



# **Processing and Characterisation of Novel Bioceramics for Load Bearing Applications**

A thesis submitted to the Faculty of Science,  
Agriculture and Engineering for the Degree of  
Doctor of Philosophy

by

**Elena Mancuso**

School of Mechanical and Systems Engineering  
Newcastle University

June 2016

*To my family and the beloved person who supported me on this journey*

## ABSTRACT

---

The use of bioceramic materials for the repair and regeneration of injured or diseased parts of the musculoskeletal system is a longstanding area of interest. However, the possibility to extend their range of applications, particularly for load-bearing bone defects and shape them into custom-built geometries is still an open challenge.

Beyond the state of the art, this research work focused on the processing and characterisation of eight novel silicate, phosphate and borate glass formulations (coded as NCLx, where x=1 to 8), containing different oxides and in diverse molar percentages. The glass frits were provided by GTS Ltd (Sheffield, UK) along with apatite-wollastonite (AW), used as comparison material.

In the first part of the work glass powders were characterised in terms of physico-chemical and biological properties. Subsequently, the glass powders were processed in form of dense bulk materials, and their sintering and mechanical behaviour was evaluated.

On the basis of the biocompatibility data, assessed using rat osteoblasts, three formulations were selected for further characterisation. *In vitro* bioactivity testing using simulated body fluid showed that after 7 days of incubation the three materials, and NCL7 in particular, showed the formation of globular shape apatite precursor precipitates, indicating the bioactive behaviour of these glasses.

In the last part of the study, 3D porous structures were manufactured *via* a binder jetting, powder-based 3D printing technology. The sintered 3D printed parts exhibited architecture and mechanical property values similar to those of AW. In addition, the *in vitro* biocompatibility indicated a biological positive response with a cell viability comparable to AW after 7 days.

The research overall has processed and characterised a range of novel bioceramic formulations, and demonstrated the potential and effectiveness of the 3DP strategy to manufacture highly reproducible ceramic-based structures.

**Keywords:** bone repair, bioceramics, additive-manufacturing, bone-substitutes.

## ACKNOWLEDGMENT

---

Throughout my PhD I have had the opportunity to meet and work with several people, whom I would like to thank sincerely and dedicate the following words.

First of all, I would like to express my gratitude for my supervisors, Kenny and Oana. During these three years they guided me through my work, encouraging my research, and at the same time they gave me the freedom to practice my ideas, collaborate with other projects, and ultimately to grow as an independent research scientist. Their advices have been priceless.

I would like to acknowledge the support of the FP7 RESTORATION project (Award CP-TP 280575-2) for funding this research.

Furthermore, I would like to thank my colleagues, with whom I shared this experience, especially Sarah and Shane that have been firstly friends, and who made my staying in Newcastle very pleasant. I would also like to acknowledge those that, with their own ideas, generated inspiring and topical discussions.

Moreover, I would like to express my sincere gratitude for the staff in the School of Mechanical and Systems Engineering. Among them I found professional and friendly people that tried to make my work in a new country as simple as possible. Particularly: Ken, Malcolm, Mike, Brian, Andy, Joanne, Tania, Linda and Chris. Their kindness and availability have been precious.

Furthermore I would like to thank the people from Chemistry and Medical School, namely Maggie, Tracey, Sharon, Isabel. To all of them goes my appreciation for their competence, and for having helped me in several occasions during my project.

A big thank you now to all my FRIENDS spread all over the world that, even though they were miles away, have been always present. Their phone or skype call, but even simply their messages, especially in unhappy moments, were invaluable. Special recognition goes to Guerino, who has always been like a big brother for me, and then PG, who after being a true friend, he has been like my mentor, and I am truly grateful for this. I would also like to extend my thankfulness to the people that although I have met in the last couple of years, they already have a special place in my heart. They supported me throughout this time, providing wise suggestions and mostly putting a smile upon my face.



Probably I do not have enough words to describe all my gratitude for my family. They always pushed and motivated me to reach my dreams, and supported my decisions with all the love that I needed, even if they were miles and miles away from me. However, I learnt that distance means so little when someone means so much. I hope to make them as happy and proud as I am in this moment.

To my dearest people that unfortunately cannot celebrate this success together with me goes a heartfelt thanks. I know that they would have been glad, probably more than me, in this occasion.

And finally my immense gratitude to “il mio topo” is beyond words. In reality, we both know that I am less capable than you with words, but I would simply like to tell you thanks for your energy, your precision and your love, that in a word are unique.

# TABLE OF CONTENTS

---

LIST OF FIGURES .....	v
LIST OF TABLES .....	xv
LIST OF ABBREVIATIONS .....	xvii
<b>CHAPTER 1. INTRODUCTION .....</b>	<b>1</b>
1.1 AIM AND OBJECTIVES OF THE WORK .....	3
1.2 THESIS STRUCTURE.....	4
<b>CHAPTER 2. HUMAN BONE TISSUE.....</b>	<b>5</b>
2.1 FUNCTION AND COMPOSITION OF HUMAN BONE.....	5
2.2 BONE STRUCTURE AND MECHANICAL PROPERTIES.....	9
2.3 BONE DEVELOPMENT, MODELLING AND REMODELLING.....	13
<b>CHAPTER 3. STATE OF THE ART IN BONE REPAIR AND REGENERATION ...</b>	<b>15</b>
3.1 CLINICAL NEED FOR BONE REPAIR AND REGENERATION .....	15
3.2 3D POROUS SUBSTITUTES FOR BONE RESTORATION .....	17
3.3 BIOMATERIALS FOR BONE TISSUE REPAIR .....	19
3.3.1 <i>Natural and synthetic polymers</i> .....	19
3.3.2 <i>Composites</i> .....	20
3.3.3 <i>Bioceramics</i> .....	21
3.3.3.1 Calcium phosphates .....	24
3.3.3.2 Apatite – wollastonite .....	26
3.3.4 <i>Bioactive glasses</i> .....	27
3.3.4.1 Silicate-based glasses .....	29
3.3.4.2 Borate-based glasses .....	32
3.3.4.3 Phosphate-based glasses.....	34
3.3.4.4 Selection of trace ions .....	36
3.3.5 <i>In vitro bioactivity of bioceramics</i> .....	44
3.4 SCAFFOLD FABRICATION TECHNOLOGIES .....	46

3.4.1	<i>Overview of additive manufacturing techniques</i>	50
3.4.1.1	Stereolithography	52
3.4.1.2	Select laser sintering	52
3.4.1.3	Fused deposition modelling	53
3.4.1.4	Powder-based three-dimensional printing	54
3.4.2	<i>Indirect powder-based 3DP for bone repair applications</i>	56
3.4.2.1	3D printed ceramic-based scaffolds	59
<b>CHAPTER 4.</b>	<b>NOVEL MATERIAL DESIGN</b>	<b>62</b>
4.1	DEVELOPMENT AND RATIONALE OF NOVEL BIOGLASS FORMULATIONS	62
<b>CHAPTER 5.</b>	<b>EXPERIMENTAL METHODS</b>	<b>68</b>
5.1	RESEARCH APPROACH	68
5.2	MATERIAL PRODUCTION	68
5.3	MATERIAL PROCESSING	70
5.3.1	<i>Glass powders</i>	70
5.3.2	<i>Bioceramic pellets</i>	70
5.3.3	<i>Indirect 3D printed bioceramic substitutes</i>	71
5.3.3.1	Powder blend preparation	72
5.3.3.2	Design of 3D structures	72
5.3.3.3	Indirect powder-based 3D printing: the process	74
5.4	CHARACTERISATION METHODS	76
5.4.1	<i>X-ray diffraction analysis</i>	76
5.4.2	<i>Hot stage microscopy</i>	76
5.4.3	<i>Morphological and microstructural characterisation</i>	77
5.4.3.1	Scanning electron microscopy	77
5.4.3.2	X-ray microtomography	77
5.4.3.3	Analysis of the porosity	78
5.4.4	<i>pH variation</i>	79
5.4.5	<i>Ion leaching evaluation</i>	79
5.4.6	<i>Shrinkage evaluation</i>	79

5.4.7	<i>Mechanical characterisation</i> .....	80
5.4.7.1	Compressive test .....	80
5.4.7.2	Three-point bending test .....	81
5.4.8	<i>In vitro bioactivity evaluation</i> .....	82
5.4.9	<i>Biological characterisation</i> .....	83
5.4.9.1	Cell culture.....	83
5.4.9.2	Glass powder cytotoxicity.....	84
5.4.9.3	In vitro evaluation of 3D printed scaffolds.....	84
5.4.9.4	Antibacterial tests.....	85

## **CHAPTER 6. RESULTS: RAW GLASS POWDERS AND BIOCERAMIC PELLETS PREPARATION AND CHARACTERISATION ..... 87**

6.1	GLASS PRODUCTION .....	87
6.2	GLASS POWDER PREPARATION.....	88
6.2.1	<i>X-ray diffraction analysis</i> .....	88
6.2.2	<i>Glass powders microstructure</i> .....	89
6.2.3	<i>Hot stage microscopy</i> .....	91
6.2.4	<i>pH variation</i> .....	95
6.2.5	<i>Ion leaching evaluation</i> .....	96
6.2.6	<i>In vitro cytotoxicity</i> .....	111
6.3	BIOCERAMIC PELLETS.....	117
6.3.1	<i>Morphological analysis</i> .....	117
6.3.2	<i>Bioceramic pellets sintering conditions</i> .....	120
6.3.3	<i>X-ray diffraction analysis before and after sintering</i> .....	121
6.3.4	<i>Sintering behaviour</i> .....	124
6.3.5	<i>Mechanical properties</i> .....	125
6.4	SELECTION OF GLASS COMPOSITIONS AS POTENTIAL BONE TISSUE-LIKE SUBSTITUTES .....	127
6.5	BIOACTIVITY EVALUATION.....	128

## **CHAPTER 7. RESULTS: MANUFACTURING OF 3D POROUS GLASS-DERIVED SUBSTITUTES ..... 137**

7.1	INDIRECT 3D PRINTED BIOCERAMIC SUBSTITUTES .....	138
7.1.1	<i>Sintering optimisation</i> .....	139
7.1.2	<i>Morphological evaluation</i> .....	141
7.1.2.1	Macrostructural observation.....	141
7.1.2.2	Microstructural observation .....	143
7.1.3	<i>Porosity and microarchitecture of the scaffolds</i> .....	144
7.1.4	<i>Mechanical properties</i> .....	148
7.1.5	<i>In vitro cellular tests</i> .....	150
7.1.6	<i>Antibacterial test</i> .....	152
<b>CHAPTER 8.</b>	<b>DISCUSSION.....</b>	<b>154</b>
8.1	INTRODUCTION .....	154
8.2	GLASS MELTING BEHAVIOUR .....	156
8.3	SINTERING TEMPERATURE SELECTION AND SINTERING BEHAVIOUR .....	156
8.4	CRYSTAL STRUCTURE EVOLUTION .....	158
8.5	MORPHOLOGICAL ANALYSIS.....	159
8.6	ION RELEASE POTENTIAL AND CYTOTOXICITY EVALUATION .....	160
8.7	APATITE-FORMING ABILITY .....	163
8.8	NOVEL GLASS FORMULATIONS PRINTABILITY .....	165
8.9	MECHANICAL PROPERTIES .....	165
8.10	NCL7 ANTIBACTERIAL PROPERTIES.....	167
<b>CHAPTER 9.</b>	<b>CONCLUSION AND FUTURE WORK.....</b>	<b>170</b>
9.1	CONCLUSIONS .....	170
9.2	FUTURE WORK.....	171
REFERENCES	.....	173

## LIST OF FIGURES

Figure 2.1: Osteoblasts, osteoclasts, osteocytes and bone lining cells: origins and locations (Marks Jr and Odgren, 2002). .....	6
Figure 2.2: Schematic representation of osteoblasts and osteoclasts pathway to bone formation (Kini and Nandeesh, 2012). .....	8
Figure 2.3: Hierarchical structure of bone, from macrostructure to sub-nanostructure (Nalla et al., 2006). .....	10
Figure 2.4: Schematic representation of bone remodelling process (Services., 2004). ....	14
Figure 3.1: Percentage of older people in the UK over the all population: 1985, 2010 and 2035 (Office for National Statistics, 2012). .....	15
Figure 3.2: Literature published between 1990 and 2015 in the area of bioceramics (Source: Scopus). .....	22
Figure 3.3: Clinical use of bioceramic materials (Hench and Wilson, 1993). .....	23
Figure 3.4: Structure of: a) crystalline silica and b) amorphous silica (Vogel, 2013). ....	28
Figure 3.5: Schematic representation of silica tetrahedron (Jones and Clare, 2012). .....	29
Figure 3.6: Schematic representation of the conversion mechanisms of a borate (3B) and 45S5 silicate (0B) glass to HA in a diluted phosphate solution (Huang et al., 2006). .....	32
Figure 3.7: SEM micrograph showing (a) human trabecular bone, and (b) 13-93B2 glass scaffold prepared using a polymer foam replication technique (Fu et al., 2009). .....	34
Figure 3.8: Schematic representation of: a) phosphate tetrahedron and b) P-O-P bond. .	35
Figure 3.9: GC-ICEL2 scaffold produced by foam replication method (Vitale-Brovarone et al., 2009). .....	36
Figure 3.10: Biological response to ionic dissolution products from bioactive glass surface (Hoppe et al., 2011). .....	37
Figure 3.11: Sequence of reactions on the surface of a bioactive glass implant (from (Gerhardt and Boccaccini, 2010)). .....	44

Figure 3.12: Common process steps for all AM techniques-based approach (re-printed by (Leong et al., 2003)).	50
Figure 3.13: The four most common and commercially available AM techniques that are used for tissue engineering scaffold fabrication (adapted from (Mota et al., 2015)).	51
Figure 3.14: 3D printing iterative phases. (1) The process starts with the spreading of a first thin layer of powder in the built area (2) and the formation of a supportive powder bed. (3) The ink-jet print-head sprays droplets of a liquid binder on the powder bed and hence the powder particles start to bond one to each other, until all the layers of the predesigned CAD file is printed. (4) The roller places the second layer of powder onto the built area and the process is repeated until the 3D structure is completed and the extra powder is removed.	57
Figure 3.15: Schematic representation of the sintering mechanism: a) particles free flowing, b) neck formations and c) voids shrinkage (reprinted by (Dorozhkin, 2010)).	59
Figure 3.16: 3D printed TCP scaffolds sintered at 1250 °C using a microwave furnace and the resulting surface morphology (inset) (Tarafder et al., 2013).	60
Figure 5.1: Specac Atlas 8T automatic hydraulic press ( <a href="http://www.specac.com/">http://www.specac.com/</a> ).	70
Figure 5.2: Flow chart describing the three stages of the 3D printed scaffold fabrication: pre-processing (yellow), processing (blue) and post-processing (green).	71
Figure 5.3: Powder blend preparation using a roller mixer.	72
Figure 5.4: CAD design of the 3DP: a) cylindrical and b) bar shape structures.	73
Figure 5.5: Commercial ZPrinter® 310 Plus 3D printer (Z Corporation, USA) and its main components ( <a href="http://www.zcorp.com">www.zcorp.com</a> ).	74
Figure 5.6: Graphic interface of ZPrint 7.10 software.	75
Figure 5.7: Compressive test performed using a Tinius Olsen universal testing machine; inset shows the specimen before the test.	80
Figure 5.8: Three-point bending test determined by an INSTRON 5567 universal testing machine.	81

Figure 5.9: Schematic representation of the three-point bending test conditions. ....	81
Figure 5.10: Morphology of rat osteoblast cells. ....	83
Figure 5.11: Staphylococcus aureus cultivation on TSA plates: (a) glass powders (bottom), bioceramic pellets (top) and (b) 3D porous scaffolds (top). ....	86
Figure 6.1: Representative image of the as-produced glass frits. ....	88
Figure 6.2: a) glass frits, b) ground using a ball milling machine, and then c) sieved to obtain fine glass powder.....	88
Figure 6.3: XRD patterns of as-synthesised glass powders (▲ hydroxylapatite, ■ $\beta$ - wollastonite, ♦ silver ● calcium sodium phosphate). ....	89
Figure 6.4: SEM analysis (magnification 1500x) showing the glass powders morphology: a) NLC1, b) NCL2, c) NCL3, d) NCL4, e) NCL6, f) NCL7, g) NCL8, and h) AW. ....	90
Figure 6.5: Shrinkage profile derived from hot stage microscopy as function of temperature for: a) NCL1, b) NCL2, c)NCL3, d) NCL4, e) NCL6, f) NCL7, g) NCL8 and h) AW.....	94
Figure 6.6: pH changes induced by the pre-sintered glass powder immersed in deionised water at 37 °C: a) with refresh and b) without refreshing the solution. ....	95
Figure 6.7: Ionic release concentrations deriving from NCL1 raw glass powders after 28 days of soaking in deionised water. ....	98
Figure 6.8: Ionic release concentrations deriving from NCL2 raw glass powders after 28 days of soaking in deionised water. ....	99
Figure 6.9: Ionic release concentrations deriving from NCL3 raw glass powders after 28 days of soaking in deionised water. ....	100
Figure 6.10: Ionic release concentrations deriving from NCL3 raw glass powders after 28 days of soaking in deionised water. ....	101
Figure 6.11: Ionic release concentrations deriving from NCL4 raw glass powders after 28 days of soaking in deionised water. ....	103



Figure 6.12: Ionic release concentrations deriving from NCL6 raw glass powders after 28 days of soaking in deionised water. ....	104
Figure 6.13: Ionic release concentrations deriving from NCL7 raw glass powders after 28 days of soaking in deionised water. ....	105
Figure 6.14: Ionic release concentration deriving from NCL8 raw glass powder after 28 days of soaking in deionised water. ....	107
Figure 6.15: Ionic release concentration deriving from NCL8 raw glass powder after 28 days of soaking in deionised water. ....	108
Figure 6.16: Ionic release concentration deriving from AW raw glass powder after 28 days of soaking in deionised water.....	109
Figure 6.17: Effect of NCL1 glass powders (measured in triplicate) on formazan formation after (a) direct and (b) indirect contact with rat osteoblast cells, evaluated through MTT assay after 1 day and 7 days in culture. Error bars represent the standard error of the mean ( $p < 0.05(*)$ and $p < 0.001(**)$ ). ....	111
Figure 6.18: Effect of NCL2 glass powders (measured in triplicate) on formazan formation after (a) direct and (b) indirect contact with rat osteoblast cells, evaluated through MTT assay after 1 day and 7 days in culture. Error bars represent the standard error of the mean ( $p < 0.05(*)$ and $p < 0.001(**)$ ). ....	112
Figure 6.19: Effect of NCL3 glass powders (measured in triplicate) on formazan formation after (a) direct and (b) indirect contact with rat osteoblast cells, evaluated through MTT assay after 1 day and 7 days in culture. Error bars represent the standard error of the mean ( $p < 0.05(*)$ and $p < 0.001(**)$ ). ....	113
Figure 6.20: Effect of NCL4 glass powders (measured in triplicate) on formazan formation after (a) direct and (b) indirect contact with rat osteoblast cells, evaluated through MTT assay after 1 day and 7 days in culture. Error bars represent the standard error of the mean ( $p < 0.05(*)$ and $p < 0.001(**)$ ). ....	113
Figure 6.21: Effect of NCL6 glass powders (measured in triplicate) on formazan formation after (a) direct and (b) indirect contact with rat osteoblast cells, evaluated through MTT	

assay after 1 day and 7 days in culture. Error bars represent the standard error of the mean ( $p < 0.05(*)$ and $p < 0.001(**)$ ). .....	114
Figure 6.22: Effect of NCL7 glass powders (measured in triplicate) on formazan formation after (a) direct and (b) indirect contact with rat osteoblast cells, evaluated through MTT assay after 1 day and 7 days in culture. Error bars represent the standard error of the mean ( $p < 0.05(*)$ and $p < 0.001(**)$ ). .....	114
Figure 6.23: Effect of NCL8 glass powders (measured in triplicate) on formazan formation after (a) direct and (b) indirect contact with rat osteoblast cells, evaluated through MTT assay after 1 day and 7 days in culture. Error bars represent the standard error of the mean ( $p < 0.05(*)$ and $p < 0.001(**)$ ). .....	115
Figure 6.24: Effect of AW glass powders (measured in triplicate) on formazan formation after (a) direct and (b) indirect contact with rat osteoblast cells, evaluated through MTT assay after 1 day and 7 days in culture. Error bars represent the standard error of the mean ( $p < 0.05(*)$ and $p < 0.001(**)$ ). .....	115
Figure 6.25: SEM micrograph (magnification 2500x) of NCL1 pellet surface at (a) low (575°C), and (b) appropriate sintering level (625°C). .....	117
Figure 6.26: SEM micrograph (magnification 2500x) of NCL2 pellet surface at (a) low (650°C), and (b) appropriate sintering level (700°C). .....	118
Figure 6.27: SEM micrograph (magnification 2500x) of NCL3 pellet surface at (a) low (550°C), and (b) appropriate sintering level (625°C); red arrows indicate necking formation. ....	118
Figure 6.28: SEM micrograph (magnification 2500x) of NCL4 pellet surface at (a) low (600°C), and (b) appropriate sintering level (625°C). .....	118
Figure 6.29: SEM: micrograph (magnification 2500x) of NCL6 pellet surface at (a) low (700°C), and (b) appropriate sintering level (725°C); red arrow indicates necking formation. ....	119

Figure 6.30: SEM micrograph (magnification 2500x) of NCL7 pellet surface at (a) low (600°C), and (b) appropriate sintering level (625°C); red arrows indicate necking formation. ....	119
Figure 6.31: SEM micrograph (magnification 2500x) of NCL8 pellet surface at (a) low (575°C), and (b) appropriate sintering level (625°C). ....	119
Figure 6.32: SEM micrograph (magnification 2500x) of AW pellet surface at (a) low (830°C), and (b) appropriate sintering level (850°C); red arrow indicates necking formation. ....	120
Figure 6.33: XRD patterns of NCL1 composition: (a) glass powder and (b) pellet sintered at 625°C. ....	121
Figure 6.34: XRD patterns of NCL2 composition: (a) glass powder and (b) pellet sintered at 700°C (● diopside). ....	121
Figure 6.35: XRD patterns of NCL3 composition: (a) glass powder and (b) pellet sintered at 625°C. ....	122
Figure 6.36: XRD patterns of NCL4 composition: (a) glass powder and (b) pellet sintered at 625°C. ....	122
Figure 6.37: XRD patterns of NCL6 composition: (a) glass powder and (b) pellet sintered at 725°C, (● calcium sodium phosphate and ■ sodium calcium magnesium phosphate). ....	122
Figure 6.38: XRD patterns of NCL7 composition: (a) glass powder and (b) pellet sintered at 625 C, (◆ silver). ....	123
Figure 6.39: XRD patterns of NCL8 composition: (a) glass powder and (b) pellet sintered at 625°C. ....	123
Figure 6.40: XRD patterns of AW composition: (a) glass powder and (b) pellet sintered at 850°C, (▲ hydroxylapatite, ■ β-wollastonite). ....	124
Figure 6.41: Average volumetric shrinkage (%) for sintered pellets (n=5). Error bars represent the standard error of the mean. ....	124

Figure 6.42: Representative stress-strain curve obtained during compression tests performed on the sintered bioceramic pellets. ....	125
Figure 6.43: a) Averaged compressive stress (for $\epsilon_c=20\%$ ) and b) compressive modulus values of dry bioceramic pellets (n=5). Error bars represent the standard error of the mean ( $p<0.05(*)$ and $p<0.001(**)$ ). ....	126
Figure 6.44: a) morphological (5Kx mag) and b) compositional analysis of the marked region of NCL2 bioceramic pellet before the immersion in SBF. c) morphological (5Kx mag) and d) compositional analysis (at %) of the marked region of NCL2 bioceramic pellet after 7 days of immersion in SBF. ....	128
Figure 6.45: a) morphological (5Kx mag) analysis with b) higher magnification inset (20Kx mag), and c) compositional analysis (at %) of the marked precipitates observed on NCL2 bioceramic pellet after 28 days of soaking in SBF. ....	129
Figure 6.46: a) morphological (5Kx mag) and b) compositional analysis of the marked region of NCL4 bioceramic pellet before the immersion in SBF. c) morphological (5Kx mag) and d) compositional analysis (at %) of the marked region of NCL4 bioceramic pellet after 7 days of immersion in SBF. ....	129
Figure 6.47: a) morphological (5Kx mag) analysis with b) higher magnification inset (20Kx mag), and c) compositional analysis (at %) of the marked precipitates observed on NCL4 bioceramic pellet after 28 days of soaking in SBF (white arrows indicate the granular structures developed on the pellet surface). ....	130
Figure 6.48: a) morphological (5Kx mag) and b) compositional analysis of the marked region of NCL7 bioceramic pellet before the immersion in SBF. c) morphological (5Kx mag) and d) compositional analysis (at %) of the marked region of NCL7 bioceramic pellet after 7 days of immersion in SBF (the red arrows indicate the micro-cracks formation on the pellet surface). ....	131
Figure 6.49: a) morphological (5Kx mag) analysis with b) higher magnification inset (20Kx mag), and c) compositional analysis (at %) of the marked precipitates observed on NCL7 bioceramic pellet after 28 days of soaking in SBF (the red arrows indicate the micro-cracks formation on the pellet surface). ....	131

Figure 6.50: a) morphological (5Kx mag) and b) compositional analysis of the marked region of AW bioceramic pellet before the immersion in SBF. c) morphological (5Kx mag) and d) compositional analysis (at %) of the marked region of AW bioceramic pellet after 7 days of immersion in SBF (the red arrows indicate the micro-cracks formation on the pellet surface). .....	132
Figure 6.51: a) morphological (5Kx mag) analysis with b) higher magnification inset (20 Kx mag), and c) compositional analysis (at %) of the marked precipitates observed on NCL7 bioceramic pellet after 28 days of soaking in SBF (the red arrows indicate the micro-cracks formation on the pellet surface). .....	133
Figure 6.52: Atomic concentration of Si, Ca and P on the upper surface of a) NCL2 and b) NCL4 bioceramic pellets after immersion in SBF at different time points. ....	133
Figure 6.53 : Atomic concentration of Si, Ca and P on the upper surface of a) NCL7 and b) AW bioceramic pellets after immersion in SBF at different time points. ....	134
Figure 6.54: Release profiles of Si, Ca and P ions for a)NCL2 and b) NCL4 bioceramic pellets immersed in SBF solution at different time intervals. ....	134
Figure 6.55: Release profiles of Si, Ca and P ions for a)NCL7 and b) AW bioceramic pellets immersed in SBF solution at different time intervals. ....	135
Figure 6.56: Averaged weight loss ( $\pm$ SE) of NCL2, NCL4, NCL7 and AW pellets after soaking in SBF solution. ....	135
Figure 6.57: Averaged pH value ( $\pm$ SE) of SBF solution for NCL2, NCL4, NCL7 and AW samples. ....	136
Figure 7.1: SEM micrographs of 3D printed green bodies: a) NCL2, b) NCL4, c) NCL7 and d) AW samples. ....	138
Figure 7.2: Heat treatments and corresponding profiles that were investigated for NCL2 3D printed green bodies. ....	139
Figure 7.3: Heat treatments and corresponding profiles that were investigated for NCL7 3D printed green bodies. ....	140

Figure 7.4: Heat treatment and corresponding profile for AW 3D printed green bodies. .....	141
Figure 7.5: NCL2 3D printed samples: a) before and b) after the sintering process. ....	141
Figure 7.6: NCL7 3D printed samples: a) before and b) after the sintering process. ....	142
Figure 7.7: AW 3D printed samples: a) before and b) after the sintering process.....	142
Figure 7.8: Average volumetric shrinkage (%) for sintered NCL2, NCL7 and AW 3D printed samples. Error bars represent the standard error of the mean.....	142
Figure 7.9: SEM micrographs of a) upper surface and b) cross section of NCL2 3D printed structure after sintering (red arrows indicate necking formation).....	143
Figure 7.10: SEM micrographs of a) top surface and b) cross section of NCL7 3D printed structure after sintering (red arrows indicate necking formation).....	143
Figure 7.11: SEM micrographs of a) top surface and b) cross section of AW 3D printed structure after sintering (red arrows indicate necking formation).....	144
Figure 7.12: Averaged open and total porosity values for sintered NCL2, NCL7 and AW 3D printed parts. Error bars represent the standard error of the mean ( $p < 0.05(*)$ ).....	145
Figure 7.13: NCL2 scaffold: (a) 3D reconstruction and (b), (c) and (d) spatial views (XY, XZ and YZ) obtained through micro-CT analysis. ....	146
Figure 7.14: NCL7 scaffold: (a) 3D reconstruction and (b), (c) and (d) spatial views (XY, XZ and YZ) obtained through micro-CT analysis. ....	147
Figure 7.15: AW scaffold: (a) 3D reconstruction and (b), (c) and (d) spatial views (XY, XZ and YZ) obtained through micro-CT analysis. ....	147
Figure 7.16: Illustrative images of 3D sintered bars after the three-point bending test.	148
Figure 7.17: Representative stress-strain curve for 3D printed porous ceramic bars, resulting from the three-point bending test (red arrows indicate the cracking phenomena during the test).....	148

Figure 7.18: Average flexural strength and flexural modulus for NCL2, NCL7 and AW 3D printed scaffolds evaluated through three-point bending test. Error bars represent standard error of the mean ( $p < 0.05(*)$ ). .....	149
Figure 7.19: Effect on formazan formation by NCL2, NCL7 and AW 3D printed scaffolds (n=6), evaluated through MTT assay after 24 hours, 3 days and 7 days in culture. Error bars represent the standard error of the mean ( $p < 0.05(*)$ , $p < 0.001(**)$ ). .....	150
Figure 7.20: Illustrative image of the zone inhibition test after 24 h incubation, performed on: NCL7 and AW glass powders (bottom) and bioceramic pellets (top) using <i>S. aureus</i> . .....	152
Figure 7.21: Inhibition halo test by using <i>S. aureus</i> strain to evaluate the antibacterial effect of NCL7 and AW 3D printed scaffold: a) general view of the agar plate, b) magnification of AW sample and c) magnification of NCL7 sample showing the inhibition zone that limited bacterial growth.....	153
Figure 8.1: Ionic concentrations of Si, P, B, Ca and Mg released into deionised water from all the formulations, without refreshing the solutions and at different time points (1, 7, 14 and 28 days). .....	161
Figure 8.2: (a) NCL7 and (b) AW bioceramic pellet after soaking in SBF for 28 days (the red arrows indicate the micro-cracks formation on the pellet surface). .....	164

## LIST OF TABLES

Table 2.1: Bone cells type, location, origin and morphology. ....	8
Table 2.2: Mechanical properties of human cortical and trabecular bone. ....	12
Table 3.1: Desirable requirements for the design of bone tissue engineered scaffolds. ..	18
Table 3.2: In vivo pre-clinical studies of load-bearing bone defects using composite scaffolds (adapted from (Pilia et al., 2013)). ....	21
Table 3.3: CaP-compounds with corresponding abbreviation, chemical formula and Ca/P molar ratio (re-adapted from (Dorozhkin, 2010)). ....	25
Table 3.4: Mechanical properties of natural bone and AW glass-ceramic (Kokubo, 2008). ....	27
Table 3.5: Composition of various silicate glasses developed over the years (Silver et al., 2001; Rahaman et al., 2011; Jones, 2013). ....	31
Table 3.6: Role of elemental ions on bone repair and regeneration. ....	39
Table 3.7: Ion concentrations (mM) of human blood plasma and SBF solution (Kokubo and Takadama, 2006). ....	45
Table 3.8: Conventional techniques for the production of bone tissue substitutes. ....	49
Table 3.9: The four most commonly used AM technologies for the production of bone tissue substitutes with their advantages (+) and disadvantages (-). ....	55
Table 3.10: Mechanical and biological properties of some ceramic-based 3D printed scaffolds. ....	61
Table 4.1: Molar composition and rationale of the novel glass formulations. ....	64
Table 5.1: Overview of the experimental work performed on: glass powders, bioceramic pellets and 3D printed bioceramic structures. ....	69
Table 5.2: Powder blend settings for ZPrinter® 310 Plus 3D printer. ....	75
Table 6.1: Production parameters for the new glass compositions. ....	87



Table 6.2: HSM results and resulting thermal parameters for NCL1, NCL2, NCL3 and NCL4.....	92
Table 6.3: HSM results and resulting thermal parameters for NCL6, NCL7, NCL8 and AW.....	93
Table 6.4: Bioceramic pellets sintering temperatures. ....	120
Table 7.1: Summary of the mechanical properties (mean $\pm$ SE) for 3D printed NCL2, NCL7 and AW porous scaffolds assessed by three-point bending test. ....	149
Table 7.2: pH values and ionic concentrations of the different DMEM extracts obtained from NCL2, NCL7 and AW specimens at specific time points.....	151
Table 8.1: Summary of the key outcomes deriving from the processing and characterisation of the novel glass formulations. ....	155
Table 8.2: Glass formulations sintering intervals obtained by HSM, and optimal sintering temperatures for dense pellets and porous scaffolds.....	156
Table 8.3: Compressive modulus (mean $\pm$ SE) of AW and dense bioceramic pellets.....	166
Table 8.4: Total porosity values (vol %) of 3D printed scaffolds (n=5) compared to human bone. The data represent the mean $\pm$ SE (* (Goldstein, 1987)). ....	166
Table 8.5: Mechanical properties (mean $\pm$ SE) of 3D printed scaffolds via powder-based indirect 3DP. ....	168

## **List of abbreviations**

additive manufacturing (**AM**)  
alkaline phosphatase (**ALP**)  
amorphous calcium phosphate (**ACP**)  
analysis of variance (**ANOVA**)  
apatite-wollastonite (**AW**)  
biphasic calcium phosphate (**BCaP**)  
bone grafts and substitutes (**BGS**)  
bone morphogenetic proteins (**BMP**)  
bone tissue engineering (**BTE**)  
carbonated hydroxyapatite (**HCA**)  
computer tomography (**CT**)  
computer-aided design (**CAD**)  
dicalcium phosphate anhydrous (**DCPA**)  
dimethylsulfoxide (**DMSO**)  
poly-D-lactide (**PDLA**)  
Dulbecco's Modified Eagle Medium (**D-MEM**)  
extracellular matrix (**ECM**)  
fetal bovine serum (**FBS**)  
fused deposition modelling (**FDM**)  
hot stage microscopy (**HSM**)  
hydroxyapatite (**HA**)  
hydroxy-terminated poly(propylene fumarate) (**HT-PPFhm**)  
hypoxia-inducible factor 1 (**HIF-1**)  
inductively coupled plasma optical emission spectrometer (**ICP-OES**)  
maltodextrine (**MD**)  
magnetic resonance imaging (**MRI**)  
mesenchymal stem cells (**MSCs**)  
osteoblast (**OB**)  
phosphate buffered solution (**PBS**)  
polycaprolactone (**PCL**)

poly-DL-lactide (**PDLLA**)  
polyethylene (**PE**)  
poly(glycolic acid) (**PGA**)  
poly-lactide (or poly- lactic acid) (**PLA**)  
poly-L-lactide (**PLLA**)  
poly(lactic-co glycolide) (**PLGA**)  
rapid prototyping (**RP**)  
scanning electron microscopy (**SEM**)  
select laser sintering (**SLS**)  
simulated body fluid (**SBF**)  
solid free form fabrication (**SFF**)  
standard error of the mean (**SE**)  
standard tessellation language (**STL**)  
stereolithography (**SLA**)  
tetracalcium phosphate (**TTCP**)  
thermally induced phase separation (**TIPS**)  
three dimensional (**3D**)  
three dimensional printing (**3DP**)  
tissue engineering (**TE**)  
tricalcium phosphate (**TCP**)  
trypticase Soy Agar (**TSA**)  
trypticase Soy Broth (**TSB**)  
ultraviolet (**UV**)  
X-ray diffraction (**XRD**)  
X-ray photoelectron spectroscopy (**XPS**)  
 $\beta$ -tricalcium phosphate ( **$\beta$ -TCP**)  
3-(4,5-dimethylthiazol-2-yl)-2,5-diphenyl tetrazolium bromide (**MTT**)

# Chapter 1. Introduction

---

Annually, more than two million bone graft procedures are performed worldwide to repair bone defects in orthopaedics, neurosurgery and dentistry (Van Lieshout *et al.*, 2011). In 2013, the global market for joint reconstruction and replacement was worth nearly €11.8 billion. In Europe the market has been estimated to increase from €3.4 billion in 2013 up to €4 billion by 2018 (*Joint Reconstruction and Replacement: Materials, Technologies, and Global Markets*, 2014).

Among the human tissues, bone has been considered one of the most transplanted, second only to blood (Giannoudis *et al.*, 2005). In addition to other important properties, bone possesses the intrinsic capacity of self-healing in response to injury (Dimitriou *et al.*, 2011). Hence, most of small skeletal fractures heal spontaneously without the need of further treatments. However, in complex clinical conditions (such as skeletal reconstruction of large load-bearing bone defects resulting from trauma, infection, tumour resection and skeletal abnormalities), or cases in which the regenerative process is compromised (like avascular necrosis, atrophic non-unions and osteoporosis), the tissue cannot heal on its own, and therefore additional reconstructive surgical interventions are required (Logeart-Avramoglou *et al.*, 2005).

Since the first reported use of a calcium sulphate to fill bone defects in 1892 (Dressmann, 1892), material-based strategies have seen remarkable progress, emerging as a promising alternative to the more common autologous tissue-based approach (Salgado *et al.*, 2004).

Particularly, in 1969 Prof. L. Hench proposed the first glass intended for bone tissue repair, later commercially known as Bioglass® (Hench, 1991; Hench, 1998b). Hench's studies represented the fundamentals to launch the field of bioactive glasses, a class of biomaterials highly and still widely investigated (Jones, 2013).

The most important feature of bioglasses is their ability to form a strong bond with soft as well as hard host tissue, and to induce cell response resulting in osteoinductive behaviour (Hench *et al.*, 1971; Xynos *et al.*, 2000b). More specifically, it has been demonstrated that when a bioglass is put in contact with biological fluids, a layer of carbonated hydroxyapatite (HCA) develops on its surface promoting material-tissue bonding (Gerhardt and Boccaccini, 2010; Chen *et al.*, 2012). In addition to the beneficial property to bond to bone, bioactive glasses degrade over time, releasing

soluble ions that promote cell proliferation, differentiation and activate gene expression (Xynos *et al.*, 2000a; Xynos *et al.*, 2001; Kanczler and Oreffo, 2008; Hoppe *et al.*, 2011)

After Bioglass<sup>®</sup> introduction, many new formulations in the silicate, phosphate and borate-based system have been designed to meet a set of requirements that are both crucial and necessary for optimised tissue-engineered substitutes (scaffolds). The purpose was to improve specific properties, such as controlled degradation rate, biocompatibility and most importantly mechanical strength (Kokubo *et al.*, 2003; Rahaman *et al.*, 2011; Will *et al.*, 2012; Kaur *et al.*, 2013). However, the possibility to extend the range of bioactive glasses applications, particularly for load-bearing bone defects, is still an open challenge.

In addition to material properties, design characteristics of bone-like substitutes are decisive aspects in bone tissue repair field (Hollister *et al.*, 2002). An accurate control on both microscopic and macroscopic level is thus necessary during the scaffold fabrication process (Henkel *et al.*, 2013). In this direction, the advances in material processing using additive manufacturing (AM) technologies are offering a promising opportunity to generate “smart”, custom-made, and ultimately patient-specific devices for bone tissue repair applications (Melchels *et al.*, 2012; Yoo, 2014; Mota *et al.*, 2015). Furthermore, along with the possibility of tailoring the device geometry according to patient needs, AM enables the fabrication of 3D implants with differences in spatial distribution of porosities, pore sizes, mechanical and chemical properties over the large scale (Henkel *et al.*, 2013). Additionally, this approach overcame the limitations of conventional techniques, and most importantly offered great benefit to the healthcare sector (Bose *et al.*, 2013; Arafat *et al.*, 2014; Giannitelli *et al.*, 2014).

Indirect powder-based 3D printing is a versatile technology (Bose *et al.*, 2013), developed in the early 1990s at MIT (Cambridge, MA), and is based on jetting of a binder solution onto a powder bed, following a layer by layer procedure (Sachs *et al.*, 1992). The advantages of this method, in the field of bone tissue repair, derive from the flexibility in material usage and the possibility of printing objects with defined geometry, controlled and interconnected structure without the use of any toxic solvent (Utela *et al.*, 2010; Butscher *et al.*, 2011; Bose *et al.*, 2013). After the success of its application for the fabrication of bioceramics scaffolds (Lee *et al.*, 2005; Leukers *et al.*, 2005; Irsen *et al.*, 2006a; Utela *et al.*, 2006b; Vorndran *et al.*, 2008; Butscher *et al.*, 2012; Cox *et al.*, 2015), the use of 3D printing technology for the production of bone-like substitutes is likely to

increase in the coming years, primarily focusing on the development of medical implants that can be customised according to patient and clinical needs.

### **1.1 Aim and objectives of the work**

Beyond the current state of the art and within the European RESTORATION (Resorbable Ceramic Biocomposites for Orthopaedic and Maxillofacial Applications) project (EU FP7 280575), this work focused on the processing and characterisation of eight novel silicate, phosphate and borate glass formulations (coded as NCLx, where x=1 to 8), containing different oxides and in diverse molar percentages, as potential biomaterials to support the repair and regeneration of load bearing bone defects.

To achieve the aim, the following specific objectives were developed:

- **OB1:** development of a series of novel glass compositions (later termed bioceramics) containing specific doping agents;
- **OB2:** evaluation of the physico-chemical and biological properties of the glass powders;
- **OB3:** evaluation of the physico-chemical, mechanical and *in vitro* bioactive properties of dense sintered bioceramic pellets;
- **OB4:** optimisation of the methodology for the fabrication of three dimensional (3D) porous glass-derived substitutes;
- **OB5:** evaluation of the physico-chemical, mechanical and biological properties of the previously fabricated 3D porous sintered substitutes.

## 1.2 Thesis structure

In order to achieve the research objectives, the overall thesis is divided into nine chapters.

The current **Chapter 1** provides an introduction to the work, highlighting the aim and the resulting objectives, and illustrates how the overall manuscript is organised.

**Chapter 2** starts with a brief overview about bone biology, covering human bone tissue function, composition, structure and mechanical properties; and it concludes with an insight on bone development, modelling and remodelling processes.

**Chapter 3** presents the current state of the art on bone tissue repair and regeneration. It begins with an introduction on the existing clinical approaches, followed by the recent progress on biomaterials used for bone tissue substitution. Specifically, it focuses on the use of bioactive glasses and the possibility to modify their compositions by adding specific and functional doping agents. Furthermore, a relevant literature review on 3D porous structures fabrication methodology is presented, along with an in-depth description of additive manufacturing technologies, in order to frame the scope of the work.

According to the emerging clinical need of developing new biomaterials with tailored physico-chemical and mechanical features, **Chapter 4** reports the rationale for the design and development of eight novel bioceramic formulations for bone tissue repair and regeneration, along with their structure and molar composition.

**Chapter 5** deals with the methodology adopted for the novel glasses production, processing (in form of glass powders, bioceramic pellets and 3D porous scaffolds *via* 3DP technology), and characterisation of their physico-chemical, biological and mechanical properties.

In **Chapter 6** are reported the main achievements resulting from the experimental work, carried out on the processing and characterisation of the as-synthesised glass powders and dense bioceramic pellets. **Chapter 7** instead presents the results deriving from the processing and characterisation of 3D printed bioceramic substitutes.

In **Chapter 8** a general discussion about the key findings resulting from the experimental work is presented; and finally, the overall project conclusions with the limitations and potential future developments are outlined in **Chapter 9**.

## Chapter 2. Human bone tissue

---

### 2.1 Function and composition of human bone

Bone is a highly complex living tissue, characterised by its stiffness (typically in the range 0.1-20GPa) and fracture toughness (typically between 0.1-12MPa·m<sup>1/2</sup>) (Fu *et al.*, 2011), repair and regeneration ability that provides internal support for all higher vertebrates (Marks Jr and Popoff, 1988). Its basic functions include: *i*) mechanical support for muscular activity, *ii*) physical protection of organs and soft tissue, and *iii*) significant flexibility without compromising the mechanical strength. Together with its protective functions, bone tissue serves as a reservoir for inorganic ions and a source of calcium necessary during the remodelling process which each bone continuously undergoes during life (Marks Jr and Popoff, 1988; Marks Jr and Odgren, 2002; Clarke, 2008).

Most biological tissues are frequently defined in terms of both structural and material properties (Pal, 2014). Bone is a composite material based on 50 to 70% minerals (inorganic phase), 20 to 40% organic matrix, 5 to 10% water content, and < 3% lipids (Clarke, 2008). The bone extracellular matrix (ECM) is composed of collagenous and non-collagenous proteins. Type I collagen is the main constituent of bone organic phase (accounting for approximately 90%) along with smaller amounts of type III, V, XI and XIII collagen. The remaining 10% of the ECM proteins weight is composed of glycoproteins, proteoglycans and growth factors including bone morphogenetic proteins (BMP), alkaline phosphatase (ALP), osteopontin, bone sialoprotein, osteocalcin, cytokines and adhesion molecules, which contribute the matrix mineralisation process, bone cell proliferation and bone cell activities (Velleman, 2000; Sommerfeldt and Rubin, 2001; Clarke, 2008; Gentili and Cancedda, 2009).

Regarding the mineral content, this is mainly made by hydroxyapatite [(Ca<sub>10</sub>(PO<sub>4</sub>)<sub>6</sub>(OH)<sub>2</sub>)] (85%) with traces of calcium carbonate (10%), calcium fluoride (2-3%) and magnesium fluoride (2-3%) (Polo-Corrales *et al.*, 2014). Hydroxyapatite (HA) crystals, characterised by a plate shape, are the smallest known biological crystals (30-50nm in length, 20-25nm wide, and 2-5nm thick) (Zipkin, 1970; Boskey, 2007; Palmer *et al.*, 2008). Unlike geological HA [(Ca<sub>5</sub>(PO<sub>4</sub>)<sub>3</sub>(OH)<sub>2</sub>)] with a Ca/P molar ratio equal to 1.67, Ca/P values in bone and dentin were found between 1.37 and 1.87 (Hing,



2004). This variation happens because bone is used by the human body as reservoir, maintaining magnesium, calcium and phosphate ions homeostasis (Palmer *et al.*, 2008).

From a material science prospective, the organic and inorganic bone components work together to confer to bone its exclusive anisotropy characteristics. The amount of mineral content is correlated to bone strength and stiffness degree, while the organic phase provides bone its flexibility. Specifically, the collagen content gives the bone the ability to support tense loads instead the bone mineral constituents give it the ability to support compressive loads (Rho *et al.*, 1998; Tranquilli Leali *et al.*, 2009).

Regarding the cellular makeup of bone, it consists of four different types of cells: osteoblasts (bone-forming), osteocytes (bone development), bone lining cells (bone protection), and osteoclasts (bone-resorbing). A first difference among bone cells is based on their origin: osteoblasts, osteocytes and bone lining cells originate from mesenchymal stem cells (MSCs), also known as osteoprogenitor cells, whereas osteoclasts originate from hemopoietic stem cells. MSCs are multipotent cells that arise from the mesenchyme during tissue development (Marion and Mao, 2006). Concerning the location, osteoblasts, osteoclasts and bone lining cells are located along the bone surface whereas osteocytes are in the internal part of the bone (Figure 2.1) (Buckwalter *et al.*, 1996).

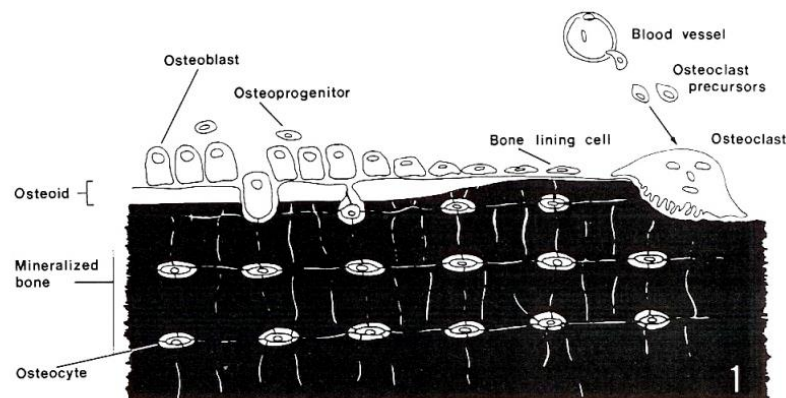


**Figure 2.1: Osteoblasts, osteoclasts, osteocytes and bone lining cells: origins and locations (Marks Jr and Odgren, 2002).**

Osteoblasts are mononucleated cells and originate from pluripotent mesenchymal stem cells of the bone marrow stroma (Owen, 1988; Pittenger *et al.*, 1999). They are functionally responsible for

ECM production and the regulation of the mineralisation process (Clarke, 2008; Neve *et al.*, 2011). During osteogenesis (the process of formation of new bone), osteoblasts secrete an amorphous matrix called osteoid predominantly consisting of type I collagen along with many non-collagenous proteins of the bone matrix, such as bone sialoprotein, osteocalcin and osteopontin (Aubin and Triffitt, 2002; Boskey, 2007; Heino and Hentunen, 2008).

Eventually, osteoblasts can become relatively inactive and form bone lining cells. Due to their inactivity these cells have fewer cytoplasmic organelles than osteoblasts, even though it has been hypothesised that bone lining cells can be osteoblast precursors (Franz-Odenaal *et al.*, 2006). In terms of morphology they are thin and elongated and cover most of bone surface in an adult skeleton (Buckwalter *et al.*, 1996; Marks Jr and Odgren, 2002).

In calcified cartilage and woven bone, mineralisation is initiated by the matrix vesicles that grow from the plasma membrane of osteoblasts to create an environment for the concentration of calcium and phosphate ions. In lamellar bone, the process is vesicle independent and seems to be started by collagen molecule components (Landis *et al.*, 1993). In both cases, collagen serves as template for initiation and propagation of mineralisation process. The mineral deposition makes the matrix impermeable. Osteoblasts surrounded by the bone matrix progress to their ultimate differentiation stage, the osteocytes. It has been estimated that osteocytes make up more than 90% of the bone cells in an adult skeleton bone. These cells are located within a space or lacuna and have long cytoplasmic process through canaliculi in the matrix to contact processes of adjacent cells. Osteocytes have the ability to communicate metabolically and electrically through gap junctions (Sheng *et al.*, 2014), which consist of arrays of intercellular channels made of integral membrane proteins called connexions (Sosinsky and Nicholson, 2005). The cellular network can sense the mechanical deformation that takes place in bone and contributes to bone formation and resorption process (Kimmel, 1993). Responsible for the bone resorption process are another class of cells, the osteoclasts. They derive from hematopoietic stem cells and the differentiation process requires cell-cell interactions via either osteoblast or osteoblast precursor cells (Figure 2.2) (Aubin and Triffitt, 2002; Karaplis, 2002; Heino and Hentunen, 2008).

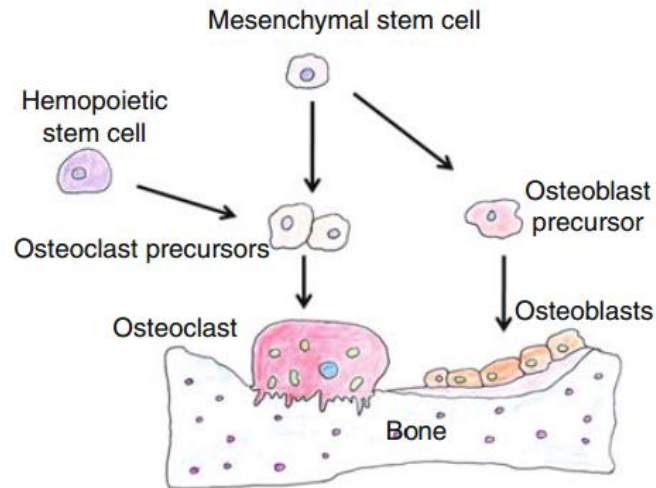


**Figure 2.2: Schematic representation of osteoblasts and osteoclasts pathway to bone formation (Kini and Nandeesh, 2012).**

A summary of bone cells location, origin and morphology can be found in Table 2.1.

**Table 2.1: Bone cells type, location, origin and morphology.**

Cell type	Location	Origin	Morphology
Osteoblasts	bone surface	mesenchymal stem cells	cuboidal cells
Osteoclasts	bone surface	hemopoietic stem cells	giant and multinucleated cells
Lining cells	bone surface	mesenchymal stem cells	thin and elongated cells
Osteocytes	inner part of the bone	mesenchymal stem cells	star-shaped cells

## 2.2 Bone structure and mechanical properties

At the microscopic level, human bone is characterised by two different types: woven and lamellar bone. Woven bone is considered primary and immature with a disoriented arrangement of collagen fibres that turn into lamellar bone during adolescence. Lamellar bone is a highly organised structure with collagen bundles oriented in the same direction (Hollinger *et al.*, 2004; Ossification, 2004).

Macroscopically bone can be divided into trabecular (also known as spongy or cancellous) bone, which forms the porous inner core, and cortical (also called compact) bone, which forms a dense outer shell (Figure 2.3(a)). Their proportions usually differ at various locations in the skeleton, but generally cortical bone accounts for 80% of the weight of the human skeleton and cancellous bone for the remaining 20% (Rho *et al.*, 1998). Considering a bone cross-section, the end of long bones (*i.e.* tibia or femur) has a hard outer surface of dense compact bone and a porous internal structure, whereas flat bones (skull, ilium and rib cage) have two thin layers of cortical bone with a variable volume of cancellous bone embedded between them.

As it was previously stated, cortical bone is highly dense and consists of a hierarchical structure, going from the solid material ( $> 3\text{mm}$ ), to the osteons ( $10\text{--}500\mu\text{m}$ ) firstly (Figure 2.3(b)), then to *lamellae* ( $3\text{--}20\mu\text{m}$ ), and finally to the collagen-mineral composite ( $60\text{--}600\text{nm}$ ) (Figure 2.3(c)) (Lovell, 1990). The osteon, containing blood vessels and nerves in the centre, forms a cylindrical structure of about  $200\text{--}250\mu\text{m}$  in diameter giving strength to cortical bone. The single *lamella* consists of collagen fibrils ( $1\mu\text{m}$ ) and they are arranged concentrically around the central Haversian canal. The thick and dense arrangement of the structure allows cortical bone to have a much higher resistance to torsional and bending forces. In contrast, cancellous bone is highly porous, consisting of a honeycomb-like network of branching bars, plates and rods, called *trabeculae*, interspersed in the bone marrow compartment (Figure 2.3(a)).

The high surface area provided by the porous *trabeculae* permits the diffusion of nutrients and circulation of growth factors. It has also been demonstrated that cancellous bone is metabolically more active and is quicker in adapting to changes in mechanical loading and unloading than cortical bone (Buckwalter *et al.*, 1996; Rho *et al.*, 1998).

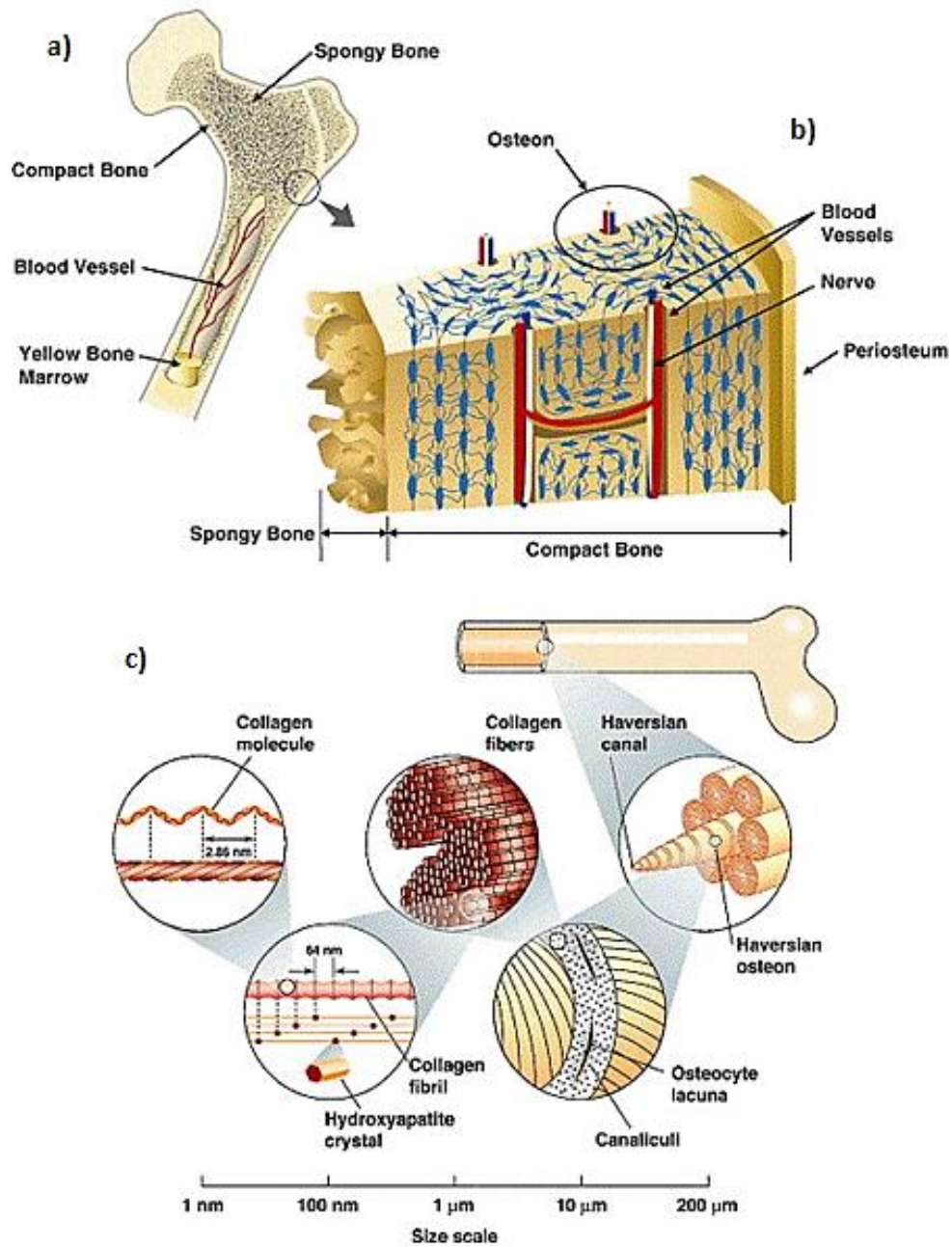


*Figure 2.3: Hierarchical structure of bone, from macrostructure to sub-nanostructure (Nalla et al., 2006).*

In addition, although the elemental composition and the materials are the same for both types of bone (Downey and Siegel, 2006), the microstructure produced by cortical bone is characterised by regular, cylindrically shaped *lamellae*. On the contrary, the microstructure of cancellous bone is composed by irregular, sinuous convolutions of *lamellae*, which allows cancellous bone to have greater resilience and better absorption of loads (Rho *et al.*, 1998).

As result of the hierarchically organised architecture and the diverse orientation of bone components, the mechanical properties of bone tissue at each anatomical level are different, varying according to the loading direction. For these reasons, bone is considered an anisotropic and heterogeneous material.

In particular, for cortical bone the mechanical properties depend mainly on the porosity (5-10%), the mineralisation level and organisation of the solid matrix. For the cancellous bone the mechanical properties are characterised by a wider range, as reported in Table 2.2, and they vary considerably around the periphery, along the length and by a factor of 2-5 from bone to bone (Downey and Siegel, 2006).

The structure-mechanical stresses relationship has been studied since 1982 in terms of Wolff's law, which states that bone and in particular long bones undergo adaptive changes during their growth in response to external mechanical stimuli (Goodship, 1987; Clarke, 2008). Furthermore, considering the heterogeneity of bone structure and the different mechanical functions, several studies (Goldstein, 1987; Kokubo *et al.*, 2003; Currey *et al.*, 2007; Gerhardt and Boccaccini, 2010; Fu *et al.*, 2011) have reported that mechanical properties for both cortical and trabecular bone should be stated in a range of rather single values, as indicated in the Table 2.2.

*Table 2.2: Mechanical properties of human cortical and trabecular bone.*

	<b>Compressive strength (MPa)</b>	<b>Flexural strength (MPa)</b>	<b>Tensile strength (MPa)</b>	<b>Young's Modulus (GPa)</b>	<b>Fracture toughness (MPa m<sup>1/2</sup>)</b>	<b>Porosity (%)</b>	<b>Reference</b>
<b>cortical bone</b>	130-200	135-193	50-151	7-25	2-12	5-10	(Evans, 1961; Reilly <i>et al.</i> , 1974; Hench, 1991; Hall, 1992; Rho <i>et al.</i> , 1995; Hernandez <i>et al.</i> , 2001)
<b>trabecular bone</b>	2-12	10-20	1-5	0.1-5	0.1-0.8	50-90	(Martin; Reilly <i>et al.</i> , 1974; Goldstein, 1987; Hench, 1991; Hall, 1992; Thompson and Hench, 1998; Hernandez <i>et al.</i> , 2001; Currey <i>et al.</i> , 2007)

### 2.3 Bone development, modelling and remodelling

As it was previously stated, bone plays a key role in a series of fundamental processes for the human body, *i.e.* growth factor and cytokine depository, acid-base equilibrium and detoxification. Additionally, given the capability of adapting its mass and morphology to functional needs, the ability of being a mineral reservoir and the capacity of self-repairing, bone tissue has been described as the ultimate “smart” material (Sommerfeldt and Rubin, 2001).

The formation of normal healthy bone takes approximately 4 to 6 months, and occurs by two developmental pathways: intramembranous ossification and endochondral ossification (Marks Jr and Odgren, 2002). Differentiation and proliferation of mesenchymal stem cells into osteoblasts occur during both processes (Heino and Hentunen, 2008). The first one describes the direct transformation of mesenchymal stem cells into osteoblasts and it is responsible for the formation of craniofacial bone, skull and parts of the clavicle and mandible. Endochondral ossification (Greek: *endon*, “within” and *chondros*, “cartilage”) arises mainly in long bones involving cartilage tissue as a precursor. In this complex and multistep process, mesenchymal progenitor cells condense and differentiate into chondrocytes, which are responsible for depositing cartilaginous structures that serve as template for developing bones (Karaplis, 2002).

During life, human bone continually grows in both longitudinal and radial directions, modelling as well as remodelling, through the collaborative action of osteoblasts, osteocytes, and osteoclasts together with growth factors (Clarke, 2008; Seeman, 2009). Modelling is the process through which bone changes its shapes subsequently to physiologic or mechanical stimuli and it occurs at a low rate throughout life (Roberts *et al.*, 2004). During this process, bone resorption and formation are two uncoupled pathways and they happen on distinct surfaces (Clarke, 2008). In contrast remodelling, which is more frequent than modelling in adults (Kobayashi *et al.*, 2003), is the process in which bone resorption precedes bone formation, occurring along specific sites on the same bone surface, in particular at the interface with the hematopoietic bone marrow (Goodship, 1987; Seeman, 2009). This mechanism guarantees tissue turnover while maintaining bone strength and mineral homeostasis in mature skeleton (Hadjidakis and Androulakis, 2006). During the remodelling process old bone is continuously removed and replaced with new bone to prevent microdamage accumulation (Turner, 1998). Furthermore, it is a lifelong process and its frequency varies according to the demands of the body (Kini and Nandeesh, 2012). Bone remodelling starts



with the differentiation of osteoclast precursors into mature multinucleated osteoclasts that are attracted at the remodelling site and then activated for the resorption phase. This stage is followed by a brief reversal phase during which the osteoblasts proliferate and differentiate into mature osteoblasts to repair the resorption defects caused by osteoclasts. Afterwards, during the much slower formation phase, some of the osteoblasts are incorporated into the bone matrix as bone-lining cells or osteocytes. Figure 2.4 summarises the four sequential phases of the overall process: activation, resorption, reversal and formation (Rucci, 2008).

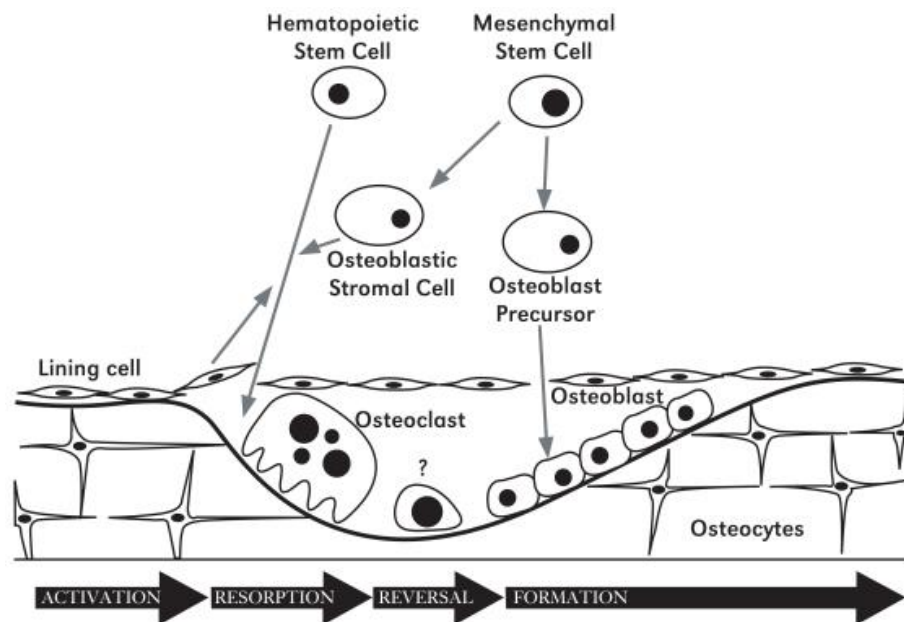


*Figure 2.4: Schematic representation of bone remodelling process (Services., 2004).*

## Chapter 3. State of the art in bone repair and regeneration

---

### 3.1 Clinical need for bone repair and regeneration

Thanks to the intrinsic regenerative capacity of bone (Einhorn, 1998; Dawson *et al.*, 2014), particularly in young people, the majority of bone fractures heal well without scar formation and with no need of further intervention (Gruber *et al.*, 2006; Dimitriou *et al.*, 2011; Dimitriou *et al.*, 2012; Oryan *et al.*, 2015). However, in patients with defects two and half times bigger than the bone radius (commonly called critical size bone defects) (Schroeder and Mosheiff, 2011), and which are caused by trauma, bone tumour resections (Cancedda *et al.*, 2007) or severe non-union fractures (permanent failure of healing following a broken bone), osteoporosis and avascular necrosis, bone regeneration is necessary in a quantity that goes beyond the normal potential for self-repair (Bosch *et al.*, 1998; Horner *et al.*, 2010; Dimitriou *et al.*, 2011).

The incidence of bone diseases such as arthritis, osteoporosis, tumours, trauma and their related symptoms is growing worldwide, and it has been estimated to double by 2020 (Amini *et al.*, 2012) due to a variety of causes, such as the life expectancy increase and the growing needs of baby-boomers. Furthermore, with the increase of the older UK population, of which 23% will be 65 and over by 2035 (Figure 3.1), the obesity rates, and a lifestyle characterised by poor physical activity (Office for National Statistics, 2012), bone tissue replacement and regeneration have become a major clinical demand.

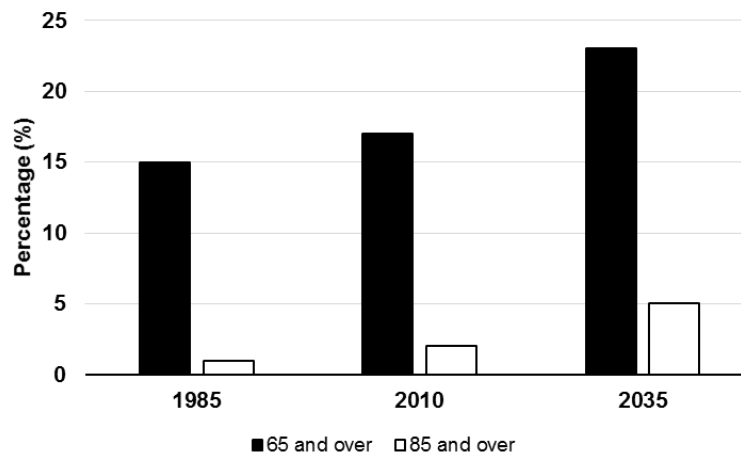


*Figure 3.1: Percentage of older people in the UK over the all population:1985, 2010 and 2035 (Office for National Statistics, 2012).*

Bone is one of the most common transplanted tissues, the second only after blood (Liu *et al.*, 2013; Oryan *et al.*, 2014). According to a new report from research and consulting firm GlobalData, the global bone grafts and substitutes (BGS) market value will increase progressively over the coming years, going from almost \$2.1 billion in 2013 to approximately \$2.7 billion by 2020, at a Compound Annual Growth Rate (CAGR) of 3.8%.

Traditional treatments for large bone defects are based on transplant of a) *autologous* bone (from the same patient), b) *allogeneic* bone (from a human cadaver), and c) *xenogeneic* bone (from an animal) (Petite *et al.*, 2000; Rose and Oreffo, 2002). Based on the use of autologous tissue, autograft procedures are considered the ‘gold-standard’ in bone grafting, showing osteogenic, osteoinductive (the process by which osteogenesis is induced) and osteoconductive (the process by which bone growth is permitted on a material’s surface) properties with the best clinical outcomes (Albrektsson and Johansson, 2001; De Long *et al.*, 2007; Brydone *et al.*, 2010). Nevertheless, their use in medical practice is limited due to their short supply and to the high percentage of donor site morbidity (Younger and Chapman, 1989). The use of allografts or xenografts could be an alternative for their high availability and low cost. However, these approaches present also risks, like infection transmission and adverse host immune response, resulting in poor outcomes (Galea *et al.*, 1998; Burg *et al.*, 2000; Mankin *et al.*, 2005; Khan *et al.*, 2008). The limitations of current treatments together with the impact on healthcare system costs encouraged interest in alternative therapeutic solutions (De Long *et al.*, 2007; Oryan *et al.*, 2014).

From a biological perspective, cells, growth factors, extracellular matrix along with cell-matrix interactions are crucial for the *in vivo* process of bone repair (Kanczler and Oreffo, 2008). However, when a critical size bone defect develops, the cells cannot migrate from one side to the other, requiring for this purpose a solid support (commonly known as scaffold) on which they can anchor and build new bone (Schroeder and Mosheiff, 2011). Scaffolds, cells, and signalling molecules are defined as basic pillars of bone tissue engineering (BTE) (Amini *et al.*, 2012). The term “tissue engineering” was introduced in the late 1980s (Nerem, 2006), although effective awareness of the concept started a decade later with the publication of a paper by Langer and Vacanti (Langer and Vacanti, 1993). They stated what is now recognised as the definition of TE: “an interdisciplinary field that applies the principles of engineering and the life sciences toward the development of biological substitutes that restore, maintain, or improve tissue functions or a whole organ” (Vacanti and Vacanti, 2013).

### 3.2 3D porous substitutes for bone restoration

3D porous constructs act as biological and mechanical support, which once implanted into the bone defect should induce and direct the growth of new tissue and restore its function (Dvir *et al.*, 2011).

Due to the complex internal and external structure, but also composition of human bone tissue, scaffolds for bone tissue repair and regeneration are governed by many interdependent and also conflicting essential prerequisites (Chen *et al.*, 2008). Currently, as many scaffold-based approaches are still experimental, there are no specific design criteria that define the properties of the so-called “ideal scaffold” for bone repair (Fu *et al.*, 2011). In 2004 Hutmacher stated: “It could be argued that there is no ‘ideal scaffold’ design *per se*, instead each tissue requires a specific matrix design with defined material properties” (Hutmacher *et al.*, 2004). The choice of appropriate materials, which is of crucial importance for scaffold-based solutions, will be investigated later in this chapter.

Besides chemistry and material selection, it is also widely stated that a scaffold intended for orthopaedic applications, should mimic the morphology, structure and function of bone tissue (Hutmacher, 2000; Hollister *et al.*, 2002; Salgado *et al.*, 2004), enhancing cell adhesion, proliferation and differentiation (Hutmacher, 2001; Stevens, 2008). According to the recent literature, a set of desirable requirements for tissue engineered scaffolds is summarised in the Table 3.1.

**Table 3.1: Desirable requirements for the design of bone tissue engineered scaffolds.**

<b>Requirement</b>	<b>Function</b>
Biocompatibility	Ability to perform its function without exhibiting any immune response in the host tissue (Hutmacher, 2000; Hutmacher, 2001)
Biodegradability	Tailoring rate of degradation according to the growth rate of the host tissue (Reis and Román, 2004)
Mechanical properties	The mechanical strength of the scaffold, which is given by the intrinsic properties of the biomaterial together with the porous architecture itself, should match the strength of natural bone even during the degradation and remodelling processes (Yang <i>et al.</i> , 2001; Wagoner Johnson and Herschler, 2011)
Porosity and pore size	The scaffold should have an interconnected porous structure that can allow fluid flow, cell migration, bone ingrowth and vascularization (Liu <i>et al.</i> , 2013). Pore dimensions in the range of 200 to 350 $\mu\text{m}$ have been found to be ideal for bone tissue in-growth (Bose <i>et al.</i> , 2012); if the pores are too small, pore occlusion by cell migration can happen (Salgado <i>et al.</i> , 2004). Furthermore, while macroporosity (pore size $> 50 \mu\text{m}$ ) plays an important role for osteogenic outcomes, an adequate microporosity (pore size $< 10 \mu\text{m}$ ) is essential in order to allow capillary ingrowth. Porosity and interconnectivity together are also essential for an accurate diffusion of nutrients and for the removal of metabolic waste (Karageorgiou and Kaplan, 2005). Additionally, the degree of porosity influences the scaffold mechanical stability, therefore its value should be in the range of strength and stiffness of the host tissue (Hutmacher, 2000; Karageorgiou and Kaplan, 2005; Loh and Choong, 2013).
Surface properties	Appropriate surface chemistry is required to promote cell attachment, differentiation and proliferation activities (Hsin and Yiwei, 2011; Mitra <i>et al.</i> , 2013)
Osteoinductivity	The scaffold should be able to induce new bone formation (osteogenesis) through molecular signalling and the recruitment of osteoprogenitor cells (Albrektsson and Johansson, 2001).
Osteoconductivity	Scaffold composition should let bone cells to adhere, proliferate and form extracellular matrix on its surface and into the pores (Albrektsson and Johansson, 2001).
Processing	The fabrication process should not affect the material properties and subsequent clinical use of the scaffold (Leong <i>et al.</i> , 2003).
Commercialisation	The processing conditions should be suitable for scaffold commercialisation at reasonable costs (Thavornnyutikarn <i>et al.</i> , 2014).

### 3.3 Biomaterials for bone tissue repair

Several materials with different compositions and microstructures have been adopted or synthesised, and subsequently processed as 3D constructs for bone tissue repair and regeneration (Bose *et al.*, 2012).

The extracellular matrix of bone is a composite of biological materials, mainly based on ceramics (*i.e.* hydroxyapatite), biological polymers (*i.e.* collagen matrix) and water. Therefore, synthetic and/or naturally occurring ceramics, polymers and their composites are the materials mainly investigated for the fabrication of bone-like substitutes (Rezwan *et al.*, 2006; Raucci *et al.*, 2012).

The next paragraphs will provide a review of the current state of art on biomaterials for bone repair, where basic and advanced characteristics will be discussed, focusing primarily on bioceramic class materials.

#### 3.3.1 Natural and synthetic polymers

Biological polymers, such as hyaluronic acid, collagen, fibrin and chitosan have seen an increasing use as promising candidates for bone repair applications (Griffith, 2000; Hutmacher, 2000; Seal *et al.*, 2001; Dalton *et al.*, 2009). They are usually biocompatible and enzymatically biodegradable materials. The main advantage from their use is the support of cell attachment, proliferation, and differentiation through the use of biofunctional molecules (Narayan, 2009). Furthermore, they have the potential to interact biologically with the host tissue, and have low immunogenic properties (Salgado *et al.*, 2004). However, depending upon the application, the rate of the previously mentioned enzymatic degradation may not be easily controlled. Therefore, it may be difficult to determine the lifespan of natural polymers *in vivo*.

Flexibility in processing, the ability to tailor their chemistry and their biodegradation rate are additional advantages of synthetic polymers (Planell *et al.*, 2009; Bose *et al.*, 2012). The most common biodegradable synthetic polymers used for 3D structures are: saturated poly- $\alpha$ -hydroxy esters, including poly(lactic acid) (PLA) and their forms (L-PLA (PLLA), D-PLA (PDLA), and mixture of D,L-PLA (PDLLA)), poly(glycolic acid) (PGA) as well as poly(lactic-co glycolide) (PLGA) copolymers (Mano *et al.*, 2004; Gentile *et al.*, 2014).

The degradation products of certain polymers (PLA, PGA) are usually removed by the natural physiological pathways. However, they may create a local acidic environment with the consequent

adverse host tissue response (Chen *et al.*, 2012). Additionally, the adoption of polymeric materials, mainly natural polymers, for bone repair and regeneration is challenging, especially for their limited abilities in achieving strong bonding with bone, and in some circumstances unsuitable mechanical properties.

In particular, for the regeneration of load-bearing bones, these polymers exhibit low elastic moduli (Griffith, 2000; Seal *et al.*, 2001), and are prone to a deformation mechanism known as creep (Lichte *et al.*, 2011). Hence, to overcome the above mentioned drawbacks, proposed strategies are: to *i*) reinforce polymers with other materials (*i.e.* bioceramics or metals) and use them as composites (section 3.3.2) or *ii*) to use ceramics themselves as unique component (section 3.3.3).

### **3.3.2 Composites**

Composites materials are those that combine two or more different materials in order to obtain better resultant outcomes, mimicking the composite structure of natural bone tissue (Davis and Leach, 2008). To improve specific properties such as fracture toughness, bioactivity and biocompatibility, at least two phases are combined together: the matrix and the dispersed phase (Wang, 2003). The matrix has the main function of filling the volume and transfer the stress to the dispersed phase, instead this last one, which is harder and stiffer, is responsible for enhancing one or more properties of the final composite (Dorozhkin, 2011).

Composite materials generally can be particle-reinforced, fibre reinforced and structural composites. Specifically for bone tissue repair, composite materials are commonly made of polymers that are used as a matrix, and then are combined with a ceramic phase (inorganic component) in order to obtain biomaterials with improved mechanical and bioactive properties (Dhandayuthapani *et al.*, 2011) and enhanced degradation profiles (Gloria *et al.*, 2010). Example of composite structures developed for load bearing segmental bone defects are reported in the Table 3.2.

**Table 3.2: In vivo pre-clinical studies of load-bearing bone defects using composite scaffolds (adapted from (Pilia *et al.*, 2013)).**

Ceramic phase	Polymeric phase	Defect area and size	Length of the study	Reference
TTCP and DCPA	PLGA	Wistar rat femur (2.3 mm)	2 weeks	(Lickorish <i>et al.</i> , 2007)
BCaP	Collagen	New Zeland white rabbit femur (20 mm)	18 weeks	(Jegoux <i>et al.</i> , 2008)
TCP	PCL	CGH/Rnu rat femur (8 mm)	3 weeks	(Rai <i>et al.</i> , 2010)
$\beta$ -TCP	PGA	Sprague-Dawley rat femur (3 mm)	12 weeks	(Cao and Kuboyama, 2010)
HA	HT-PPFhm	Rabbit femur (4 mm)	48 weeks	(Jayabalan <i>et al.</i> , 2010)
Bioglass	Collagen-phosphatidylserine	Sprague-Dawley rat femur (3.5 mm)	6 weeks	(Xu <i>et al.</i> , 2011)

### 3.3.3 Bioceramics

Referring to the definition of Hench, “bioceramics are those ceramics used for the repair and reconstruction of diseased or damaged parts of the musculoskeletal system” (Hench, 1991). More recently the definition of bioceramics have been extended to “a large class of specially designed ceramics for the repair and reconstruction of diseased or damaged parts of the body” (Baino *et al.*, 2015).

Bioceramics, such as hydroxyapatite, calcium phosphates and bioactive glasses are the most investigated biomaterials for orthopaedic and maxillofacial applications, as demonstrated by the considerable amount of literature that has been published in this specific field (Figure 3.2).

The growing interest in the use of these materials is due to their versatile properties, which can be tailored according to their composition, and their ability to form a direct physical bond to bone *via* the formation of an apatite layer on the surface of the implant (Hench, 1998c; Ducheyne and Qiu, 1999; Kokubo *et al.*, 2003).



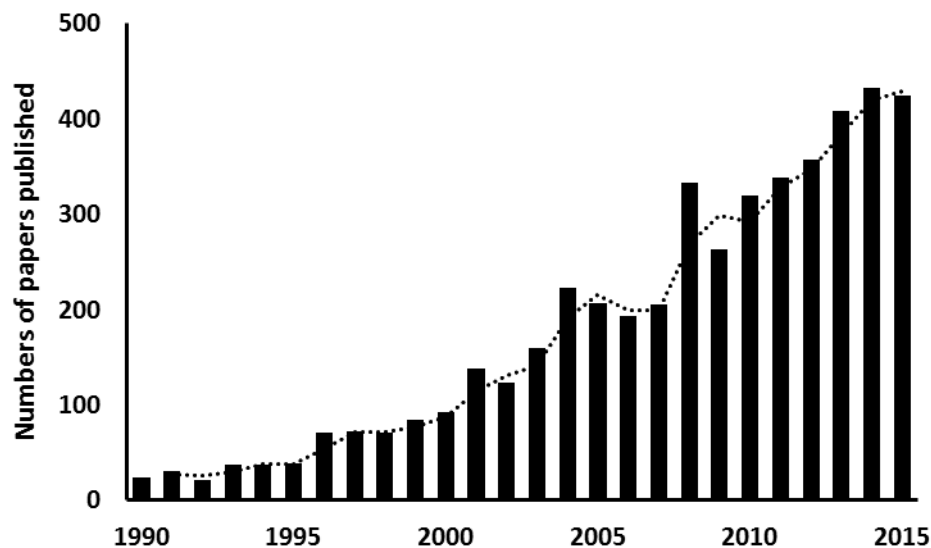


**Figure 3.2: Literature published between 1990 and 2015 in the area of bioceramics (Source: Scopus).**

Generally, the term bioceramic is used to cover a broad class of biomaterials, specifically: bioactive glasses such as Bioglass<sup>®</sup>, glass-ceramics such as AW, and ceramics such as synthetic HA (Hench, 1999). Traditionally, bioceramics have been used very successfully within the human body for a wide range of applications as shown in Figure 3.3. Specifically, orthopaedics and dentistry are the favourite areas. Classic applications involve bone fillers and dental implants in form of dense or porous substitute, injectable cement pastes and prosthesis surface coating (Hench, 1991; Hench, 1998a; Hench, 1998b).

Currently, this class of biomaterials are proposed for a broader range of clinical applications that goes beyond bone tissue engineering field (*i.e.* otoryngological implants and keratoprotheses). Miguez-Pacheco *et al.*, reviewed the use of bioactive glasses for soft tissue repair, finding eight different novel applications, from cardiac tissue and nerve regeneration to laryngeal and lung tissue repair (Miguez-Pacheco *et al.*, 2015). Ocular surgery is another clinical field where bioceramics are playing an important role (Baino and Vitale-Brovarone, 2015).

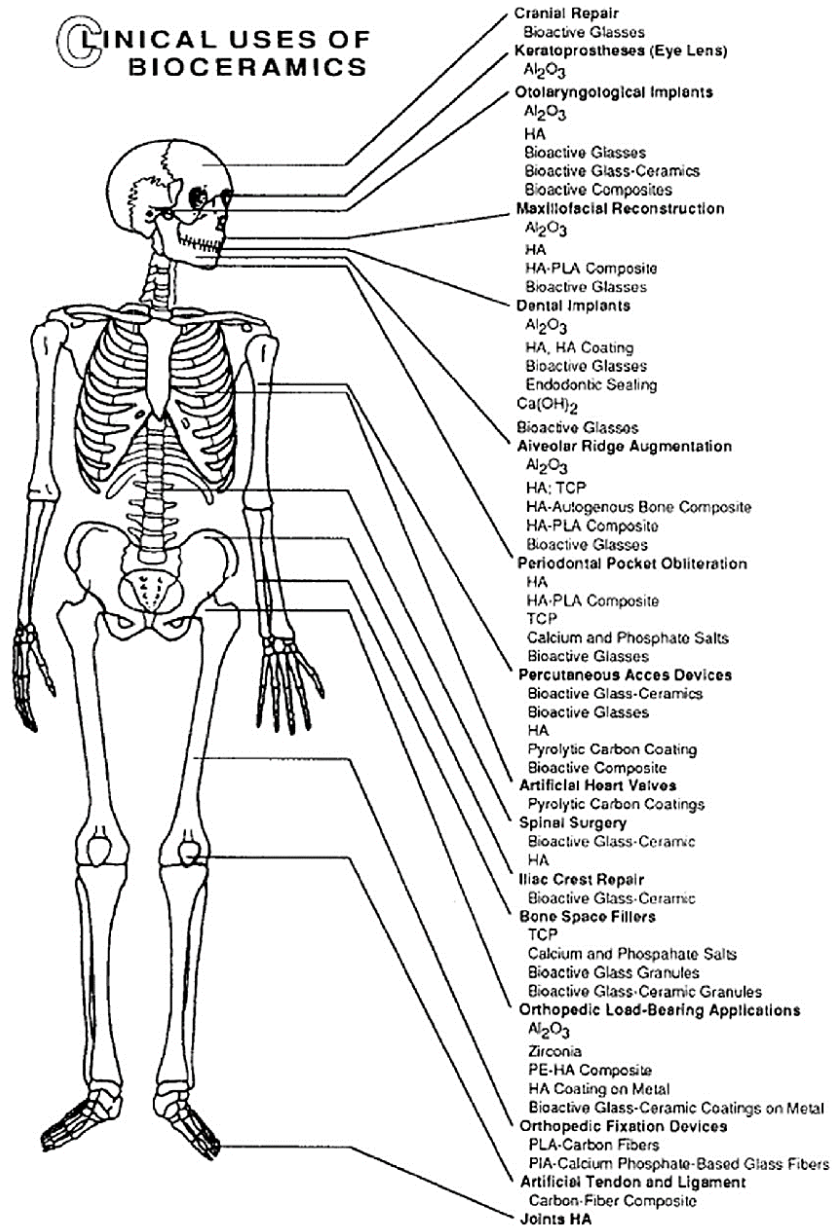


*Figure 3.3: Clinical use of bioceramic materials (Hench and Wilson, 1993).*

According to their biological behaviour and the interaction with the host tissue, bioceramics may be effectively *bioinert* (alumina, zirconia), *bioactive* (Bioglass® and AW), and *bioresorbable* (TCP) (Hench, 1998b; Bairo *et al.*, 2015).

For the purpose of medical devices, the term bioinert refers to a material that, once implanted in the host tissue, induces a minimal level of adverse response in the surrounding physiological environment (Best *et al.*, 2008).

In a general sense a bioactive material has been defined as a material able to induce a specific biological activity (Williams, 2009). In 1990, Kokubo described the capacity of a material to develop an HA-like layer on its surface, when immersed in a simulated body fluid (SBF) solution, as indication of its bioactivity (Kokubo *et al.*, 1990). More precisely, for the case of bone tissue, a bioactive material is a material that, when in a biological environment, forms a carbonated hydroxyapatite surface layer, leading to a strong bone-tissue bonding and eventually promoting the natural bone regeneration (Kokubo and Takadama, 2006; Erol-Taygun *et al.*, 2013).

Bioresorbable materials degrade over time and are intended to be replaced by the natural host tissue (Stevens, 2008). The optimal material should adapt its degradation kinetic to the living tissue formation process, which usually is slower, and then be resorbed (Chen *et al.*, 2012). This aspect sometimes is a challenge during the design process, although recent works have shown the possibility to tailor the degradation rate of bioceramics by manipulating their formulation, making them an emerging research field within the medical device industry (Huang *et al.*, 2006; Yao *et al.*, 2007; Fu *et al.*, 2010a).

### **3.3.3.1 Calcium phosphates**

Due to the similarity with the mineral component of human bone, calcium phosphate ceramics have been extensively used as biomaterials for the repair and regeneration of bone tissue for the last 30 years (Barrère *et al.*, 2006).

There are different forms of CaP ceramics available in nature, the most commonly investigated in the field of BTE are: HA,  $\beta$ -tricalcium phosphate ( $\beta$ -TCP) and biphasic calcium phosphate (BCP) (Best *et al.*, 2008; Dorozhkin, 2010; Samavedi *et al.*, 2013). A detailed list of CaP compounds, their abbreviations, the chemical formula, and Ca/P molar ratio are reported in Table 3.3.

**Table 3.3: CaP-compounds with corresponding abbreviation, chemical formula and Ca/P molar ratio (re-adapted from (Dorozhkin, 2010)).**

Compound	Abbreviation	Chemical formula	Ca/P ratio
Monocalcium phosphate monohydrate	MCPM	$\text{Ca}(\text{H}_2\text{PO}_4)_2 \cdot \text{H}_2\text{O}$	0.5
Monocalcium phosphate anhydrous	MCPA or MCP	$\text{Ca}(\text{H}_2\text{PO}_4)_2$	0.5
Dicalcium phosphate dihydrate	DCPD	$\text{CaHPO}_4 \cdot 2\text{H}_2\text{O}$	1.0
Dicalcium phosphate anhydrous	DCPA or DCP	$\text{CaHPO}_4$	1.0
Octacalcium phosphate	OCP	$\text{Ca}_8(\text{HPO}_4)_2(\text{PO}_4)_4 \cdot 5\text{H}_2\text{O}$	1.33
$\alpha$ -Tricalcium phosphate	$\alpha$ -TCP	$\alpha\text{-Ca}_3(\text{PO}_4)_2$	1.5
$\beta$ -Tricalcium phosphate	$\beta$ -TCP	$\beta\text{-Ca}_3(\text{PO}_4)_2$	1.5
Amorphous calcium phosphates	ACP	$\text{Ca}_x\text{H}_y(\text{PO}_4)_z \cdot n\text{H}_2\text{O}$ , $n = 3 - 4.5$	1.2 – 2.2
Calcium-deficient hydroxyapatite	CDHA	$\text{Ca}_{10-x}(\text{HPO}_4)_x(\text{PO}_4)_{6-x}(\text{OH})_{2-x}$ ( $0 < x < 1$ )	1.5 – 1.67
Hydroxyapatite	HA or HAp	$\text{Ca}_{10}(\text{PO}_4)_6(\text{OH})_2$	1.67
Fluorapatite	FA or FAp	$\text{Ca}_{10}(\text{PO}_4)_6\text{F}_2$	1.67
Oxyapatite	OA or OAp	$\text{Ca}_{10}(\text{PO}_4)_6\text{O}$	1.67
Tetracalcium phosphate	TTCP	$\text{Ca}_4(\text{PO}_4)_2\text{O}$	2

HA is the most widely used CaP because it shares chemical similarities to inorganic component of bone tissue (Yoshikawa and Myoui, 2005). Although it is not highly soluble, it supports nucleating sites for the precipitation of apatite crystals in culture medium (Bohner and Lemaitre, 2009).

TCP is a biodegradable bioceramic with a Ca/P molar ratio of 1.5. It exists in two different phases, which are  $\alpha$  and  $\beta$ . Both phases are less stable than HA and therefore more soluble in aqueous environments. Despite their similarities in chemical composition,  $\alpha$ -TCP is more soluble than  $\beta$ -TCP, but from a clinical perspective  $\beta$ -TCP is considered to be osteoconductive and osteoinductive, and hence more widely used in bone regeneration than  $\alpha$ -TCP (Barrère *et al.*, 2006; Samavedi *et al.*, 2013). As previously stated, depending on the situation, it might be necessary for an implant to

resorb slowly before being replaced by the host tissue. For this reason, a combination of HA and TCP has been investigated, in which the higher TCP/HA ratio leads to a higher dissolution rate (Best *et al.*, 2008; Dorozhkin, 2010). CaP ceramics represent a class of tuneable biomaterials with exclusive properties, they are used in different areas of the human skeleton (*e.g.* treatment of bone defects, maxillofacial applications, spinal fusion and bone augmentation). However, how calcium phosphate properties help osteoinductivity/osteoconductivity are still unanswered questions (Samavedi *et al.*, 2013), and for this reason they are a class of materials still actively being researched (Jarcho, 1981; Matsumine *et al.*, 2004; Saikia *et al.*, 2008; Sun and Yang, 2015; Wang *et al.*, 2015).

### 3.3.3.2 *Apatite – wollastonite*

In the early 1970s Hench was developing the Bioglass<sup>®</sup> composition at University of Florida. Around the same time in Japan Kokubo *et al.* were the first to develop a new bioceramic material, known as apatite-wollastonite (AW) glass-ceramic (Kokubo *et al.*, 1982; Magallanes-Perdomo *et al.*, 2011). AW is a formulation composed by small apatite particles and reinforced by wollastonite crystalline phases in a glassy matrix (Best *et al.*, 2008). The nominal composition (wt%) comprises MgO (4.6%), CaO (44.7%), SiO<sub>2</sub> (34%), P<sub>2</sub>O<sub>5</sub> (16.2%) and CaF<sub>2</sub> (0.5%) (Kokubo, 2008).

This bioceramic possesses the highest mechanical properties in comparison to other bioactive glasses and glass-ceramics, because of wollastonite and apatite crystals' presence. Furthermore, its exceptional ability to form strong chemical bonds with bone tissue has been widely demonstrated (Kokubo and Takadama, 2006; Kokubo, 2008; Park and Ozturk, 2013).

AW has been adopted for a broad range of medical applications, either in a powder form as bone filler, as porous structures or as a bulk material (Kokubo, 1999; Kokubo *et al.*, 2003) and showed excellent biocompatibility *in vitro* and *in vivo* (Ohsawa *et al.*, 2004; Dyson *et al.*, 2007; Lee *et al.*, 2015).

With regard to the mechanical properties of this material, Table 3.4 demonstrates that dense AW has considerably higher compressive as well as bending strength than human cortical bone.

**Table 3.4: Mechanical properties of natural bone and AW glass-ceramic (Kokubo, 2008).**

	Natural bone	AW glass-ceramic
Bending strength (MPa)	30-190	200-220
Compressive strength (MPa)	90-230	1000
Elastic modulus (GPa)	3.8-17	120

### **3.3.4 Bioactive glasses**

Over the last four decades bioactive glasses for orthopaedic and maxillofacial applications have attracted the interest of many researchers, playing an important role for bone tissue repair and regeneration, thanks to their outstanding osteoconductive and osteoinductive properties, as well as bioactivity and customable degradation rate (Hench, 1999; Rahaman *et al.*, 2011; Jones, 2013).

Bioactive glasses represent the subset of biomaterials designed mainly for hard and soft bone tissue repair and regeneration (Rahaman *et al.*, 2011; Jones and Clare, 2012; Jones, 2013). So far different methods have been adopted to process them, predominantly as 3D porous structures, and several new strategies have been proposed to manipulate their compositions, and the parameters that affect their performance in biomedical applications (*i.e.* chemistry, microstructure, thermal behaviour, fabrication method, porosity, mechanical properties) (Lee *et al.*, 2013; Bretcanu *et al.*, 2014; Rahaman *et al.*, 2014; Brauer, 2015; Miguez-Pacheco *et al.*, 2015).

As far as the glass production method is concerned, bioactive glasses are generally prepared *via* sol-gel or melting-quenching process. The sol-gel route consists in the formation of a gel from a solution containing the compositional precursors. Through a reaction at room temperature, nanoparticles are assembled together to obtain a wet inorganic network, forming a gel, which is subsequently dried and heated to form a glass (Hench and West, 1990). In the melt-derived route, which is the production method selected for this study, the precursors are homogenised, and then melted in a platinum crucible at high temperatures typically in the range 1200 - 1500 °C. Afterwards, the molten glass is poured into moulds in order to obtain solid blocks or is quenched in cold water or oil to obtain glass “frits”, ready to be further processed (O'Donnell, 2012). If the cooling process is sufficiently quick, no crystallisation will occur and the result will be an

amorphous structure, known as *glass*; otherwise a *glass-ceramic*, with a combination of a crystalline phase and a residual glassy phase will form (Figure 3.4) (Tilley, 2013).

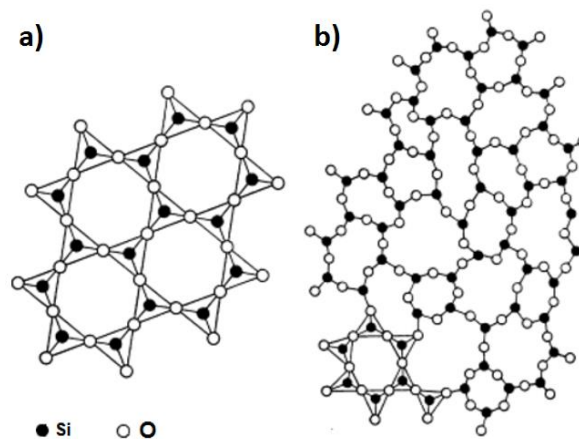


**Figure 3.4: Structure of: a) crystalline silica and b) amorphous silica (Vogel, 2013).**

Whether the resulting material will be a glass or a glass-ceramic, three different components are generally associated to their structure:

- i) the network formers, which are the basic and stand-alone pillars of the structure, and include silicon dioxide ( $\text{SiO}_2$ ), phosphorous pentoxide ( $\text{P}_2\text{O}_5$ ) and boron trioxide ( $\text{B}_2\text{O}_3$ ). These oxides represent the building unit of silicate, phosphate and borate-based glasses respectively;
- ii) the network modifiers, which are usually oxides of alkali or alkaline-earth metals that break-up the glass network, and modify the glass structure, as the name suggest, (*i.e.* sodium, calcium and strontium);
- iii) the intermediate oxides, which can help the glass formers or modifiers during the process (*i.e.* aluminium and iron), but they do not form glasses by themselves (Vogel, 2013).

### 3.3.4.1 Silicate-based glasses

Silicate-based glasses are by far the most common and most widely investigated bioactive glasses for orthopaedic applications. They are based on the 3D glass-forming  $\text{SiO}_2$  network in which Si is fourfold coordinate to O, as shown in Figure 3.5 (Rahaman *et al.*, 2011).

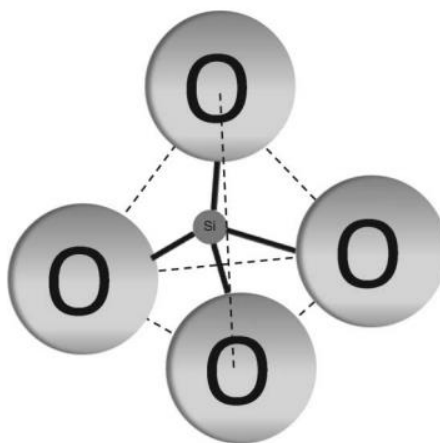


*Figure 3.5: Schematic representation of silica tetrahedron (Jones and Clare, 2012).*

Furthermore, these materials present an open structure that allows the arrangement of alkali and alkali-earth cations ( $\text{Na}^+$ ,  $\text{K}^+$ ,  $\text{Ca}^{2+}$ , etc.), which cause the breaking of the Si–O–Si bonds and the formation of non-bridging oxygen groups as network modifiers (Scholze, 2012).

The concentration of non-bridging groups is one of the crucial stage during the bioactive process, since, as described by Hench, they are responsible of the dissolution of silica and the consequent formation of silanol groups at the glass surface, which are considered the nucleation centres of the apatite formation (Kokubo, 1990; Hench and Wilson, 1993). At this stage a silica-rich layer ( $\sim 1\text{--}2\mu\text{m}$  thickness) is formed on the surface of the glass, followed by the nucleation of an amorphous calcium phosphate (ACP) layer, which incorporates  $(\text{OH})^-$  and  $(\text{CO}_3)^{2-}$  from the solution and finally crystallise as an HCA layer (Hench, 1991).

The most widely investigated bioglass for biomedical applications, with a composition in the  $\text{Na}_2\text{O-CaO-SiO}_2\text{-P}_2\text{O}_5$  system, belongs to the silicate-based glass group. It was synthesised by Hench *et al.* in the 1970s, designated as bioglass 45S5, and it is now commercially known as Bioglass<sup>®</sup> (Hench, 1998b).

Bioglass<sup>®</sup> has been extensively studied because of its ability of forming an HCA layer on the glass surface (known as bioactivity) when in contact with body fluids, through the mechanism that will



be detailed described in paragraph 3.3.5. The bioactive behaviour of Bioglass<sup>®</sup> is accomplished by:

- i) the low amount of SiO<sub>2</sub> (less than 60mol%), if compared to more chemically stable silicate glasses;

- ii) the high content of NaO<sub>2</sub> and CaO;

- and iii) the high CaO/P<sub>2</sub>O<sub>5</sub> ratio (wt%) (Hench, 1998b).

The development of this glass revolutionised the definition of biomaterial, moving the perspective from inert to a material that, interacting with the human body, is capable to elicit a specific biological response (Hench *et al.*, 1971). Additionally, the osteoconductive as well as the osteoinductive behaviour of 45S5 bioglass has long been established, as it does not only support the regeneration at bone-implant interface, but also far away from that region (Kaur *et al.*, 2013).

Furthermore, 45S5 bioglass<sup>®</sup> has been used in clinical practice since 1985 in the form of particulate for dental applications (Perioglas<sup>®</sup>, Novabone, USA), and afterwards as dense material or in form of granules for bone defect filling (Baino and Vitale-Brovarone, 2011).

However, although Bioglass<sup>®</sup> was demonstrated to be an excellent material, considered for long time the gold standard for bone tissue regeneration, it suffers from several drawbacks. Specifically, the difficulties are related to the material processing in form of 3D porous scaffolds, due to the limited ability of this glass in sintering. This aspect arises because 45S5 bioglass<sup>®</sup> tends to crystallise above 1000 °C, leading to poor densification of the structure with the consequent weaker and less interconnected structure, accompanied by the formation of micro-cracks and poor mechanical strength (Gerhardt and Boccaccini, 2010). Furthermore, the 45S5<sup>®</sup> glass devitrifies during the sintering process, which has the effect of reducing the rate of HA precipitation. (Brink, 1997; Chen *et al.*, 2006; Yao *et al.*, 2007). Additionally, other weaknesses in the use of Bioglass<sup>®</sup> include: its slow degradation kinetic with the consequent difficulties to match the formation rate of new tissue, and the abrupt pH variations of the biological microenvironment, due to the increase in the concentration of ions such as Na<sup>+</sup> and Ca<sup>2+</sup>, especially in the short term when the degradation is faster (Huang *et al.*, 2006; Rahaman *et al.*, 2011; Fu *et al.*, 2012).

Two decades after Bioglass<sup>®</sup> discovery, a new silicate-based glass was developed to overcome its processing limitations. The new composition, termed 13-93 glass, is based on the 45S5 Bioglass<sup>®</sup> composition, but has higher silica content (53wt%) and K<sub>2</sub>O and MgO as additional network modifiers (see Table 3.5 for the detailed composition). This glass showed an enhanced viscous

flow behaviour, less tendency to crystallize, and in the form of porous scaffold it exhibited porosity content and mechanical properties comparable to those of cancellous bone (Brink, 1997; Fu *et al.*, 2007).

The bioactive behaviour of the 13-93 glass was demonstrated by the formation of an HA layer on the surface of 13-93-derived scaffold surface, in less than 7 days of immersion in SBF, indicating its potential of bonding to bone (Fu *et al.*, 2007). Furthermore, *in vivo* studies demonstrated the ability of the 13-93 formulation in supporting tissue ingrowth (Fu *et al.*, 2010b). As XRD investigations confirmed, this glass remained amorphous even after the sintering treatment (Fu *et al.*, 2007). Table 3.5 reports the composition of some silicate bioactive glasses mainly investigated in the literature.

**Table 3.5: Composition of various silicate glasses developed over the years (Silver *et al.*, 2001; Rahaman *et al.*, 2011; Jones, 2013).**

Composition (wt%)	45S5	13-93	58S	70S30C	77S	13-93B1
SiO <sub>2</sub>	45	53	58.2	71.4	80	34.4
K <sub>2</sub> O	0	12	0	0	0	11.7
Na <sub>2</sub> O	24.5	6	0	0	0	5.8
MgO	0	5	0	0	0	4.9
P <sub>2</sub> O <sub>5</sub>	6	4	9.2	0	4	3.8
B <sub>2</sub> O <sub>3</sub>	0	0	0	0	0	19.9
CaO	24.5	20	32.6	28.6	16	19.5

Worldwide many researchers have used the SiO<sub>2</sub>-Na<sub>2</sub>O-CaO-P<sub>2</sub>O<sub>5</sub> system and particularly its ancestor (the 45S5 bioactive glass), as template materials to develop new silica-based formulations (Krishnan and Lakshmi, 2013). Nevertheless, the possibility to tailor the glass properties, altering the main formulation by using different oxides, is currently an open challenge for the design of more complex compositional systems (Jones, 2013).

### 3.3.4.2 Borate-based glasses

Recent studies have shown the possibility to control the degradation rate of bioactive glasses by tailoring their composition (Deliormanli, 2013). Specifically, by partially or totally replacing the  $\text{SiO}_2$  in 45S5 and 13-93 with  $\text{B}_2\text{O}_3$ , the glass degradation rate can cover a wider range, and in this way the bone regeneration can be easily attained (Huang *et al.*, 2006; Yao *et al.*, 2007). In 1990 Brink *et al.* proposed the first borosilicate glass for biomedical applications, in which various proportions of  $\text{B}_2\text{O}_3$  were used (Brink, 1997). Borate-based glasses are very reactive materials with low chemical durability; hence, they degrade faster and convert more completely to HA than silicate-based, such as 45S5 and 13-93 glass (Huang *et al.*, 2006).

In a study conducted by Huang *et al.*, the gradual replacement of  $\text{SiO}_2$  with  $\text{B}_2\text{O}_3$  in the parental glass resulted in a substantial increase of HA conversion in diluted phosphate solutions. Furthermore, unlike silicate glasses, borate-based materials form an HCA layer directly on the surface of the underlying unreacted glass, without the formation of a borate-rich layer as intermediate stage (schematically shown in Figure 3.6) (Huang *et al.*, 2006).

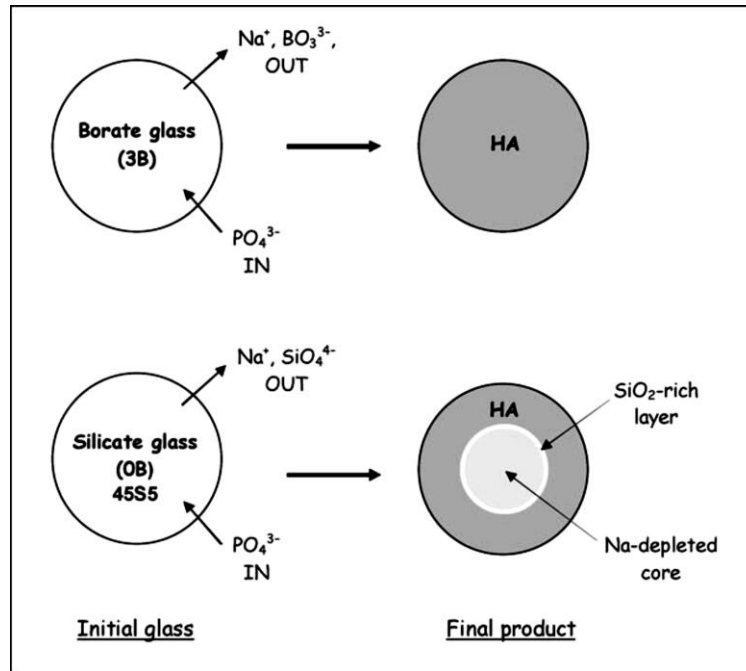


**Figure 3.6:** Schematic representation of the conversion mechanisms of a borate (3B) and 45S5 silicate (0B) glass to HA in a diluted phosphate solution (Huang *et al.*, 2006).

According to the amount of silica replaced, the bioactive process and thus the conversion rate to HA of the resulting B<sub>2</sub>O<sub>3</sub> composition can be controlled within a wide range (from hours to months) (Baino and Vitale-Brovarone, 2011). Moreover, from a material processing perspective, some borate-containing glasses exhibited a more controllable sintering behaviour than Bioglass<sup>®</sup>, becoming very promising candidates for scaffold production (Liang *et al.*, 2008).

The first borate-based scaffolds were produced in 2005 by soft pressing of the glass powders (Rahaman *et al.*, 2005). More recently Fu *et al.* used the polymer foam replication method to successfully produce 13-93B2 (22mol% CaO, 6mol% Na<sub>2</sub>O, 8mol% MgO, 8mol% K<sub>2</sub>O, 18mol% SiO<sub>2</sub>, 36mol% B<sub>2</sub>O<sub>3</sub>, and 2mol%P<sub>2</sub>O<sub>5</sub>) 3D porous borate-derived scaffolds, which showed a microstructure and mechanical properties similar to trabecular bone (see Figure 3.7) (Fu *et al.*, 2009). However, Liu *et al.* demonstrated that the degradation process significantly influenced the mechanical properties of 13-93B2 scaffolds. In fact, after 15 days of immersion in phosphate solution, the scaffold mechanical strength decreased from 6.2 to 2.8MPa (Liu *et al.*, 2009; Xin *et al.*, 2010).

B<sub>2</sub>O<sub>3</sub>-based compositions support cell proliferation *in vitro* and enhance tissue formation *in vivo*. However, the leaching out phenomena of certain level of boron (> 0.65mM) from the glass exhibited a toxic effect during static *in vitro* cell culture (Fu *et al.*, 2009). This cytotoxic effect was not observed *in vivo*, where borate bioactive glasses regenerated tissue as effectively as silicate-based glasses (Jung *et al.*, 2013), and they also produced a level of boron in the blood much lower than the toxic threshold (Liu *et al.*, 2010). The main reason of this different behaviour was ascribed to the fact that during the *in vivo* study, being a fully dynamic system, the fluids were continuously replaced and the pH values were closer to the environment (Jones and Clare, 2012).

Conclusively, *i*) the easier processing route, with respect to silicate-derived scaffolds, *ii*) the possibility to tailor their degradation according to tissue regeneration rate, *iii*) the more controllable conversion rate to HA, and *iv*) the microarchitecture similarity to human trabecular bone make B<sub>2</sub>O<sub>3</sub>-based glasses promising materials for clinical applications as bone substitutes. Additionally, the potential of borate-based compositions has been exploited as carriers for the release of elemental ions essential for bone repair and regeneration (Liang *et al.*, 2008; Xiao *et al.*, 2009; Liu *et al.*, 2010; Hoppe *et al.*, 2011). Currently, the main issue related to the use of borate-based glasses is the toxicity of boron released in solution. Brown *et al.* performed an *in vitro* study in static

conditions and found that boron concentration higher than 2.5mM produced a significant inhibition of MC3T3 cell proliferation (more than 50%) (Brown *et al.*, 2009). Furthermore, it has been reported that boron content >250-350mg (per kg of mass) caused adverse toxic disorders during *in vivo* trials on rabbit models (Nielsen). A partial answer to the potential negative effect of boron release has been found in the dilution of phosphorous pentoxide to contain the toxicity of the medium (Huang *et al.*, 2006; Ning *et al.*, 2007; Yao *et al.*, 2007; Jung *et al.*, 2013).

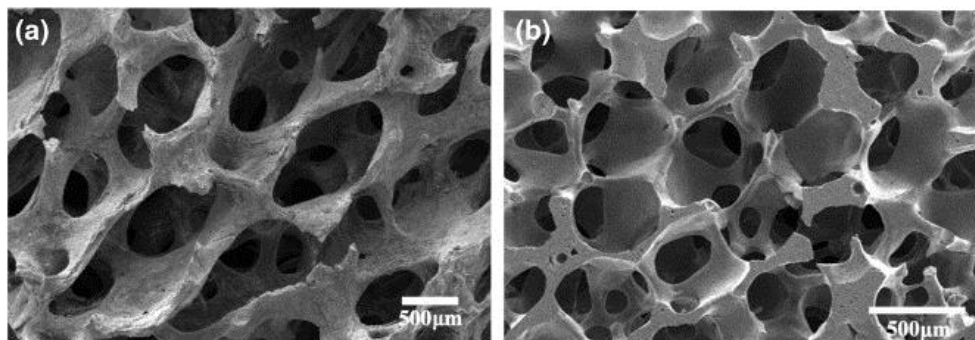


**Figure 3.7: SEM micrograph showing (a) human trabecular bone, and (b) 13-93B2 glass scaffold prepared using a polymer foam replication technique (Fu *et al.*, 2009).**

### 3.3.4.3 Phosphate-based glasses

The growing need of designing new biomaterials capable to resorb once they have attained their function, and with no adverse effects for the human body, led to the development of a novel class of bioactive glasses (Knowles, 2003). As the name suggests, phosphate glasses are based on the  $P_2O_5$  as glass former, and the  $[PO_4]$  tetrahedron, for which a phosphorous atom is surrounded by four oxygen atoms (Figure 3.8 (a)), and that represents the basic unit in their structure. The asymmetric nature of the  $[PO_4]$  unit is considered to be the reason of the low durability of these glasses. Furthermore, in the P-O-P bond (Figure 3.8 (b)), three of the four oxygen atoms are free, conferring them more flexibility in the orientation of the tetrahedral (Kaur *et al.*, 2013). Hence, the higher number of free oxygen atoms in phosphate glasses, with respect to silicate glasses, offers a wider range of possible bond formation (Hoppe, 1996).

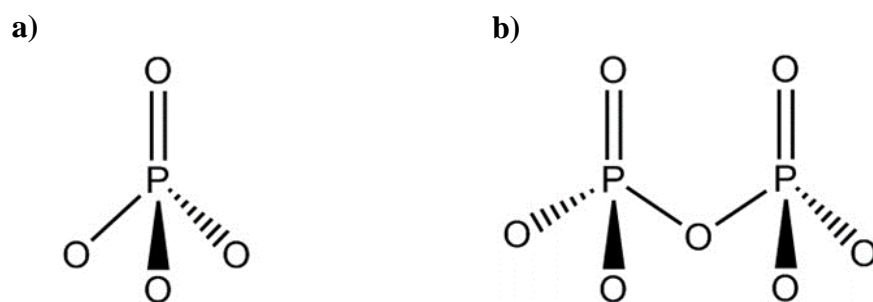


**Figure 3.8: Schematic representation of: a) phosphate tetrahedron and b) P-O-P bond.**

$P_2O_5$ -containing glasses in the  $CaO-Na_2O-P_2O_5$  system have been demonstrated to have distinctive dissolution properties in aqueous-based fluids, which can be tailored and predicted by adding appropriate oxides into the main composition (Abou Neel *et al.*, 2009b). Besides, depending on their composition, their solubility can vary from hours to weeks, and in general it rises by increasing the  $P_2O_5$  content (Abou Neel *et al.*, 2009b; Jones and Clare, 2012). Furthermore, the use of  $CaO$  and  $Na_2O$  as network modifiers makes the composition of phosphate-based glasses very similar to the mineral phase of bone, conferring them additional clinical potential as synthetic bone grafts (Knowles, 2003). In addition, this class of bioactive glasses have been considered very smart materials, since they can be synthesised and doped with specific ions such as zinc, strontium, copper or fluoride, which are elements able to induce a precise biological response and enhance their biocompatibility (Baino and Vitale-Brovarone, 2011; Kaur *et al.*, 2013).

Phosphate bioactive glasses have been used for different biomedical applications, going from soft to hard bone tissue, in form of bulk or powders, and in combination with polymers (Navarro *et al.*, 2004; Leonardi *et al.*, 2010; Novajra *et al.*, 2011; Bretcanu *et al.*, 2014; Sun and Yang, 2015; Tarafder *et al.*, 2015), as fibres for nerve repair (Jeans *et al.*, 2007), and also as antimicrobial delivery devices (Abou Neel *et al.*, 2005; Neel *et al.*, 2005; Valappil *et al.*, 2007). At present only few phosphate-based compositions have been used to produce 3D porous scaffolds for bone repair and regeneration, in comparison to the most common silica-containing glasses.

In 2004, Navarro *et al.* processed phosphate glass powders by  $H_2O_2$  foaming method, and the result was a 3D scaffold with a microstructure very similar to trabecular bone (Navarro *et al.*, 2004). Later on, Abou Neel and her research group produced strontium-doped phosphate based glasses using different amount of  $SrO$  (from 0 to 5mol%). The substitution of  $Na_2O$  with  $SrO$  in the original composition affected considerably the properties of the glass, increasing its density, transition temperature and degradation rate (Abou Neel *et al.*, 2009a). Additionally, another research group,

affiliated at Politecnico di Torino (Turin, Italy), exploited phosphate glasses properties for bone tissue applications. They developed a new bioactive glass (GC-ICEL2) and processed it as phosphate-derived scaffolds (see Figure 3.9) (Vitale-Brovarone *et al.*, 2009). GC-ICEL2 scaffolds enhanced the proliferation and differentiation of bone marrow stromal cells, and they were found to be bioactive and bioresorbable after soaking in different media, exhibiting an architecture similar to trabecular bone (Vitale-Brovarone *et al.*, 2009; Vitale-Brovarone *et al.*, 2011; Bretcanu *et al.*, 2014). More recently, the same research group produced bone-like scaffolds by co-sintering silicate and phosphate-based glasses. The resulting 3D structures revealed to be a promising strategy to customise osteoinductivity, dissolution rate and bioactive properties (Novajra *et al.*, 2015).



**Figure 3.9:** GC-ICEL2 scaffold produced by foam replication method (Vitale-Brovarone *et al.*, 2009).

#### **3.3.4.4 Selection of trace ions**

Over the last four decades, a significant amount of research work has been carried out on bioactive glasses as promising materials for producing scaffolds intended for bone repair and regeneration (Hench, 1999; Jones *et al.*, 2006; Rahaman *et al.*, 2011; Jones, 2013; Brauer, 2015). Figure 3.10 describes the biological response to ionic dissolution products of bioactive glasses through a schematic overview, according to the evidences reported in the literature (Hoppe *et al.*, 2011).

The main potential of this class of bioceramics is the possibility of customising their properties by doping the main composition with network modifiers and/or intermediate oxides (Murphy *et al.*, 2009; Fu *et al.*, 2010a; Fu *et al.*, 2010c; Murphy *et al.*, 2010; Pan *et al.*, 2010; Hoppe *et al.*, 2011; Baines *et al.*, 2013; Kaur *et al.*, 2013). To this extent, it has been demonstrated that slight changes in the glass formulation can substantially affect the material behaviour, particularly the physico-chemical and mechanical properties, dissolution rate, bioactivity and bioresorbability (Franks *et al.*, 2000; Huang *et al.*, 2006; Fu *et al.*, 2010a; Murphy *et al.*, 2010; Sharma *et al.*, 2012; Wu *et al.*, 2013).

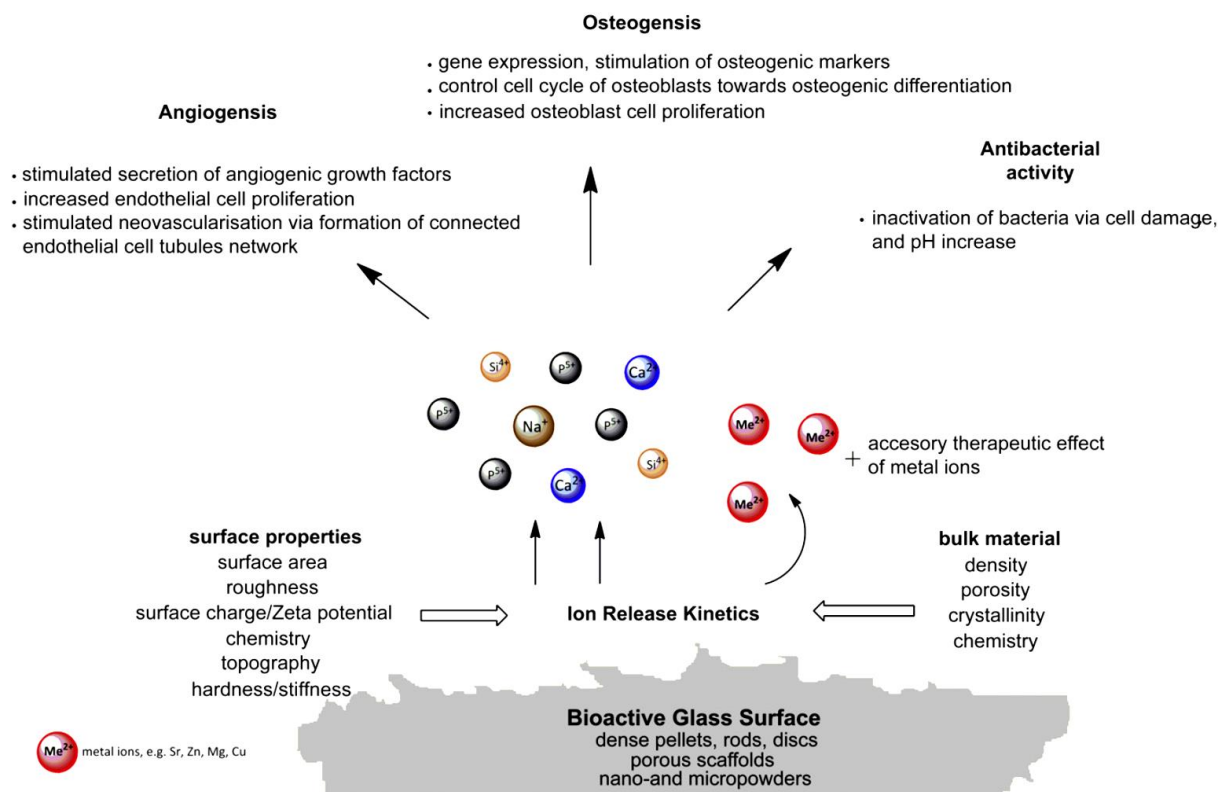


**Figure 3.10: Biological response to ionic dissolution products from bioactive glass surface (Hoppe *et al.*, 2011).**

Furthermore, several studies investigated how the release of specific ions from the glass network (*i.e.* Cu, Zn, Fe, Cr, Sr, Al, Ag, and Mg) can promote cell proliferation and differentiation, activate gene expression, and in some cases exhibit antibacterial properties (Bellantone *et al.*, 2002; Branda *et al.*, 2002; Singh *et al.*, 2009). Additionally, Table 3.6 reports some of the most important elements that are vital constituents of human body, and at the present also considered potential glass network modifiers, with their main function on bone tissue metabolism, regeneration and mineralisation (Murphy *et al.*, 2009; Murphy *et al.*, 2010; Hoppe *et al.*, 2011).

Trace ions like V, Mo, Bi Al, Cr, Y, and La have been recently used as dopants, since they are known to be involved in the bone metabolism, and also because they play a physiological role in angiogenesis, growth and mineralisation of bone tissue (Demling, 2009; Chellan and Sadler, 2015).

At present, an extensive literature have been published describing the ion incorporation as network modifiers, and their effect on SiO<sub>2</sub>, P<sub>2</sub>O<sub>5</sub>, and B<sub>2</sub>O<sub>3</sub>-based glass compositions (Murphy *et al.*, 2009; Fu *et al.*, 2010a; Fu *et al.*, 2010c; Murphy *et al.*, 2010; Pan *et al.*, 2010; Hoppe *et al.*, 2011). Most of the existing studies have investigated the effect of doped bioglasses on the bioactive properties



and HA formation (Li *et al.*, 1992; Branda *et al.*, 2002; Rahaman *et al.*, 2005; Yao *et al.*, 2005; Zhang *et al.*, 2009; Zhao *et al.*, 2010; Oudadesse *et al.*, 2011; Deliormanli, 2013; Zhang *et al.*, 2013; Macon *et al.*, 2015). Furthermore, the influence of network modifiers on the mechanical properties and biocompatibility have been also widely examined (Eslami *et al.*, 2010; Balagna *et al.*, 2011; Novajra *et al.*, 2011; Zheng *et al.*, 2012; Tarafder *et al.*, 2015). Additionally, Mourino *et al.*, considered the use of metallic ions as therapeutic agents and the need to design strategies for controlling their release (Mourino *et al.*, 2012).

**Table 3.6: Role of elemental ions on bone repair and regeneration.**

ELEMENT	ROLE	REFERENCE
<b>Magnesium (Mg)</b>	It plays a key role in bone metabolism, mineralisation of calcified tissues, directly stimulating osteoblast proliferation; it is an also active component of several enzymes.	(Tsuboi <i>et al.</i> , 1994; Rude <i>et al.</i> , 2003)
<b>Copper (Cu)</b>	Essential for hematologic and neurologic systems, helps in iron absorption, important in maintaining bone matrix and bone density, and plays a significant role in angiogenesis.	(Finney <i>et al.</i> , 2009; Josko, 2011; Hordyjewska <i>et al.</i> , 2014)
<b>Cobalt (Co)</b>	It stimulates angiogenesis via regulation of the hypoxia-inducible factor 1 (HIF-1).	(Chachami <i>et al.</i> , 2004; Wan <i>et al.</i> , 2008)
<b>Zinc (Zn)</b>	Essential in cellular metabolism and cofactor in metabolism of vitamins, DNA synthesis and cell division, as well as tissue repair and wound healing process.	(Demling, 2009; Josko, 2011)
<b>Manganese (Mn)</b>	It activates several important enzyme systems and it is involved in the synthesis of proteoglycans in cartilage.	(Soetan <i>et al.</i> , 2010)
<b>Strontium (Sr)</b>	It plays stimulatory effect on bone formation. Helpful in calcification of bones and teeth, bone healing, bone resorption.	(Marie <i>et al.</i> , 2001; Marie, 2010)
<b>Silver (Ag)</b>	It shows antibacterial and antimicrobial properties.	(Chellan and Sadler, 2015)
<b>Fluorine (F)</b>	It prevents dental caries and increases bone mechanical properties.	(Soetan <i>et al.</i> , 2010; Chellan and Sadler, 2015)
<b>Silicon (Si)</b>	Essential in bone mineralisation, component of connective tissues, stimulates collagen I formation and osteoblast differentiation; it is also associated with the formation and calcification of hard tissue	(Carlisle, 1970; Reffitt <i>et al.</i> , 2003; Nielsen and Poellot, 2004)
<b>Calcium (Ca)</b>	Constituent of bones and teeth, favours osteoblast proliferation, differentiation and ECM mineralisation.	(Heaney, 2008; Soetan <i>et al.</i> , 2010)
<b>Phosphorus (P)</b>	Essential for calcium phosphate deposition and extracellular matrix mineralisation.	(Boskey, 2003; Boskey, 2007; Soetan <i>et al.</i> , 2010)
<b>Iron (Fe)</b>	It enhances bone metabolism, particularly osteoblast proliferation, differentiation, and calcification.	(Beard, 2001; Gaston and Simpson, 2007; Yamasaki and Hagiwara, 2009)
<b>Boron (B)</b>	It helps in bone formation and stimulates RNA synthesis in fibroblast cells.	(Dzondo-Gadet <i>et al.</i> ; Uysal <i>et al.</i> , 2009)
<b>Selenium (Se)</b>	Essential nutrient for the body, protects the organism from harmful free radicals.	(Lee, 2010)

In 1994, Vrouwenvellder *et al.* showed how modifying the basic 45S5 glass network with small substitutions or additions of certain ions like iron, titanium, fluorine or boron affected the bioactive behaviour of the resulting formulations. Specifically, the incorporation of CoO, ZnO, and MgO delayed the HA formation, while the use of titanium increased proliferation and osteoblast expression. Furthermore, the addition of boron, iron and fluorine lowered the osteoblast activity with respect to the un-doped formulation (Vrouwenvellder *et al.*, 1994). Singh *et al.* doped borosilicate glasses with specific amounts of iron (5, 10 and 15wt%), and evaluated the bioactive properties by immersion in SBF solution. After 36 days of soaking, only the compositions with a percentage of iron between 10 and 15% showed the formation of an apatite layer (Singh and Bahadur, 1999). Later on, the same research group investigated the structural and bioactive effects of Al, Cr, Y and La on calcium borosilicate glasses. In particular,  $Y_2O_3$  and  $Cr_2O_3$  containing glasses formed an HA layer after 25 days of immersion in SBF, whereas no signs of apatite crystals were detected for  $Al_2O_3$  and  $La_2O_3$  doped glasses, which instead exhibited higher dissolution rate, proving that modifying the glass composition, the durability and bioactive properties were affected (Singh *et al.*, 2009).

Bioactive glasses doped using ZnO have also been widely investigated. Oudadesse *et al.* studied the effect of Zn on the bioactive and cytotoxic behaviour of a silicate-based glass. According to the obtained results, the Zn-doped glass slowed down the Ca and P ionic release in SBF, and thus the chemical reactivity. However, the release of  $Zn^{2+}$  did not influence directly the cell viability, which was more affected by particle size and release rate (Oudadesse *et al.*, 2011). Another study has shown that the incorporation of Zn (5mol%) in a sol-gel based bioglass produced a positive effect on cell attachment and pH balance in SBF solution. Furthermore, in the same work, it has demonstrated that Zn addition increased ALP activity and osteoblast proliferation (Balamurugan *et al.*, 2007).

Recently, trace elements of  $SiO_2$  and ZnO in conjunction with a 3D printed technology were used to produce 3D porous  $\beta$ -TCP scaffolds. The use of silica and zinc oxide improved  $\beta$ -TCP osteoinductivity by modulating collagen I and osteocalcin production. Furthermore, it was found that neovascularization increased up to three times in the doped material with respect to the pure  $\beta$ -TCP, used as control. Overall, this research findings indicated the addition of  $SiO_2$  and ZnO as a possible alternative to introduce osteoinductive properties to CaPs, avoiding the use of biological or pharmacological agents (Fielding and Bose, 2013).

Vitale-Brovarone research group investigated the effects of different ion-doped bioactive glasses. Specifically, they demonstrated how the addition of different amounts (0, 2.5 and 5mol%) of  $\text{TiO}_2$  to a phosphate-based glass showed reduced solubility and improved *in vitro* biocompatibility (Novajra *et al.*, 2011). Furthermore, they evaluated the biocompatibility and antibacterial response of a silver-doped bioactive glass in the system  $\text{SiO}_2\text{-CaO-CaF}_2\text{-Na}_2\text{O-K}_2\text{O-P}_2\text{O}_5\text{-MgO}$ . The produced Ag-containing scaffolds were able to inhibit bacteria adhesion and proliferation, however they showed a negative effect on osteoblast cell-like viability, making necessary the optimisation of Ag content (Balagna *et al.*, 2011). Moreover, the same research group investigated the *in vitro* behaviour of  $\text{SiO}_2\text{-CaO-Na}_2\text{O-K}_2\text{O-P}_2\text{O}_5\text{-MgO}$  glass introducing two different amounts of manganese oxide (0.25 and 0.5mol%). The presence of Mn for both compositions seemed to delay the bioactive process with respect to the parental glass. However, no cytotoxic effect was found, and interestingly the addition of Mn promoted osteoblast proliferation and ALP expression (Miola *et al.*, 2014).

As stated above, a broad range of biomedical applications based on the release of therapeutic ions integrated in an organic matrix have been proposed (Hum and Boccaccini, 2012; Vallet *et al.*, 2012; Cordero-Arias *et al.*, 2015; Stähli *et al.*, 2015). Metallic ions such as  $\text{Cu}^{2+}$ ,  $\text{Sr}^{2+}$  and  $\text{Co}^{2+}$  are being considered cost-effective and safer alternatives for enhancing the biological impact of bioglasses, if compared to growth factors and gene therapies. Furthermore, they can be easily processed, are stable at high temperatures and have a tuneable release kinetic (Mourino *et al.*, 2012).

At present, there is a large volume of published studies on the ability of copper to stimulate angiogenesis and proliferation of endothelial cells during *in vitro* culture (Hu, 1998; Finney *et al.*, 2009; Gerard *et al.*, 2010; Wu *et al.*, 2013). Furthermore, the use of copper, as network modifier, has also shown an osteogenic effect in enhancing the differentiation of MSCs into osteoblast cells (Rodriguez *et al.*, 2002; Wu *et al.*, 2013).

Different inorganic matrixes, including silicate (Wu *et al.*, 2013; Stähli *et al.*, 2015), borate (Erol *et al.*, 2012; Wang *et al.*, 2014; Zhao *et al.*, 2015) and phosphate glasses (Neel *et al.*, 2005; Stähli *et al.*, 2013) have been used in order to incorporate Cu ions, whose effects on bone tissue repair and regeneration were examined. In 2013, 45S5 glass scaffold were produced *via* foam replication method and doped using different CuO percentages (0.1, 1 and 2.5wt%). *In vitro* experiments in SBF solution were performed on the Cu-containing samples, which revealed high bioreactivity as

confirmed by the fast formation of HCA layer on their surface. Furthermore, the possibility to tailor the Cu degradation of the novel designed Cu-doped bioglasses, according to the culture conditions, make them promising candidate materials for regenerative medicine and mainly for bone tissue healing (Hoppe *et al.*, 2013).

Later on, Wang *et al.* evaluated the ionic release effects of Cu-doped (0 – 3wt%) borate-based glasses *in vitro* and *in vivo*. The nucleation of HA tested in SBF solution decreased slowly with the increase of Cu in the glass, whereas the Cu ions leaching in solution increased with the increase of copper amount. These findings were promising in predicting that borate-based scaffolds could act as carrier systems for the controlled release of Cu ions (Wang *et al.*, 2014).

Furthermore, the Cu-derived scaffolds showed no detrimental effects on human MSCs viability, and they further enhanced ALP activity by increasing culture time and Cu content. Most interestingly, Wang *et al.* found that after *in vivo* implant in rat calvarial defects, the scaffolds with the highest Cu content (3wt%) exhibited superior ability to stimulate bone regeneration and angiogenesis with respect to the undoped borate scaffolds used as control (Wang *et al.*, 2014).

Strontium-containing bioactive glasses are another class of doped bioglasses that have been broadly considered in the literature (Marie *et al.*, 2001; Meunier *et al.*, 2002; Pan *et al.*, 2010; Zhao *et al.*, 2010; Vickers, 2013). Particularly, strontium has been shown to have a beneficial effect when treating osteoporosis-affected patients, as it has the ability to stimulate new bone deposition in osteoblasts and to inhibit osteoclasts and thus bone resorption (Bonnelye *et al.*, 2008). Gentleman *et al.* proved that Sr-doped silicate glasses enhanced bone cell activity. In particular, replacing the amount of calcium in the system  $\text{SiO}_2\text{-P}_2\text{O}_5\text{-Na}_2\text{O-CaO}$  with strontium (up to 100%), the osteoblast activity was improved and the osteoclast differentiation inhibited (Gentleman *et al.*, 2010). Hesarakı *et al.* using a Sr-containing bioactive glass concluded that strontium addition enhanced ALP activity and increased proliferation of rat calvaria osteoblast cells (Hesarakı *et al.*, 2010). Recently, Sr-doped AW scaffolds have been produced using different mol% of SrO. The formulation having 6.2mol% of strontium showed better performance in terms of bioactivity and osteogenic differentiation of human mesenchymal stem cells (MSCs) (Vickers, 2013).

Lately, the adoption of cobalt-doped bioactive glasses for bone tissue applications have been considered as well. Melt-derived 13-93 glass compositions were prepared by Hoppe *et al.* using 1wt% and 5wt% of CoO. The Co-containing bioactive scaffolds were tested in SBF solution;

interestingly, the kinetic of CaP layer formation was similar for both the doped compositions. However, for the samples with higher amount of Co an amorphous CaP layer was formed on the top of their surface after 7 days in immersion, whereas a mixed Ca-P-Si rich layer with HCA characteristics, and similarly to the un-doped 13-93 glass, was detected on the samples with less Co content. Furthermore, according to the degradation test results, the Co concentration after 21 days was within a therapeutic range (~2ppm), making them a potential platform for controlled Co release (Hoppe *et al.*, 2014). In the same year Vyas *et al.* tested the bioactive properties of Co-doped silicate glasses, where the original SiO<sub>2</sub> content (45wt%) was partially replaced with cobalt (0.5, 1, 1.5 and 2wt% respectively). It was concluded, partially conversely with Hoppe *et al.* findings (Hoppe *et al.*, 2014), that the increasing of cobalt amount positively affected the bioactive behaviour of the glass (Vyas *et al.*, 2015).

Additionally, cobalt ions have been known to induce hypoxia conditions and thus stimulate angiogenesis via regulation of the hypoxia-inducible factor 1 (HIF-1), whose role has been identified crucial for angiogenesis and skeleton regeneration (Chachami *et al.*, 2004; Emans *et al.*, 2007; Wan *et al.*, 2008). Moving from these consideration, Hoppe *et al.* used the same Co-containing glasses, analysed in their previous study (Hoppe *et al.*, 2014), to evaluate the biocompatibility of cobalt-derived glass particulates and 3D porous scaffolds in culture with osteoblast-like cells and human dermal micro endothelial cells. The formulation with 1 wt % of CoO exhibited better *in vitro* biocompatibility with respect to 5 wt % CoO-containing glass, which showed a cytotoxic effect during *in vitro* culture; in addition, the glass doped with less cobalt content slightly enhanced mitochondria activity.

Similar outcomes were obtained using human endothelial cells, leading to conclude that 1 wt % Co-containing glass can be considered a promising candidate as hypoxia mimicking material in the field of bone tissue applications; instead, the increase in cobalt amount showed a negative effect on physiological fluids, assuming that it may outreach the acceptable threshold (Hoppe *et al.*, 2015).

### 3.3.5 *In vitro* bioactivity of bioceramics

Bioactivity and bone bonding mechanisms have been widely investigated. As previously mentioned, bioactivity is the ability of a material to bond to the host tissue through the formation of an HA-like layer (Kokubo and Takadama, 2006). According to the literature, bioceramics were the first class of materials to display bioactive behaviour (Hench, 1998b). Specifically, the concept was introduced by Hench at the beginning of 70's, when he described the bonding process of 45S5 bioglass to bone as a process based on the formation of a carbonated hydroxyapatite (HCA) layer on the surface of the material in contact with the host tissue (Hench, 1991).

The sequence of reaction events involved during the bond formation between bone and a bioactive glass, initially proposed by Hench and subsequently modified by Gerhardt and Boccaccini (Hench, 1998b; Gerhardt and Boccaccini, 2010), is reported in the Figure 3.11 below.

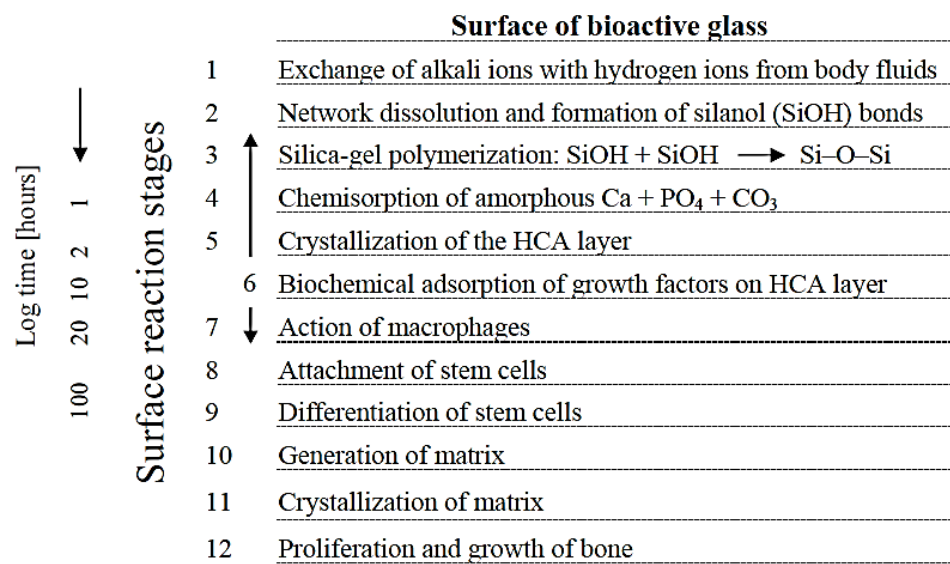


**Figure 3.11: Sequence of reactions on the surface of a bioactive glass implant (from (Gerhardt and Boccaccini, 2010)).**

Later on, Kokubo discovered that also AW glass-ceramic showed bioactive behaviour, bonding to bone *in vivo* (Kokubo, 1990), and in 1991 he stated that “*the essential requirement for an artificial material to bond to living bone is the formation of bone-like apatite on its surface when implanted in the living body, and that this in vivo apatite formation can be reproduced in a simulated body fluid*” (Navarro *et al.*, 2008). This was the origin of *in vitro* bioactivity tests.

The solution proposed by Kokubo was an a-cellular fluid with an ionic concentration almost equal to human blood plasma (Table 3.7). Since Kokubo protocol development, the *in vitro* apatite formation on the surface of a material, when immersed in SBF, has been considered a useful method of assessing potential *in vivo* bioactivity of a new material (Kokubo *et al.*, 1990; Kokubo and Takadama, 2006).

**Table 3.7: Ion concentrations (mM) of human blood plasma and SBF solution (Kokubo and Takadama, 2006).**

	Na <sup>+</sup>	K <sup>+</sup>	Mg <sup>2+</sup>	Ca <sup>2+</sup>	Cl <sup>-</sup>	HCO <sub>3</sub> <sup>-</sup>	HPO <sub>4</sub> <sup>2-</sup>	SO <sub>4</sub> <sup>2-</sup>
Human blood plasma	142.0	5.0	1.5	2.5	103.0	27.0	1.0	0.5
SBF	142.0	5.0	1.5	2.5	148.8	4.2	1.0	0

Although a large number of studies for the bioactivity evaluation are based on the protocol proposed by Kokubo (Wu and Xiao, 2009), the strength of this test method for the assessment of bone-bonding ability has not been scientifically demonstrated. Furthermore, numerous modifications of both ion concentration as well as test method conditions have been suggested to investigate the bioactive behaviour of new implants (Salinas and Vallet-Regi, 2013):

- i)* the refresh of the solution at set time points;
- ii)* the renewal of the solution through a dynamic system;
- iii)* the use of a different buffer and the reaching of a physiological carbonate ions concentration;
- iv)* the modification of SBF solution by adding plasma proteins such as albumin.

More recently, a new unified method for the assessment of the apatite-forming ability of bioactive glasses has been proposed. The aim of the study was to provide a valid protocol, in particular for bioactive glass samples with high surface area, and to verify its reproducibility over a wide number of research groups. Based on the modification of the ISO standard 23317:2012, which fixes the surface area to solution volume ratio when comparing samples, and is performed in static conditions, the new proposed method uses fixed mass per solution volume ratio and agitated solution. Furthermore, the method involved 10 laboratories of 8 different countries and it was validated through a round robin test (Macon *et al.*, 2015).



### 3.4 Scaffold fabrication technologies

As described in paragraph 3.2, in bone tissue engineering 3D porous scaffolds are essential pillars to guide tissue growth and regeneration. Hence, after the selection of an adequate bone matrix-like biomaterial, which depends on the biological and mechanical properties of the anatomic site that needs to be replaced, another important aspect of TE approach is the selection of an appropriate processing technology to fulfil the scaffold requirements.

Polymer foam replication is the most widely exploited technique to produce bioactive glass and glass-ceramic scaffolds (Renghini *et al.*, 2009; Fu *et al.*, 2010a; Baino *et al.*, 2013). In addition to this method, a variety of different technologies have been developed through the years to produce 3D porous glass and glass-ceramic scaffolds, including sol-gel (Bielby *et al.*, 2002; Sepulveda *et al.*, 2002; Jones and Hench, 2003a; Rainer *et al.*, 2008; Correia *et al.*, 2015), organic phase burning-out (Brovarone *et al.*, 2006; Fu *et al.*, 2007; Vitale-Brovarone *et al.*, 2008), thermally induced phase separation (TIPS) (Yin *et al.*, 2003; Fabbri *et al.*, 2010), and freeze casting (Zhang *et al.*, 2005; Deville *et al.*, 2006b; Song *et al.*, 2006; Mozafari and Moztarzadeh, 2014). An overview of these so-called *conventional techniques* together with their main advantages and disadvantages is reported in Table 3.8 (Rezwan *et al.*, 2006; Baino and Vitale-Brovarone, 2011; Fu *et al.*, 2011; Rahaman *et al.*, 2011; Jones, 2013; Lu *et al.*, 2013; Gao *et al.*, 2014). All the above mentioned methods bring to scaffolds with different morphologies, structures and properties.

Specifically, polymer burning-out was the technique used to produce the first example of bioceramic scaffold for bone regeneration (Bellucci *et al.*, 2011). In this case, the ceramic powder is mixed with an organic pore former (porogen) that is subsequently removed during a thermal treatment necessary to consolidate the inorganic phase. Generally, the scaffold produced with this method are characterised by low porosity and limited interconnectivity (Brovarone *et al.*, 2006). Foam replication method was introduced for the first time in 2006 by Chen *et al.* (Chen *et al.*, 2006), and it has been widely investigated since then. It is a relatively inexpensive processing technique, based on the use of a polymeric sponge, which is impregnated in a bioceramic-based slurry. Afterwards, during a heat treatment, the polymeric template is burned out and the ceramic phase is sintered. This technique leads to the production of scaffolds with controllable pore size, high porosity (> 80%) and better interconnectivity than polymer burning-out method (Bretcanu *et al.*, 2008; Vitale-Brovarone *et al.*, 2011). However, the greater porosity is associated to high

brittleness and low mechanical properties, which represent the main drawbacks of this technique. For this reason, Bellucci *et al.* considered the development of alternative strategies highly necessary. Specifically, whereas in the original method the exceeding slurry was removed by squeezing the sample, and the green bodies (un-sintered specimens) were left to dry before the sintering process, in the new protocol the samples were kept entirely loaded of slurry, which was previously mixed with PE particles and that led to an increased and more controlled final porosity (Bellucci *et al.*, 2011).

Sol-gel phase separation, TIPS and freeze casting also belong to the class of conventional techniques for scaffold production.

Sol-gel scaffold fabrication is a versatile method based on the preparation of a sol-gel glass of desired composition, and consequent foaming of the sol by the addition of a surfactant, followed by condensation and gelation reactions. The obtained foamed solutions are then cast into moulds, and after a drying process, they are sintered to produce consolidated structures (Jones *et al.*, 2004; Rainer *et al.*, 2008). Through this technique it is possible to obtain glass or glass-ceramics in different forms, including hierarchical porous architectures, ultra-fine or spherical-shaped powders, ceramic fibres, thin-film coatings and microporous inorganic membranes (Raucci *et al.*, 2010; Chen, 2011). The peculiarity of this method is related to the nanopores (2–50nm) resulting from the sol-gel process and the interconnected macropores (10–500µm) deriving from the foaming process. However, because of the resulting nanopores, which lead to a higher surface area, the scaffolds undergo a fast degradation process (Sepulveda *et al.*, 2002; Fu *et al.*, 2011). Furthermore, the sol-gel-derived scaffolds have low strength, therefore they are not suitable for load-bearing applications (Jones *et al.*, 2006).

The phase separation route involves the use of a polymer that is dissolved in an organic solvent. Once a homogeneous polymer-based solution is formed, glass or glass-ceramic powders are added and a mixture is obtained. To induce phase separation, the polymer solution is cooled rapidly, and a porous structure is produced after evaporation of the solvent via sublimation and following stabilisation (Boccaccini and Maquet, 2003). The large number of variables on which the methodology is based (including polymer and solvent selection, concentration of polymer, and phase separation temperature) allows tailoring of the properties of the final porous structures

(Molladavoodi *et al.*, 2013). However, the possibility of solvent residue and the sensitivity of the method to slight changes in the parameters, limit the use of this technique (Cao *et al.*, 2006).

Regarding the freeze casting method, this is based on the rapid freezing of a colloidal suspension, using an organic solvent (*i.e.* water, camphene or camphene mixture), and the casting of the solution in a non-porous mould. After sublimation of the solvent and a drying process, the 3D constructs are sintered to consolidate their structures (Deville, 2008). The main advantage of this method lies in the preparation process, which is easy and does not require expensive equipment (Sofie and Dogan, 2001; Thavornnyutikarn *et al.*, 2014). Furthermore, this technique allows to control the directionality of the porosity by the solidification conditions yielding porous ceramics with a specific macro-porosity (Deville *et al.*, 2006a; Deville *et al.*, 2006b; Fu *et al.*, 2010b). However, as for the TIPS technique, also for this method the solvent residue present in the structure can be harmful to biological tissues (Sachlos *et al.*, 2003; Zhu and Chen, 2013).

Despite the fact that conventional fabrication methods have been widely used over the last three decades to produce promising scaffolds for medical applications (Morsi *et al.*, 2008), most of the scaffold requirements (*i.e.* pore geometry, pore size, shape and interconnectivity) cannot be fully controlled with many of them. Moreover, depending on the fabrication method used, the 3D scaffold also lacks of the mechanical strength necessary to withstand stress and forces of the living tissues (*i.e.* sol-gel method) (Jones *et al.*, 2006). In addition, some of these processing techniques use organic solvents, and the presence of their toxic residues can cause severe inflammatory response (*i.e.* TIPS and freeze casting). Furthermore, most of these methods are manual, resulting in poor reproducibility over the large scale and inconsistent outcomes (Leong *et al.*, 2003; Sachlos *et al.*, 2003; Zhu and Chen, 2013).

Based on these observations scaffold fabrication for bone repair and regeneration remains a research challenge. Therefore, the emerging need for novel 3D constructs with tailored physico-chemical and mechanical features has led to the development of new manufacturing technologies (Utela *et al.*, 2008; Melchels *et al.*, 2012; Thavornnyutikarn *et al.*, 2014; Mota *et al.*, 2015). The aim of next section is to describe and review the state of the art of additive manufacturing (AM) techniques, for the design and fabrication of scaffolds for bone tissue repair.

**Table 3.8: Conventional techniques for the production of bone tissue substitutes.**

METHOD	DESCRIPTION	ADVANTAGES	DISADVANTAGES
<b>Organic phase burning-out</b>	A blend is obtained by mixing glass particles and organic phase, after they are thermally treated to remove the organic phase and sinter the glass.	- No organic solvents	- Residual of porogens - Low porosity (<60%) and limited interconnectivity
<b>Foam replication</b>	Impregnation of a polymeric sponge template in a glass-based slurry followed by a thermal treatment to remove the organic phase and sinter the glass.	- No organic solvents - Control of porosity and pore size	- Possibility of an inhomogeneous coating of the foam - Low mechanical strength (2-20MPa)
<b>Sol-gel</b>	A solution of metal alkoxides leads to the formation of the sol phase, made by solid particles that then will condense in gel-like materials. After a drying process the so obtained material is treated at high temperature.	- Hierarchical pore structure - Interconnected macropores - Nanoporous texture	- Many variables affect the final morphology ( <i>i.e.</i> glass particles, surfactant, gelation time) - Low mechanical strength (0.3-2.3MPa)
<b>Thermally induced phase separation (TIPS)</b>	A polymer mixed with/without glass particles, is dissolved in a solvent and a liquid-liquid or solid-liquid phase separation is obtained by lowering the temperature. The solvent is removed by sublimation to give a porous structure.	- Incorporation of biologically active molecules - High porosity	- Slight changes in the parameters ( <i>i.e.</i> type of polymer, glass particles, and solvent used) affect the morphology of the scaffold - Possibility of solvent residues
<b>Freeze casting</b>	The method involves the rapid freezing of colloidally-stable suspension of particles in a nonporous mold. The frozen solvent is removed by sublimation to avoid cracking prior to sintering.	- Oriented microstructure - High mechanical strength in the direction of orientation	- Small pore size (10–40µm) - Possibility of solvent residues

### 3.4.1 Overview of additive manufacturing techniques

The use of AM, or also called solid free form fabrication (SFF), rapid prototyping (RP) or more recently 3D printing processes, to produce custom-made devices with well-designed architecture, has become a fast-developing research field in the last few years (Thavorniyutikarn *et al.*, 2014; Mota *et al.*, 2015). The concept of AM was introduced for the first time by Chuck Hull in 1986 via his patented stereolithography (SLA) process (Hull, 1986). Since its launch, many applications advanced from the outstanding and time-saving capabilities of its production method (Arafat *et al.*, 2014; Giannitelli *et al.*, 2014; Yoo, 2014). According to ASTM F2792, AM is defined as “the process of joining materials to make objects from three-dimensional model data usually layer upon layer” (F2792, 2012). Conversely to the conventional fabrication methods that remove material from a bulk, using AM techniques 3D objects are built through a layer-by-layer approach via the processing of solid filament, liquid or powder stock materials (Hutmacher *et al.*, 2004; Bartolo *et al.*, 2009). AM provides exclusive methods to produce accurate (macro-architecture as well as microstructure) and consistent (mechanical properties, porosity and interconnectivity) bone-like substitutes matching patient’s defects (Sun *et al.*, 2004). The above mentioned advances have led to a growing interest in the development of novel scaffolds with a tailored architecture and customizable properties as well as enhanced *in vitro* behaviour. Leong *et al.* (2003) reported the common steps of AM techniques in a flowchart (Figure 3.12).

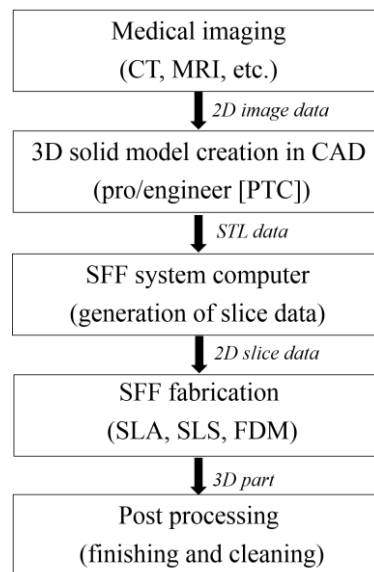


**Figure 3.12: Common process steps for all AM techniques-based approach (re-printed by (Leong *et al.*, 2003)).**

In summary, medical images of the anatomic site are acquired by computer tomography (CT) or magnetic resonance imaging (MRI). The 2D image data are then treated by computer-aided design (CAD) software, and afterward the obtained 3D model is converted into a standard tessellation language (STL) file. Subsequently the .stl file is sliced into layers and loaded in the AM machine. According to the fabrication process, the 3D build parts can need further finishing and cleaning work. At present, different AM techniques have been widely explored for TE scaffold fabrication, although none of those proposed has been acknowledged as a gold standard approach. The four techniques represented in the Figure 3.13 have been recognised as the most commonly used strategies for the production of TE substitutes (Melchels *et al.*, 2012), namely they are:

a) Stereolithography, b) Selective laser sintering, c) Fused deposition modelling and d) Powder-based three dimensional printing.

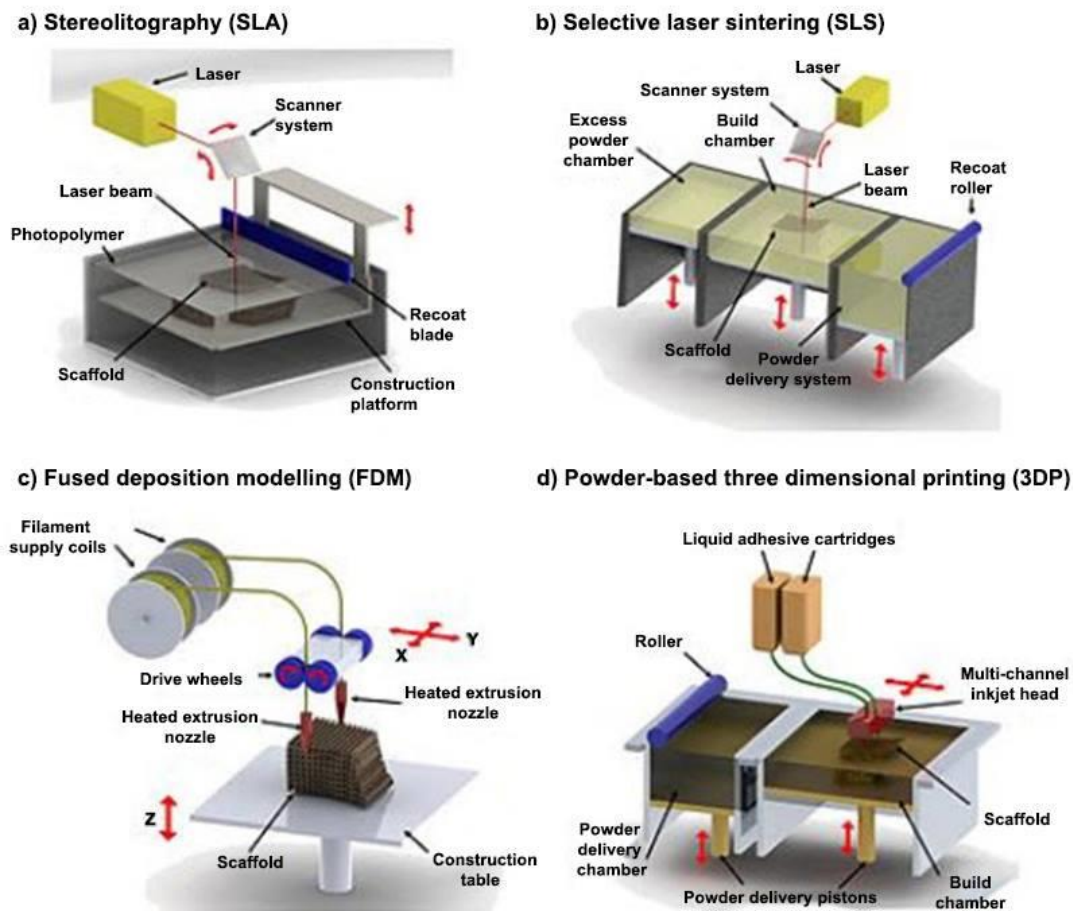


**Figure 3.13:** The four most common and commercially available AM techniques that are used for tissue engineering scaffold fabrication (adapted from (Mota *et al.*, 2015)).

#### 3.4.1.1 Stereolithography

Stereolithography (SLA) is the oldest AM technology (Hull, 1986). The process, as schematically described in Figure 3.13, uses ultraviolet (UV) light or laser to polymerise layer-by-layer a photosensitive polymer. Once one layer is completed, the construction platform is vertically lowered to a given distance and a new uniform layer of resin is placed on the top of the previous solidified one. The process is repeated until the 3D object is completed. Further actions include the removal of non-polymerised resin and the post-curing of the printed 3D part under UV light (Thavornnyutikarn *et al.*, 2014; Mota *et al.*, 2015). This approach has been applied to fabricate 3D scaffolds from polymers, bioceramics and composite materials (Chu *et al.*, 2002; Cooke *et al.*, 2003; Melchels *et al.*, 2009; Arcaute *et al.*, 2010). SLA technology can also be used to produce hydrogel/polymer scaffolds in combination with cells for soft tissue engineered applications. The success of cell encapsulation is determined by several elements, such as UV light intensity, exposure time and free radical formation (Lu *et al.*, 2006; Park *et al.*, 2011). However, considerable shortcomings (for example the shrinkage of the structure during the production process, the necessity of a support and the presence of a toxic resin) limit the use of this technique.

#### 3.4.1.2 Select laser sintering

Select laser sintering (SLS) process is based on the use of a high intensity laser beam such as CO<sub>2</sub> that selectively sinters regions of powder-based material placed in a powder bed until the formation of a powder layer. After the generation of the first layer, the powder bed is vertically lowered by one layer thickness and the new layer of powder is spread mechanically by a roller on the top of the previous one. In this technology the non-sintered powder serves as support for the build-up of the next layers. The process is iteratively repeated until the 3D structure is finalised (Thavornnyutikarn *et al.*, 2014; Mota *et al.*, 2015). TE constructs based on polymers, ceramics and metals have been produced using the SLS technique. In 2005 Ciardelli *et al.* developed a select laser sintered scaffold of PCL and a polysaccharide (starch, gellan and dextran), finding a promising and easy method to improve PCL biocompatibility (Ciardelli *et al.*, 2005). Usually, TE scaffolds produced *via* SLS technique show low mechanical properties, however Goodridge *et al.* (2007), using a SLS method, fabricated an apatite-mullite glass-ceramic with good surface finish and mechanical properties (flexural strength around 16 MPa) in the range of cancellous bone (Goodridge *et al.*, 2007). Very recently, Lee *et al.* used SLS to produce 3D porous AW scaffolds.

MSC-seeded and unseeded AW scaffolds were tested *in vivo* using MF1 nude mice. Osteoid formation and tissue in-growth were observed after 4 weeks and without the need for osteogenic pre induction, demonstrating that SLS custom-designed scaffolds enhance *in vivo* biocompatibility and osteoconductive capacity of AW glass ceramics (Lee *et al.*, 2015). Furthermore, the use of SLS technology has been extended to polymer/ceramic composites; however, despite the advantages of this method, the performance of 3D porous constructs depends on the combination of the above described process parameters (Thavornyutikarn *et al.*, 2014).

#### **3.4.1.3 Fused deposition modelling**

Fused deposition modelling (FDM) was developed and commercialised by Stratasys Inc. in 1992. It is based on the melting and extrusion of material (usually a thermoplastic polymer) onto a platform. The filament of material is provided by two rotating rollers to a mobile nozzle, which moves in *x* and *y* direction, as shown in the Figure 3.13. Through an orifice in the extruder head the material can be deposited on a platform. After fabrication of the first layer and when the material is solidified, the platform moves downwards in *z*-direction and the process is repeated layer-by-layer until the 3D object is completed (Thavornyutikarn *et al.*, 2014; Mota *et al.*, 2015).

Although a variety of material can be used to produce FDM scaffolds, polymer or composite-based scaffolds are the most investigated. A PCL-HA composite was the first scaffold produced using the FDM technique by Hutmacher *et al.* (Hutmacher, 2000). Later on, different scaffolds were printed using PCL, and in 2009, PCL scaffolds fabricated *via* FDM were approved by FDA for craniofacial applications (Low *et al.*, 2009). In addition, in 2010 PCL and PCL-TCP bi-layered constructs were investigated for the repair and regeneration of osteochondral defects (Ho *et al.*, 2010).

The use of FDM technique allows the manufacture of interconnected porous scaffolds with an extremely reproducible architecture, with no need of solvents, and at a quite low maintenance costs (Kalita *et al.*, 2003). However, the major limitations of this strategy are: *i*) the use of materials in the form of filament with specific diameters, and *ii*) the effect that the high operating temperatures (sometimes up to 280°C) can have on the raw material properties (Sung-Hoon *et al.*, 2002; Thavornyutikarn *et al.*, 2014; Carneiro *et al.*, 2015).



#### **3.4.1.4 Powder-based three-dimensional printing**

Three-dimensional printing (3DP) is an ink-jet printing technology, developed at MIT (Cambridge, MA) in 1989 (Sachs *et al.*, 1992). It is used to produce complex 3D solid objects by jetting a liquid-based binder onto a bed of loose powder. 3DP technology has been largely used to create 3D tissue substitutes from a wide range of materials (Bose *et al.*, 2013).

Although the first published study using this technique was about the use of a mixture of PLGA and NaCl (Kim *et al.*, 1998), bioceramics such as HA, bioactive glasses, TCP, but also polymers and hydrogels have been then processed using 3DP technology (Leukers *et al.*, 2005; Seitz *et al.*, 2005; Butscher *et al.*, 2011). Among the different AM methodology, 3DP has been considered a versatile technique, which became popular for the production of scaffolds for bone tissue engineering applications (Bose *et al.*, 2013).

For the manufacture of medical devices the main advantages of this technology derive from the possibility to fabricate 3D custom substitutes with defined design, controlled and interconnected porosity, with a wide range of materials, and also without the contamination problems related to the use of toxic solvents (Leukers *et al.*, 2005; Detsch *et al.*, 2011; Bose *et al.*, 2013). However, process parameter optimisation, appropriate binder selection, and removal of the loose powder after printing are important features that need to be considered for the final success of the printed parts (Butscher *et al.*, 2012). All these parameters will be analysed in major detail in the next section (3.4.2).

The key parameters together with advantages and disadvantages of the AM techniques mostly used for TE scaffold fabrication are summarised in the Table 3.9. Indirect 3DP was adopted in this research project as a method to process bioceramic powders to create 3D structures, and it is described in greater detail in the next paragraph (3.4.2.1).

**Table 3.9: The four most commonly used AM technologies for the production of bone tissue substitutes with their advantages (+) and disadvantages (-).**

TECHNIQUE	PARAMETERS	ADVANTAGES (+)/ DISADVANTAGES (-)	REFERENCE
SLA	Layer thickness: 25-100 $\mu\text{m}$	+ High accuracy and good surface finish; possibility of cell encapsulation;	(Melchels <i>et al.</i> , 2009; Melchels <i>et al.</i> , 2010;
	Resolution: 14-150 $\mu\text{m}$	- support structure needed; photopolymer needed; possible use of toxic resins; possible shrinkage during polymerisation.	Butscher <i>et al.</i> , 2011; Mota <i>et al.</i> , 2015)
SLS	Layer thickness: 75-150 $\mu\text{m}$	+ No support structure needed; solvent free; fast process;	(Dalton <i>et al.</i> , 2009; Swift and Booker, 2013;
	Resolution: 50-1000 $\mu\text{m}$	- heat transfer generated by the laser; difficulties to remove trapped powder; poor surface finish.	Thavornnyutikarn <i>et al.</i> , 2014; Mota <i>et al.</i> , 2015)
FDM	Layer thickness: 50-750 $\mu\text{m}$	+ No support structure needed; no material trapped; solvent free;	(Zein <i>et al.</i> , 2002; Kalita <i>et al.</i> , 2003; Leong <i>et al.</i> , 2003; Swift
	Resolution: 100-500 $\mu\text{m}$	- high temperature needed; mechanical anisotropy; thermoplastic polymers needed; filament preparation necessary.	and Booker, 2013; Thavornnyutikarn <i>et al.</i> , 2014)
3DP	Layer thickness: 50-150 $\mu\text{m}$	+ Wide material range; no support structure needed; cost-effective; fast process (10 min for 20 scaffolds); solvent free;	(Utela <i>et al.</i> , 2008; Butscher <i>et al.</i> , 2011;
	Resolution: 50-300 $\mu\text{m}$	- poor surface finish; low green body strength to handle the samples; depowdering process necessary; powder can be trapped in the pores.	Melchels <i>et al.</i> , 2012; Bose <i>et al.</i> , 2013; Mota <i>et al.</i> , 2015)

### 3.4.2 Indirect powder-based 3DP for bone repair applications

3DP is a powder-based methodology, whose working stages are schematically represented in Figure 3.14. During the process a liquid binder (usually a water-based solution) is jetted, using an ink-jet print-head, onto a powder bed of loose material. The particles are then bonded together and the first 3D layer is produced.

After the printing of this first layer, the powder bed is lowered in the  $z$ -direction and a new layer of loose powder is spread on the top of the previous one in the  $x$ - $y$  plane. As in the case of SLS, also in this process the powder bed acts as a physical support for the printed part. Following a layer-by-layer approach, each step is repeated until the predesigned object is concluded. The 3D printed part, technically called a green body or unfinished part, needs then the removal of the loose powder and depending on the material (*i.e.* HA, TCP or AW)(Seitz *et al.*, 2005; Santos *et al.*, 2012; Alharbi, 2015) the consolidation of the structure by thermal treatment (Butscher *et al.*, 2011).

It is important to note that before starting the process, and after the material selection, thorough optimisation of the printing parameters, *e.g.* layer thickness, powder packing density, powder wettability, powder flowability as well as binder drop volume, is necessary to obtain a good outcome (Bose *et al.*, 2013). For any new powder-based material the optimisation process may require long time; this can be considered one of the major shortcomings of 3DP technique.

Once the material has been chosen, the preparation of the powder (in terms of particle size and distribution) is a crucial step for the quality of the final 3D printed part, as it will affect the sinterability, pore dimension, surface area and surface finish (Cima and Cima, 1996; Sachs, 2000). The powder formulation is the first stage of the 3DP process, followed by the selection of the binder and possible additives (Utela *et al.*, 2008).

There are different ways of binding the powder; among these the most commonly used are organic (*i.e.* polyvinyl) or inorganic (*i.e.* colloidal silica) liquids and in-bed adhesives (*i.e.* maltodextrin (MD) or sucrose) (Cima *et al.*, 1995; Brecht and Anderson, 1999; Feenstra, 2005; Suwanprateeb and Chumnanklang, 2006). Liquid binders are the most versatile methods as they work with almost any material (Brecht *et al.*, 2003). However, in the case of organic binders, they can dry in the printhead, causing the obstruction of the nozzle (Greil, 2000). The use of an in-bed binder is an alternative method: a powder-based component is added to the starting formulation and it binds the particles after interaction with a sprayed liquid (Irsen *et al.*, 2006a). Even though, it is a time

consuming process, as it requires the further step of mixing two materials any time a new powder is processed, it reaches higher green body strengths if compared to liquid binders (Utela *et al.*, 2010).

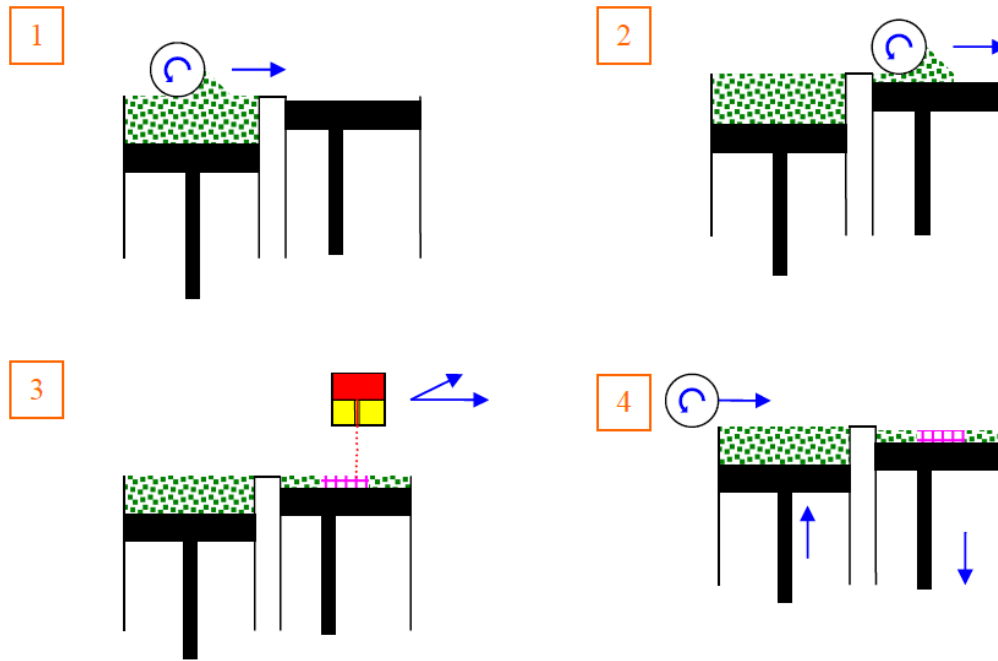


**Figure 3.14: 3D printing iterative phases. (1) The process starts with the spreading of a first thin layer of powder in the built area (2) and the formation of a supportive powder bed. (3) The ink-jet print-head sprays droplets of a liquid binder on the powder bed and hence the powder particles start to bond one to each other, until all the layers of the predesigned CAD file is printed. (4) The roller places the second layer of powder onto the built area and the process is repeated until the 3D structure is completed and the extra powder is removed.**

Additives are generally added to the raw material to influence the post-processing behaviour and the resulting properties of the sintered parts (Bose *et al.*, 2002). Particularly, a ceramic powder can be mixed together with polymeric grains, with the same or different particle sizes (Utela *et al.*, 2010). The addition of polymeric material, which will burn out during the heat treatment, will produce a ceramic structure with a degree of porosity and a level of interconnectivity that depends on the percentage as well as grain dimensions of the porogen (Seitz *et al.*, 2005; Vorndran *et al.*, 2008).

Regarding the printing parameters, the *layer thickness*, which depends partially on the material particle size, should be a compromise value to avoid *i)* binder penetration and over spreading (in the case of very thin layers), and *ii)* high saturation and difficulties for the powders to bond with possibility of displacement (in the case of too thick layers) (Tarafder *et al.*, 2013). The *powder packing density* is the density of powder that the roller spreads in the powder bed. If the resulting layer is not homogenous, specimen resolution and shape of the geometry can be compromised (Gibson *et al.*, 2014). The *flowability* of the powder plays a crucial role during the spreading phase, as it defines the spreading capability of the material (Schulze, 1995), but also during the *depowdering* process, which will be clarified later on in this paragraph (Butscher *et al.*, 2011). As the final resolution is usually at least twice the dimension of the powder particle size (Vacanti *et al.*, 2001), using fine powder is convenient to achieve high resolutions. However, dry and fine particles tend to agglomerate causing poor flowability, hence, a compromise between flowability and resolution is necessary (Butscher *et al.*, 2011).

Furthermore, another important aspect for the printing accuracy is the *powder wettability*. This parameter is generally related to surface energy and chemistry of the particles (Spori *et al.*, 2008). In particular, low wettability generates brittle binder-powder composites, resulting in low green body strength, whereas high wettability causes widespread of binder limiting the printing resolution (Hogekamp and Pohl, 2004; Butscher *et al.*, 2012). The *green strength* is another essential requirement of printed objects. It defines the mechanical properties immediately after the printing process and before the sintering treatment. An appropriate green strength is important to maintain handle ability, and to meet the final mechanical properties of the 3D printed part, since it influences the strength after the sintering treatment (Cox *et al.*, 2015). The depowdering process, which can be either manual or mechanical, is the last step of the printing procedure, and it is carried out to remove the loose powder from the printed specimens (Butscher *et al.*, 2011).

Subsequently, a heat treatment needs to be performed on the green bodies to burn out the binder and any additives used, and consolidate the structure. *Sintering* is the most important post-processing step, which provides an increased mechanical strength to the 3D printed object. Every material has specific sintering temperature, usually defined as the temperature where the maximal densification rate is being reached (Palmour *et al.*, 2013), although many factors such as grain size, specimen dimensions, heating rate, phase transformations, liquid phase formation and porosity can

affect the sintering properties of a material and its densification behaviour (Muralithran and Ramesh, 2000; Dorozhkin, 2010).

Additionally, during the sintering process the composition (*i.e.* phase changes), mechanical and structural properties of a material are also influenced (Butscher *et al.*, 2011). In most cases, heat treatment allows a structure to retain its shape, even though the process can cause a significant degree of sample shrinkage (Dorozhkin, 2010). This phenomenon can be compensated by scaling the initial CAD model according to a pre-determined correction factor (Shanjani *et al.*, 2010). Figure 3.15 shows the particles distribution before and during the sintering treatment and the resulting shrinkage behaviour.

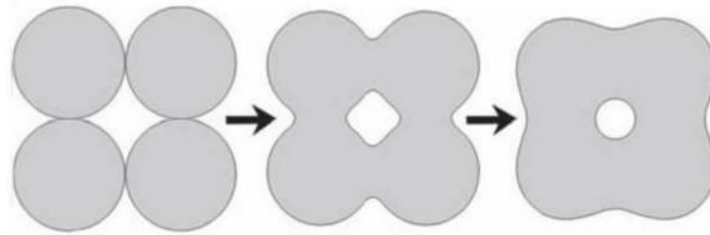


**Figure 3.15: Schematic representation of the sintering mechanism: a) particles free flowing, b) neck formations and c) voids shrinkage (reprinted by (Dorozhkin, 2010)).**

#### **3.4.2.1 3D printed ceramic-based scaffolds**

The use of 3DP technology has been widely documented for BTE applications, mainly processing bioactive ceramics, such as tricalcium phosphates, bioactive glasses and HA (Leukers *et al.*, 2005; Seitz *et al.*, 2005; Tarafder *et al.*, 2013; Cox *et al.*, 2015).

In recent years, several composite materials have been investigated for 3DP scaffold production using the combination of different ceramics or ceramics and polymers (Gbureck *et al.*, 2007; Khalyfa *et al.*, 2007; Will *et al.*, 2008). In 2005 Seitz *et al.* stated the applicability of 3DP methodology for the fabrication of a porous HA scaffold with internal channels between 450 and 570 $\mu$ m (Seitz *et al.*, 2005).

In 2010, Warnke *et al.* evaluated the biocompatibility of HA 3D printed scaffold and their ability to promote and support human osteoblast proliferation. Interestingly, their results found the superior biocompatibility of HA scaffold compared to the commercial available Geistlich BioOss<sup>®</sup>, a bone substitute material derived from the mineral portion of bovine bone. (Warnke *et al.*, 2010).

Later on, Tarafder *et al.* developed a 3D printed and microwave sintered  $\beta$ -TCP, with a high degree of interconnectivity along the structure (Figure 3.16) (Tarafder *et al.*, 2013). In another study, conducted in 2015 by Tarafder *et al.*, the properties of  $\beta$ -TCP scaffolds were improved, doping the main composition with SrO and MgO. A significant increase in mechanical strength was achieved as well as higher osteoid, bone and haversian canal formation, which are essential conditions for early wound healing and mineralisation *in vivo* (Tarafder *et al.*, 2015).

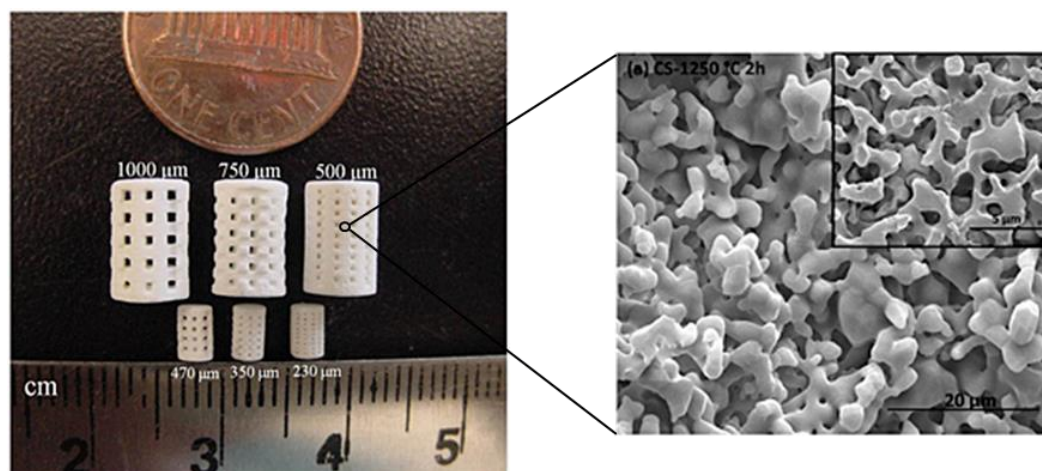


**Figure 3.16: 3D printed TCP scaffolds sintered at 1250 °C using a microwave furnace and the resulting surface morphology (inset) (Tarafder *et al.*, 2013).**

In addition to *in vitro* experiments, Habibovic *et al.* demonstrated how 3D printed brushite (dicalcium phosphate dihydrate) and monetite (dicalcium phosphate anhydrous) cements, with a controlled open porosity, enhance *in vivo* osteoconduction (Habibovic *et al.*, 2008).

More recently, Inzana *et al.* fabricated a 3D printed collagen-calcium phosphate composite *via* inkjet printing, and afterwards they assessed the healing performance using a critically sized murine femoral defect. After 9 weeks of implant the bone substitutes confirmed their osteoconductive properties (Inzana *et al.*, 2014). Furthermore, according to *in vivo* studies, 3D printed ceramic scaffolds hold great potential for bone tissue repair, showing invaluable biocompatibility and osteoconductivity (Habibovic *et al.*, 2008; Will *et al.*, 2008; Inzana *et al.*, 2014).

In Table 3.10 is reported a summary of mechanical and biological properties of the most investigated 3D printed ceramic-based substitutes intended for bone tissue applications.

In conclusion, despite the disadvantages of powder-based 3DP mentioned in this paragraph, and also described in Table 3.10, the broad range of biomaterials and the variety of designs that are

achievable with this technology makes it a promising and versatile approach for custom medical device production.

**Table 3.10: Mechanical and biological properties of some ceramic-based 3D printed scaffolds.**

Material	Sintering condition	Mechanical properties	Biological properties	Reference
HA	1250°C/2h	compressive strength: 21.2±2.2 MPa (dense part)	Cells were seeded on the scaffolds and cultivated under static and dynamic setups. This last method showed better results with a deep cell proliferation into the HA structure.	(Leukers <i>et al.</i> , 2005; Seitz <i>et al.</i> , 2005)
HA	1250°C/2h	compressive strength: 21.2±2.2 MPa (dense part)	Cell viability tests showed superior biocompatibility of HA scaffolds to BioOss®	(Seitz <i>et al.</i> , 2005; Warnke <i>et al.</i> , 2010)
β-TCP	1400°C	compressive strength: 8.66± 0.11 MPa (% porosity 46.07±8.52)	<i>In vitro</i> cytotoxic assays showed a good cell–scaffold interaction, thus revealing the scaffolds' biocompatibility	(Santos <i>et al.</i> , 2012)
β-TCP/ Bioglass	1000°C	bending strength: 14.9 ± 3.6 MPa	–	(Bergmann <i>et al.</i> , 2010)
HA/AW	1300°C/3h	bending strength: 35.22±6.56 MPa (% porosity 30.00±1.50)	<i>In vitro</i> tests showed that osteoblast cells attach and attain normal morphology on the surface of the 3D printed scaffolds.	(Suwanprateeb <i>et al.</i> , 2009)
Brushite	-	bending strength: 5.2 MPa	<i>In vivo</i> implantation of both brushite and monetite scaffolds showed their osteoinductive potential.	(Habibovic <i>et al.</i> , 2008;
Monetite	134°C/2h	bending strength: 3.9MPa		Klammert <i>et al.</i> , 2010)
TTCP/ β-TCP	1200°C/6h 1400°C/6h	compressive strength: 1.3±0.1MPa 3.9±0.1MPa	MC3T3-E1-cells grew on the scaffolds as adherent cell showing the increase in ALP activity over the 3 weeks in culture.	(Khalyfa <i>et al.</i> , 2007)
TTCP/ CaSO <sub>4</sub>	1000°C/6h	compressive strength: 0.1±0.01MPa	-	



## Chapter 4. Novel material design

---

### 4.1 Development and rationale of novel bioglass formulations

Bioactive glasses are one of the last glass subgroups that have been explored, revealing as promising materials for the production of 3D structures for bone tissue repair (Hench, 1999; Jones, 2013; Krishnan and Lakshmi, 2013).

However, since their discovery in 1969 by Hench, there are still several criticisms related to the clinical use of this class of biomaterials (Hench and Jones, 2015). Firstly, whether or not glass dissolution products have a positive effect on adult stem cells is still an open debate; secondly, they have often resulted inadequate when used in load-bearing bone defects, due to their low tensile strength and fracture toughness. Ultimately, there are no large-scale porous bioactive glasses on the market, thus their commercial success is limited (Rahaman *et al.*, 2011; Hench and Jones, 2015).

Based on the current state of the art, eight novel silicate, phosphate and borate glass formulations (coded as NCL<sub>x</sub>, where  $x=1,\dots,8$ ), containing different oxides and in diverse molar percentages, were initially proposed for this research. Specifically, ions such as Ca, Na, K and Mg were incorporated in all the glass compositions as they are essential elements for all living organisms, and they stimulate the cellular and sub-cellular processes of bone formation (Bracci *et al.*, 2009).

Furthermore, trace ions like Sr, Cu, Co or Zn are recognised for their anabolic effects in bone metabolism (Nielsen, 1990; Saltman and Strause, 1993; Meunier *et al.*, 2002; Pan *et al.*, 2010). Ag<sub>2</sub>O was selected since it is known to provide antibacterial effects if used as doping agent (Luo *et al.*, 2010; Balagna *et al.*, 2011). Sr, which can accumulate in bone due to its chemical similarity to Ca, has been widely investigated for its therapeutic potential in bone metabolism, and also for its property of reducing the incidence of fractures in osteoporotic patients (Gentleman *et al.*, 2010; Wu *et al.*, 2011; Tarafder *et al.*, 2015). Cu and/or Zn ions were incorporated for the importance of these elements in maintaining the bone matrix and bone density (Cousins, 1998); additionally, Cu helps collagen formation and plays an important role during angiogenesis, and Zn shows anti-inflammatory effects (Hu, 1998; Rodriguez *et al.*, 2002; Lai and Yamaguchi, 2005; Lang *et al.*, 2007; Finney *et al.*, 2009; Gerard *et al.*, 2010; Wu *et al.*, 2013). CaF<sub>2</sub> has been considered a promising network modifier since it has been demonstrated that F-doped bioactive glasses enhance

the formation of fluorapatite, which is chemically more stable than biological HA (Brauer *et al.*, 2010). Finally, Al and Fe were selected in order to increase the mechanical strength of the glasses (Hoppe *et al.*, 2011; Sharma *et al.*, 2012).

The molar compositions, along with the rationale and innovative characteristics of the novel materials with respect to previously developed glass formulations, are reported in Table 4.1.

**Table 4.1: Molar composition and rationale of the novel glass formulations.**

CODE	COMPOSITION (mol%)	RATIONALE	REFERENCE
NCL1		<p><b>Aim:</b> to develop a material with osteogenic properties, mainly determined by the presence of a high amount of silica.</p> <p><b>Network former:</b> <b>SiO<sub>2</sub></b>.</p> <p><b>Selected dopants</b></p> <p><b>Ca and P:</b> main components of biological apatite;</p> <p><b>Na, K and Mg:</b> essential elements for all living organisms, which stimulate the cellular and sub-cellular processes of bone formation;</p> <p><b>(Zn + Mn + Cu):</b> enhance the osteointegration of the material;</p> <p><b>SrO</b> reduce the incidence of fractures in osteoporotic patients;</p> <p><b>V:</b> beneficial effects during the normal development and metabolism of the skeleton;</p> <p><b>(Te + Bi):</b> improve the sinterability of the material.</p>	<p>(Yamaguchi, 1998; Silver <i>et al.</i>, 2001; Xynos <i>et al.</i>, 2001; Zreiqat <i>et al.</i>, 2002; Dietrich <i>et al.</i>, 2009; Gentleman <i>et al.</i>, 2010; Wu <i>et al.</i>, 2011; Sansone <i>et al.</i>, 2013; Tarafder <i>et al.</i>, 2015)</p>
	<p>40SiO<sub>2</sub> - 5P<sub>2</sub>O<sub>5</sub> - 8Na<sub>2</sub>O - 10CaO - 8K<sub>2</sub>O - 5MgO - 5MnO<sub>2</sub> - 5ZnO - 10SrO - 1CuO - 1Bi<sub>2</sub>O<sub>3</sub> - 1TeO<sub>2</sub> - 1V<sub>2</sub>O<sub>5</sub></p>		
NCL2		<p><b>Aim:</b> intended to develop a load-bearing material with osteogenic properties and tailored degradation rate.</p> <p><b>Network former:</b> <b>SiO<sub>2</sub></b>.</p> <p><b>Selected dopants</b></p> <p><b>P<sub>2</sub>O<sub>5</sub>, B<sub>2</sub>O<sub>3</sub>, MgO, and MnO<sub>2</sub>:</b> regulate the degradation process of the glass;</p> <p><b>B<sub>2</sub>O<sub>3</sub>, CaO, CaF<sub>2</sub>, Na<sub>2</sub>O and P<sub>2</sub>O<sub>5</sub>:</b> help the acellular bioactivity;</p> <p><b>Ca and P:</b> as for composition NCL1;</p> <p><b>Na, K:</b> as for composition NCL1;</p> <p><b>Al, Fe and F:</b> increase the mechanical properties;</p> <p><b>Se:</b> improve the healing process;</p> <p><b>Li, Mo, Cr:</b> known as trace elements in the human body.</p>	<p>(Abou Neel <i>et al.</i>, 2005; Demling, 2009; Hoppe <i>et al.</i>, 2011; Chen <i>et al.</i>, 2012; Sharma <i>et al.</i>, 2012; Whitney and Rolfes, 2013)</p>
	<p>45SiO<sub>2</sub> - 5P<sub>2</sub>O<sub>5</sub> - 2B<sub>2</sub>O<sub>3</sub> - 4Na<sub>2</sub>O - 15CaO - 3K<sub>2</sub>O - 8MgO - 2MnO<sub>2</sub> - 5Al<sub>2</sub>O<sub>3</sub> - 2CaF<sub>2</sub> - 5Fe<sub>2</sub>O<sub>3</sub> - 1Li<sub>2</sub>O - 1MoO<sub>3</sub> - 1SeO<sub>2</sub> - 1Cr<sub>2</sub>O<sub>3</sub></p>		

CODE	COMPOSITION (mol%)	RATIONALE	REFERENCE
NCL3	25SiO <sub>2</sub> - 2P <sub>2</sub> O <sub>5</sub> - 35B <sub>2</sub> O <sub>3</sub> - 6Na <sub>2</sub> O - 7CaO - 5K <sub>2</sub> O - 5MgO - 2Al <sub>2</sub> O <sub>3</sub> - 3TiO <sub>2</sub> - 5Fe <sub>2</sub> O <sub>3</sub> - 1Li <sub>2</sub> O - 1BaO - 1CoO - 1V <sub>2</sub> O <sub>5</sub> - 1Cr <sub>2</sub> O <sub>3</sub>	<i>Aim:</i> to develop a material with improved degradation rate and appropriate level of bioactivity as well as mechanical properties. <i>Network former:</i> B <sub>2</sub> O <sub>3</sub> . <i>Selected dopants</i>	(Carlisle, 1970; Carlisle, 1981;
		<b>Si:</b> essential for metabolic process, bone tissue formation and calcification <b>Ca and P:</b> as for composition NCL1; <b>Na, K and Mg:</b> as for composition NCL1; <b>V:</b> beneficial effects during the normal development and metabolism of the skeleton; <b>Co:</b> influences the thermal stability, sinterability and microstructure <b>(Al + Fe + Li + Ti):</b> responsible for the material strength; <b>Ba and Cr:</b> known as trace elements in the human body.	Singh and Bahadur, 1999; Singh and Srinivasan, 2010; Hoppe <i>et al.</i> , 2011; Vyas <i>et al.</i> , 2015)
NCL4	20SiO <sub>2</sub> - 5P <sub>2</sub> O <sub>5</sub> - 40B <sub>2</sub> O <sub>3</sub> - 5Na <sub>2</sub> O - 5CaO - 5K <sub>2</sub> O - 5MgO - 5ZnO - 5SrO - 2CaF <sub>2</sub> - 1CuO - 1MoO <sub>3</sub> - 1SeO <sub>2</sub>	<i>Aim:</i> to develop a material with tailored degradation rate and osteogenic effects. <i>Network former:</i> B <sub>2</sub> O <sub>3</sub> . <i>Selected dopants</i>	(Yamaguchi, 1998; Marion <i>et al.</i> , 2005; Lang <i>et al.</i> , 2007; Bonnelye <i>et al.</i> ,
		<b>Si:</b> as for composition NCL3; <b>Ca and P:</b> as for composition NCL1; <b>Na, K and Mg:</b> as for composition NCL1; <b>Zn:</b> plays anti-inflammatory role and helps bone formation; <b>Sr:</b> as for composition NCL1; <b>CaO, CaF<sub>2</sub>, Na<sub>2</sub>O and P<sub>2</sub>O<sub>5</sub>:</b> help the acellular bioactivity; <b>Cu, Mo and Se:</b> known as trace elements in the human body.	2008; Liang <i>et al.</i> , 2008; Fu <i>et al.</i> , 2010c; Gentleman <i>et al.</i> , 2010; Pan <i>et al.</i> , 2010; Hoppe <i>et al.</i> , 2011)

CODE	COMPOSITION (mol%)	RATIONALE	REFERENCE
NCL5	45P <sub>2</sub> O <sub>5</sub> - 7Na <sub>2</sub> O - 10CaO - 6K <sub>2</sub> O - 10MgO - 5ZnO - 5MnO <sub>2</sub> - 10SrO - 1TiO <sub>2</sub> - 1Sb <sub>2</sub> O <sub>3</sub>	<p><i>Aim:</i> to develop a resorbable glass with controlled degradation rate.</p> <p><i>Network former:</i> P<sub>2</sub>O<sub>5</sub>.</p> <p><i>Selected dopants</i></p> <p><b>Ca:</b> involved in bone metabolism, enhances osteoblast proliferation, differentiation and ECM mineralisation;</p> <p><b>Na, K and Mg:</b> essential elements for all living organisms, which stimulate the cellular and sub-cellular processes of bone formation;</p> <p><b>(MgO, TiO<sub>2</sub>, MnO<sub>2</sub> and SrO):</b> regulate the degradation rate of the glass</p> <p><b>Zn:</b> as for composition NCL4;</p> <p><b>Sr:</b> as for composition NCL1.</p>	<p>(Yamaguchi, 1998;</p> <p>Maeno <i>et al.</i>, 2005;</p> <p>Barrère <i>et al.</i>, 2006; Lang <i>et al.</i>, 2007; Bonnelye <i>et al.</i>, 2008; Abou Neel <i>et al.</i>, 2009a; Gentleman <i>et al.</i>, 2010; Leonardi <i>et al.</i>, 2010; Hoppe <i>et al.</i>, 2011; Novajra <i>et al.</i>, 2011; Vitale-Brovarone <i>et al.</i>, 2011; Lakhkar <i>et al.</i>, 2013)</p>
NCL6	8SiO <sub>2</sub> - 50P <sub>2</sub> O <sub>5</sub> - 10B <sub>2</sub> O <sub>3</sub> - 8Na <sub>2</sub> O - 10CaO - 3K <sub>2</sub> O - 10MgO - 2MnO <sub>2</sub> - 2CaF <sub>2</sub> - 1CuO - 1CoO - 1Cr <sub>2</sub> O <sub>3</sub>	<p><i>Aim:</i> to develop a resorbable glass with controlled degradation rate, and improved mechanical strength.</p> <p><i>Network former:</i> P<sub>2</sub>O<sub>5</sub>.</p> <p><i>Selected dopants</i></p> <p><b>Si:</b> as for composition NCL3;</p> <p><b>B:</b> stimulates bone formation; also, B<sub>2</sub>O<sub>3</sub> helps the bioresorbability of the glass;</p> <p><b>Ca:</b> as for composition NCL5;</p> <p><b>Na, K and Mg:</b> as for composition NCL5;</p> <p><b>(Mg + F):</b> improve the microhardness of the glass;</p> <p><b>(Cu + Co +Cr):</b> enhance the sintering ability.</p>	<p>(Saranti <i>et al.</i>, 2006; Sun <i>et al.</i>, 2010; Hoppe <i>et al.</i>, 2011; Mourino <i>et al.</i>, 2012)</p>

CODE	COMPOSITION (mol%)	RATIONALE	REFERENCE
NCL7	50SiO <sub>2</sub> - 5P <sub>2</sub> O <sub>5</sub> - 15Na <sub>2</sub> O - 15CaO - 2K <sub>2</sub> O - 3MgO - 5AgO - 2TiO <sub>2</sub> - 2Fe <sub>2</sub> O <sub>3</sub> - 1CuO	<p><b>Aim:</b> intended to develop a material with antibacterial properties, mainly determined by the presence of silver oxide, and a good level of bioactivity.</p> <p><b>Network former:</b> SiO<sub>2</sub>.</p> <p><b>Selected dopants</b></p> <p><b>Ca and P:</b> main component of biological apatite;</p> <p><b>Na, K and Mg:</b> essential elements for all living organisms, which stimulate the cellular and sub-cellular processes of bone formation;</p> <p><b>Ag:</b> exhibits inhibitory effects on bacteria growth;</p> <p><b>Ti, Fe and Cu:</b> enhance osteoblast proliferation and activity;</p> <p><b>(Ti + Fe):</b> increase the mechanical properties of the material.</p>	(Vrouwenvellder <i>et al.</i> , 1994; Valappil <i>et al.</i> , 2007; Luo <i>et al.</i> , 2010; Balagna <i>et al.</i> , 2011; Hoppe <i>et al.</i> , 2011)
NCL8	45SiO <sub>2</sub> - 5P <sub>2</sub> O <sub>5</sub> - 2B <sub>2</sub> O <sub>3</sub> - 10Na <sub>2</sub> O - 15CaO - 5K <sub>2</sub> O - 5MgO - 5MnO <sub>2</sub> - 1ZnO - 1Fe <sub>2</sub> O <sub>3</sub> - 1SrO - 2.5CaF <sub>2</sub> - 0.5CuO - 0.5CoO - 0.5MoO <sub>3</sub> - 0.5SeO <sub>2</sub> - 0.5Cr <sub>2</sub> O <sub>3</sub>	<p><b>Aim:</b> intended to develop a material with osteogenic properties and tailored degradation rate for non-load bearing applications.</p> <p><b>Network former:</b> SiO<sub>2</sub>.</p> <p><b>Selected dopants</b></p> <p><b>P<sub>2</sub>O<sub>5</sub>, B<sub>2</sub>O<sub>3</sub>, MgO, and MnO<sub>2</sub>:</b> as for composition NCL2;</p> <p><b>B<sub>2</sub>O<sub>3</sub>, CaO, CaF<sub>2</sub>, Na<sub>2</sub>O and P<sub>2</sub>O<sub>5</sub>:</b> as for composition NCL2;</p> <p><b>Na, K, Mg:</b> as for composition NCL1</p> <p><b>Zn, Sr, Cu, Co, Mo, Se and Cr:</b> known as trace elements in the human body.</p>	(Murphy <i>et al.</i> , 2010; Hoppe <i>et al.</i> , 2011; Chen <i>et al.</i> , 2012; Whitney and Rolfes, 2013)

## Chapter 5. Experimental methods

---

### 5.1 Research approach

In order to obtain gradual confirmation of the feasibility of the main aim of this study, the overall research project was developed through three sequential stages:

- i)* glass powders preparation and characterisation;
- ii)* bioceramic pellets preparation and characterisation (dense materials);
- iii)* 3D printed bioceramic structures preparation and characterisation (porous materials).

An overview of the experimental work carried out during each phase is reported in Table 5.1.

Starting with the production of the new glasses (described in paragraph 5.2), this chapter deals with the material processing (reported in paragraph 5.3), and the characterisation methods performed during each stage (presented in paragraph 5.4).

### 5.2 Material production

The novel glasses were produced and supplied by Glass Technology Service (GTS) Ltd (Sheffield, UK) along with AW that will be used as comparison material. Briefly, the individual components (reported in Table 4.1) of each formulation were weighed out and then mixed together to obtain a uniform blend ready to be processed. Subsequently, the glass mixtures were melted in platinum crucibles for times and temperatures, which varied according to the composition.

.

**Table 5.1: Overview of the experimental work performed on: glass powders, bioceramic pellets and 3D printed bioceramic structures.**

MATERIAL	EXPERIMENTAL WORK	COMMENTS	CHAPTER
Glass powders	Crystallinity (XRD) Morphological characterisation (SEM) Thermal properties (HSM) pH variation in dH <sub>2</sub> O Ionic release (ICP-OES) <i>In vitro</i> cytotoxicity assessment	During the first stage of the work the processing and characterisation of all the novel glass formulations were performed.	6
Bioceramic pellets	Sintering condition optimisation Morphological characterisation (SEM) Shrinkage evaluation Crystallinity (XRD) Mechanical properties assessment	In the second stage the processing to bioceramic pellets and the subsequent characterisation of the sintered dense structures was carried out.	6
Bioceramic pellets	<i>In vitro</i> bioactivity tests (SBF)	On the basis of the physico-chemical, mechanical and biological characterisation results, only three formulations were selected for bioactivity tests.	6
3D printed bioceramic scaffolds	Sintering condition optimisation Morphological characterisation (SEM) Shrinkage evaluation Porosity and micro-architecture (microCT) evaluation Mechanical properties assessment <i>In vitro</i> cytotoxicity assessment <i>In vitro</i> antibacterial tests	In the last part of the work, the three formulations previously selected were processed to porous 3D printed scaffolds ( <i>via</i> a powder-based 3DP technology), and subsequently characterised.	7



## 5.3 Material processing

### 5.3.1 Glass powders

Glass frits of all the materials were ground in a one-bowl zirconia ball milling machine (Planetary Mono Mill Pulverisette 6, Fritsch GmbH, Germany) using a rotational speed of 400rpm for 30 min (10 min each repetition). The obtained powders were then sieved using a mechanical sieve shaker (Impact Test Equipment Ltd, UK) to have a final particle size about 20 $\mu$ m and below 53 $\mu$ m (Boccaccini *et al.*, 2007).

### 5.3.2 Bioceramic pellets

Dense bioceramic pellets were processed from fine glass powders, previously sieved as described in section 5.3.1. Firstly the raw material ( $0.35\pm0.01$ g) was carefully mixed together with isopropanol solution (Sigma-Aldrich, UK) in the proportion 3:1 (w/w), until the particles bound together and a paste-like texture was formed. Then it was left to dry for about 40s at room temperature. Afterwards, the mixture was placed into a 10mm cylindrical die and cold pressed using an automatic hydraulic press (Specac-Atlas<sup>TM</sup> 8T, Specac Ltd., UK) for 2 minutes under a load of 1 tonne (Figure 5.1).



**Figure 5.1:** Specac Atlas 8T automatic hydraulic press (<http://www.specac.com/>).

Subsequently, the pressed pellets, also called green bodies, were treated through a sintering process to consolidate their structure. As reported in chapter 2, the sintering temperature is usually defined as the temperature where the maximal densification rate is being reached (Palmour *et al.*, 2013). Hence, the pressed green bodies were placed in a furnace (Carbolite 1200 CWF, Carbolite GmbH,

Germany) and heat treated according to the results derived from the hot stage microscopy analysis that will be described in section 5.4.2.

### 5.3.3 Indirect 3D printed bioceramic substitutes

Figure 5.2 schematically represents the three different phases of the entire 3D printing fabrication process: *i)* pre-processing, *ii)* processing and *iii)* post-processing, which are described in detail in the following paragraphs.

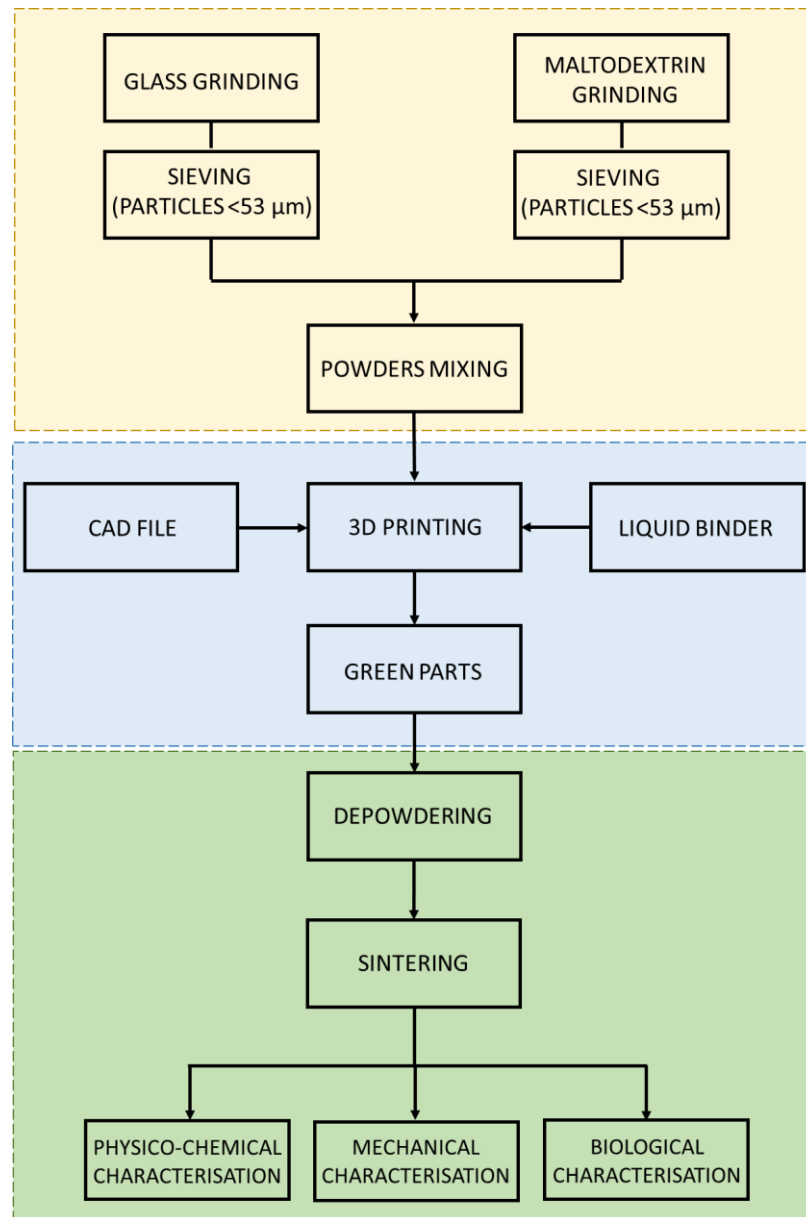


**Figure 5.2:** Flow chart describing the three stages of the 3D printed scaffold fabrication: pre-processing (yellow), processing (blue) and post-processing (green).

#### 5.3.3.1 Powder blend preparation

Once received from GTS Ltd., the starting materials were processed to glass powders according to the procedure reported in the paragraph 5.3.1. As the particle size affects the printing results as well as the properties of the final parts (Sachs *et al.*, 1992; Bredt *et al.*, 2003; Utela *et al.*, 2008; Bergmann *et al.*, 2010; Butscher *et al.*, 2012; Farzadi *et al.*, 2015), for this study the range of particle diameters was chosen between 0 and 53 $\mu$ m.

Subsequently, each powder formulation was mixed together with MD (Oneon, Bristol, UK) in the same range of particle size. Before the printing process, to achieve a homogeneous mixture, the two base materials (70wt.% of glass powders and 30wt.% of MD) were blended for 1h using a roller mixer (Stuart, SRT6) (Figure 5.3).



**Figure 5.3: Powder blend preparation using a roller mixer.**

MD was used as an in-bed and solid binder to improve the printing behaviour of the powder, and to react with the jetted liquid binder, enhancing the adhesion between the glass particles but also leading to a porous final structure.

The liquid binder (zb®60), which consists of a water-based solution, was purchased from EMCO Education Ltd, UK.

#### 5.3.3.2 Design of 3D structures

Two different geometries were drawn using Autodesk Inventor® (Autodesk, USA): a cylindrically shape with height of 2.25mm and 10.35in diameter, and a bar shape with height 5mm, width 6mm and length 40mm, as reported in Figure 5.4.

The CAD files were then saved in .stl format, and processed by the ZCorp 310 software, prior to printing.

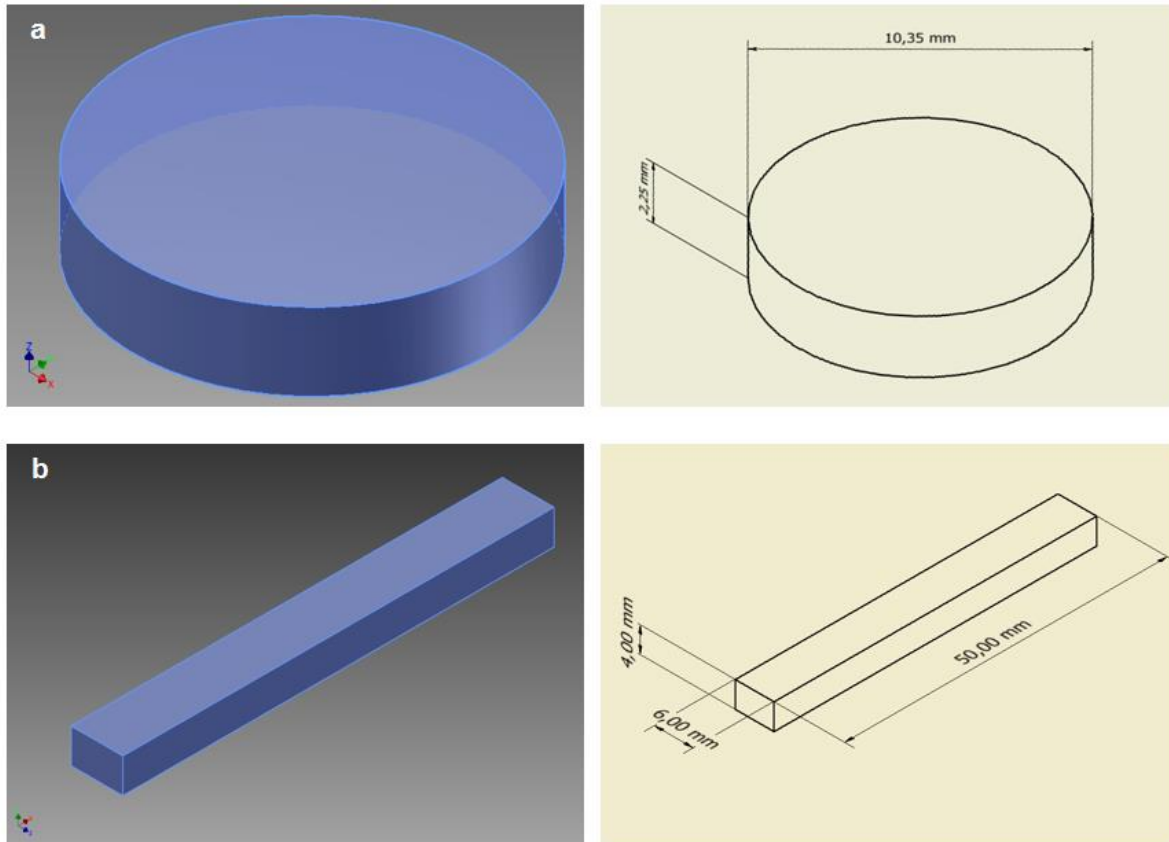


**Figure 5.4:** CAD design of the 3DP: a) cylindrical and b) bar shape structures.

### 5.3.3.3 Indirect powder-based 3D printing: the process

A commercial ZPrinter® 310 Plus 3D printer (Z Corporation, USA), illustrated with all its main components in Figure 5.5, was used to print all the samples of this research study. Before starting the process, the blended powder was poured into the build area and pressed to get a firm layer. Once a flat and compact surface was obtained, the feed piston was moved up to the same level as the build piston.

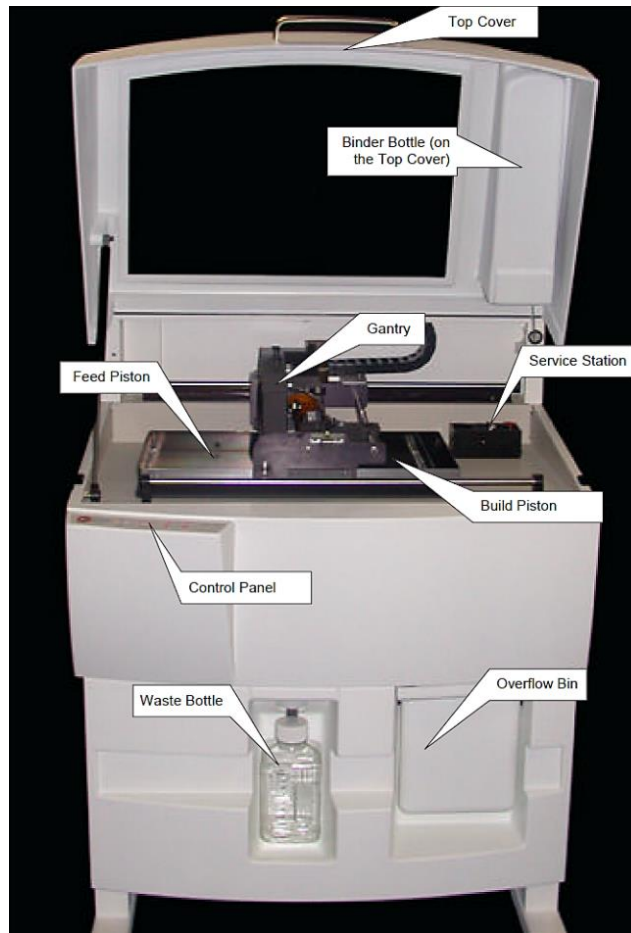


**Figure 5.5: Commercial ZPrinter® 310 Plus 3D printer (Z Corporation, USA) and its main components**  
([www.zcorp.com](http://www.zcorp.com)).

The printing parameters were adjustable through the Z310 Plus software (graphic interface is shown in Figure 5.6). They were selected on the basis of the optimisation process developed and described by Alharbi (Alharbi, 2015), and maintained the same for all the powder blends (see Table 5.2).

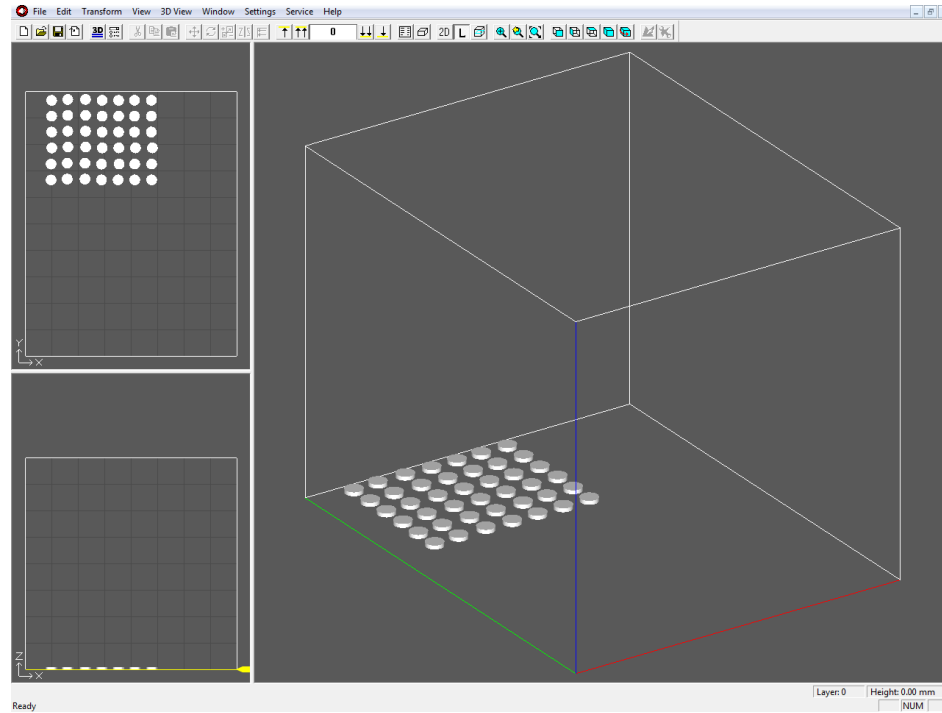


**Figure 5.6: Graphic interface of ZPrint 7.10 software.**

**Table 5.2: Powder blend settings for ZPrinter® 310 Plus 3D printer.**

Layer thickness (mm)	Saturation level		Binder/volume ratio		Bleed compensation		
0.1	Shell	Core	Shell	Core	X	Y	Z
	100%	100%	0.21	0.10	Off	Off	Off

After the printing process was completed, which usually took approximately 10min to print 20 cylindrical scaffolds and 12min to print 10 bars (see CAD model in Figure 5.4), the green parts were left to dry overnight before being removed from the build area. Once taken out, any loose powder still present on the specimens was cleaned out using an air blower. The green bodies, with a relatively weak and delicate structure were thermally post-processed through a sintering treatment, using the same equipment described in section 5.3.2. A number of different heat treatments, according to the results derived from the hot stage microscopy (section 5.4.2), were evaluated to burn out the organic binder from the green bodies and to sinter the glass powders, obtaining mechanically competent porous structures.

## 5.4 Characterisation methods

Various techniques were applied to characterise firstly the glass powders, then the bioceramic pellets and finally the 3D printed structures. These include: hot stage microscopy (HSM) to evaluate the sintering parameters, scanning electron microscopy (SEM) to assess particles and structure morphology, and X-ray diffraction (XRD) to investigate the crystalline composition. Tests in simulated body fluid (SBF) were also performed to assess the bioactive behaviour of the new materials. Furthermore, pH variation analysis as well as ionic release in different liquid solutions and at specific time points were measured. Additionally, the mechanical and biological properties in different conditions were evaluated. Details of these techniques and their experimental settings are given in the following sections.

### 5.4.1 X-ray diffraction analysis

To investigate the presence of crystalline phases in the novel materials, XRD analysis was performed using a PANalytical X'Pert Pro MPD, powered by a Philips PW3040/60 X-ray generator fitted with an X'Celerator detector. Diffraction data was acquired by exposing powder samples to Cu-K $\alpha$  X-ray radiation, which has a characteristic wavelength ( $\lambda$ ) of 1.5418Å. X-rays were generated from a Cu anode supplied with 40kV and a current of 40mA.

The data were collected over a  $2\theta$  range between 5-80°  $2\theta$ , with a step size equal to 0.0334°, a counting time per step of 200 seconds using the scanning X'Celerator detector. Fixed anti-scatter and divergence slits of 1° were used together with a beam mask of 10mm. All scans were carried out in 'continuous' mode.

Phase identification was carried out by means of the PANalytical X'Pert HighScore Plus© software, in conjunction with the ICDD Powder Diffraction File 2 Database (2004), ICDD Powder Diffraction File 4 - Minerals (2014) and the Crystallography Open Database (February 2013; [www.crystallography.net](http://www.crystallography.net)).

### 5.4.2 Hot stage microscopy

The sintering ability of the novel glass powders was determined by using hot stage microscopy (Misura®, Expert System Solutions, Italy). This technique allowed the quantification of the sintering interval by measuring the variation of the sample dimensions during the heating treatment (Bretcanu *et al.*, 2009).

The test was performed in air to approximate the conditions inside the furnace chamber during the heating process, which develops with a rate of 10°C/min up to 1200°C. The samples for HSM analysis were prepared by manually pressing the glass powders into a small cylindrical die (2x3mm) and placed on a 10x15x1 mm alumina support. During the process the specimens were observed by a video camera and images of the changing sample profile were acquired up to 1450°C. Afterwards, the shrinkage–temperature curves were analysed and the shrinkage at different temperatures was calculated from the reduction of the sample dimensions, using the following formula:

$$\text{shrinkage (\%)} = \frac{A_0 - A_T}{A_0} \times 100$$

where  $A_0$  ( $\text{mm}^2$ ) is the area of the sample at instant  $(t - 1)$  and  $A_T$  ( $\text{mm}^2$ ) is the area at instant  $t$ .

### ***5.4.3 Morphological and microstructural characterisation***

#### ***5.4.3.1 Scanning electron microscopy***

To assess the glass particle morphology and the bioceramic pellet surface, microstructural observations were determined by scanning electron microscope, (Philips XL30 ESEM FEG, which is fitted with a Rontec Quantax system for the EDS analysis). Furthermore, morphological analysis were conducted before and after the sintering process of the specimens to determine if the heat treatment had any detrimental effect on bulk structure. The formation of neck struts and appropriate densification level were examined.

Before the imaging acquisition, the specimens were sputtered with a thin layer of gold (approximately 10nm, sputter time 40s at 40mA), and afterward analysed. All the images were taken at an operation voltage of 20 kV, and working distance between 5 and 10mm.

#### ***5.4.3.2 X-ray microtomography***

Scaffold architecture and structural interconnectivity was also investigated by micro-computed tomography (micro-CT; XRadia/Zeiss VersaXRM-410). The scanner was set at a voltage between 60 and 80kV and a current of 248A, and the samples were scanned with an isotropic voxel size of 2.4µm by approximately 1600 slices covering the sample height. Afterward, the scanned 2D slices



were reconstructed to give 3D views of the entire structure using Avizo Fire software (Durham University, UK).

#### 5.4.3.3 Analysis of the porosity

The open porosity of the samples, which represent the percentage of pores that are penetrated by an immersion liquid or that are connected with the atmosphere, was measured according to the BS EN 623-2:1993 using Archimedes method with the following formula:

$$\text{Open porosity (\%)} = \frac{(m_2 - m_1)}{(m_2 - m_3)} \times 100$$

Samples were weighed by means of a density determination kit in an analytical balance (Kern ABT220-5DM). The dry weight of the samples was recorded as  $m_1$ . Then, they were immersed in distilled water to force the liquid to fill the pores of the samples until no bubbles emerged from the water baker and the submerged mass ( $m_3$ ) was measured. Afterward, the specimens were taken out and re-weighed to calculate the wet mass ( $m_2$ ) in air.

Five specimens for each group were tested to calculate the average porosity. The results were expressed as mean  $\pm$  standard error of the mean (SE).

The total porosity, given by the sum of the close and open porosity, was measured according to the formula:

$$\text{Total porosity (\%)} = 1 - \frac{m_s}{\rho V_s} \times 100$$

where  $m_s$  is the dry mass of the sample,  $\rho$  is the density of the material and  $V_s$  is the volume of the sample. Five specimens for each group were tested to calculate the average porosity. The results were expressed as mean  $\pm$  standard error of the mean.

The density of the material in turn was calculated through the pycnometer method (ISO 1183-1:2004), using the formula reported below:

$$\rho = \rho_l \frac{m_2}{(m_1 + m_2 - m_3)}$$

where  $\rho_l$  is the density of the liquid,  $m_1$  is the mass of the liquid in the pycnometer filled completely with liquid,  $m_2$  is the mass of the sample material and  $m_3$  is the mass of the sample and liquid together in the pycnometer. The average of five specimens for each composition was considered.

#### ***5.4.4 pH variation***

A pH meter (Mettler Toledo Ltd., UK) was used to measure the effect induced by the novel glass compositions on the pH variation. The meter was calibrated with standard solutions (at pH 4 and 7) every time before use. Specifically, the pH values induced by raw glass powder, considered the most critical scenario, were measured daily up to 7 days to verify its confinement within a “physiological range”. Un-sintered glass powders with a concentration of 10 mg/ml were immersed in deionised water (Veolia Water Technologies, UK) and incubated under an atmosphere of 5% CO<sub>2</sub> and 95% air at 37°C. Two different tests were performed: *i*) an extreme condition, without changing the solution, and *ii*) a more realistic one to simulate the physiological fluids exchange, refreshing the solution every 48h.

#### ***5.4.5 Ion leaching evaluation***

In order to evaluate the ionic release potential of each composition, raw glass powders were immersed in deionised water (Veolia Water Technologies, UK) at a concentration of 10 mg/ml and stored in static condition at 37°C. After each storage period, the specimens were removed *via* filtration, and filtrates retained for ionic content analysis.

The ion concentration was measured using an inductively coupled plasma optical emission spectrometer (ICP-OES) Spectro-Ciros-Vision (Sheffield University, UK), which allows simultaneous multi-element analysis following the calibration of the instrument by introduction of standards of known concentrations of the elements of interest.

#### ***5.4.6 Shrinkage evaluation***

In most cases, heating treatments cause the shrinkage of ceramic samples. Specifically, the structure retains its shape producing a significant degree of reduction of its dimensions. Hence, dimensional changes of the sintered specimens were carefully evaluated. The following formula was applied to calculate the volumetric shrinkage that occurred during the sintering treatment of bioceramic pellets and 3D printed structures:

$$\text{Volumetric shrinkage (\%)} = \frac{V_1 - V_2}{V_1} \times 100$$

where  $V_1(mm^3)$  is the volume of the sample before sintering and  $V_2(mm^3)$  is the volume of the sample after sintering. To measure the dimensions of the specimens a digital caliper (accuracy of  $\pm 0.02mm$ ) was used (Mitutoyo Ltd, UK).

#### **5.4.7 Mechanical characterisation**

##### **5.4.7.1 Compressive test**

The mechanical properties of the sintered pellets were measured using a Tinius Olsen, universal testing machine (Figure 5.7). In this study, cylindrical samples were prepared with diameters of about  $8.5 \pm 0.5$  mm and a thickness of about  $2.5 \pm 0.3$  mm.

Five pellets for each composition were evaluated at room temperature and in dry conditions, according to previous work (Prakasam *et al.*, 2015). For all the experimental tests, the machine was equipped with a 25 kN load cell and the cross-head speed was set at 1 mm/min. Since the specimens were too hard, they did not reach the failure point, hence the stress ( $\sigma_c$ ) after the 20% of the initial deformation ( $\epsilon_c$ ) was calculated rather than the compressive strength of the dense pellets. The compressive modulus ( $E_c$ ) was determined as the slope of the initial linear part of the stress-strain curve (C773, 1988). All the results were expressed as mean  $\pm$  SE.

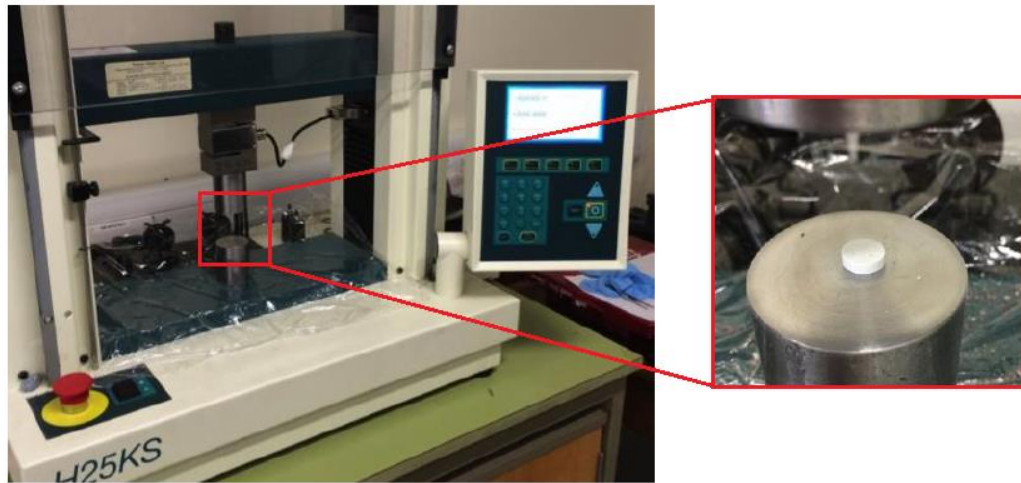


**Figure 5.7: Compressive test performed using a Tinius Olsen universal testing machine; inset shows the specimen before the test.**

#### 5.4.7.2 Three-point bending test

Regarding the mechanical properties of the 3D printed structures, flexural strength and flexural modulus were determined by a three-point bending test, using an INSTRON 5567 testing machine (Figure 5.8).



**Figure 5.8:** Three-point bending test determined by an INSTRON 5567 universal testing machine.

The conditions of the test were performed according to the ASTM C1161 – 13 standard. Beam shaped specimens with dimensions of 40x4x3mm were produced; the cross-head speed of the machine was set at 1mm/min, and the support span length at 20mm. A load cell of 1kN was used, and five replicates were tested (Figure 5.9).

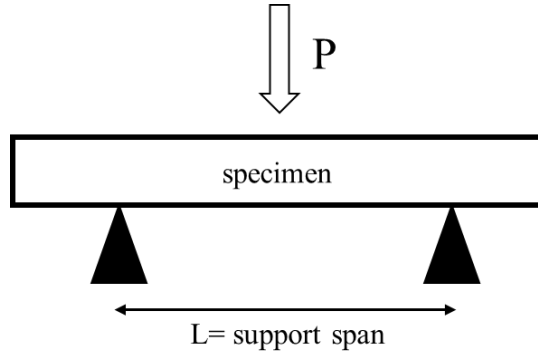


**Figure 5.9:** Schematic representation of the three-point bending test conditions.

The flexural strength ( $\sigma_f$ ) was calculated according to the following equation:

$$\sigma_f = \frac{3PL}{2bd^2}$$

where  $P$  represents the applied load (N),  $L$  (mm) is the support span length,  $b$  (mm) is the sample width and  $d$  is the depth (mm). The flexural modulus ( $E_f$ ) was calculated according to the following equation:

$$E_f = \frac{L^3 m}{4bd^3}$$

where  $L$  (mm) represents the support span length,  $m$  (N/mm) is the gradient (*i.e.* slope) of the initial linear part of the load deflection,  $b$  (mm) is the sample width, and  $d$  (mm) is the sample depth. All the results were expressed as mean  $\pm$  SE.

#### 5.4.8 *In vitro* bioactivity evaluation

In order to assess the bioactive potential of the novel materials, raw glass powders were processed as sintered pellets (following the procedure described in section 5.3.2) and then soaked in 10 ml of a simulated body fluid (SBF) solution prepared according to Kokubo's protocol (Kokubo and Takadama, 2006).

The specimens were incubated at constant temperature (37°C) for various time points (1, 3, 7, 14 and 28 days), refreshing the solution every 2 days. At the end of each time interval the specimens were removed from SBF, then abundantly rinsed with deionised water (Veolia Water Technologies, UK) and dried at room temperature. The pH of the solutions was measured using the equipment reported in paragraph 5.4.4 and the ion leaching was evaluated according to the procedure described in paragraph 5.4.5. Furthermore, the structural characteristics and chemical composition of the upper surface of the samples were investigated by SEM/EDS (experimental set-up described in section 5.4.3.1). Moreover, the sample solubility was quantitatively assessed by measuring the weight loss of the immersed pellets after 1, 3, 7, 14 and 28 days of soaking, using an analytical balance (Kern ABT220-5DM), according to the following formula

$$\text{Weight loss (\%)} = \frac{M_{bi} - M_{af}}{M_{bi}} \times 100$$

where  $M_{bi}$  is the mass of the sample before the immersion and  $M_{af}$  is the mass of the sample after the immersion.

Additionally, to quantitatively evaluate the composition of the precipitates, X-ray photoelectron spectroscopy (XPS) was performed using Theta Probe (Thermo Scientific, East Grinstead, UK),

with a micro-focused AlKa X-ray source (1486.6eV), operated with a 400µm spot size (100W power). Survey spectra were collected at a pass energy of 200eV, with the spectrometer operated in standard (not angle-resolved) lens mode. The results were expressed as the average of three points of each sample surface.

#### ***5.4.9 Biological characterisation***

The *in vitro* cytotoxicity of the novel glass formulations was evaluated *via* metabolic activity using the MTT (3-(4,5-dimethylthiazol-2-yl)-2,5-diphenyl tetrazolium bromide) colorimetric assay according to ISO 10993-5 (Standard, 2009), firstly on the glass powders and afterward on the 3D printed scaffolds.

##### ***5.4.9.1 Cell culture***

Rat calvaria osteoblast (OB) cells at early passages (Figure 5.10), provided by Institute of Cellular Medicine (Medical School, Newcastle University, UK), were cultured in T75 flasks at 37°C in a humidified incubator with 5% CO<sub>2</sub>, using Dulbecco's Modified Eagle Medium (D-MEM, Gibco®) supplemented with 10% fetal bovine serum (FBS), 1% penicillin-streptomycin and 1% glutamine (Gibco®). When 70-80% confluent, the flasks were washed twice with 5mL of phosphate buffered solution (PBS, Lonza) and afterward trypsinised using 1.5mL of trypsin-EDTA (Gibco®) and incubated for 5 minutes at 37°C, 5% CO<sub>2</sub>. The detachment of the cells from the flasks was monitored using light microscopy. When the cells were detached, 8.5mL of fresh D-MEM was added to neutralise the trypsin. The cell suspension was placed in a tube and centrifuged for 5min at 1200rpm. The supernatant was carefully removed and the cell pellet was re-suspended in an appropriate amount of media for cell counting using a haemocytometer.

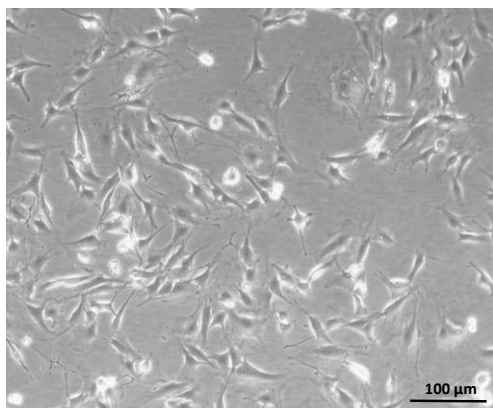


***Figure 5.10: Morphology of rat osteoblast cells.***

#### 5.4.9.2 *Glass powder cytotoxicity*

Cells were seeded at a density of  $1 \times 10^4$  cells/well in 96-well plates and incubated at 37°C for 24 hours. The glass powders were firstly sterilised using 100% ethanol solution, and then preconditioned for 24h in D-MEM at three different concentrations (0.1, 1 and 10mg/ml), in order to stabilise the pH variation due to the ionic exchange process between the powder surface and medium. The cells seeded on cell culture plate (0 mg/ml) were used as controls. Each condition was set up in triplicate. After 24 hours of incubation for the cells, two different experiments were performed:

- i) *direct method*, according to which the pre-conditioned DMEM solutions with the glass powders were directly added to each well without filtering, diluting or buffering;
- ii) *indirect method*, in which case after 24h of immersion in DMEM, the pre-conditioned glass powders were filtrated using a 0.22µm microbiological filter. The filtrated solutions were then added to each well for indirect cytotoxicity testing.

The plates were then incubated for other 24h and the cytotoxic effect was measured exposing each well to MTT solubilisation. The MTT (Sigma–Aldrich, UK) substrate was prepared in a D-MEM solution at a final concentration of 0.5mg/ml. After each time point, 100 µl of MTT solution was added to each well and incubated at 37°C for another 4 h. MTT was taken up only by active cells and reduced in their mitochondria to insoluble purple formazan granules. The medium was then removed and 100µl of dimethyl sulfoxide (DMSO) was added to dissolve the precipitated formazan. The absorbance of the solution was evaluated spectrophotometrically at a wavelength of 570nm, and acquired using a Sunrise microplate reader (Tecan Group Ltd., Switzerland).

The absorbance values from three replicates were averaged and statistically analysed using two-way analysis of variance (ANOVA) followed by Bonferroni *post hoc* analysis. P-values < 0.05 (\*) were considered statistically significant, whereas P-values < 0.001 (\*\*) were considered very significant.

#### 5.4.9.3 *In vitro evaluation of 3D printed scaffolds*

For the *in vitro* biological characterisation, bioceramic 3D printed scaffolds (8mm diameter and 2mm height) were firstly sterilised in autoclave (10 min at 121°C), and then, similarly to the glass powders, they were preconditioned for 24h in D-MEM. After the preconditioning time, rat OB cells

were seeded at a density of  $50 \times 10^5$  cells/ml onto the top surface of the scaffolds placed in a 24-well plate. Once the cells were seeded, they were left undisturbed in an incubator at 37 °C for 1 h to allow their attachment. Then, an additional 1ml of culture medium was added to each well in order to provide the right amount of nutrients to the cells. Fresh medium was replaced every 2 days.

The MTT solution was prepared according to the experimental procedure described in section 5.4.9.2. After 1, 3 and 7 days of culture, 1 ml of MTT solution was added to each well and incubated at 37°C for another 4 h. The medium was then removed and 500µl of DMSO was added to dissolve the precipitated formazan. Each time point of the assay was carried out in triplicate for both direct and indirect methods and six samples were tested for each of the two methods. The cells seeded on the polystyrene standard culture microplate were used as a conventional 2-D control. Also in this case, the absorbance of the solution was evaluated spectrophotometrically at a wavelength of 570nm, and acquired using the Sunrise microplate reader (Tecan Group Ltd., Switzerland).

The results were reported as the averaged absorbance levels of six replicates. A two-way analysis of variance (ANOVA) followed by Bonferroni *post hoc* analysis was performed to determine the statistical significance of the differences in the absorbance values. P-values < 0.05(\*) were considered statistically significant whereas P-values < 0.001(\*\*) were considered very significant.

Additionally, in order to evaluate the effect of the 3D printed scaffolds on the culture conditions, the pH of the medium as well as the resulting ionic release, determined by means of ICP-OES, were measured up to 7 days in culture.

#### **5.4.9.4 Antibacterial tests**

The antibacterial potential of NCL7 formulation was assessed through the inhibition zone test (or also called agar diffusion test) ('Performance Standards for Antimicrobial Disk Susceptibility Tests; Approved Standard—Eleventh Edition ', 2012) in collaboration with the Dental School of Newcastle University (Oral Biology Dpt.), using *Staphylococcus aureus* provided by Cramlington Hospital (UK) from an infected joint. The test was performed on: *i*) glass powder solutions (particle size 0-53µm), prepared using deionised water (concentration 10mg/l), *ii*) sintered bioceramic pellets, and *iii*) sintered 3D printed porous bioceramic scaffolds. For this purpose, a Trypticase Soy Broth (TSB) was prepared dissolving *S. aureus* disk in 20ml of TSB, and incubated at 37°C in order to allow the bacterial colonies to growth. After 24 hours of incubation, 100µl of the suspension was spread on a pre-dried Trypticase Soy Agar (TSA) plate. Before performing the test,



all the samples were sterilised in autoclave (121°C for 10min). Afterwards, the following steps were performed:

- i) 10µl of glass powder solutions were added on the top of sterile paper discs, previously placed aseptically on the bottom half of the TSA plate (Figure 5.11(a));
- ii) bioceramic pellets were aseptically placed on the top half of the TSA plate (Figure 5.11(a));
- iii) 3D printed porous bioceramic scaffolds were aseptically placed on another TSA plate (Figure 5.11(b)).

Once the specimens were positioned, the TSA plates were incubated at 37°C. After 24 hours, the inhibition zones, if present, were observed as a halo around the samples where bacteria had not grown. 10µl Erythromycin solution (40mg/ml) was used as a positive control and AW as comparison material like for all the other experiments of this study. All tests were performed in triplicate.

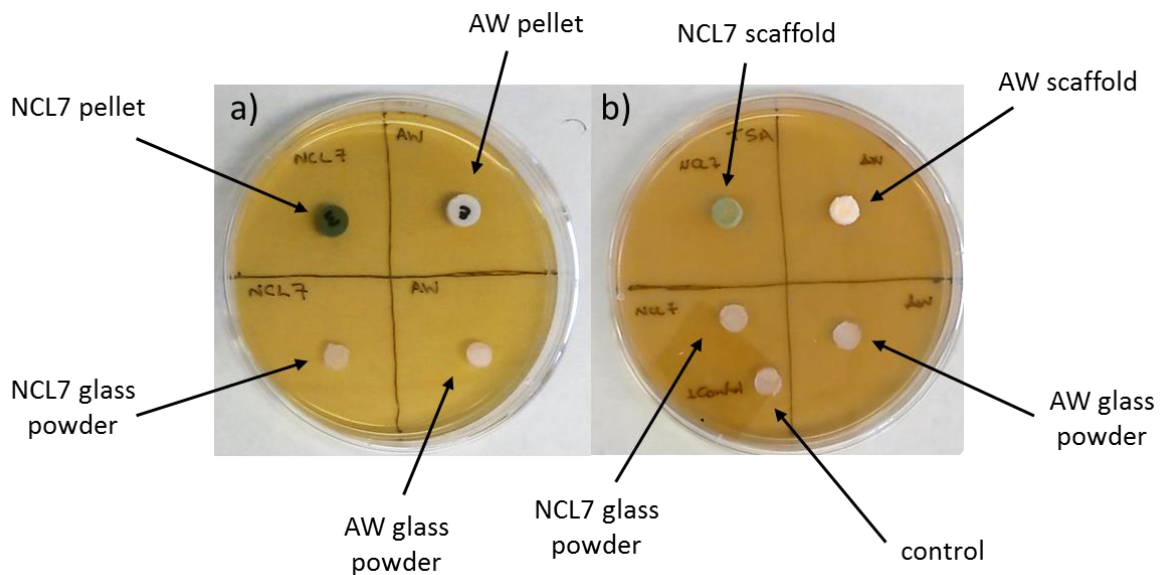


**Figure 5.11: *Staphylococcus aureus* cultivation on TSA plates: (a) glass powders (bottom), bioceramic pellets (top) and (b) 3D porous scaffolds (top).**

## Chapter 6. Results: raw glass powders and bioceramic pellets preparation and characterisation

In this chapter the results obtained from the experimental study conducted on the novel raw glass powders and on dense bioceramic pellets are presented.

### 6.1 Glass production

Once the individual components (reported in Table 4.1) of each formulation were mixed, they were melted in platinum crucibles for times and temperatures shown in Table 6.1. Afterwards, the glass melts were quenched in water, and glass frits (Figure 6.1) were obtained as last stage of the industrial process.

*Table 6.1: Production parameters for the new glass compositions.*

Glass code	Melting temperature	Melting time	Casting temperature (°C)	Comments
NCL1	1450° C	2 hours	1425	Very fluid glass could be melted at lower fusion temperature
NCL2	1450° C	2 hours	1425	Very fluid glass could be melted at lower fusion temperature
NCL3	1450° C reduced to 1400° C after 30 min, then to 1350° C after a further 30 min	2 hours	1350	Extremely fluid at 1450° C, melting reduced to 1350° C to cast, still fluid
NCL4	1450° C reduced to 1300° C after 30 min	2 hours	1300	Extremely fluid at 1450° C, melting reduced to 1300° C to cast, still very fluid. High level of evaporation noted and damage to crucible
NCL5	1500° C	4 hours	n/a	Would not form a glass at this temperature
NCL6	1450° C	2 hours	1425	Very fluid glass could be melted at lower fusion temperature
NCL7	1450° C	2 hours	1425	Fluid at 1450° C
NCL8	1450° C	2 hours	1425	Very fluid glass at 1450° C could be melted at lower fusion temperature



**Figure 6.1: Representative image of the as-produced glass frits.**

As reported in Table 6.1, during the synthesis process the composition NCL5 could not form a glass at 1500°C, which was the highest temperature reached by the furnace, so that the number of glass formulations was reduced to seven.

## 6.2 Glass powder preparation

The glass frits (Figure 6.2(a)), ground using a zirconia ball mill (Figure 6.2(b)), were sieved to obtain fine powder in the range 0-53μm as shown in Figure 6.2(c).



**Figure 6.2: a) glass frits, b) ground using a ball milling machine, and then c) sieved to obtain fine glass powder.**

### 6.2.1 X-ray diffraction analysis

The XRD patterns of the raw materials are reported in Figure 6.3. For NCL1, NCL2, NCL3, NCL4, and NCL8 the presence of a broad peak, common for glass samples, indicated the completely amorphous nature of these compositions. The amorphous peak was detected at  $2\theta$  values between  $25^\circ$  and  $30^\circ$ , and confirmed that NCL1, NCL2, NCL3, NCL4 and NCL8 formulations were free from any detectable crystalline phase.

Different patterns were detected for NCL6 formulation, which showed a glass-ceramic nature with a crystalline phase identified as calcium sodium phosphate (ICDD ref. code 01-074-1950).

Moreover, for the NCL7 composition a silver crystalline phase (ICDD ref. code 04-003-1425) was detected. Regarding the as-poured AW composition, the presence of hydroxylapatite phase (ICDD ref. code 01-080-6260) proved the glass-ceramic nature of this material, in agreement with the material investigation provided by GTS Ltd. Furthermore, a less intense  $\beta$ -wollastonite phase (ICDD ref. code 04-010-0710) was also observed in this composition.

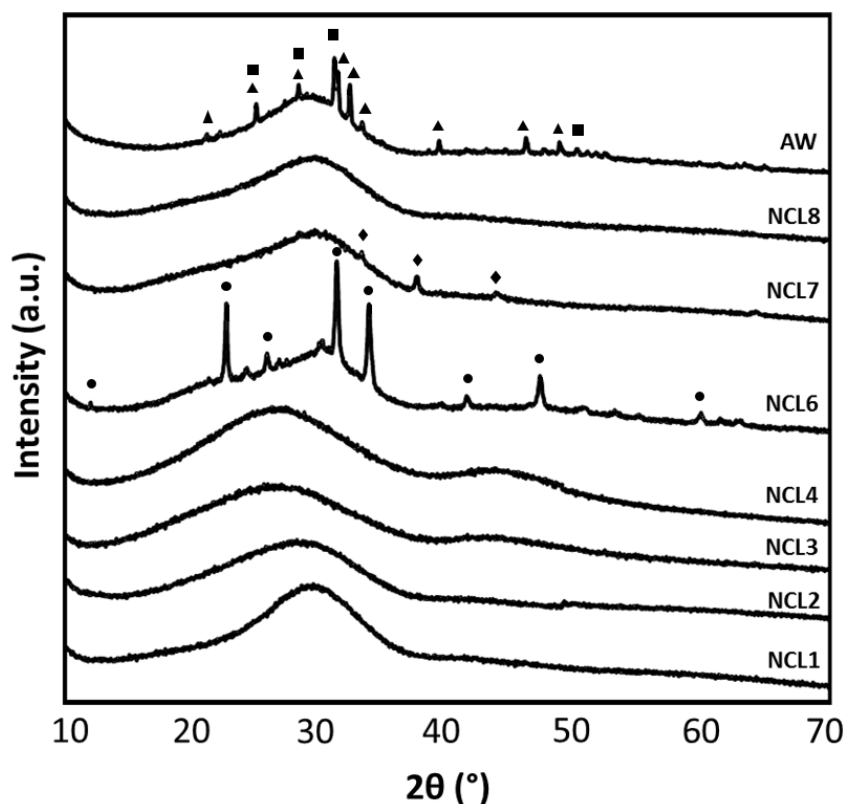


**Figure 6.3:** XRD patterns of as-synthesised glass powders ( $\blacktriangle$  hydroxylapatite,  $\blacksquare$   $\beta$ -wollastonite,  $\blacklozenge$  silver  $\bullet$  calcium sodium phosphate).

### 6.2.2 Glass powders microstructure

SEM analysis was performed in order to investigate the raw material microstructures. All the specimens were firstly gold-coated, and then analysed at an accelerating voltage of 20kV and working distance about 8.5mm. Figure 6.4(a-h) show the morphology of as-synthesised glass powders: where non-spherical and irregular shape particles can be observed. All the compositions were characterised by sharp edge particles. Furthermore, it can be seen that for all the glasses most of the particles were very fine, (ranging from 20 $\mu$ m to 53 $\mu$ m), with the presence also of grains smaller than 10 $\mu$ m, which tended to compact producing aggregates.

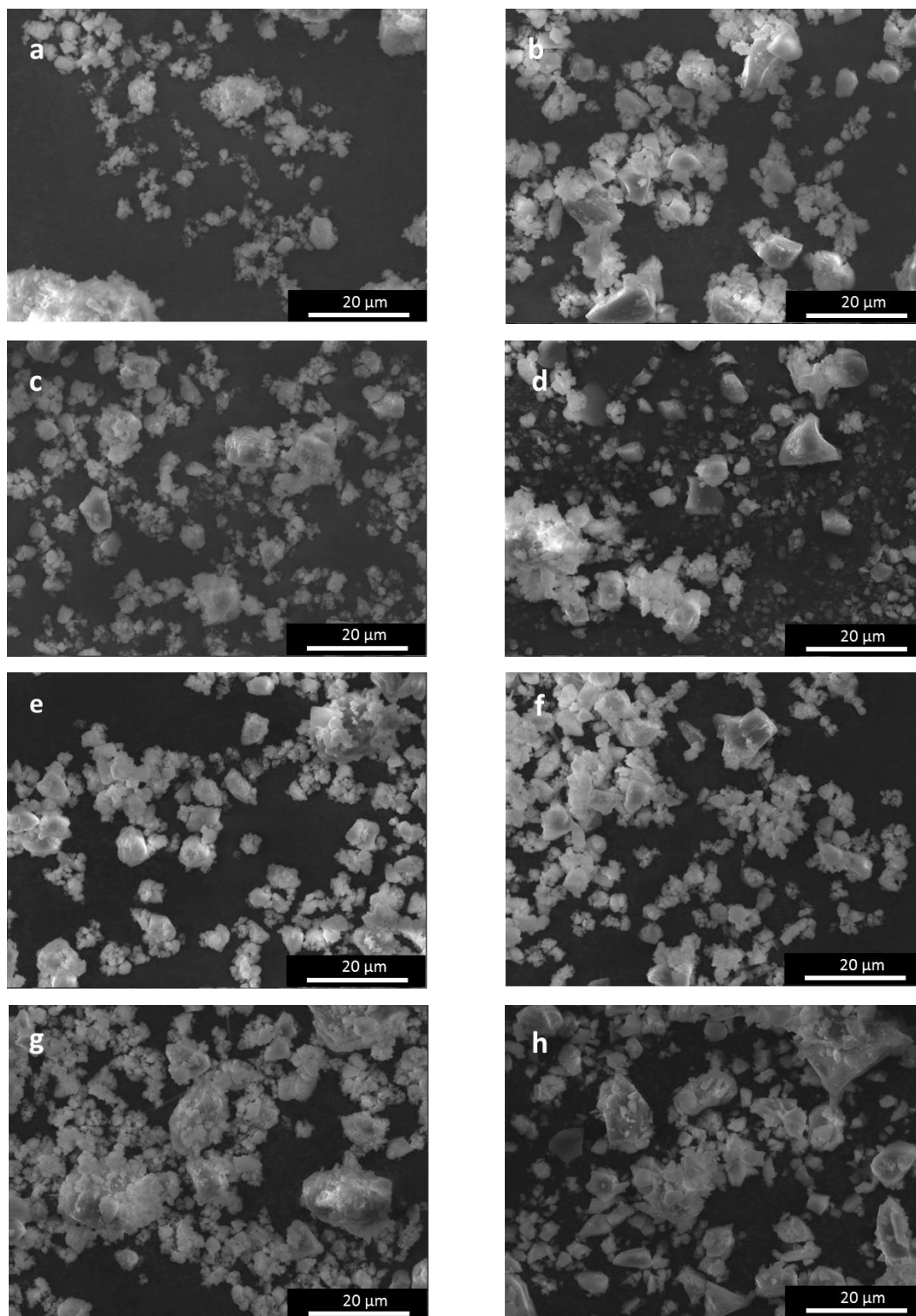




















**Figure 6.4:** SEM analysis (magnification 1500x) showing the glass powders morphology: a) NLC1, b) NCL2, c) NCL3, d) NCL4, e) NCL6, f) NCL7, g) NCL8, and h) AW.

### 6.2.3 Hot stage microscopy



















Table 6.2 and Table 6.3 summarise the morphological information and inferred thermal properties from the HSM. The experiments started at room temperature ( $T_R$ ) with heating rate of  $10^\circ\text{C}/\text{min}$  up to  $1450^\circ\text{C}$ . All the specimens maintained their initial rectangular shape before the first shrinkage temperature ( $T_{FS}$ ), which varied between  $550^\circ\text{C}$  and  $1225^\circ\text{C}$  (see Figure 6.5(a-h)). For temperatures higher than the corresponding  $T_{FS}$ , the samples started to shrink until the temperature of maximum shrinkage ( $T_{MS}$ ).

The alterations of sample dimensions during the sintering process are reported in Figure 6.5(a-h). Figure 6.5(a-b, f-g) reveal also how the silicate-based specimens (NCL1, NCL2, NCL7 and NCL8), before reaching the melting status at complete melting temperature ( $T_{CM}$ ), started to expand up to their temperature of maximum volume ( $T_{MV}$ ). Furthermore, these silicate-based glasses showed a similar thermal profile, whereas the phosphate-based (NCL6) had a thermal curve (Figure 6.5(e)) more comparable to the borate-based glasses (NCL3 and NCL4) (Figure 6.5(c-d)).

*Table 6.2: HSM results and resulting thermal parameters for NCL1, NCL2, NCL3 and NCL4.*

COMPOSITION	T <sub>R</sub>	T <sub>FS</sub>	T <sub>MS</sub>	T <sub>MV</sub>	T <sub>CM</sub>
NCL1	 25°C	 575°C	 785°C	 875°C	 1025°C
NCL2	 25°C	 600°C	 730°C	 1050°C	 1175°C
NCL3	 25°C	 555°C	 625°C	----	 760°C
NCL4	 25°C	 550°C	 650°C	----	 782°C

*Table 6.3: HSM results and resulting thermal parameters for NCL6, NCL7, NCL8 and AW.*

COMPOSITION	T <sub>R</sub>	T <sub>FS</sub>	T <sub>MS</sub>	T <sub>MV</sub>	T <sub>CM</sub>
NCL6	 25°C	 580°C	 775°C	---	 912°C
NCL7	 25°C	 575°C	 785°C	 975°C	 1025°C
NCL8	 25°C	 500°C	 730°C	 875°C	 1020°C
AW	 25°C	 800°C	 1225°C	---	 1330°C



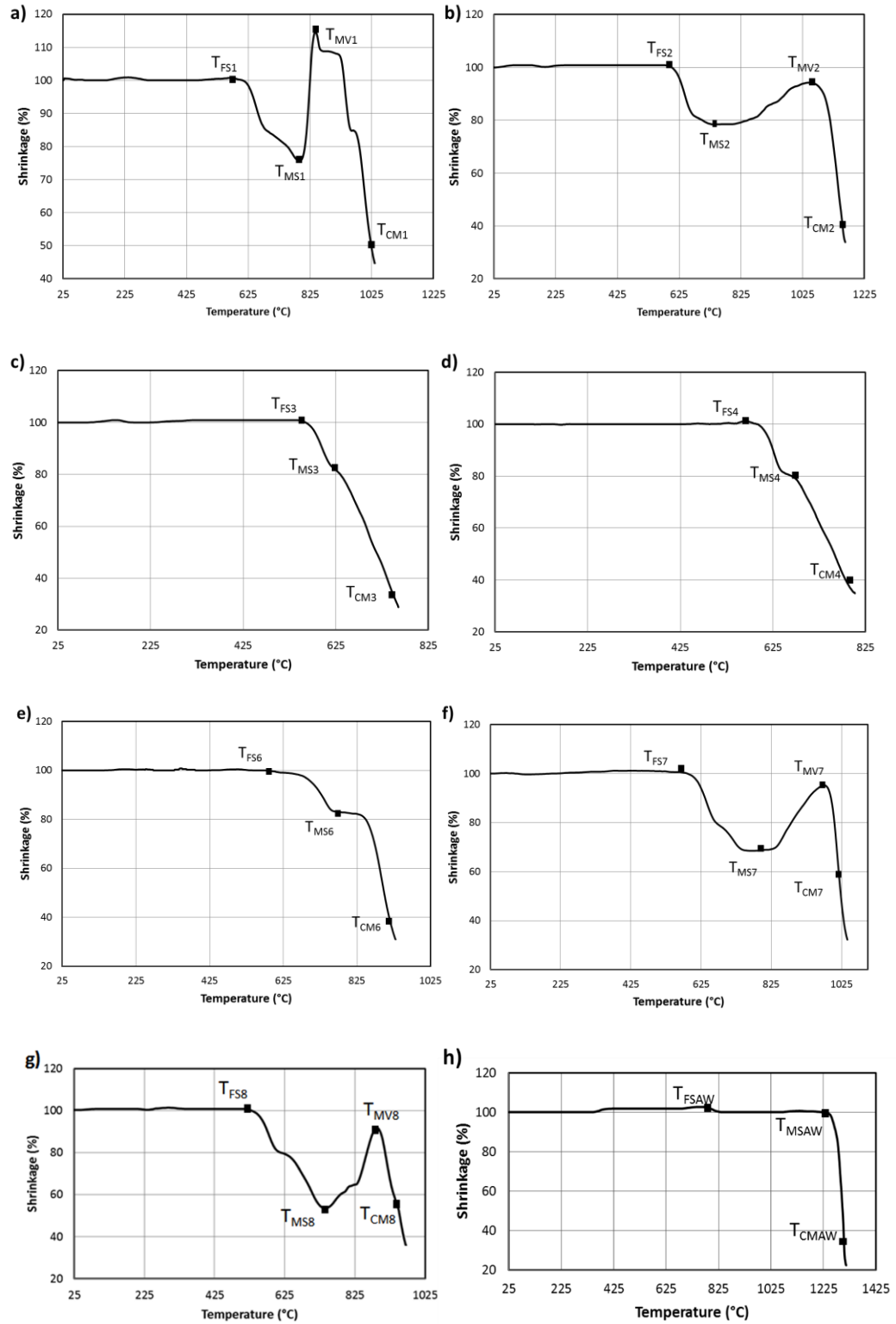


**Figure 6.5: Shrinkage profile derived from hot stage microscopy as function of temperature for: a) NCL1, b) NCL2, c) NCL3, d) NCL4, e) NCL6, f) NCL7, g) NCL8 and h) AW.**

#### 6.2.4 pH variation

The pH changes of the pre-sintered glasses, measured in deionised water at 37 °C and for a concentration of 10mg/ml, are shown in Figure 6.6. The pH varied between 8.5 and 11.3 for both refreshed (Figure 6.6(a)) and non-refreshed solutions (Figure 6.6(b)). For the condition with refresh, the solution was changed every two days, whereas for the non-refreshed condition the solution remained the same for all the experiment durations, and it reached pH saturation values after 3 days.

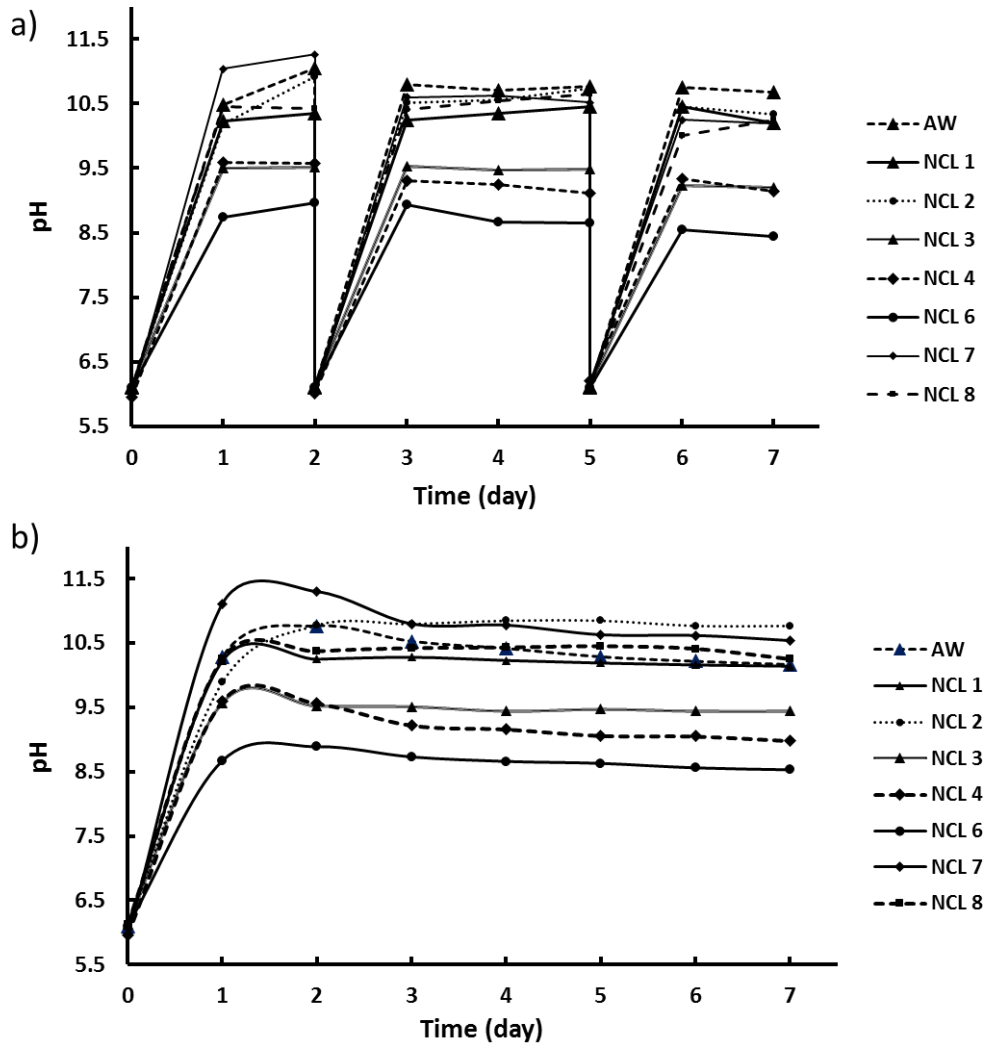


Figure 6.6: pH changes induced by the pre-sintered glass powder immersed in deionised water at 37 °C: a) with refresh and b) without refreshing the solution.

### ***6.2.5 Ion leaching evaluation***

Figure 6.7 shows the results of ion release from NCL1 glass powders, soaked in deionised water up to 28 days, and quantified using an ICP-OES. Specifically:

- the release of Si constantly increased up to 14 days, where it reached a plateau with 135mg/l;
- P, Mn, Zn, Bi and Cu concentrations all dropped significantly over the first 7 days, and showed similar kinetic profiles over the 28 days, whereas
- Mg release dropped from 1.99 to 0.08 mg/l after 28 days in immersion;
- K, Na, Te, and Va concentrations all rose steadily over the first 14 days;
- Ca concentration increased during the first days of immersion, reaching a peak after 7 days with 22.5mg/l, whereas Sr release constantly rose until the end of the immersion time, varying between 6.85mg/l and 25.9 mg/l.

Regarding NCL2 composition (silicate-based glass with 45mol% of SiO<sub>2</sub>), according to the results reported in Figure 6.8, the following considerations can be taken:

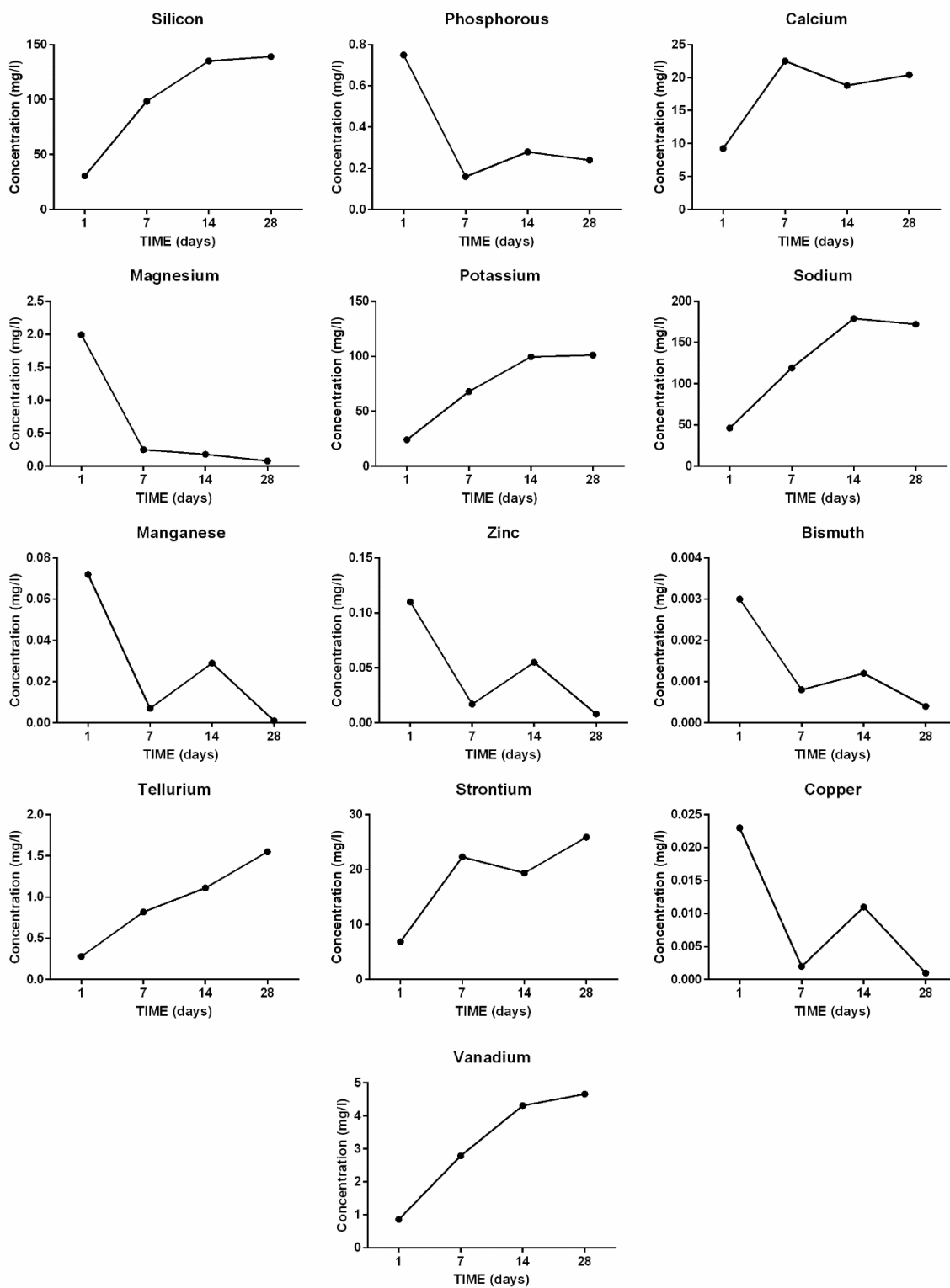
- similarly to NCL1 composition, Si concentration increased constantly during the 28 days of immersion, although in this case the maximum value reached was 85.9mg/l after the last time point;
- P, Ca, Mg, Mn, Al and Fe all showed a decrease in the ion concentration levels in the initial stages, followed by a sudden growth after 14 days of soaking;
- K, Na, B, Cr, Mo, Li and Se concentrations were characterised by a gradual increase during the overall period.

Figure 6.9 and Figure 6.10 report the ionic release trends for NCL3 composition, which is a borate-based glass (35mol% of B<sub>2</sub>O<sub>3</sub>). In this case:

- the release of boron presented a constant increase reaching 590mg/l after 28 days in immersion, whereas Si and P concentrations showed no significant variations over the entire period;
- Ca, Mg, K, Na (Figure 6.9), Li and Va (Figure 6.10) all showed an increment going from 1 to 28 days of soaking;

- Mn displayed a decrease in the ion concentration levels in the initial stages, followed by a sudden growth after 14 days of soaking, whereas Al, Fe, Co, and Ti were characterised by a jagged kinetic profiles (Figure 6.10);
- Cr and Ba release showed similar slightly curved profiles over the 28 days.

## NCL1



**Figure 6.7: Ionic release concentrations deriving from NCL1 raw glass powders after 28 days of soaking in deionised water.**

## NCL2

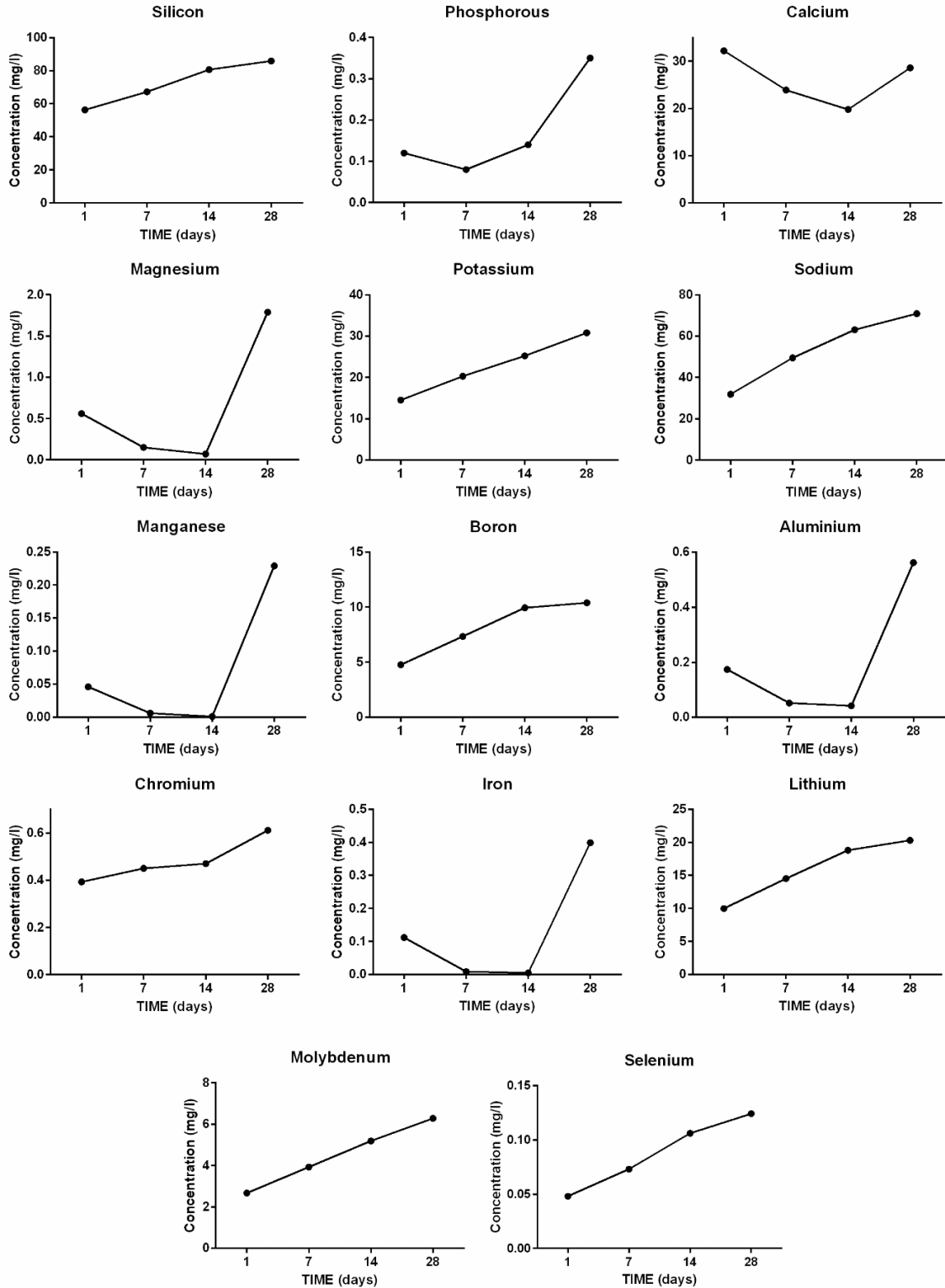


*Figure 6.8: Ionic release concentrations deriving from NCL2 raw glass powders after 28 days of soaking in deionised water.*

## NCL3

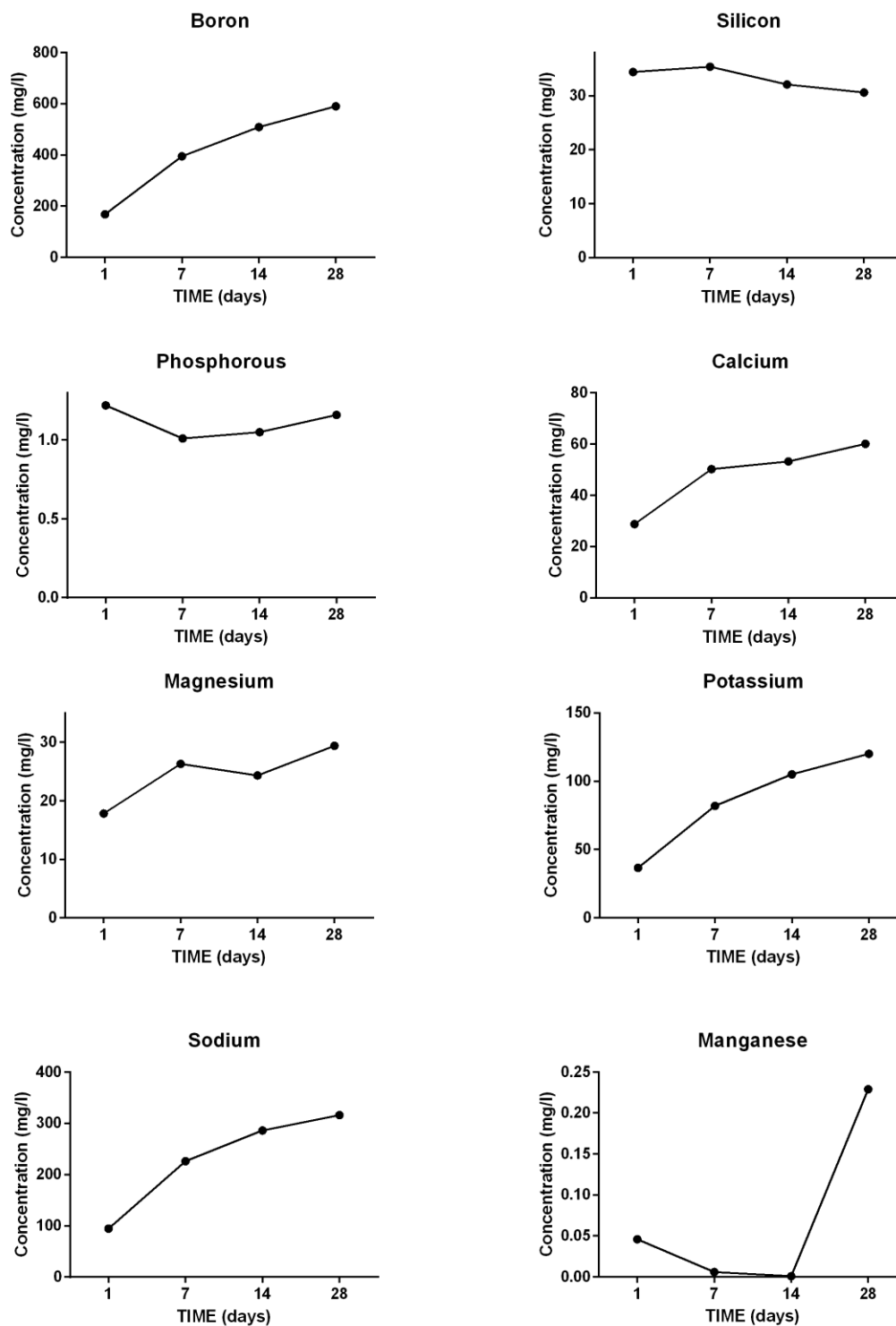


*Figure 6.9: Ionic release concentrations deriving from NCL3 raw glass powders after 28 days of soaking in deionised water.*

## NCL3

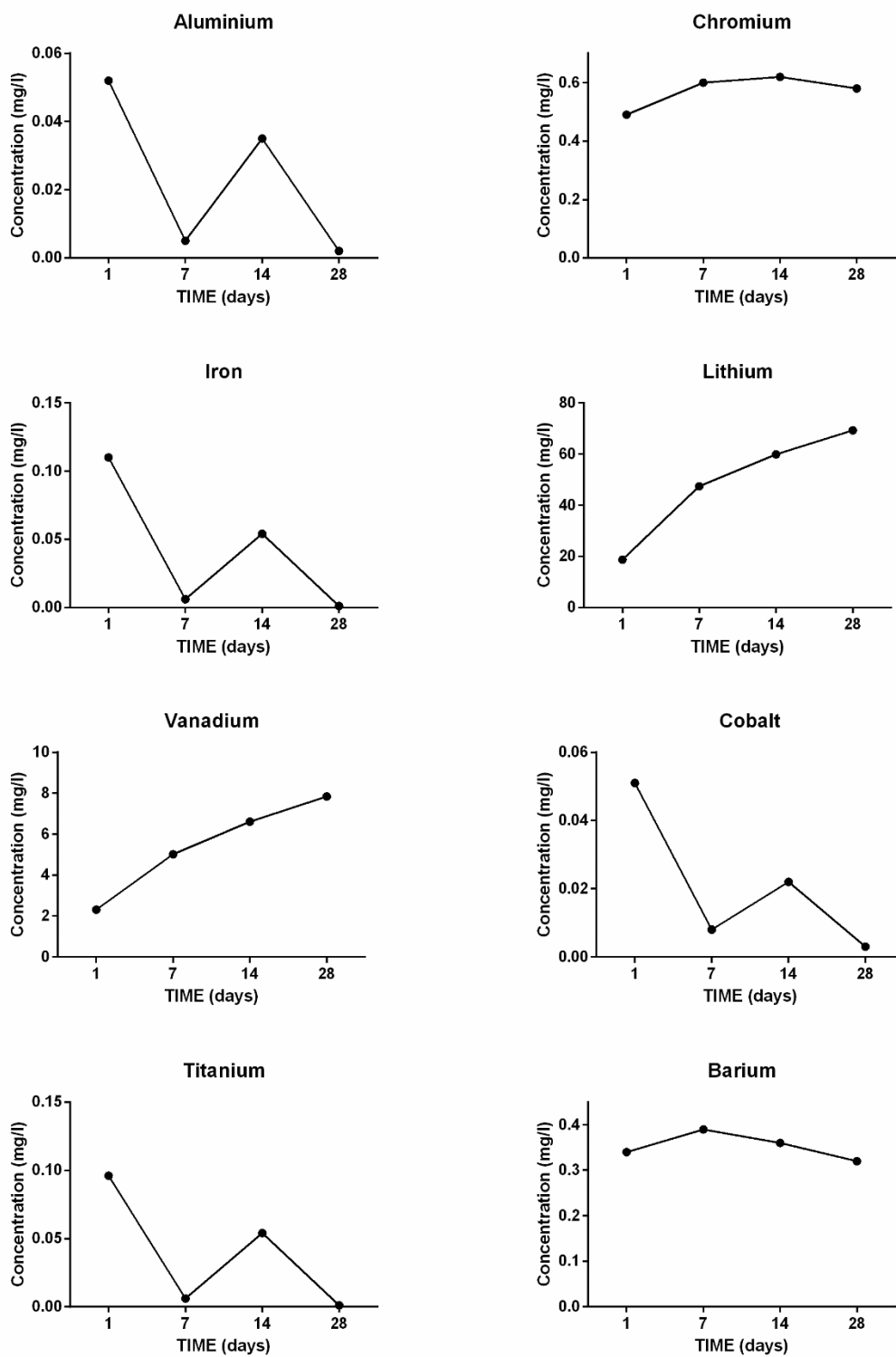


*Figure 6.10: Ionic release concentrations deriving from NCL3 raw glass powders after 28 days of soaking in deionised water.*



NCL4 is a borate-based glass with a higher content of boron (40mol% of  $B_2O_3$ ) compared to NCL3 composition (35mol% of  $B_2O_3$ ). As reported in Figure 6.11:

- boron concentration rose quickly over the first 14 days, reaching 800mg/l after 28 days;
- phosphorous release profile was characterised by a progressive decrease during the 28 days;
- silicon concentration showed a gradual increment during the initial 7 days, followed by a slow decrease;
- Ca, Mg, K and Na release reached a plateau after 14 days;
- Mo, Se and Sr all rose gradually up to 28 days;
- Zn and Cu both displayed very low levels after 28 days of immersion.

As NCL5 composition was not synthesised, NCL6 (50mol% of  $P_2O_5$ ) was the only phosphate-based glass out of the 8 initial proposed. According to the results reported in

Figure 6.12 the following considerations can be taken:

- phosphorous release profile had a continuous increase going from 52.7mg/l at day 1 to 130mg/l at day 28;
- the kinetic profiles of Si, K, Na, Co and B were quite comparable, and particularly they were characterised by a drop in their levels after 14 days;
- Ca and Mn concentrations decreased gradually over the all interval;
- Mg ionic release rose steadily over the 28 days, whereas Cr concentration was almost constant;
- a zigzag profile arose from Cu release.

In Figure 6.13 are reported the ionic release profiles for composition NCL7. This formulation is the silicate-based glass with the highest silicon content (50mol% of  $SiO_2$ ). For this glass:

- the Si concentration increased very rapidly during the first 7 days and then almost steadily up to 28 days;
- P, Ca, Mg and Cu concentrations slightly dropped over the first 7 days and afterward they restarted to rise;
- Fe and Ti were subjected to a drop in their concentration levels already after the first 7 days in immersion, where small amount could be detected. A similar drop was showed by silver

release, which instead after 7 days and up to 28 days in immersion maintained values above zero.

- K and Na concentrations were described by very similar profiles, which gradually increased over the 28 days of immersion.

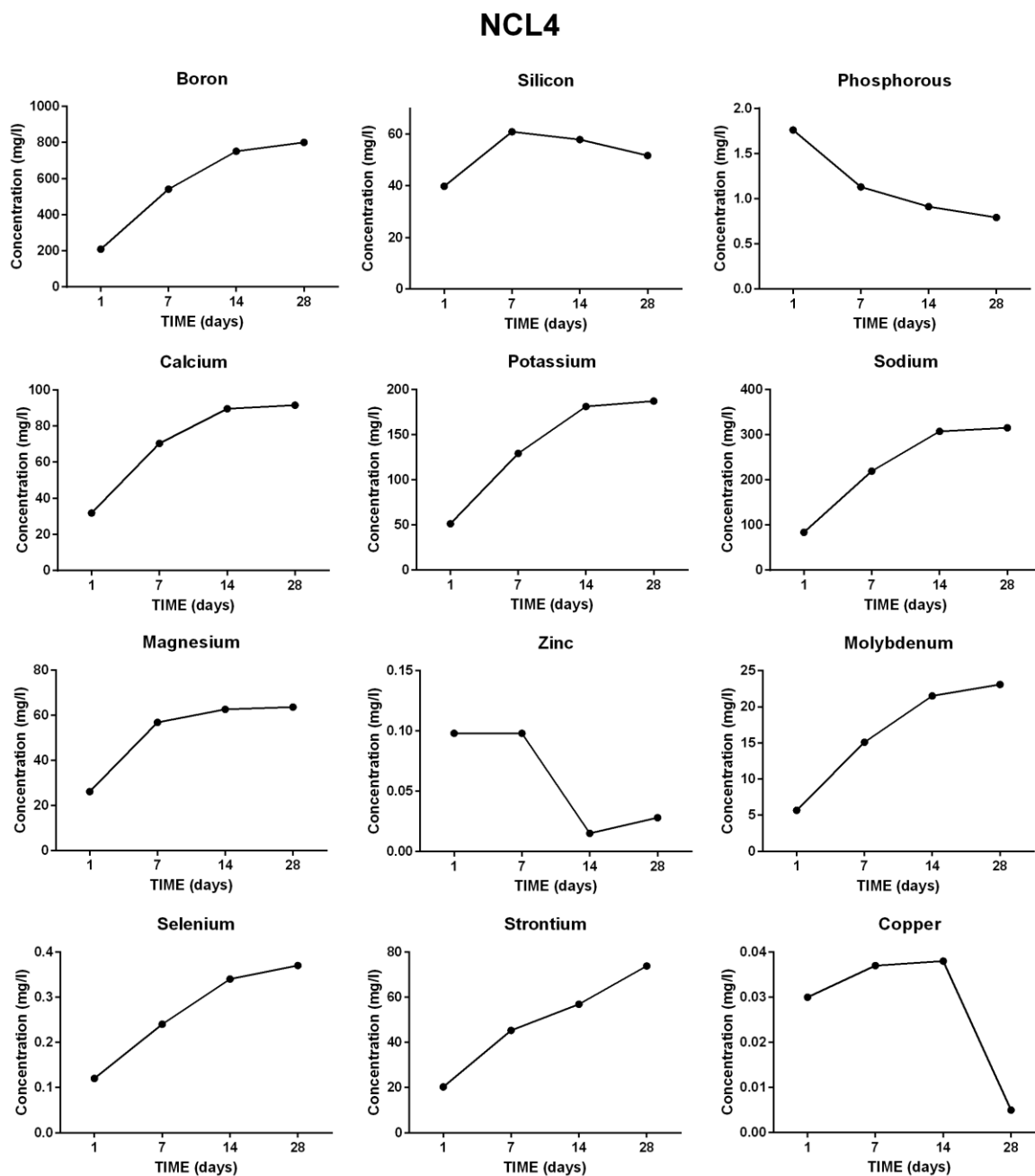


**Figure 6.11: Ionic release concentrations deriving from NCL4 raw glass powders after 28 days of soaking in deionised water.**

## NCL6

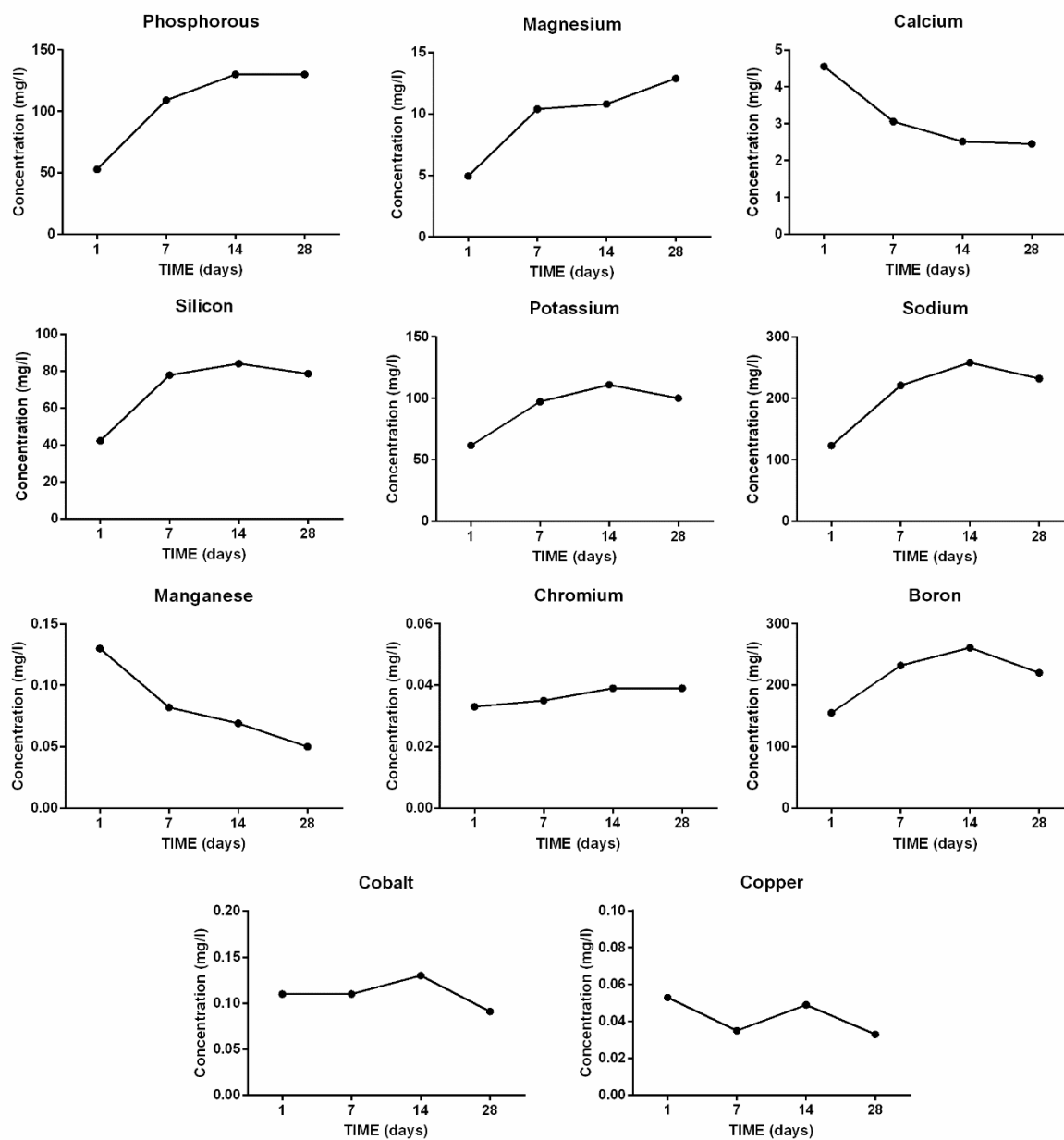


*Figure 6.12: Ionic release concentrations deriving from NCL6 raw glass powders after 28 days of soaking in deionised water.*

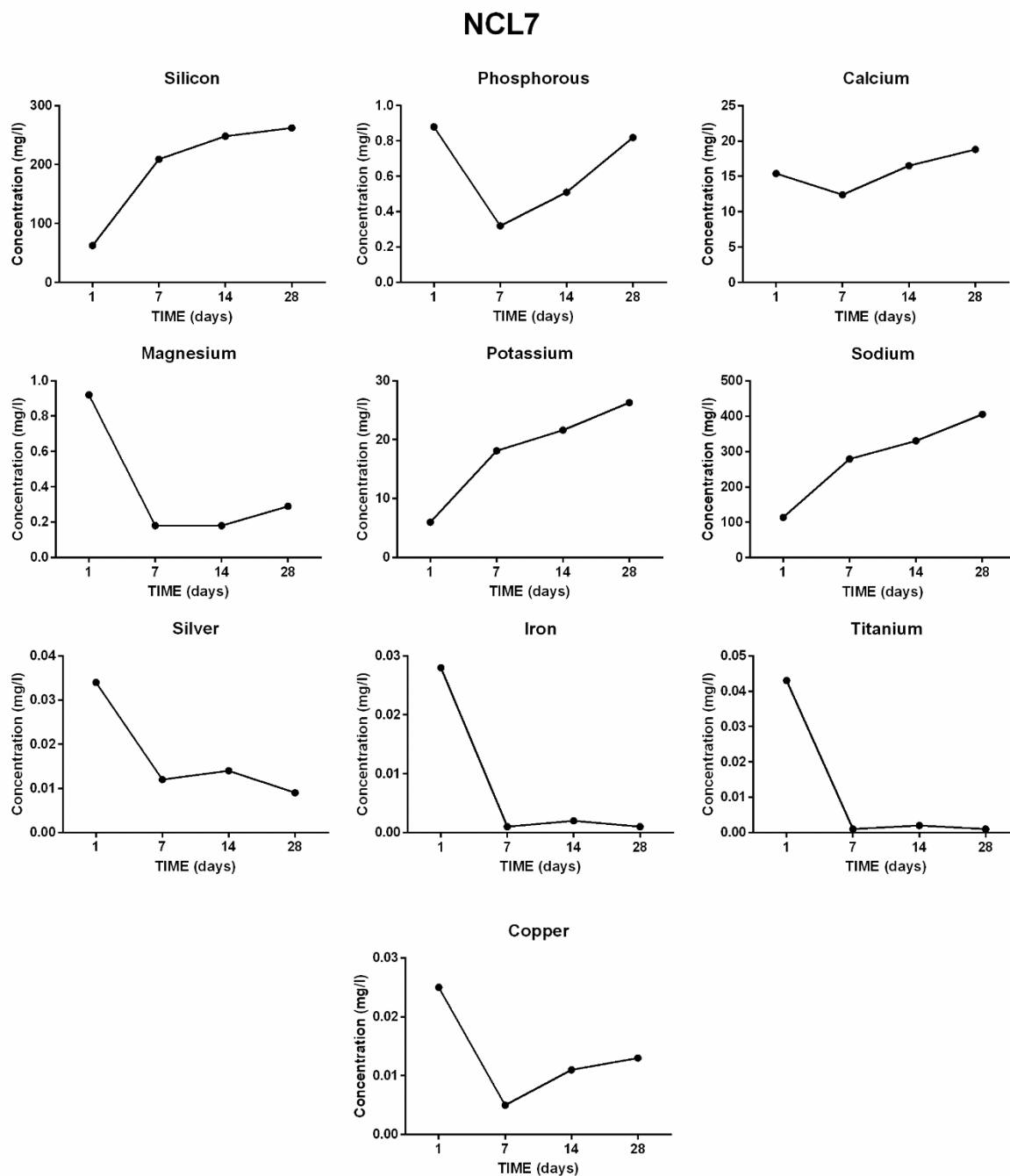


**Figure 6.13:** Ionic release concentrations deriving from NCL7 raw glass powders after 28 days of soaking in deionised water.

The last composition that will be presented is a silicate-based glass with the same silicon content of NCL2 (45mol% of SiO<sub>2</sub>). As shown in Figure 6.14 and Figure 6.15:

- silicon was characterised by a gradual increase, reaching 167mg/l at day 28;
- the release profiles of K, Na, B, Cr, Mo and Se, similarly to Si, steadily rose up to the end of the considered interval;
- Mg, Mn, Zn, Fe, Cu and Co all dropped significantly over the first 7 days;
- the level of Sr reached a peak at day 7 and then started to progressively decrease;
- P and Ca profiles were characterised by a similar trend of NCL7 composition, with a significant drop after the first 7 days in immersion, followed by rapid increase up to 28 days.

As comparison, Figure 6.16 reports the ionic release profiles deriving from AW glass-ceramic. In this case:

- silicon release reached a peak at day 14 with 85mg/l, and afterward started gradually to decrease arriving at 68.1mg/l at day 28;
- P and Ca elements had quite comparable profiles, showing a minimum in the concentration values at day 7, followed by a gradual growth up to day 28;
- the Mg ionic release varied over the period showing no clear trend.

## NCL8

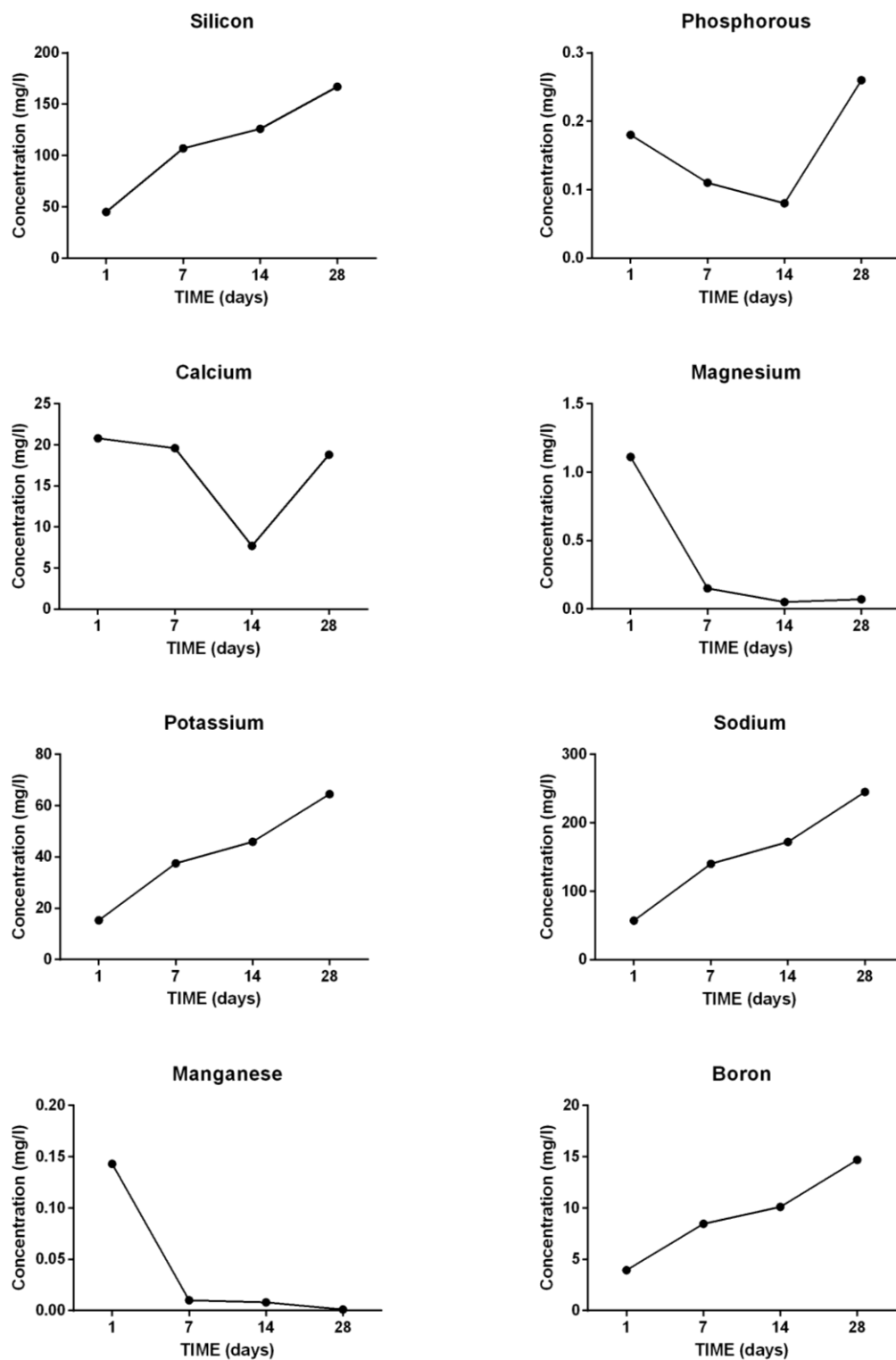


*Figure 6.14: Ionic release concentration deriving from NCL8 raw glass powder after 28 days of soaking in deionised water.*

## NCL8

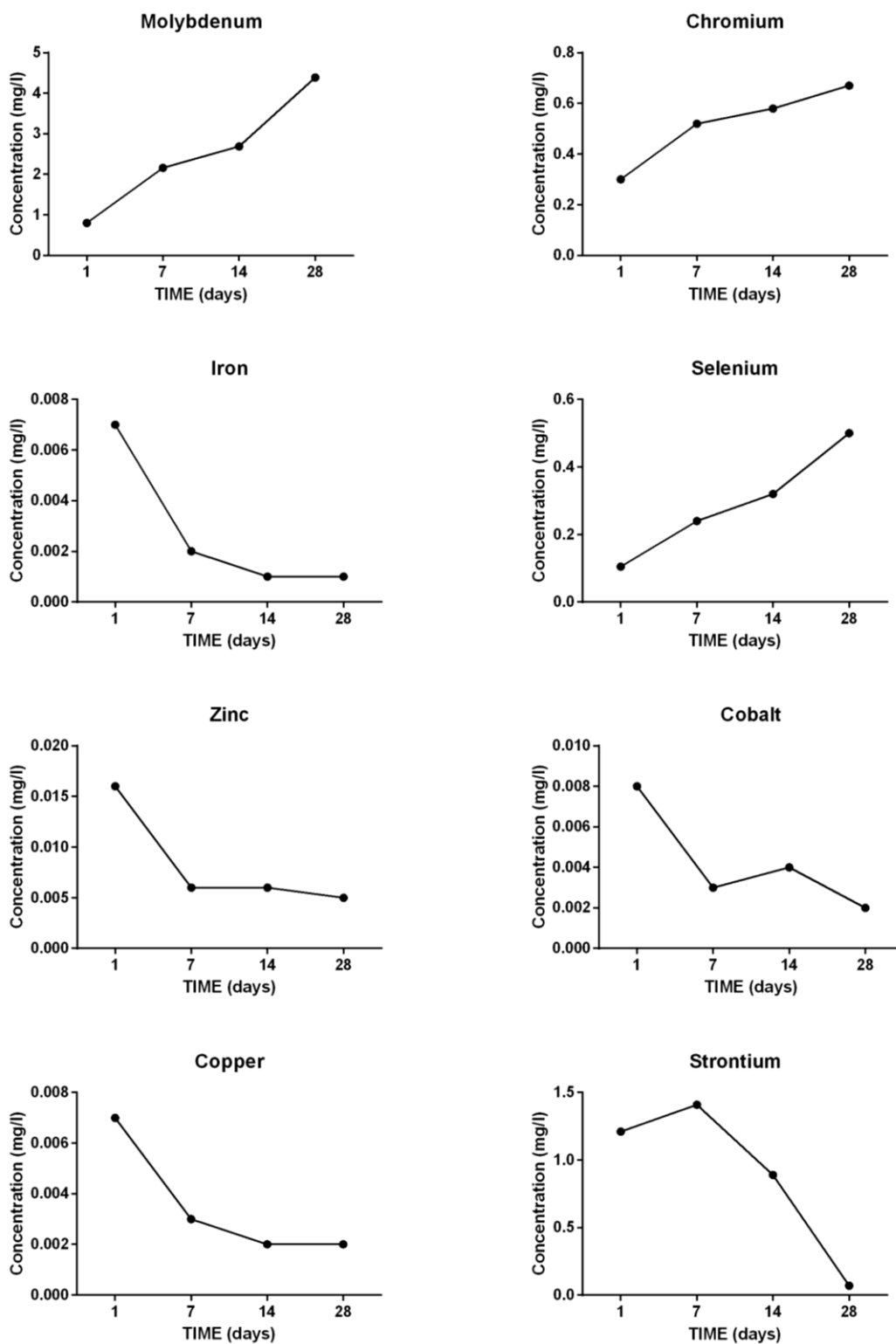


*Figure 6.15: Ionic release concentration deriving from NCL8 raw glass powder after 28 days of soaking in deionised water.*

## AW

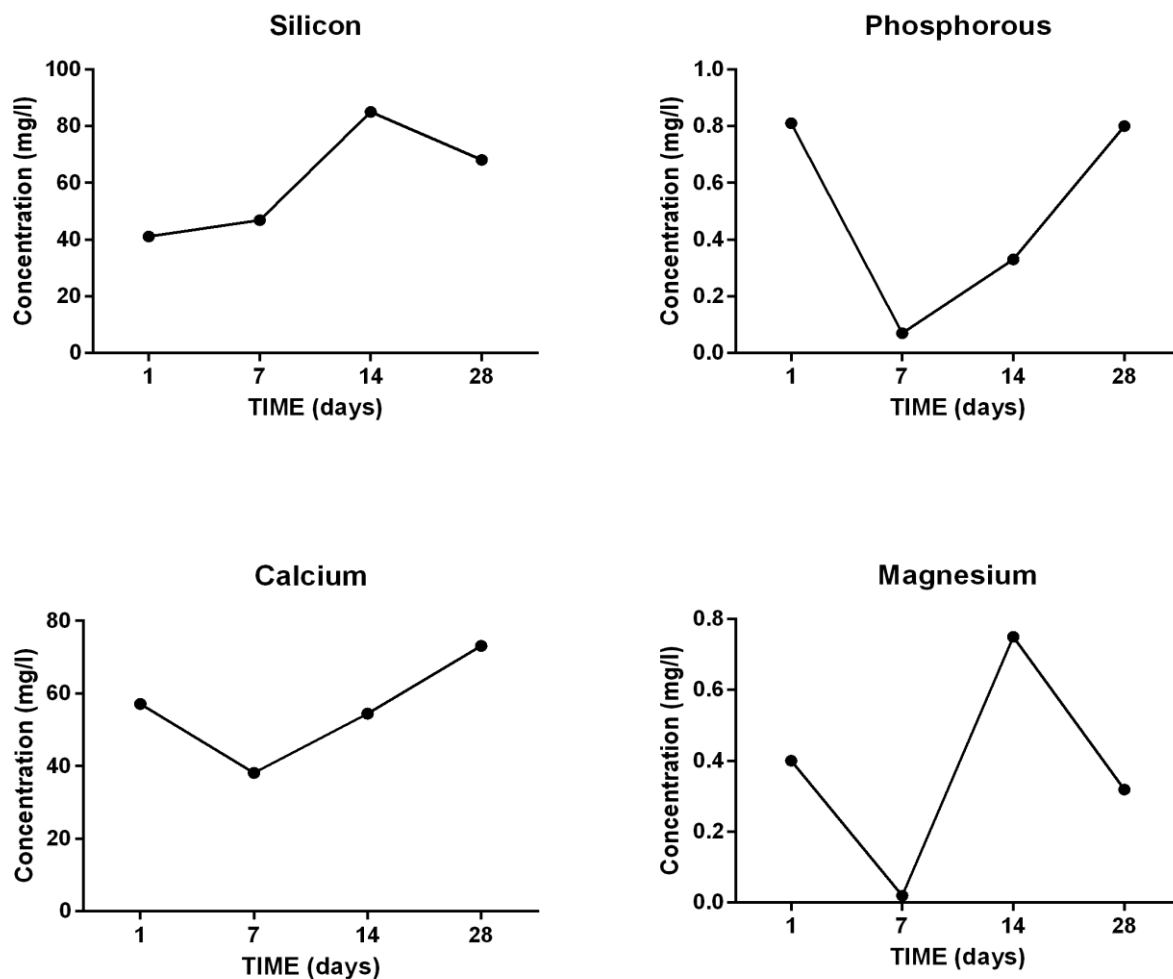


*Figure 6.16: Ionic release concentration deriving from AW raw glass powder after 28 days of soaking in deionised water.*

From the results obtained through the ICP analysis, it was possible to draw the following general considerations:

- for NCL1 and NCL7 compositions, which are both silicate-based glasses, the release of silicon followed the same trend over the 28 days, characterised by a steadily increase over the first 14 days and then remained nearly constant;
- NCL2 and NCL8 compositions showed a different silicon release profile with respect to NCL1 and NCL7 formulations. In the first case, most likely the presence of boron in the



glass matrix contributed to gradually rise up silicon release until the end of the considered interval. Furthermore, silicon and boron in these compositions displayed the same trend;

- as network former, boron was released very quickly in comparison to silicon and phosphorous, and it displayed a progressive increase all over the interval either for NCL3 and NCL4 compositions;
- the presence of boron in the glass formulation, even as intermediate oxide, enhanced the release of other elements in the composition (*i.e.* vanadium and phosphorous from NCL3 glass with respect to their release from NCL1 composition);
- silicon release from borate-based glasses was more correlated to the amount of boron rather than its content in the glass matrix, as the results from NCL3 and NCL4 demonstrated;
- as main network former, phosphorous in NCL6 composition was released more slowly than boron from NCL3 and NCL4 formulations.

### 6.2.6 *In vitro* cytotoxicity

In order to evaluate the cytotoxicity effect on rat osteoblast cells, all the novel powder-based biomaterials at different concentrations were tested through MTT assay, after one and seven days in culture. As described in paragraph 5.4.9.2, two different test conditions were assessed:

- i) the direct contact of the cells with the raw glass powders and
- ii) the indirect contact based on the filtering of the glass powders eluate.

Figure 6.17 highlights the effect of NCL1 composition. According to the results reported in Figure 6.17(a), for direct condition over the 7 days culture period, the cell viability was fairly constant for concentrations of 0.1 and 1mg/l of glass powder in media, but concentrations of 10mg/l of glass in media had a clear detrimental effect on viability.

Regarding indirect condition (Figure 6.17(b)), no harmful outcomes were detected for concentration of 0.1 and 1mg/l of glass powder in media, whilst concentrations of 10mg/l of glass in media had a detrimental effect on cell viability after 7 days in culture; condition B, no harmful outcomes were detected up to 1 mg/l. However, the negative effect of NCL1 glass powders on cells mitochondrial activity arose significantly going from 1 to 10 mg/l in both tested conditions with absorbance values close to zero.

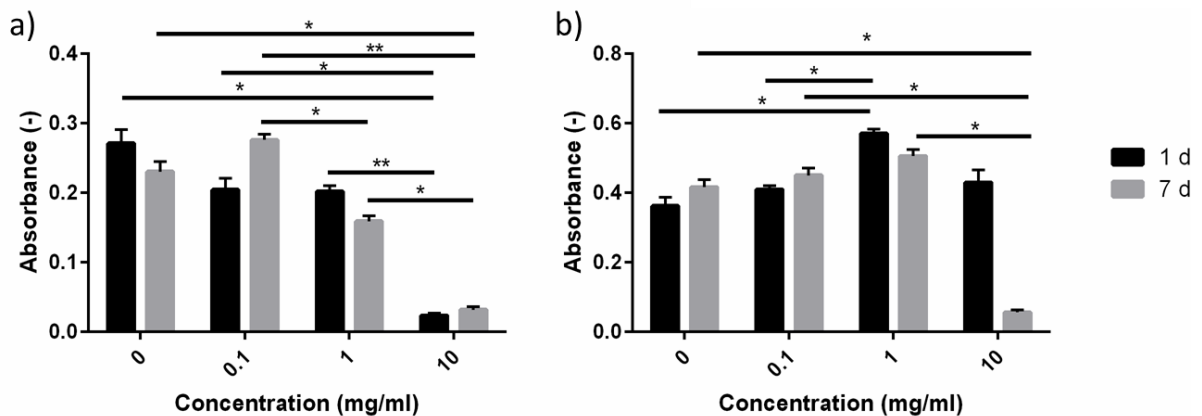


**Figure 6.17: Effect of NCL1 glass powders (measured in triplicate) on formazan formation after (a) direct and (b) indirect contact with rat osteoblast cells, evaluated through MTT assay after 1 day and 7 days in culture. Error bars represent the standard error of the mean ( $p < 0.05$ (\*) and  $p < 0.001$ (\*\*)).**

Regarding composition NCL2, whose effects on rat OB cells are reported in Figure 6.18, the following considerations can be taken: for the direct condition (Figure 6.18(a)) the cell viability was fairly constant for concentrations of 0.1 and 1mg/l of glass powder in media over the 7 days culture, but concentrations of 10mg/l of glass in media had a clear detrimental effect on viability. Overall, this formulation showed no detrimental influence on rat osteoblast mitochondrial activity by indirect contact (Figure 6.18(b)), either after 1 and 7 days in culture.

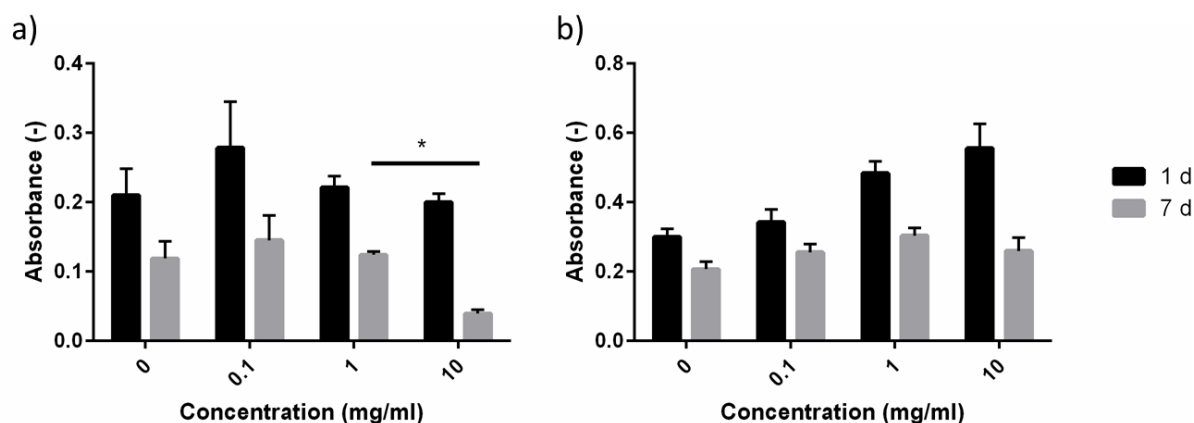


**Figure 6.18:** Effect of NCL2 glass powders (measured in triplicate) on formazan formation after (a) direct and (b) indirect contact with rat osteoblast cells, evaluated through MTT assay after 1 day and 7 days in culture. Error bars represent the standard error of the mean ( $p < 0.05$ (\*) and  $p < 0.001$ (\*\*)).

Consequences of NCL3 composition on rat osteoblasts mitochondrial activity are displayed in Figure 6.19. Although for indirect condition the material did not show any significant negative effect on cells activity after 1 day in culture and at low concentrations (Figure 6.19(b)), for both conditions a significant detrimental behaviour was found at the highest concentration tested (10 mg/l) with respect to the control (0 mg/l) after 7 days in culture.

Figure 6.20 shows the MTT assay results for NCL4 formulation, which highlights a decrease in the cell mitochondrial activity after 7 days in culture, detected for both tested methods. No significant negative effects associated to the use of this glass powder were observed for the indirect method.

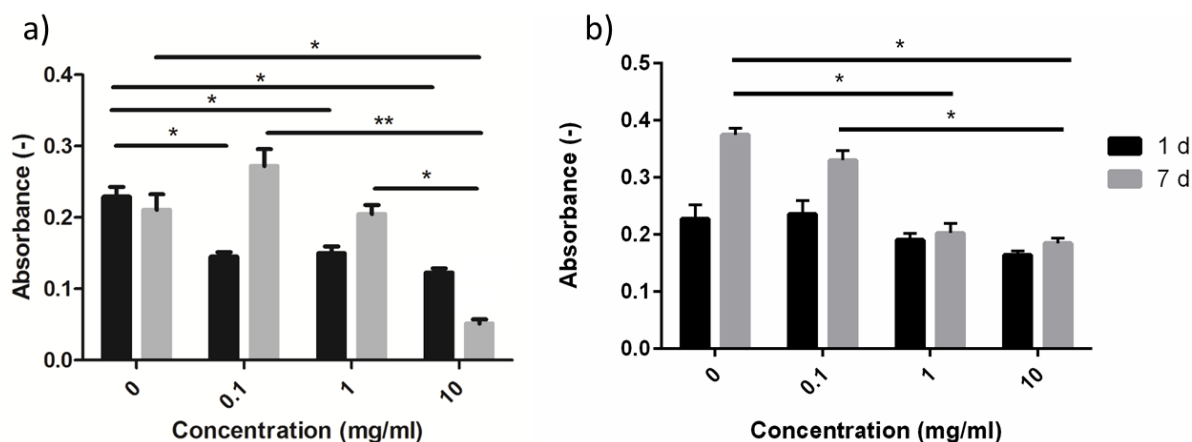


**Figure 6.19:** Effect of NCL3 glass powders (measured in triplicate) on formazan formation after (a) direct and (b) indirect contact with rat osteoblast cells, evaluated through MTT assay after 1 day and 7 days in culture. Error bars represent the standard error of the mean ( $p < 0.05$ (\*) and  $p < 0.001$ (\*\*)).

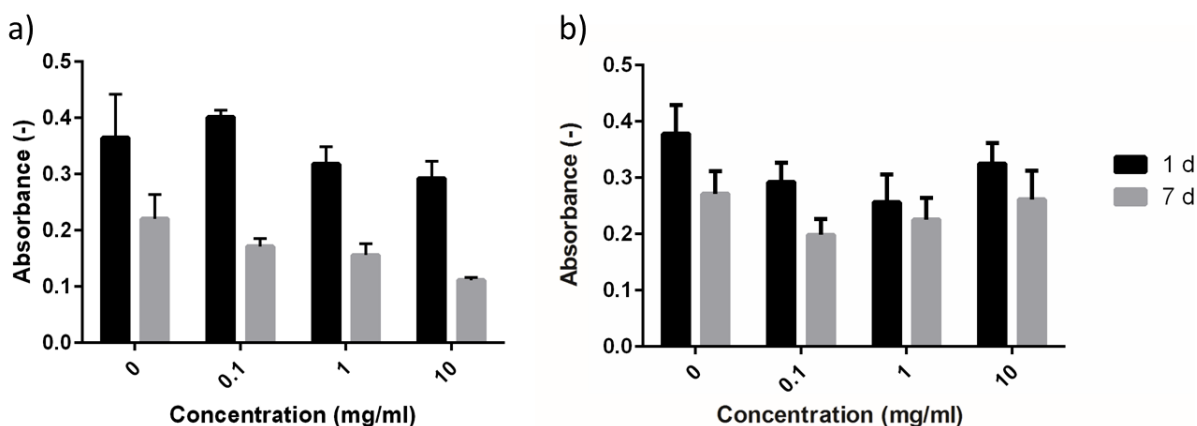


**Figure 6.20:** Effect of NCL4 glass powders (measured in triplicate) on formazan formation after (a) direct and (b) indirect contact with rat osteoblast cells, evaluated through MTT assay after 1 day and 7 days in culture. Error bars represent the standard error of the mean ( $p < 0.05$ (\*) and  $p < 0.001$ (\*\*)).

Concerning glass composition NCL6, as reported in Figure 6.21, no remarkable effects were showed after 1 day in culture for both test set-up, although for the direct method (Figure 6.22 (a)) the cell mitochondrial activity was approximately constant for concentrations of 0.1 and 1mg/l of glass powder in media over the 7 days culture period, but by increasing the concentrations up to 10mg/l an evident cytotoxic effect on viability was observed with absorbance values very close to zero. For the indirect method (Figure 6.22 (b)), the cells mitochondrial activity decreased by increasing the amount of glass powders in media, after both 1 and 7 days in culture, showing a detrimental effect for rat OB mitochondrial activity.

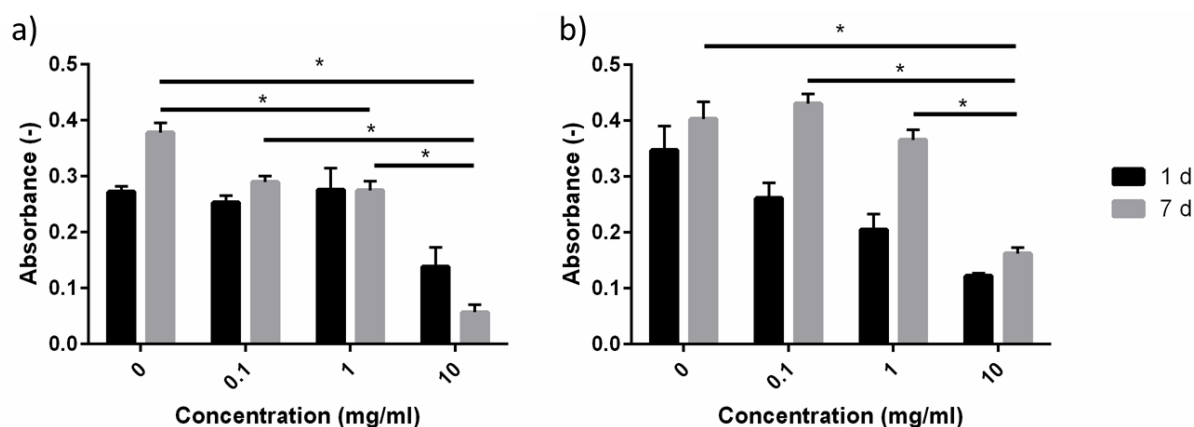


**Figure 6.21:** Effect of NCL6 glass powders (measured in triplicate) on formazan formation after (a) direct and (b) indirect contact with rat osteoblast cells, evaluated through MTT assay after 1 day and 7 days in culture. Error bars represent the standard error of the mean ( $p < 0.05$ (\*) and  $p < 0.001$ (\*\*)).

Figure 6.22 shows the effect of NCL7 glass powder on cell mitochondrial activity. As can be observed, the presence of glass powders in direct contact, and at high concentrations, slightly affected rat OB mitochondrial activity (Figure 6.22 (a)). Tests performed according to indirect method revealed no cytotoxic effect and a positive influence of NCL7 composition on rat OB cell viability, which increased over the 7 days in culture.

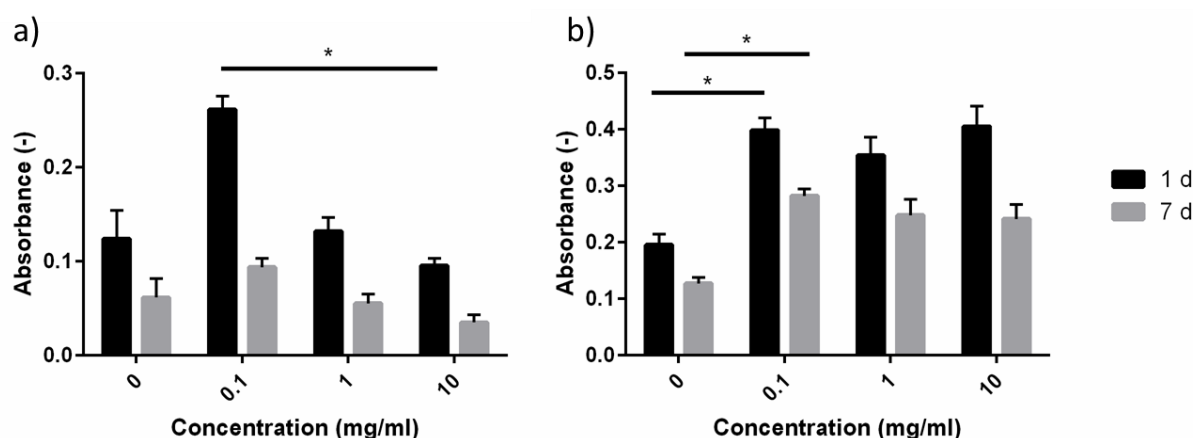


**Figure 6.22:** Effect of NCL7 glass powders (measured in triplicate) on formazan formation after (a) direct and (b) indirect contact with rat osteoblast cells, evaluated through MTT assay after 1 day and 7 days in culture. Error bars represent the standard error of the mean ( $p < 0.05$ (\*) and  $p < 0.001$ (\*\*)).

The last of the novel compositions, NCL8 silicate-based glass, showed a cytotoxic effect on cell viability after both 1 and 7 days in culture tested by direct contact. For the indirect method a decrease of rat OB activity was found particularly after 7 days in culture, and by increasing the

glass powder concentration (Figure 6.23), proving the harmful influence of this formulation on rat OB viability.

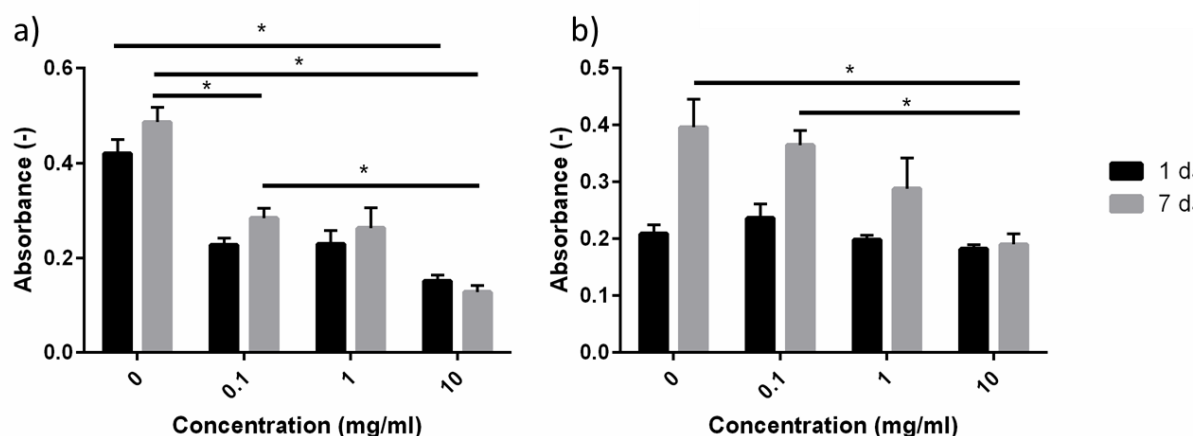


**Figure 6.23:** Effect of NCL8 glass powders (measured in triplicate) on formazan formation after (a) direct and (b) indirect contact with rat osteoblast cells, evaluated through MTT assay after 1 day and 7 days in culture. Error bars represent the standard error of the mean ( $p < 0.05$ (\*) and  $p < 0.001$ (\*\*)).

Ultimately, Figure 6.24 reports the data for AW glass powder. Similarly to composition NCL7, also in this case glass powder in direct contact with cells, and at high concentrations slightly compromised their mitochondrial activity (Figure 6.24 (a)).

However, indirect test condition (Figure 6.24(b)) showed that nevertheless an initial drop after the first 24 hours in culture, rat osteoblast mitochondrial activity improved after the longer time point.

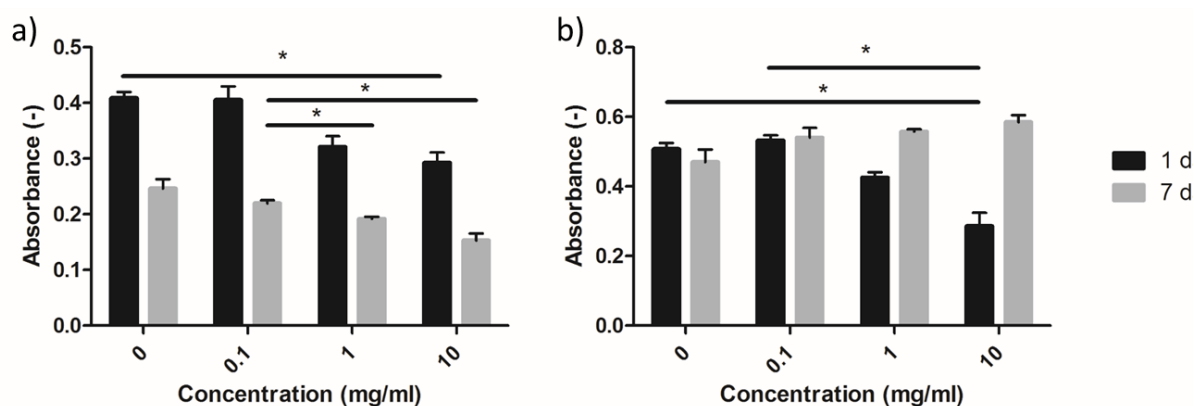


**Figure 6.24:** Effect of AW glass powders (measured in triplicate) on formazan formation after (a) direct and (b) indirect contact with rat osteoblast cells, evaluated through MTT assay after 1 day and 7 days in culture. Error bars represent the standard error of the mean ( $p < 0.05$ (\*) and  $p < 0.001$ (\*\*)).

In light of the MTT assay results, performed on raw glass powders, the following consideration can be taken:

- NCL1, NCL3, NCL6 and NCL8 formulations showed a detrimental effect on cell mitochondrial activity at all the concentrations tested, and either for direct and indirect contact test;
- NCL2, NCL4 and NCL7 compositions showed similar outcomes of AW glass-ceramic; specifically, these compositions influenced negatively cell viability following a direct contact test with high concentrations of glass powders in media, whereas they showed high cell mitochondrial activity for the indirect condition and after 7 days in culture;
- based on the *in vitro* test findings, given the high number of doping agent in each formulation, no significant correlations can be drawn between the *in vitro* glass behaviour and their structure.

### 6.3 Bioceramic pellets

This section presents the results of the experimental work conducted on bulk dense structures and prepared following the procedure described in paragraph 5.3.2. Once the pellets were pressed, they were placed in a chamber furnace. In order to assess their sintering behaviour, several thermal treatments were performed in the range 550-850°C for 1 hour (heating rate 10°C/min), according to HSM results.

#### 6.3.1 Morphological analysis

SEM investigations were performed onto bioceramic pellet surfaces to evaluate the effect of different heating treatments on sample morphology, and to further assess their sintering level. Figure 6.25 to Figure 6.32 report the pellet surface of each composition after two of the several heating treatments that were investigated. Micrographs (a) of Figure 6.25 to Figure 6.32 show a poor sintering level for all the formulations, where glass particles started to aggregate, but they were not properly sintered. The microstructures reported in micrographs (b) of Figure 6.25 to Figure 6.32 demonstrate how an increase in the heating temperatures leads to an appropriate densification status, as a result of increased liquid phase. Particularly for NCL1, NCL3, NCL6, NCL7, NCL8 and AW compositions the formation of sintering necks (red arrows in the figures) became evident.

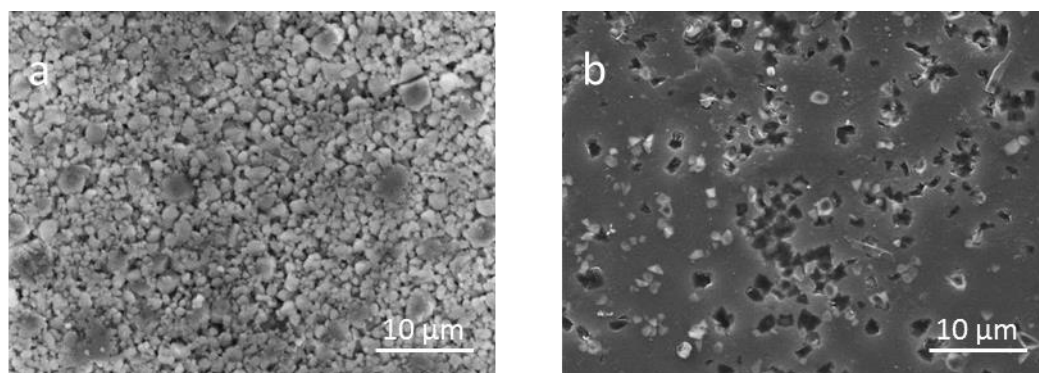


**Figure 6.25: SEM micrograph (magnification 2500x) of NCL1 pellet surface at (a) low (575°C), and (b) appropriate sintering level (625°C).**



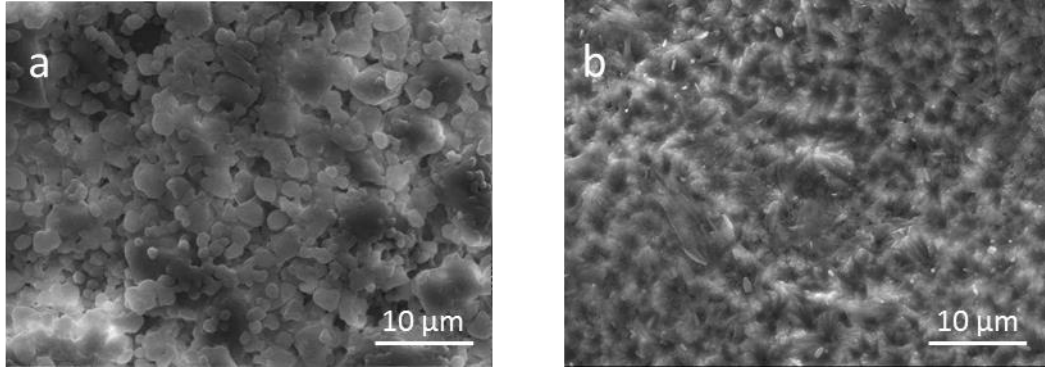


**Figure 6.26:** SEM micrograph (magnification 2500x) of NCL2 pellet surface at (a) low (650°C), and (b) appropriate sintering level (700°C).

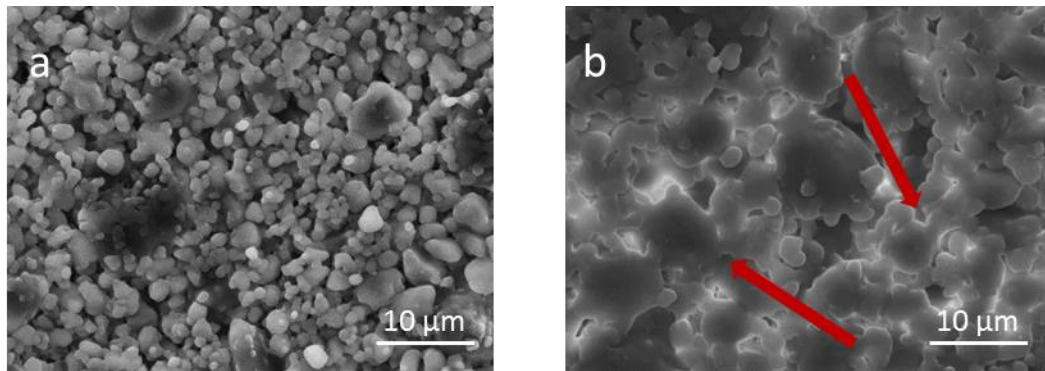


**Figure 6.27:** SEM micrograph (magnification 2500x) of NCL3 pellet surface at (a) low (550°C), and (b) appropriate sintering level (625°C); red arrows indicate necking formation.

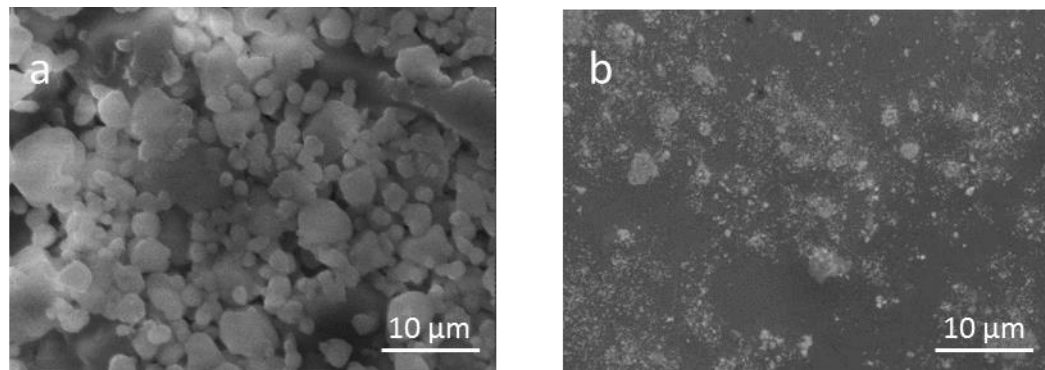


**Figure 6.28:** SEM micrograph (magnification 2500x) of NCL4 pellet surface at (a) low (600°C), and (b) appropriate sintering level (625°C).

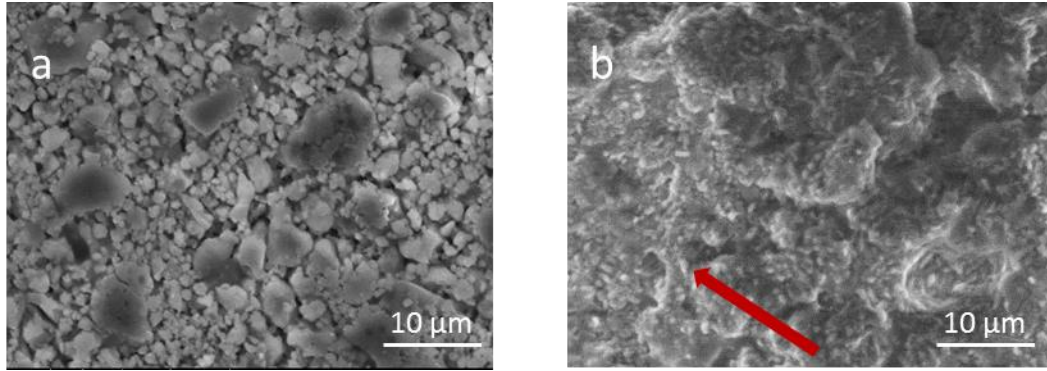


**Figure 6.29:** SEM: micrograph (magnification 2500x) of NCL6 pellet surface at (a) low (700°C), and (b) appropriate sintering level (725°C); red arrow indicates necking formation.

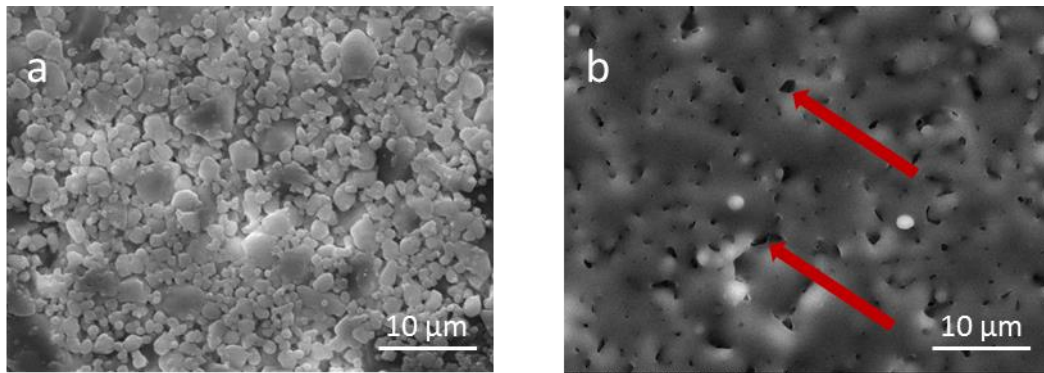


**Figure 6.30:** SEM micrograph (magnification 2500x) of NCL7 pellet surface at (a) low (600°C), and (b) appropriate sintering level (625°C); red arrows indicate necking formation.

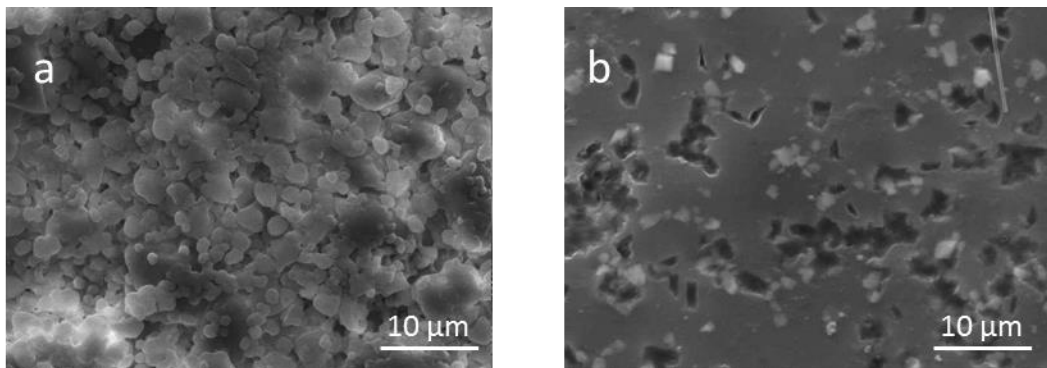


**Figure 6.31:** SEM micrograph (magnification 2500x) of NCL8 pellet surface at (a) low (575°C), and (b) appropriate sintering level (625°C).

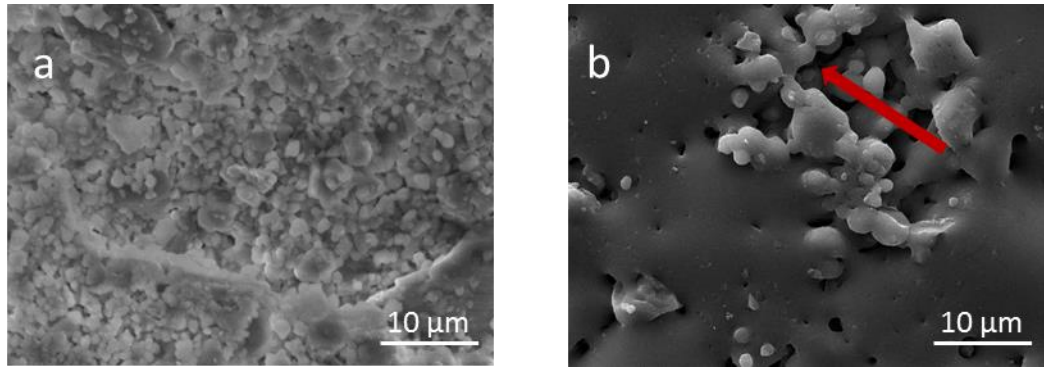


**Figure 6.32:** SEM micrograph (magnification 2500x) of AW pellet surface at (a) low (830°C), and (b) appropriate sintering level (850°C); red arrow indicates necking formation.

### 6.3.2 Bioceramic pellets sintering conditions

In light of the SEM microstructural observations, and after a thorough qualitative analysis, the heating treatment temperatures that provided the best densification degree of the bioceramic pellets, and hence mechanically competent structures are shown in Table 6.4 below.

**Table 6.4:** Bioceramic pellets sintering temperatures.

CODE	COMPOSITION	SINTERING TEMPERATURE (°C)
NCL1	Silicate-based	625
NCL2	Silicate-based	700
NCL3	Borate-based	625
NCL4	Borate-based	625
NCL6	Phosphate-based	725
NCL7	Silicate-based	625
NCL8	Silicate-based	625
AW	Silicate-based	850

### 6.3.3 X-ray diffraction analysis before and after sintering

XRD spectra for all 7 compositions and AW, before and after sintering, are reported in Figure 6.33 to Figure 6.40. NCL1, NCL3, NCL4, and NCL8 formulations maintained the same amorphous status also after the sintering treatment (see Figure 6.33, Figure 6.35, Figure 6.36 and Figure 6.39). Crystalline phases developed during the sintering treatments of NCL2 formulation (Figure 6.34) were identified as diopside phase (ICDD ref. code 01-073-6374).

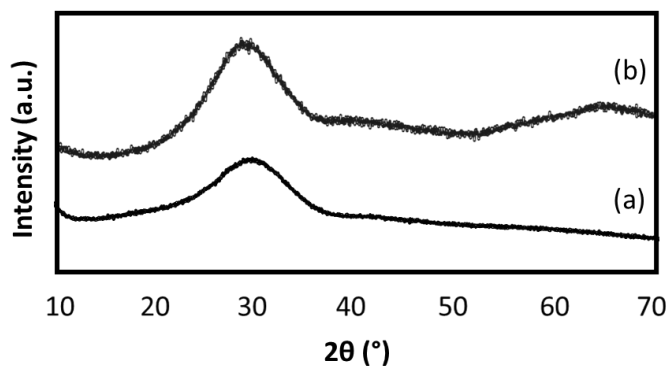


Figure 6.33: XRD patterns of NCL1 composition: (a) glass powder and (b) pellet sintered at 625°C.

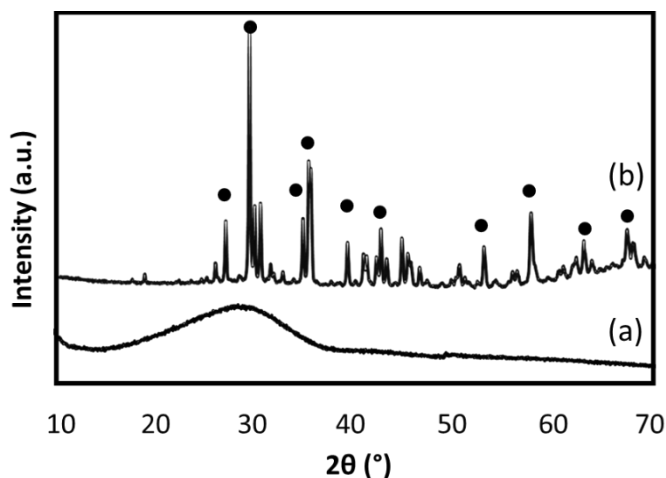
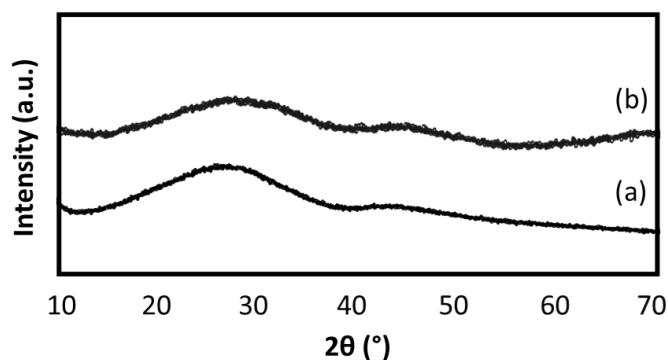
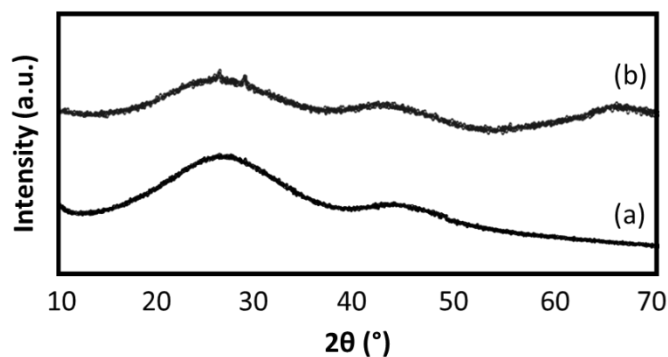


Figure 6.34: XRD patterns of NCL2 composition: (a) glass powder and (b) pellet sintered at 700°C (● diopside).



**Figure 6.35:** XRD patterns of NCL3 composition: (a) glass powder and (b) pellet sintered at  $625^{\circ}\text{C}$ .



**Figure 6.36:** XRD patterns of NCL4 composition: (a) glass powder and (b) pellet sintered at  $625^{\circ}\text{C}$ .

NCL6 sample was not completely amorphous before sintering. Peaks corresponding to calcium sodium phosphate were detected on NCL6 glass powder (Figure 6.37(a)).

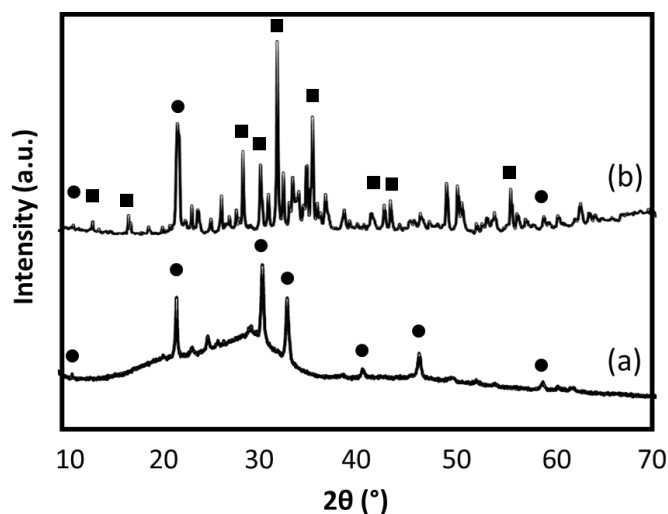


**Figure 6.37:** XRD patterns of NCL6 composition: (a) glass powder and (b) pellet sintered at  $725^{\circ}\text{C}$ , (● calcium sodium phosphate and ■ sodium calcium magnesium phosphate).

The heat treatment contributed to the further development of a crystalline phase, as shown in Figure 6.37(b), with the growth of a sodium calcium magnesium phosphate phase (ICDD ref. code 00-045-0136).

Figure 6.38 displays the XRD pattern of the NCL7 formulation. This glass was almost amorphous, as a very low amount of Ag was detected before the sintering treatment. The intensity of Ag peaks (ICDD ref. code 04-003-1425) increased after sintering.

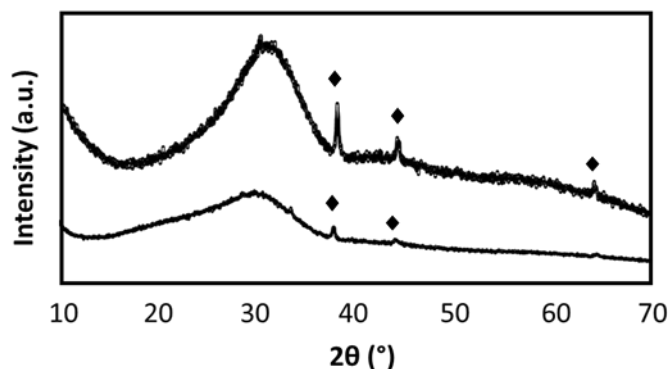


**Figure 6.38:** XRD patterns of NCL7 composition: (a) glass powder and (b) pellet sintered at 625 C, (♦ silver).

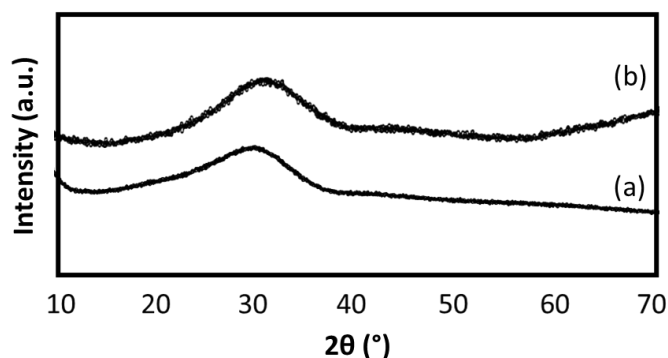


**Figure 6.39:** XRD patterns of NCL8 composition: (a) glass powder and (b) pellet sintered at 625°C.

Figure 6.40 shows the XRD results of the glass powder and sintered A-W pellet. Although the crystalline phases remained the same (hydroxylapatite and  $\beta$ -wollastonite), after the sintering process the sintered material showed more intense peaks (Figure 6.40(b)) with respect to the raw glass-powder (Figure 6.40(a)), confirming the glass-ceramic nature of this formulation.

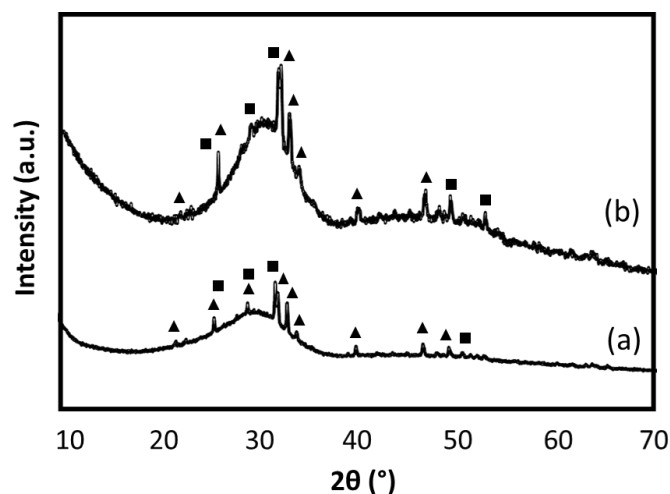


*Figure 6.40: XRD patterns of AW composition: (a) glass powder and (b) pellet sintered at 850°C, (▲ hydroxylapatite, ■  $\beta$ -wollastonite).*

#### 6.3.4 Sintering behaviour

Figure 6.41 reports the volumetric shrinkage (%) of the novel bioceramic pellets calculated according to the formula described in paragraph 5.4.6, and following the sintering conditions reported in Table 6.4. For all materials the volumetric shrinkage was between 29% and 36%.

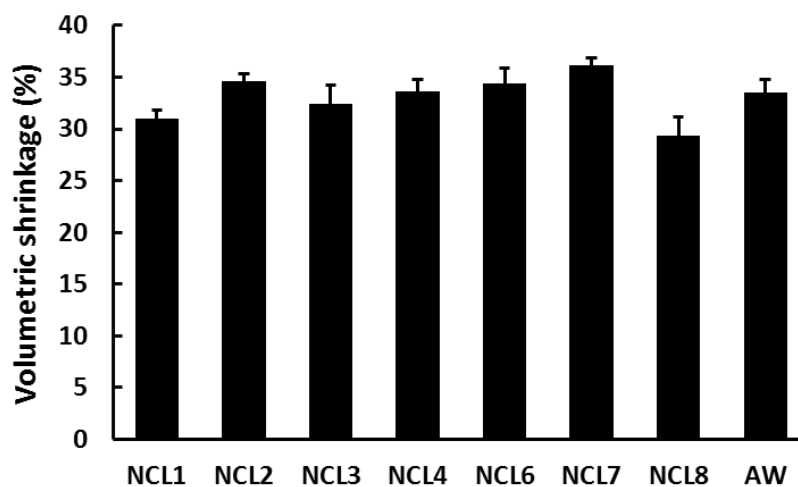


*Figure 6.41: Average volumetric shrinkage (%) for sintered pellets (n=5). Error bars represent the standard error of the mean.*

### 6.3.5 Mechanical properties

A representative stress-strain curve of the sintered bioceramic pellets, assessed in compression using a Tinius Olsen universal testing machine, is reported in Figure 6.42. The curve indicated that the stress increased linearly with increasing compressive strain.

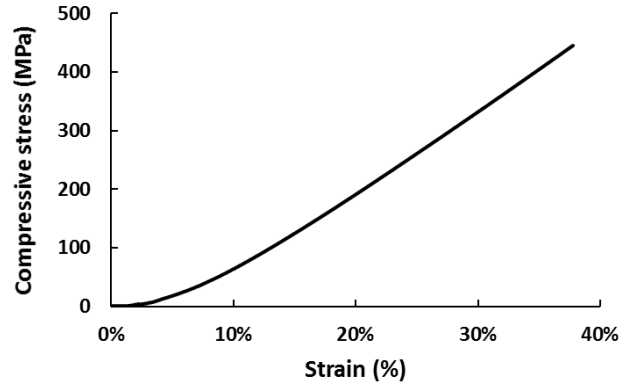


**Figure 6.42:** *Representative stress-strain curve obtained during compression tests performed on the sintered bioceramic pellets.*

The averaged compressive stress at 20% ( $\sigma_{20}$ ) of the strain, and compressive modulus ( $E_c$ ) data are shown in Figure 6.43. All the seven bioceramic pellets had a  $\sigma_{20}$  higher than the one of AW, with NCL8 showing the highest value ( $286 \pm 11$  MPa). According to the results obtained (Figure 6.43(a)), a part from composition NCL7, the silicate-based glasses (NCL1, NCL2 and NCL8) showed a small but significant increase for both  $E_c$  and  $\sigma_{20}$  compared to AW. No significant differences were found for phosphate and borate-based formulations.

Regarding the compressive modulus (Figure 6.43(b)), very significant differences ( $p < 0.001$ ) were observed for the NCL1 and NCL8 compositions, and significant differences ( $p < 0.05$ ) for NCL2 and NCL3 compositions in comparison to AW glass-ceramic. However, all the glasses showed  $\sigma_{20}$  values in excess of 150 MPa, and modulus values in excess of 1.2 GPa.



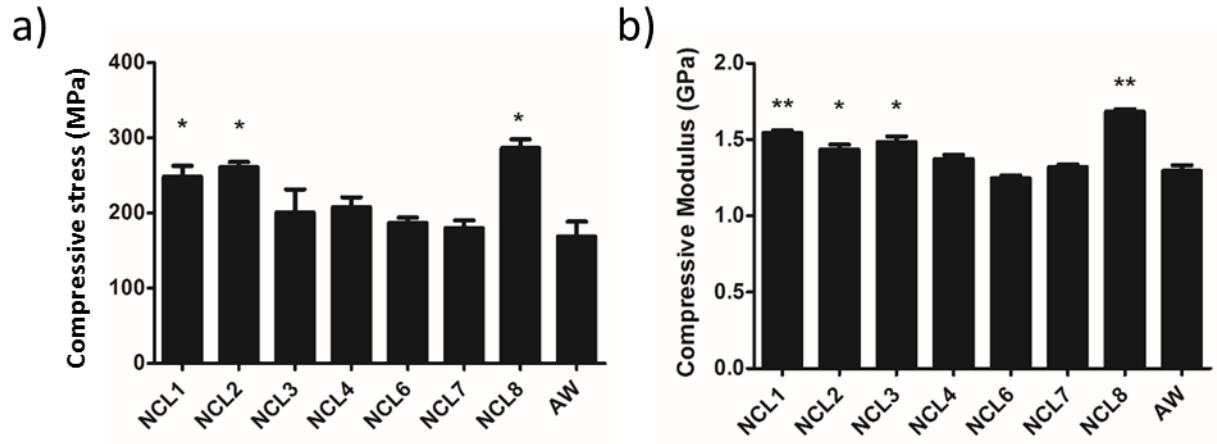


*Figure 6.43: a) Averaged compressive stress (for  $\epsilon_c=20\%$ ) and b) compressive modulus values of dry bioceramic pellets ( $n=5$ ). Error bars represent the standard error of the mean ( $p<0.05(*)$  and  $p<0.001(**)$ ).*

#### 6.4 Selection of glass compositions as potential bone tissue-like substitutes

Considering the stringent criteria necessary for the design of 3D bone-like substitutes (previously presented in Table 3.1), the development of novel biomaterials for bone tissue repair remains a highly challenging task. However, those set of requirements can be considered an essential guideline for accepting or improving a material response according to specific clinical situation demands. Along with appropriate physico-chemical properties necessary to match the characteristics of the host tissue (*i.e.* degradation rate, surface chemistry) (Reis and Román, 2004; Mitra *et al.*, 2013), a crucial aspect for the effective success of bone substitutes for load-bearing applications is a good balance between porosity of the structure and its mechanical proprieties (Chu *et al.*, 2002; Hsin and Yiwei, 2011; Loh and Choong, 2013). As described in Table 3.1, a highly interconnected porous structure is essential to enable fluid flow, cell migration, bone ingrowth and vascularization (Liu *et al.*, 2013). However, porosity affects the mechanical behaviour of the structure, since strength and stiffness gradually decrease when the volume fraction of pores increases (Vitale-Brovarone *et al.*, 2010).

In light of the results presented in paragraph 6.3.5, which showed the mechanical performance of the new formulations in form of dense bioceramic pellets, similar properties were found with respect to the widely applied AW glass-ceramic (Kokubo, 2008), particularly for NCL4, NCL6 and NCL7 compositions. Hence, all the formulations could be considered potential biomaterials for bone repair applications. However, since a biomaterial should perform its function without exhibiting any immune response in the host tissue, another important aspect, that it is worth to consider, concerns the *in vitro* biocompatibility (Hutmacher, 2000; Hutmacher, 2001). Particularly, the cytotoxicity of novel developed biomaterials is a key issue that should be addressed prior to pre-clinical trials (Hollinger, 2011). In paragraph 6.2.6 the *in vitro* cytotoxicity data resulting from raw glass powders were presented. The results of the tests revealed that for the direct method, and high concentration of glass powder (10mg/l), cell mitochondrial activity was significantly affected by the presence of the glass particles. On the other hand, the indirect method indicated that after 7 days in culture and at the highest concentration tested NCL2, NCL4 and NCL7 showed no significant differences with respect to the control (similarly to AW glass-ceramic behaviour). On the basis of the MTT results, and considering the assumption according to which the biocompatibility of new materials is a key concern for the following clinical application, only NCL2, NCL4 and NCL7 formulations were selected for further characterisation.

## 6.5 Bioactivity evaluation

This paragraph presents the results obtained from SBF testing on selected bioceramic pellets (NCL2, NCL4, NCL7 and AW).

The SEM micrographs and EDS analysis of the top surface of NCL2 dense pellets before immersion in SBF solution and after 7 days of soaking are shown in Figure 6.44(a-b) and Figure 6.44(c-d) respectively. No signs of precipitate formation were detected on the sample surface after 7 days of soaking.

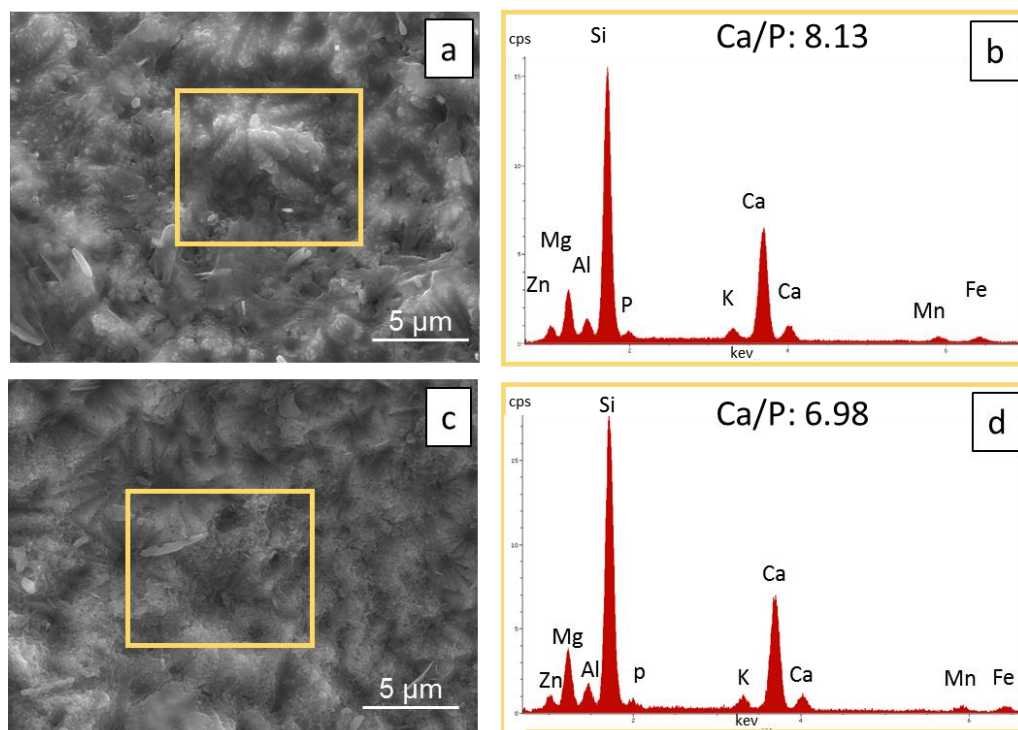


**Figure 6.44:** a) morphological (5Kx mag) and b) compositional analysis of the marked region of NCL2 bioceramic pellet before the immersion in SBF. c) morphological (5Kx mag) and d) compositional analysis (at %) of the marked region of NCL2 bioceramic pellet after 7 days of immersion in SBF.

However, after 28 days in immersion, NCL2 specimens developed a homogeneous rough layer on their surface (Figure 6.45(a-b)), even though no HCA formation was detected (see EDS spectra in Figure 6.45(c)).

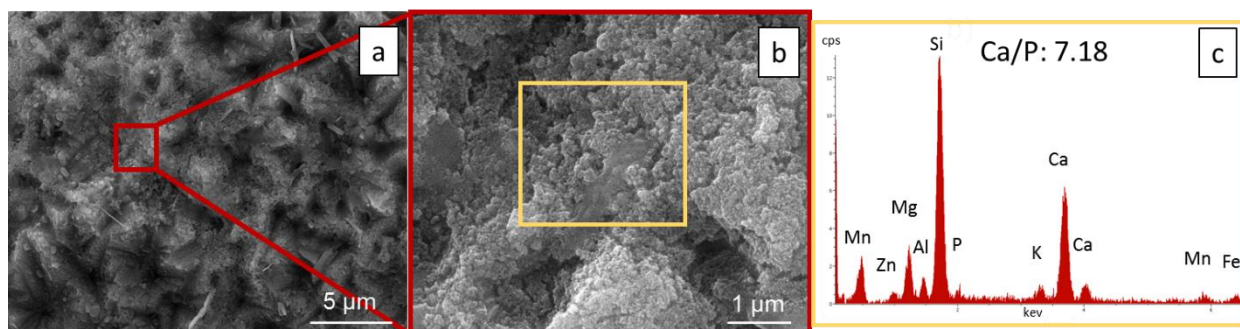


**Figure 6.45: a) morphological (5Kx mag) analysis with b) higher magnification inset (20Kx mag), and c) compositional analysis (at %) of the marked precipitates observed on NCL2 bioceramic pellet after 28 days of soaking in SBF.**

Regarding NCL4 composition, Figure 6.46 shows the SEM micrographs and EDS compositional analysis of the top surface, before (Figure 6.46(a-b)) and after 7 days (Figure 6.46(c-d)) of soaking in SBF solution. As suggested by the SEM analysis and EDS spectra, globular shaped agglomerates rich in calcium and phosphorous (Ca/P=0.76) (Figure 6.46(d)) precipitated on the sample surface, during the 7 days of immersion.

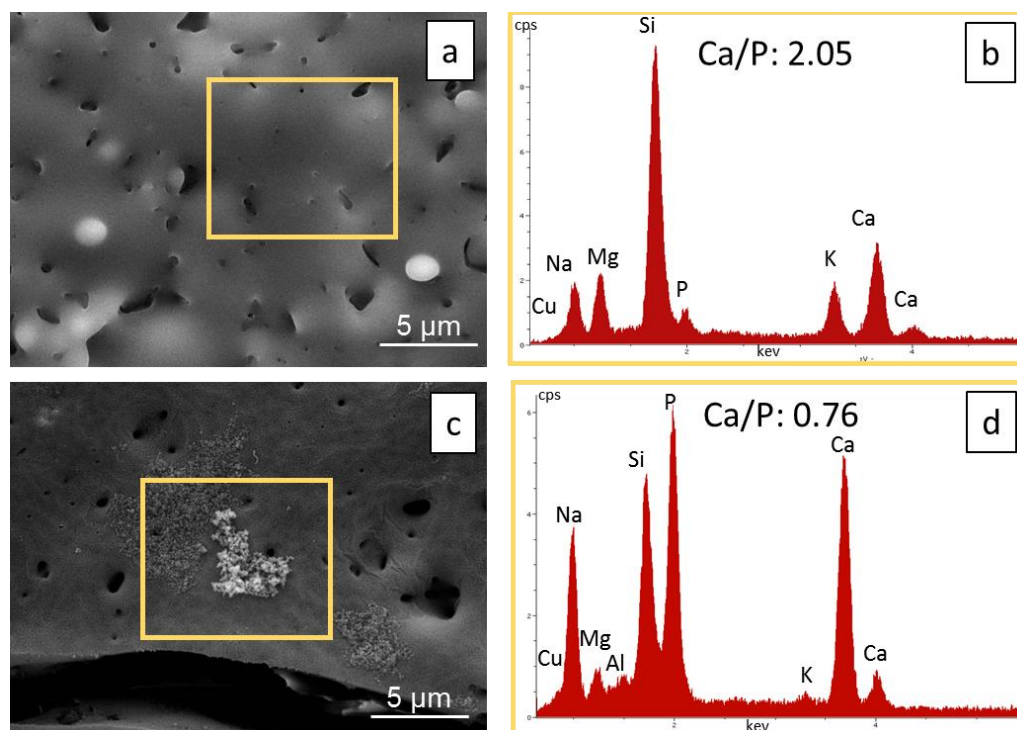


**Figure 6.46: a) morphological (5Kx mag) and b) compositional analysis of the marked region of NCL4 bioceramic pellet before the immersion in SBF. c) morphological (5Kx mag) and d) compositional analysis (at %) of the marked region of NCL4 bioceramic pellet after 7 days of immersion in SBF.**

After 28 days of immersion, more granular structures (see white arrows in Figure 6.47(b)) were observed on the NCL4 pellets surface, with the Ca/P ratio that moved from 0.76 at day 7 to 1.08 at day 28 (see spectra in Figure 6.47(c)).

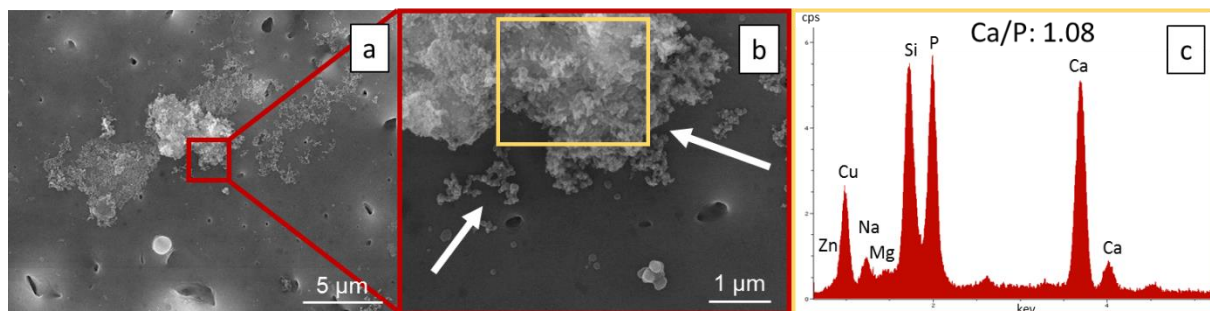
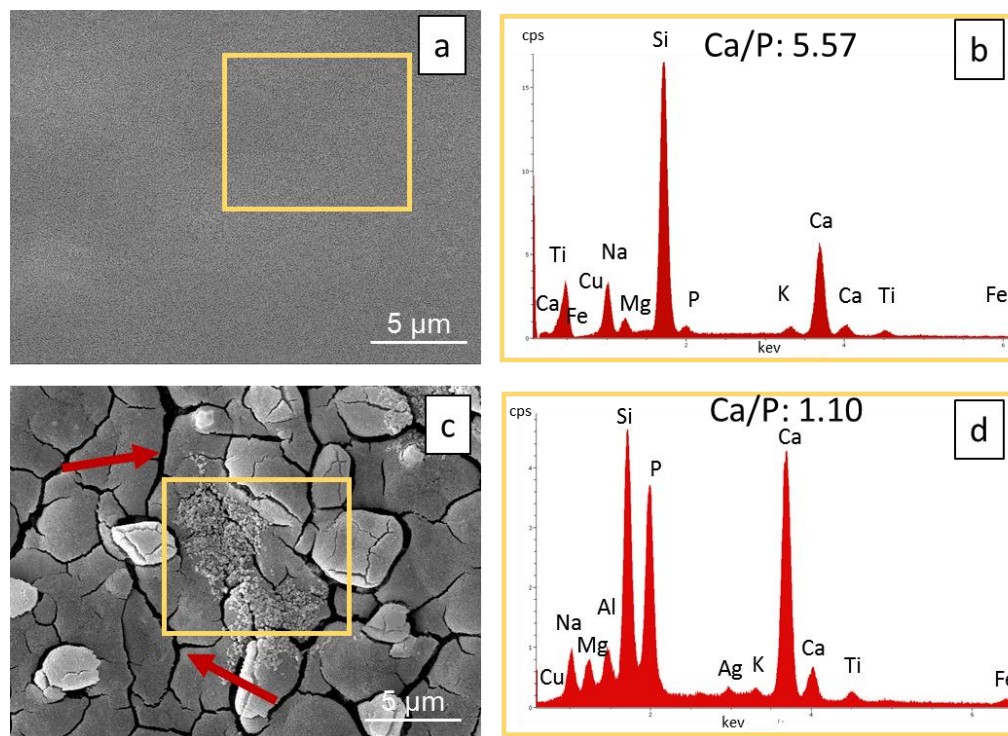


**Figure 6.47: a) morphological (5Kx mag) analysis with b) higher magnification inset (20Kx mag), and c) compositional analysis (at %) of the marked precipitates observed on NCL4 bioceramic pellet after 28 days of soaking in SBF (white arrows indicate the granular structures developed on the pellet surface).**

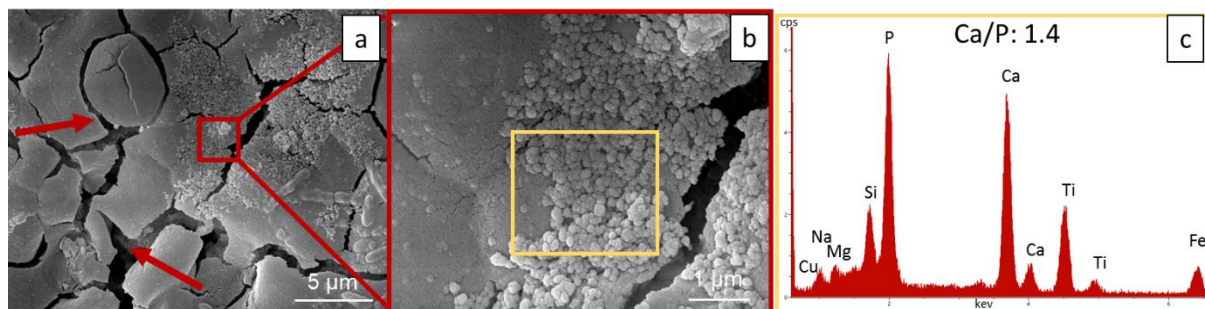
The top surface SEM imaging and the corresponding EDS spectra for NCL7 bioceramic pellets, before and after 7 days of soaking in SBF, are reported in Figure 6.48(a-b) and Figure 6.48(c-d) respectively. Also in this case no apatite formation was detected after 7 days. Although, similarly to NCL4 composition, globular shaped agglomerates were identified on the sample surface, with a Ca/P ratio of 1.10, as reported in the EDS analysis (see Figure 6.48(d)). However, Figure 6.48(c) documents the formation of micro-cracks (indicated by the red arrows in the figure), and the presence of a thin silica-rich layer, which usually forms during the first steps of the bioactivity process.

In fact, after 28 days of immersion in SBF, the micro-cracks development on the pellets surface (see Figure 6.49(a)) became more pronounced. Calcium phosphate agglomerates with a cauliflower-like shape precipitated on the NCL7 sample surface, as can be observed in Figure 6.49(b). In addition, the Ca/P ratio of the precipitates increased from 1.1 at day 7 to 1.4 at day 28 (Figure 6.49(c)), which may be considered an HA precursor, thus indicating the potential bioactive behaviour of NCL7 composition.



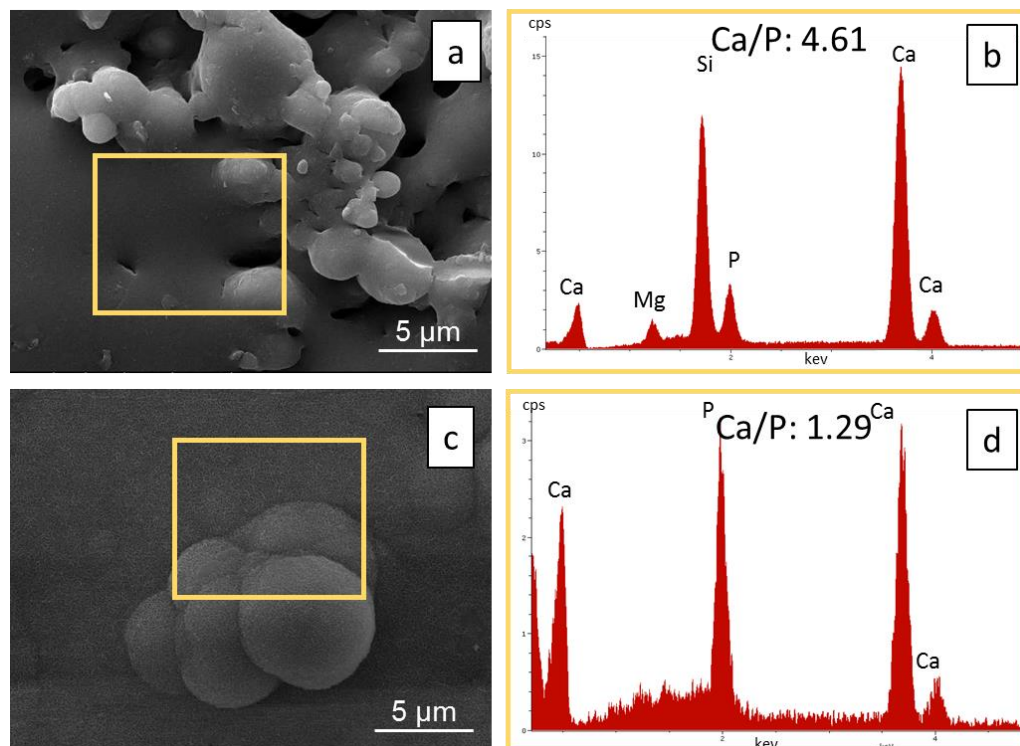


**Figure 6.48:** a) morphological (5Kx mag) and b) compositional analysis of the marked region of NCL7 bioceramic pellet before the immersion in SBF. c) morphological (5Kx mag) and d) compositional analysis (at %) of the marked region of NCL7 bioceramic pellet after 7 days of immersion in SBF (the red arrows indicate the micro-cracks formation on the pellet surface).



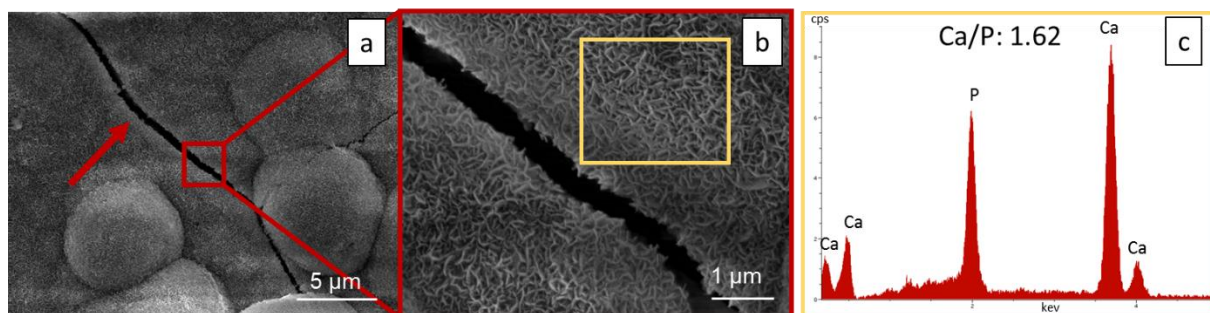
**Figure 6.49:** a) morphological (5Kx mag) analysis with b) higher magnification inset (20Kx mag), and c) compositional analysis (at %) of the marked precipitates observed on NCL7 bioceramic pellet after 28 days of soaking in SBF (the red arrows indicate the micro-cracks formation on the pellet surface).

Regarding AW composition (Figure 6.50), the upper surface of the pellets after one week of immersion (see Figure 6.50(c)) was homogenously covered by a thin layer of apatite enriched in Ca and P (see Figure 6.50(d)), proving the quick bioactive process that characterised this material.



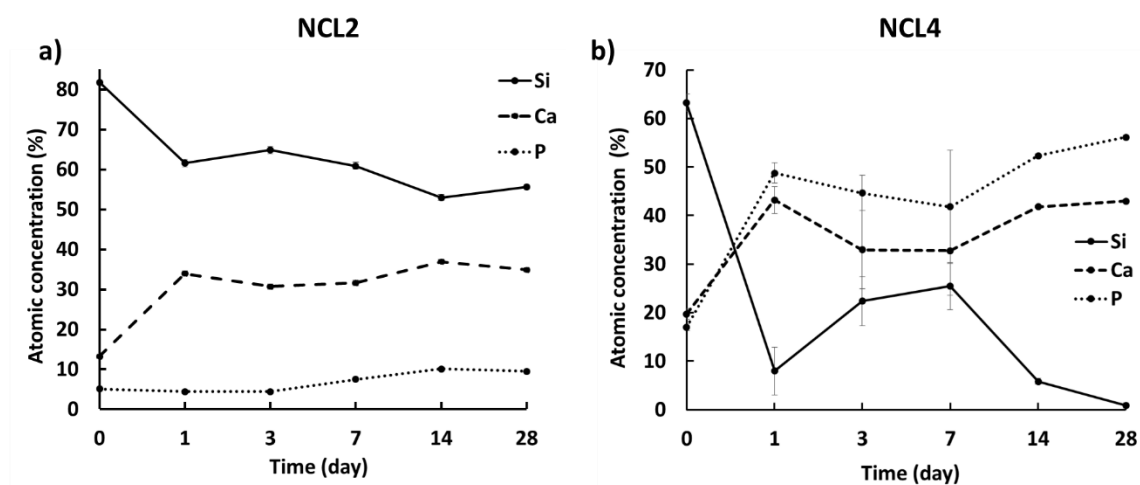
**Figure 6.50: a) morphological (5Kx mag) and b) compositional analysis of the marked region of AW bioceramic pellet before the immersion in SBF. c) morphological (5Kx mag) and d) compositional analysis (at %) of the marked region of AW bioceramic pellet after 7 days of immersion in SBF (the red arrows indicate the micro-cracks formation on the pellet surface).**

SEM analysis together with the EDS spectra of AW after 28 days in SBF immersion are shown in Figure 6.51. The high bioactive potential of AW glass-ceramic has already been widely investigated in the literature (Magallanes-Perdomo *et al.*, 2011; Park and Ozturk, 2013). However, in this study the extensively documented bioactive properties of AW formulation, were proved by: *i)* the precipitation of a homogeneous needle-like layer rich in Ca and P (see Figure 6.51(a)), *ii)* the micro-cracks formation (Figure 6.51(b)), and *iii)* most importantly by the Ca/P ratio of around 1.62 (Figure 6.51(c)) that is nearly equal to the composition of human bone hydroxyapatite (Ca/P=1.67) (Palmer *et al.*, 2008).



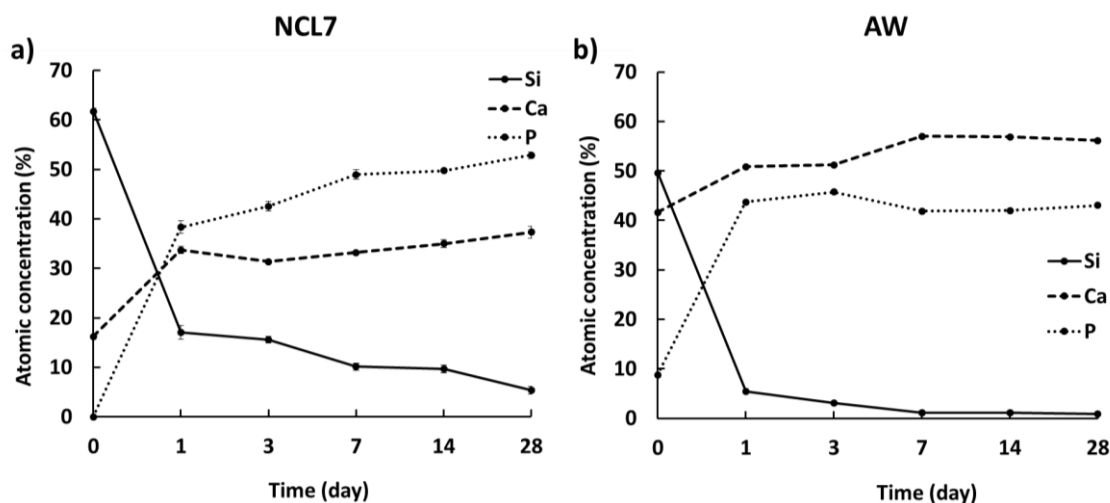
**Figure 6.51:** *a) morphological (5Kx mag) analysis with b) higher magnification inset (20 Kx mag), and c) compositional analysis (at %) of the marked precipitates observed on NCL7 bioceramic pellet after 28 days of soaking in SBF (the red arrows indicate the micro-cracks formation on the pellet surface).*

In addition to the semi-quantitative analysis performed, a quantitative elemental characterisation of the sample surfaces before and after soaking in SBF was assessed by XPS, in order to evaluate the atomic concentration of the main elements (Si, Ca and P) potentially involved in the bioactivity process. The XPS analysis evidenced that after 28 days of soaking in SBF, silicon content decreased for all the investigated compositions (Figure 6.52 and Figure 6.53). Conversely, the atomic concentration of calcium and phosphorous slightly increased for all the pellets, as consequence of the formation of CaP precipitates on their top surface. Specifically, for NCL2 phosphorous (at.%) remained almost steady (~9.5 after 28 days in immersion), while for the other compositions it reached values above 40%. The concentration of calcium instead increased beyond 30% for all the formulations.



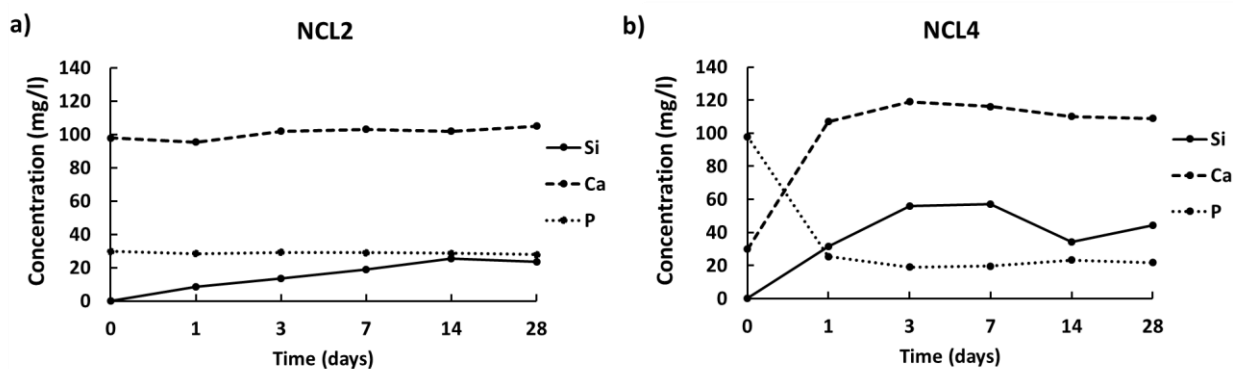
**Figure 6.52:** *Atomic concentration of Si, Ca and P on the upper surface of a) NCL2 and b) NCL4 bioceramic pellets after immersion in SBF at different time points.*





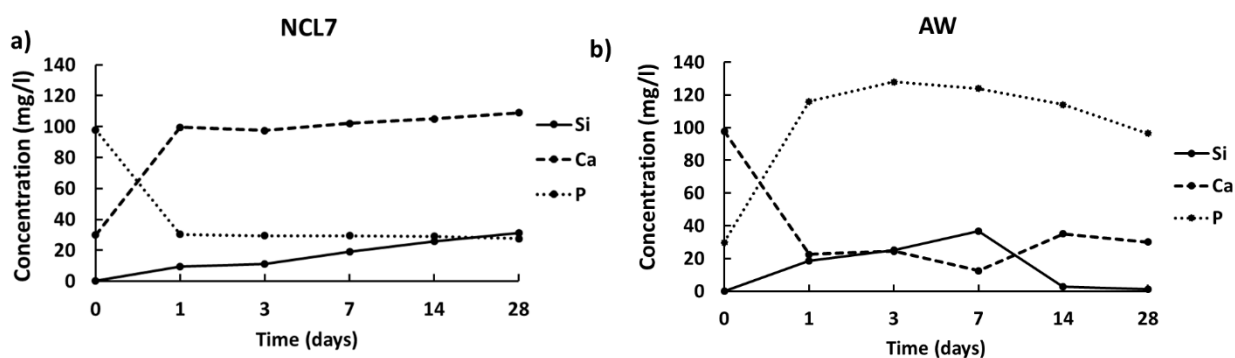
**Figure 6.53 : Atomic concentration of Si, Ca and P on the upper surface of a) NCL7 and b) AW bioceramic pellets after immersion in SBF at different time points.**

Ion leaching variation of Si, Ca, and P from bioceramic pellets, soaked in SBF solution at different time intervals, was evaluated using ICP – OES analysis. As evidenced in Figure 6.54(a), for NCL2 the concentration of Ca and P released in solution was almost constant for the all immersion time points; instead Si increased gradually up to day 14 and then started to decrease slowly. For NCL4 bioceramic pellets (see Figure 6.54(b)) the release of Ca increased rapidly during the early stage of immersion and then remained around 110mg/l until the end of the soaking time, whereas P concentration decreased rapidly from 100mg/l to 25mg/l after 1 day of soaking, and then maintained a level around this value up to 28 days of soaking in SBF. Si release increased up to 3 days in immersion, then after a steady profile between day 3 and 7, it showed a “zig-zag” variation up to day 28.



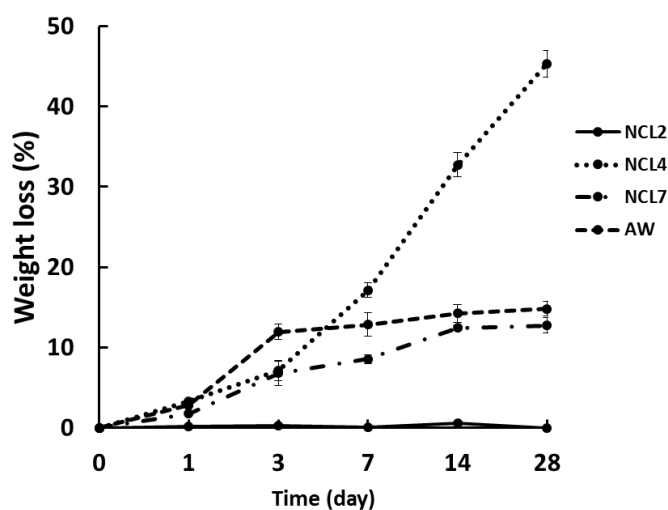
**Figure 6.54: Release profiles of Si, Ca and P ions for a) NCL2 and b) NCL4 bioceramic pellets immersed in SBF solution at different time intervals.**

Figure 6.55 reports the results for composition NCL7 and AW formulations. The variation of Ca and P for NCL7 samples had a quite specular profile as well as a similar range of values. The release of silicon from NCL7 composition in SBF solution showed a gradual increase from 0 to 28 days. For AW composition (Figure 6.55(b)) Ca content decreased rapidly during the early stage, and then fluctuated around 22mg/l with the increasing immersion time. P reached 116mg/l after 24 hours in immersion, and then declined slowly to 96.5mg/l at day 28. After a slow growth with a peak at day 7 (36.8mg/l), silicon dropped to almost zero at day 28.



**Figure 6.55:** Release profiles of Si, Ca and P ions for a) NCL7 and b) AW bioceramic pellets immersed in SBF solution at different time intervals.

The *in vitro* biodegradation behaviour of the fabricated pellets was further studied by measuring the weight loss of the samples, up to 28 days in SBF immersion, as function of the storage time (Figure 6.56).



**Figure 6.56:** Averaged weight loss ( $\pm$ SE) of NCL2, NCL4, NCL7 and AW pellets after soaking in SBF solution.

As expected, the weight loss for NCL4 samples was higher with respect to the other specimens, confirming that borate-based glasses have a faster dissolution rate, in accordance with the literature (Yao *et al.*, 2007; Liu *et al.*, 2010; Deliormanli, 2013; Wang *et al.*, 2014). NCL7 and AW showed a similar trend all over the considered interval, with a mass loss around 12% and 14% respectively, after 28 days of soaking, whereas no marked sign of degradation was found for NCL2 formulation. The degradation process of a bioactive glass takes place by ionic exchange of soluble ions, which, depending on the glass composition, influence the pH of the surrounding media (Rahaman *et al.*, 2011). In order to evaluate the hydrolytical stability of the bioceramic pellets after immersion in SBF, the pH changes during the 28 days of immersion were assessed.

Figure 6.57 reports the pH values measured during 28 days of immersion. As it can be observed, all the compositions were characterised by a low pH variation over the period, which ranged between 7.44 and 7.74.

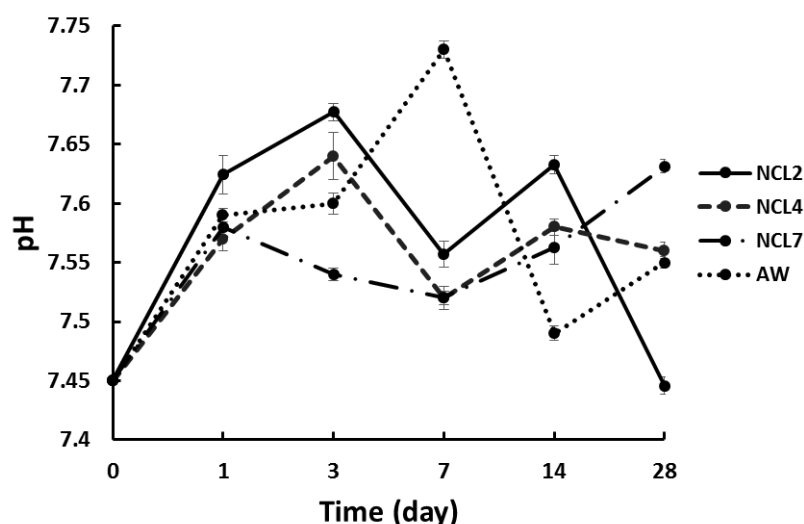


**Figure 6.57:** Averaged pH value ( $\pm$ SE) of SBF solution for NCL2, NCL4, NCL7 and AW samples.

## Chapter 7. Results: manufacturing of 3D porous glass-derived substitutes

---

### 7.1 Introduction

The use of AM technology for the production of bone-like substitutes has been predicted to increase in the coming years, primarily focusing on the development of medical implants that can be customised according to patient and clinical needs. Among the different computer-aided fabrication techniques, indirect powder-based 3D printing is such a versatile technology that has been widely used to produce scaffolds from a broad variety of materials (Bose *et al.*, 2013). The advantages of this method, in the field of bone tissue engineering, derive from *i*) the flexibility in material usage and *ii*) the possibility of printing objects with defined geometry, controlled and interconnected structure without the use of any toxic solvent (Utela *et al.*, 2010; Butscher *et al.*, 2011; Bose *et al.*, 2013). Several studies in the literature investigated the potential of powder-based 3DP technology to process ceramic-based materials alone or in combination with other blended compounds for bone tissue applications, however the lack of appropriate mechanical properties is still their major limitation (Lee *et al.*, 2005; Leukers *et al.*, 2005; Irsen *et al.*, 2006b; Utela *et al.*, 2006a; Vorndran *et al.*, 2008; Butscher *et al.*, 2012; Cox *et al.*, 2015).

The main objectives of the last part of this work are:

- i) to manufacture 3D porous glass-derived substitutes *via* powder-based 3DP technology, using the three novel glass formulations that showed appropriate mechanical and biological properties during the first two stages of the study,
- ii) to characterise them in terms of physico-chemical, mechanical and biological performance.

For powder-based 3D printing systems, grain size and grain size distribution of the starting materials are crucial factors for the physical characteristics of the final 3D printed parts. Specifically, they must be taken into account during the manufacturing of porous tissue substitutes, since they directly influence porosity, which in turn has been seen to impact cell attachment, proliferation and differentiation, and equally importantly the resulting mechanical properties of the implant (Spath *et al.*, 2015).

In the current study, a ZCorp 310 3D printer was used as processing route to create 3D bone-like substitutes based on blends of glass powder - MD (70:30 w/w) as precursor materials. The particle range (between 0 and 53  $\mu\text{m}$ ) of the raw materials was chosen according to the work performed by Alharbi, where different blend of AW-MD were used to investigate the feasibility of powder-based 3DP technology, and its potential utility for bone tissue engineering applications (Alharbi, 2015).

## 7.2 Indirect 3D printed bioceramic substitutes

Figure 7.1 displays the microstructures of NCL2, NCL4, NCL7 and AW green bodies resulting from the indirect 3D printing process. As can be observed from Figure 7.1(b), composition NCL4 showed a very brittle and less compact structure with respect to the other formulations and resulted not suitable for further processing and characterisation.

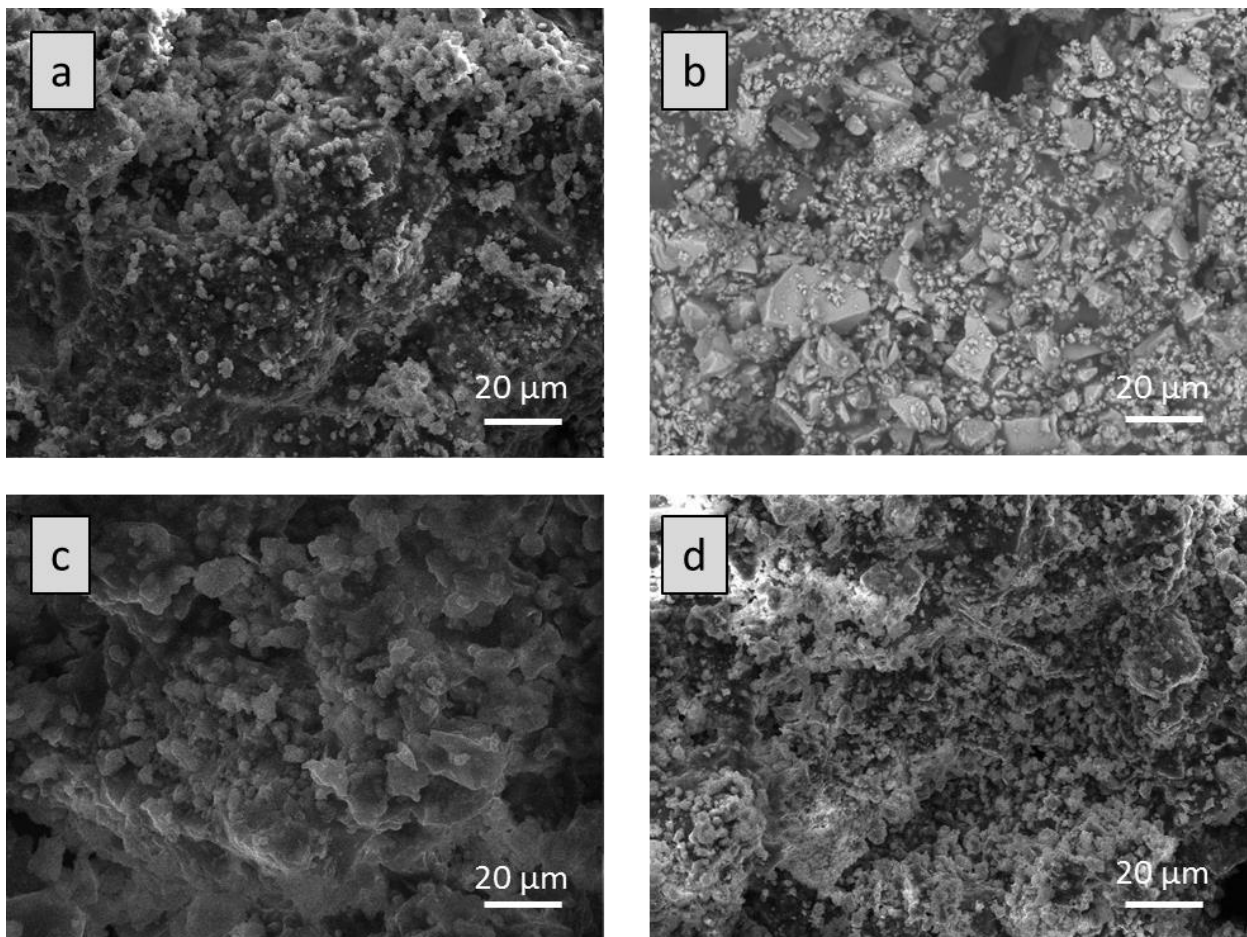


*Figure 7.1: SEM micrographs of 3D printed green bodies: a) NCL2, b) NCL4, c) NCL7 and d) AW samples.*

### 7.2.1 Sintering optimisation

Once the green bodies were printed, the indirect stage of the process started. Different thermal treatments were performed and optimised on both NCL2 and NCL7 compositions in order to obtain mechanically competent 3D porous parts with appropriate structural integrity. Figure 7.2 displays the three sintering profiles evaluated for NCL2 3D printed green bodies. The heat treatment 1 was a one-step treatment, on the basis of the results obtained from the HSM, and already evaluated for the sintering of dense bioceramic pellets. For the heat treatment 2, an intermediate step at 400°C was investigated to allow a better nucleation of the glass particles; however, many micro-cracks developed in the structures during the sintering process.

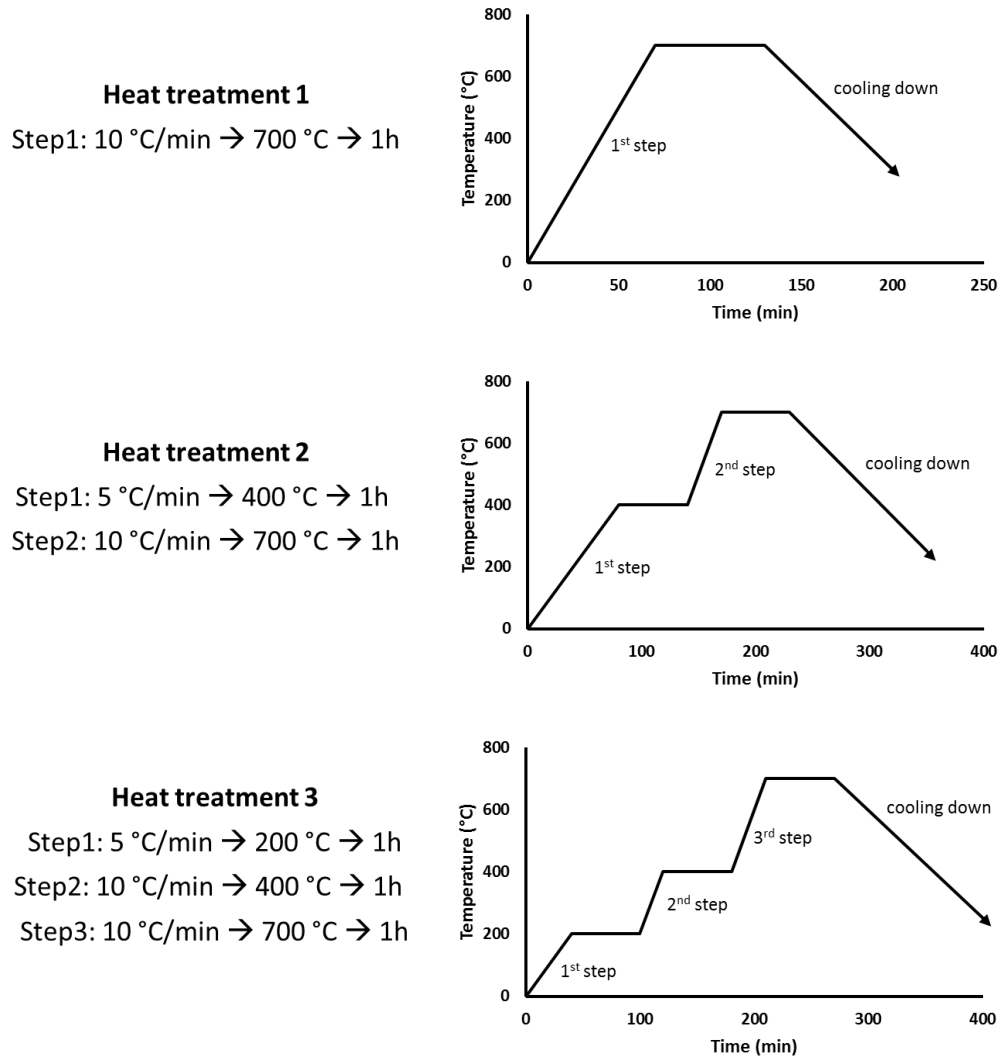


*Figure 7.2: Heat treatments and corresponding profiles that were investigated for NCL2 3D printed green bodies.*

Hence, considering the presence of the polymer-based binder, the thermal cycle was modified to remove completely the sacrificial porogen without losing the sample integrity. A third and longer (5°C/min) step was added to the previous heat treatment in order to permit the burning-out of the binder and the gradual consolidation of the bioceramic structure. Similar considerations were adopted for composition NCL7, for which the corresponding heating profiles are illustrated in Figure 7.3. The maximum heating temperature, in this case was 625°C. In the end, the heat treatment 3 in Figure 7.2 and in Figure 7.3 was selected as the more appropriate for the sintering of NCL2 and NCL7 3D printed green parts respectively.

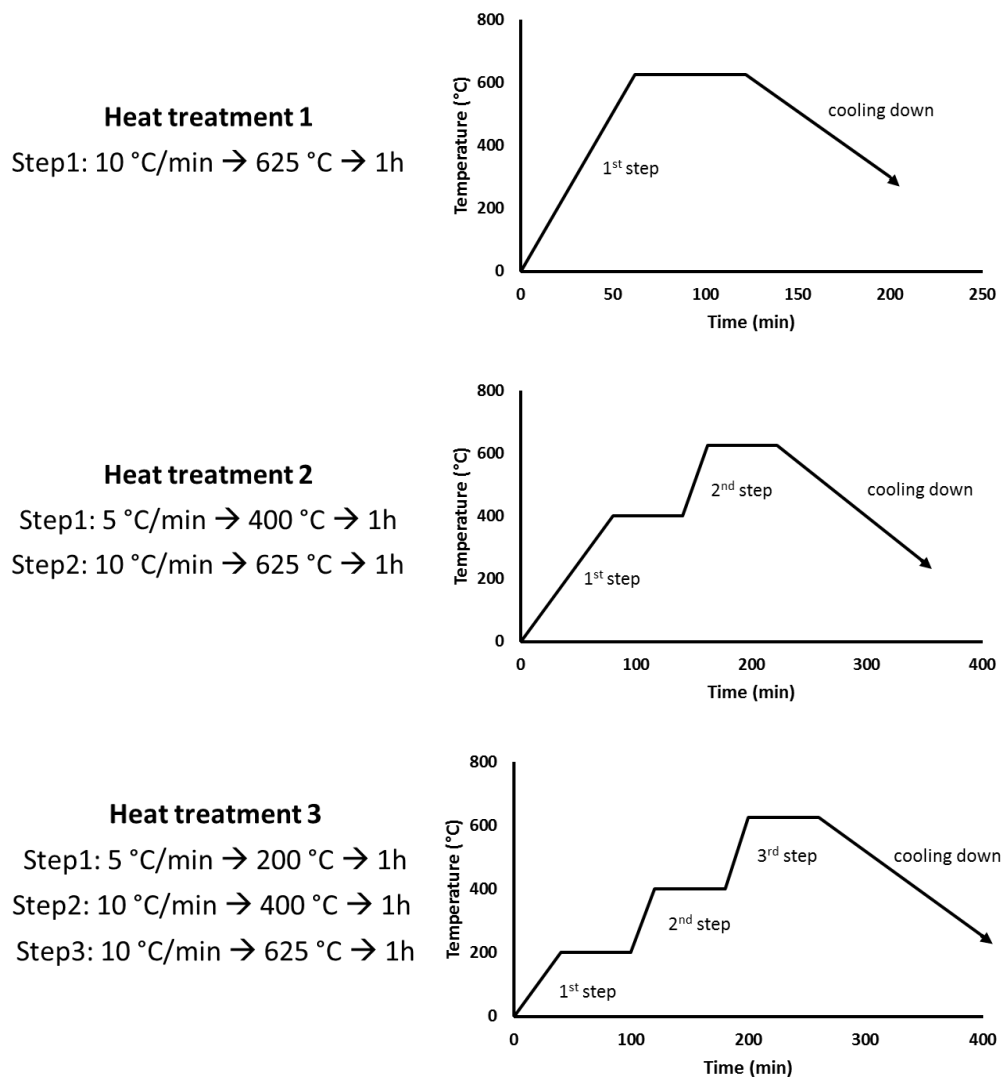


*Figure 7.3: Heat treatments and corresponding profiles that were investigated for NCL7 3D printed green bodies.*

For all the heat treatments each step consisted of heating the green bodies (with specific heating rate) up to desired temperature, followed by dwelling for 1 hour. At the end of each treatment the samples were left to cool down in the furnace chamber.

The sintering conditions of AW were selected on the basis of previous studies, and are reported in Figure 7.4 below (Xiao *et al.*, 2008).

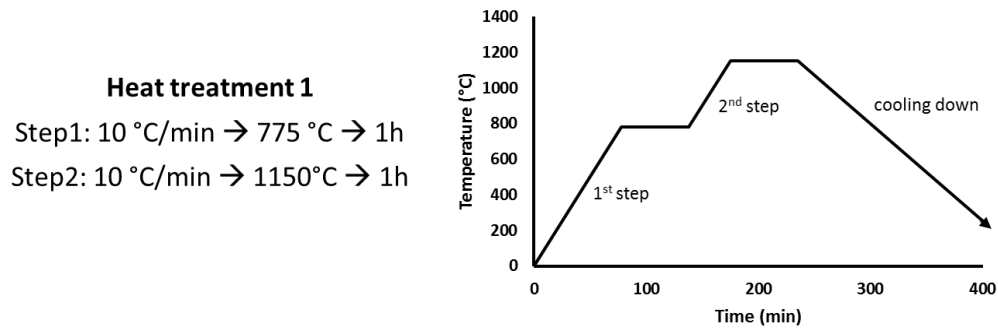
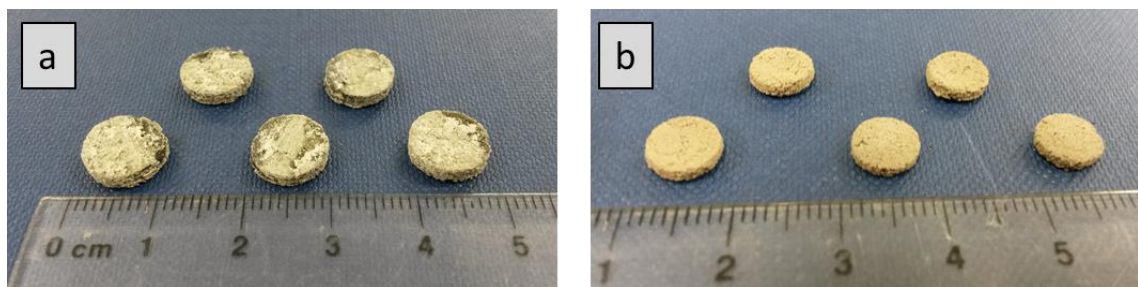


**Figure 7.4: Heat treatment and corresponding profile for AW 3D printed green bodies.**

## 7.2.2 Morphological evaluation

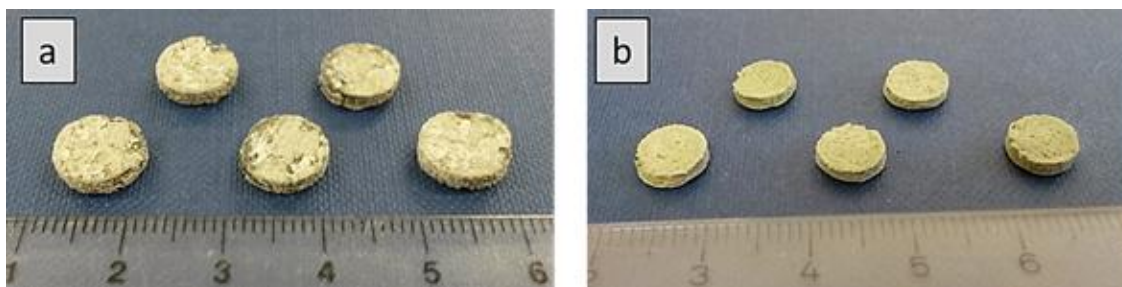
### 7.2.2.1 Macrostructural observation

Figure 7.5, Figure 7.6 and Figure 7.7 display NCL2, NCL7 and AW 3D printed structures respectively before (micrograph(a)) and after (micrograph(b)) the sintering. This qualitative comparison highlights that the green bodies showed a good level of integrity already after the printing process, and that the post-processing phase led to a more connected and harder structures with no shape distortion.



**Figure 7.5: NCL2 3D printed samples: a) before and b) after the sintering process.**





**Figure 7.6:** NCL7 3D printed samples: a) before and b) after the sintering process.

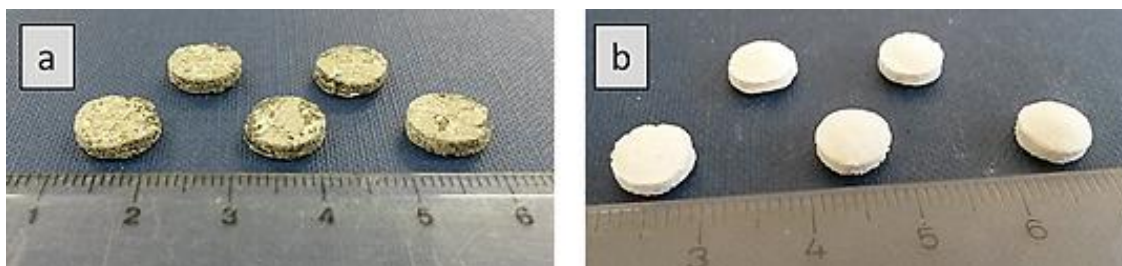


**Figure 7.7:** AW 3D printed samples: a) before and b) after the sintering process.

As expected, the thermal treatments, during which the liquid and solid binders were burned off, produced a reduction of the sample dimensions between 49% and 57%. However, no significant differences were measured for the shrinkage values of the two compositions in comparison to AW scaffolds (Figure 7.8).

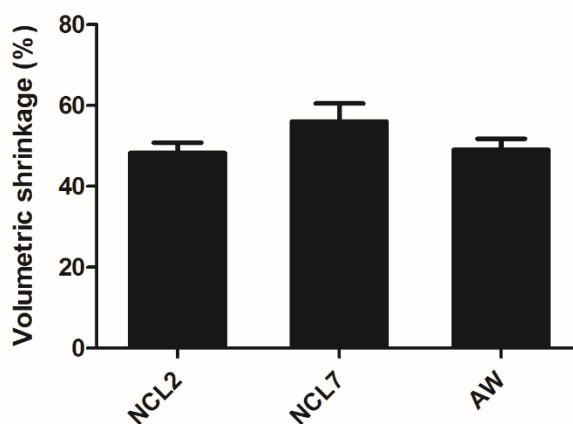


**Figure 7.8:** Average volumetric shrinkage (%) for sintered NCL2, NCL7 and AW 3D printed samples.

*Error bars represent the standard error of the mean.*

### 7.2.2.2 Microstructural observation

SEM analysis was performed on NCL2, NCL7 and AW 3D printed structures to evaluate the effect of sintering treatment on samples morphology. Figure 7.9 shows the top surface (micrograph(a)) and cross section (micrograph(b)) of NCL2 3D printed structure, following the heat treatment 3 described previously in Figure 7.2. Figure 7.9 reveals that thermal treatment led to neck formation (see red arrows), driven by the mix of small and big particles, and to a diffuse strut roughness, which was enhanced by the presence of many micro-particles, as demonstrated by surface morphology of the green body (see Figure 7.1 (c)).

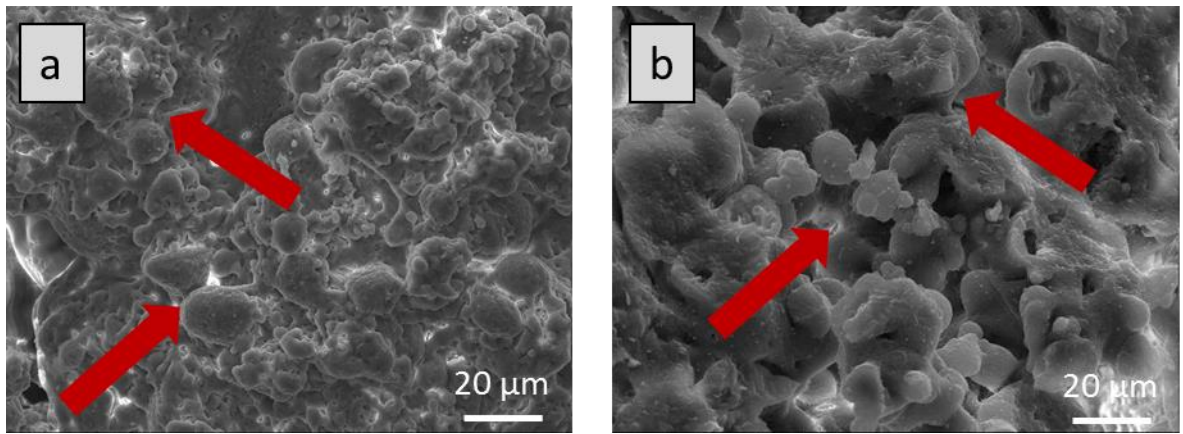


**Figure 7.9: SEM micrographs of a) upper surface and b) cross section of NCL2 3D printed structure after sintering (red arrows indicate necking formation).**

The upper surface and internal structure of NCL7 3D printed scaffold, after sintering, are shown in Figure 7.10.

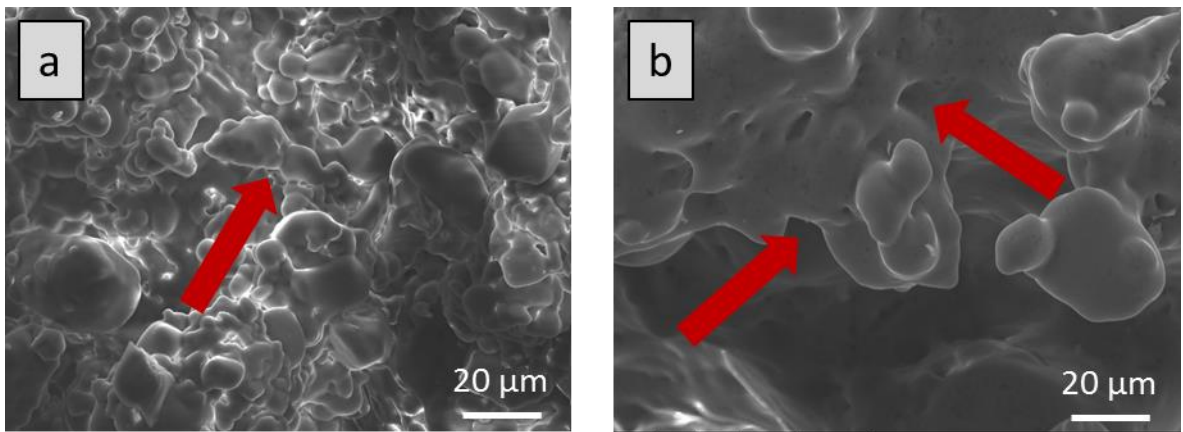


**Figure 7.10: SEM micrographs of a) top surface and b) cross section of NCL7 3D printed structure after sintering (red arrows indicate necking formation).**

If compared to the green body, the sintered structure exhibited a very high degree of densification, demonstrating that a good level of sintering was achieved, since it was impossible to identify the original sharp grain boundaries of the glass powders. Furthermore, the resulting morphology consisted in a smooth and also interconnected 3D network.

Figure 7.11 reports the surface and internal morphology of sintered 3D printed AW sample. The thermal treatment led to a consolidate structure, characterised by a rough and dense surface with fine crystalline grains. Figure 7.11(b) highlights the presence of a distributed micropore-based network (pore size about 20 $\mu$ m).

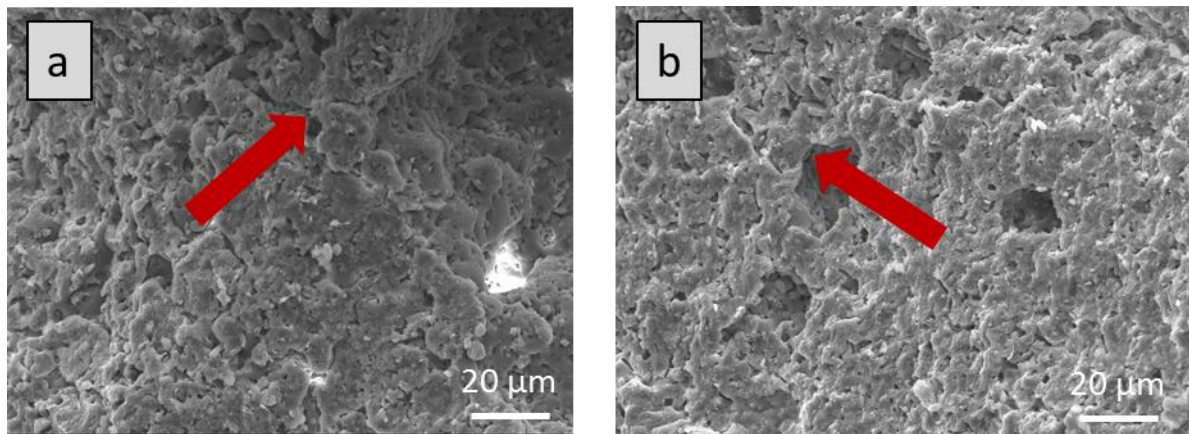


**Figure 7.11: SEM micrographs of a) top surface and b) cross section of AW 3D printed structure after sintering (red arrows indicate necking formation).**

### ***7.2.3 Porosity and microarchitecture of the scaffolds***

On the basis of the results reported in Figure 7.12, which compare open and total porosity of NCL2, NCL7 and AW 3D printed parts after sintering, open porosity values varied between 15% and 23%, while total porosity values were found to vary from 28% to 38%. Significant differences were observed for NCL2 open porosity values in comparison to those of NCL7 3D printed scaffolds. No significant differences were found for the new compositions with respect to AW glass-ceramic; even though, NCL2 showed the lowest porosity and AW the highest, whereas NCL7 sintered samples exhibited an intermediate porosity level.

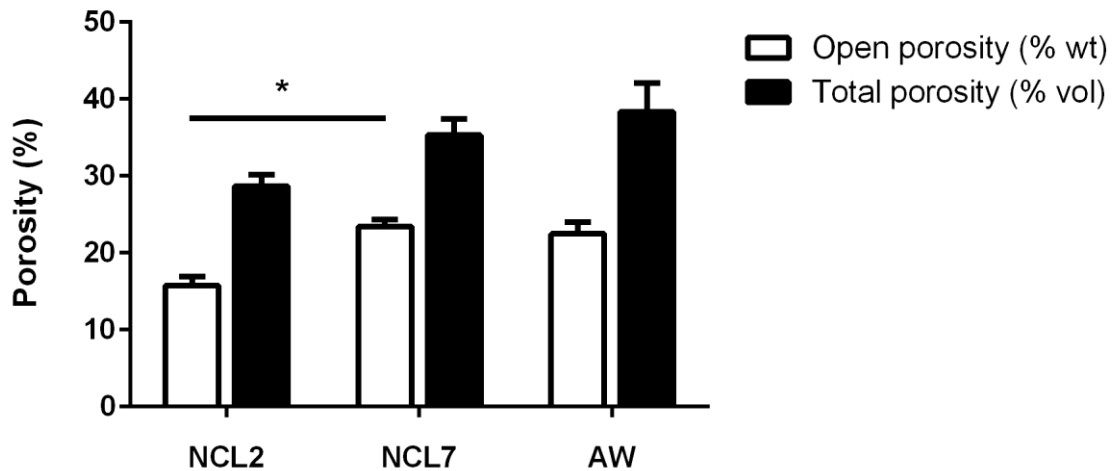


**Figure 7.12: Averaged open and total porosity values for sintered NCL2, NCL7 and AW 3D printed parts. Error bars represent the standard error of the mean ( $p < 0.05(*)$ ).**

These outcomes were confirmed by the micro-CT analysis, performed to evaluate the microarchitecture of the 3D printed sintered scaffolds. 3D reconstructions together with the representation of three spatial views (XY, XZ and YZ) of the bioceramic-derived structures are shown in Figure 7.13, Figure 7.14 and Figure 7.15 for NCL2, NCL7 and AW scaffolds respectively.

Both porosity and interconnectivity are known to be desirable requirements of engineered scaffolds, necessary for the proper diffusion of nutrients and for metabolic waste removal (Salgado *et al.*, 2004).

Although the same glass powder/maltodextrin ratio was used to make all the bioceramic samples, composition NCL2 exhibited lower micro-porosity, showing a heterogeneous distribution of the pores. Additionally, in Figure 7.13(c-d) the presence of macro-channels, which crossed the structure, can be observed.

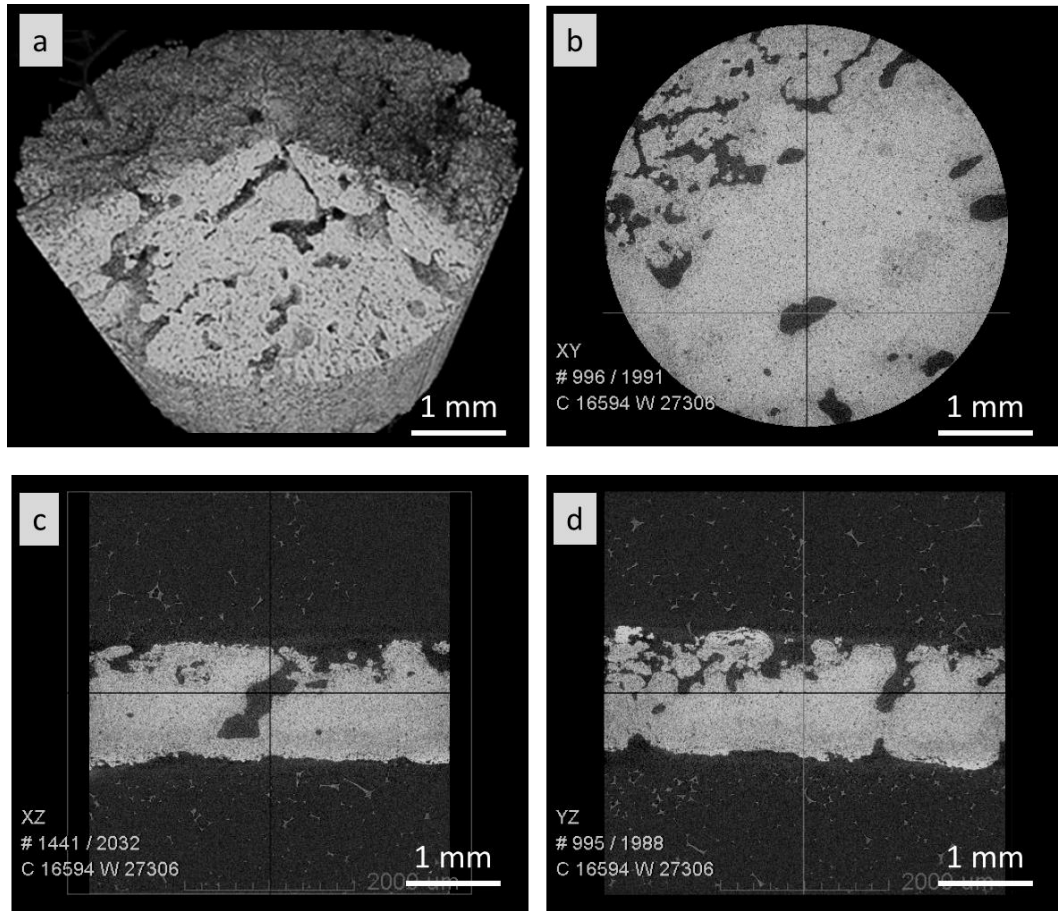


**Figure 7.13: NCL2 scaffold: (a) 3D reconstruction and (b), (c) and (d) spatial views (XY, XZ and YZ) obtained through micro-CT analysis.**

Conversely, NCL7 micro-CT data (Figure 7.14) revealed an architecture characterised by a homogeneous widespread network of micro and macro-pores, which presence is crucial for fluid flow, cell migration, bone ingrowth and vascularisation. According to the different spatial views represented in Figure 7.14(b-c-d), a good level of interconnectivity throughout the structure was achieved.

3D representation of NCL7 was found highly similar to AW-based structure. In good agreement with previous studies (Alharbi, 2015), AW samples were successfully sintered showing a homogeneous distribution of micro and macro pores along with an interconnected architecture (Figure 7.15(b-c-d)).



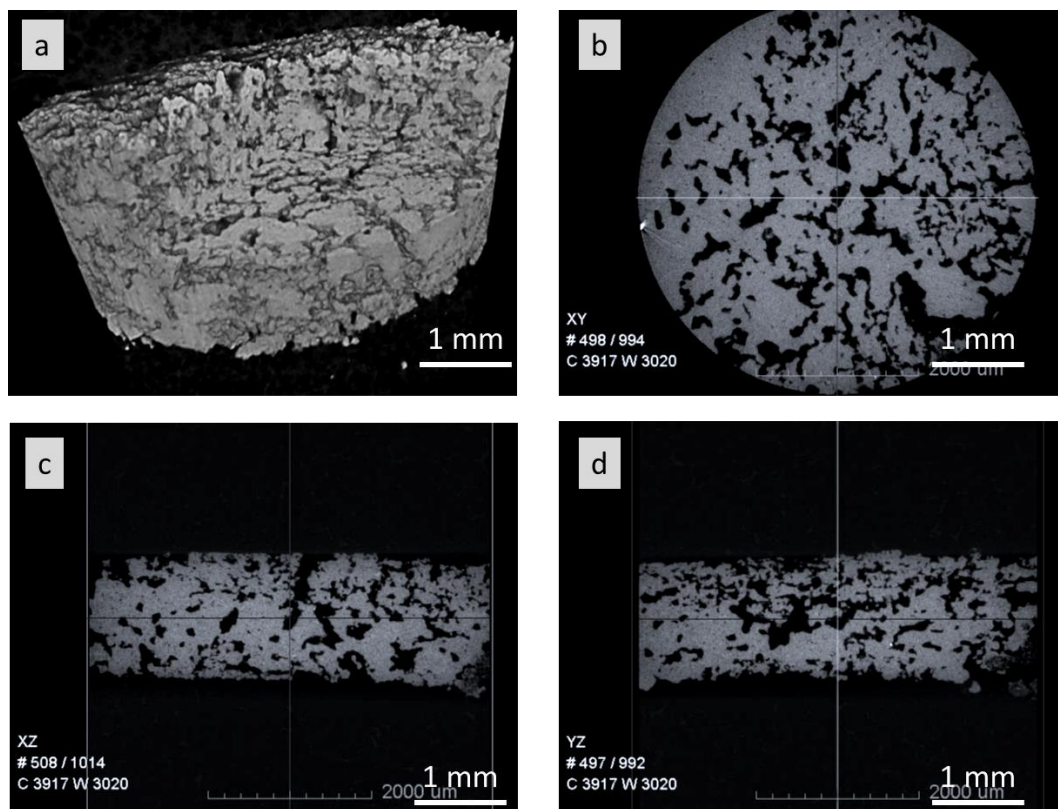


*Figure 7.14: NCL7 scaffold: (a) 3D reconstruction and (b), (c) and (d) spatial views (XY, XZ and YZ) obtained through micro-CT analysis.*

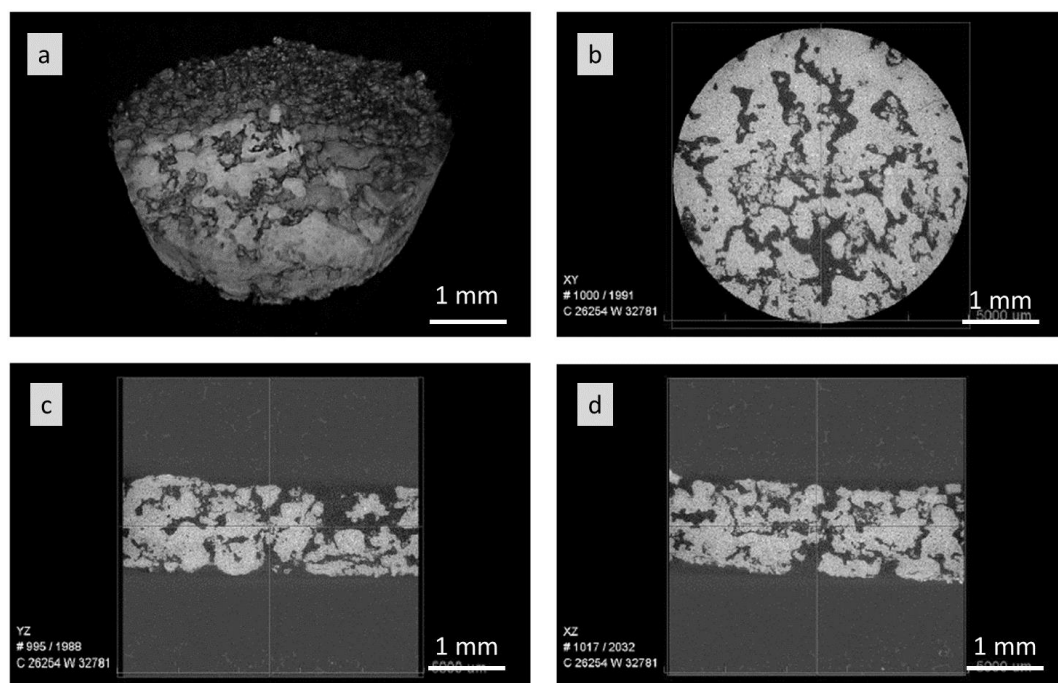


*Figure 7.15: AW scaffold: (a) 3D reconstruction and (b), (c) and (d) spatial views (XY, XZ and YZ) obtained through micro-CT analysis.*

#### 7.2.4 Mechanical properties

In order to assess the mechanical characteristics of the NCL2, NCL7 and AW 3D printed bioceramic structures, a three-point bending test was performed (Figure 7.16), according to the ASTM C1161 – 13 standard, using an INSTRON 5567 testing machine.



*Figure 7.16: Illustrative images of 3D sintered bars after the three-point bending test.*

The mechanical property values of the printed samples were evaluated from the stress-strain curves, resulting from the bending test (Figure 7.17).

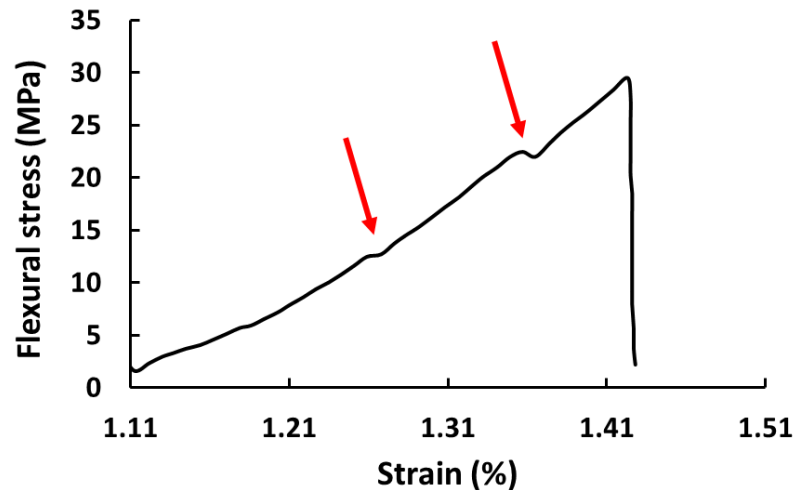


*Figure 7.17: Representative stress-strain curve for 3D printed porous ceramic bars, resulting from the three-point bending test (red arrows indicate the cracking phenomena during the test).*

The stress-strain curves presented similar trends, characterised by an almost linear profile with some stress oscillation (see red arrows in Figure 7.17), likely due to pore collapsing or either porous structure cracking during the test.

Figure 7.18 reports the flexural strength and modulus values calculated for NCL2, NCL7 and AW structures. NCL2 was characterised by the highest mechanical properties. However, no significant differences were found for the novel 3D printed scaffolds in comparison to AW, whereas NCL2 scaffolds showed flexural strength values significantly higher than NCL7 bars.

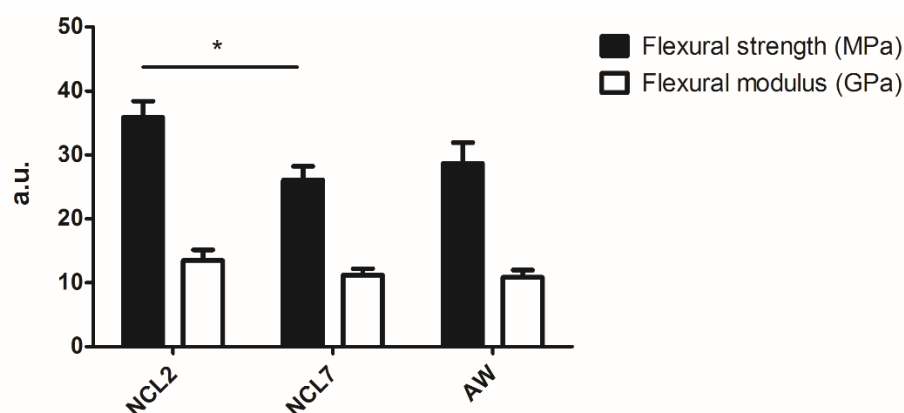


**Figure 7.18:** Average flexural strength and flexural modulus for NCL2, NCL7 and AW 3D printed scaffolds evaluated through three-point bending test. Error bars represent standard error of the mean ( $p < 0.05(*)$ ).

A summary of the mechanical properties values for NCL2, NCL7 and AW printed bars is reported in Table 7.1. According to these data, even though the starting materials were different, it can be concluded that using the same glass powder-porogen ratio, 3D printed structures with comparable mechanical properties can be obtained.

**Table 7.1:** Summary of the mechanical properties (mean±SE) for 3D printed NCL2, NCL7 and AW porous scaffolds assessed by three-point bending test.

SAMPLE	FLEXURAL STRENGTH (MPa)	FLEXURAL MODULUS (GPa)
NCL2	35.84±2.5	13.47±1.7
NCL7	26.08±2.1	11.20±0.9
AW	28.64±3.2	10.86±1.1



### 7.2.5 In vitro cellular tests

Figure 7.19 reports the effect of 3D printed scaffolds on rat OB mitochondrial activity tested by MTT colorimetric assay up to 7 days in culture.

According to the absorbance values shown in Figure 7.19, no significant differences were detected for the novel 3D printed scaffolds in comparison to 3D printed AW after each considered time point.

Furthermore, it can be highlighted that, although NCL2 showed a slightly increase of absorbance values after 7 days in culture, compared to those after 3 days, the absorbance values for NCL2 scaffolds after 7 days were significantly lower ( $p < 0.001$ ) than those measured for the control sample (CTRL), represented by the polystyrene culture plate, and 3D printed NCL7 scaffolds.

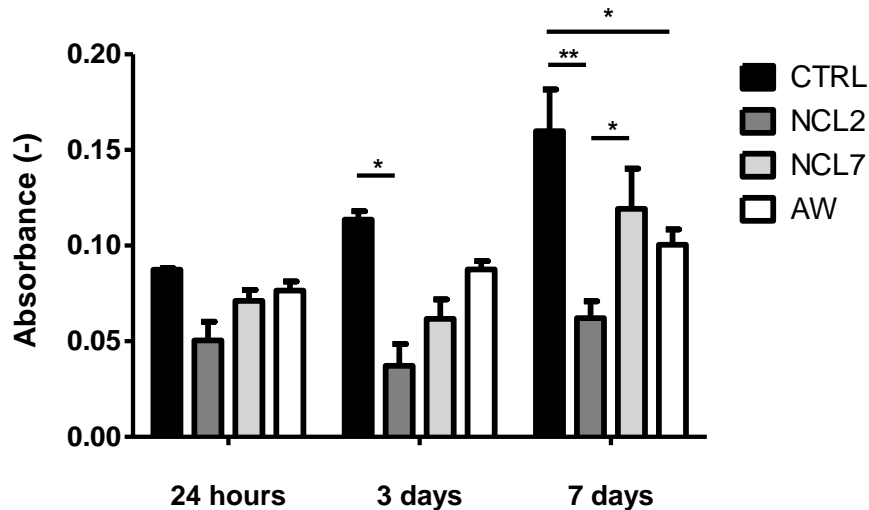


**Figure 7.19:** Effect on formazan formation by NCL2, NCL7 and AW 3D printed scaffolds ( $n=6$ ), evaluated through MTT assay after 24 hours, 3 days and 7 days in culture. Error bars represent the standard error of the mean ( $p < 0.05$ (\*),  $p < 0.001$ (\*\*)).

Additionally, Table 7.2 displays the pH values of the conditioning media and the results obtained from the ICP analysis, considering the common elements of the three compositions (Si, P, Ca and Mg) after 7 days of immersion in DMEM solution. Acellular DMEM solution alone was used as control.

**Table 7.2: pH values and ionic concentrations of the different DMEM extracts obtained from NCL2, NCL7 and AW specimens at specific time points.**

	NCL2			NCL7			AW			DMEM		
	24 h	3 d	7 d	24 h	3 d	7 d	24 h	3 d	7 d	24 h	3 d	7 d
<b>pH (mg/l)</b>	8.17	7.99	7.96	8.27	8.05	7.88	8.19	8.08	7.99	7.16	7.10	7.05
<b>Si (mg/l)</b>	5.49	2.11	1.59	22	16.8	34.1	1.49	13.15	16.85	0.25	0.25	0.25
<b>P (mg/l)</b>	3.7	2.5	2.7	5.2	8.2	10.5	4.6	0.5	2.6	29.5	29.5	29.5
<b>Ca (mg/l)</b>	4.8	2.3	4.6	2.6	9.7	22.9	10.4	17.8	28.8	65.1	65.1	65.1
<b>Mg (mg/l)</b>	2.1	0.8	0.7	2.1	0.8	4	2.2	2.2	2	19.8	19.8	19.8

Novel 3D printed scaffolds, immersed in DMEM (having an initial pH of 7), produced a pH increase, in particular after 24 hours of soaking. The pH values, whose variation is commonly caused by the ion exchange phenomena between the samples and DMEM solution, started to decrease slowly after 3 days in culture for both NCL2 and NCL7. However, the pH values ranged between 7.88 and 7.96 after seven days, similarly to AW glass-ceramic.

According to Table 7.2, which reports the ionic concentration of the pure extracts, calculated by subtracting the DMEM ionic content, there are no remarkable correlations between incubation time and concentration of ions released in DMEM solution. However, NCL7 resulted in the highest values for silicon and phosphorous values release in DMEM solution, while AW produced the highest released of calcium ions.

### 7.2.6 Antibacterial test

In order to evaluate the possible antibacterial properties of NCL7 composition, due to the presence of silver in its formulation, an inhibition zone test was performed on raw powders, sintered pellets and 3D printed scaffolds using *S. aureus*.

As reported in Figure 7.20, no inhibition zone for bacterial growth was detected for raw powders and bioceramic pellets after 24h in incubation.

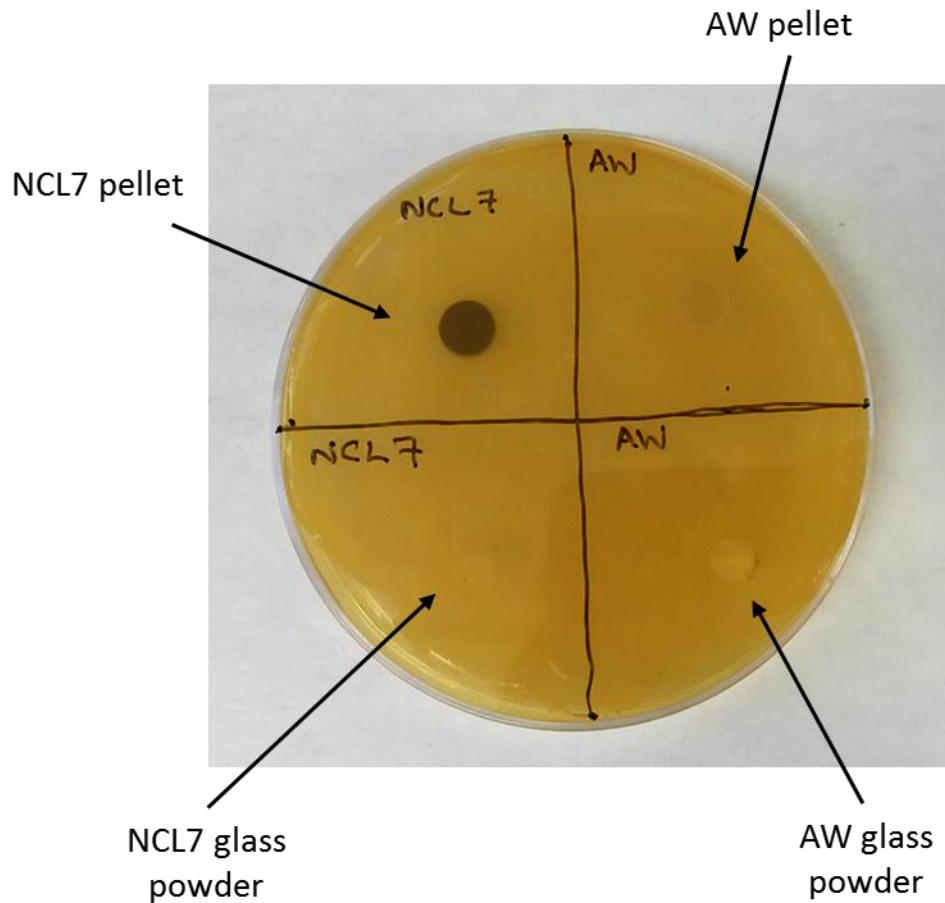


**Figure 7.20: Illustrative image of the zone inhibition test after 24 h incubation, performed on: NCL7 and AW glass powders (bottom) and bioceramic pellets (top) using *S. aureus*.**

According to the qualitative analysis performed on the agar plate containing the porous samples (Figure 7.21(a)), also no antibacterial activity was revealed by AW specimens (see inset Figure 7.21(b)), since no antibacterial agents were present in the AW main composition.

Surprisingly, a different behaviour was found for the porous NCL7 scaffolds, when compared to the dense bioceramic pellets. As shown in Figure 7.21(b), only NCL7 3D printed samples were able to create a zone where the bacterial growth was slightly inhibited. Although the halo was limited with respect to the positive control, the test revealed the potential antibacterial activity of porous NCL7-derived scaffolds, presumably due to silver ions diffusion in the area close to the sample.

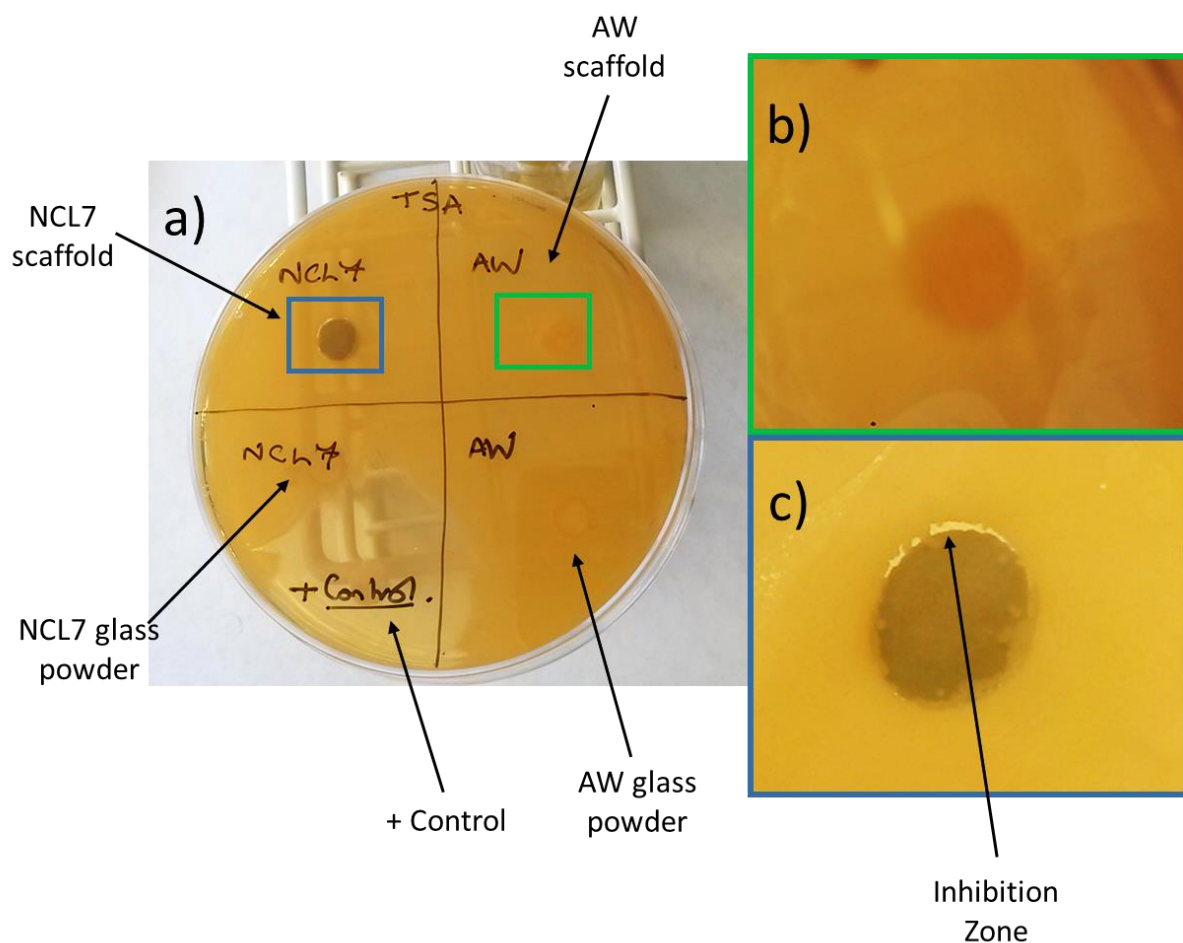


**Figure 7.21: Inhibition halo test by using *S. aureus* strain to evaluate the antibacterial effect of NCL7 and AW 3D printed scaffold: a) general view of the agar plate, b) magnification of AW sample and c) magnification of NCL7 sample showing the inhibition zone that limited bacterial growth.**

## Chapter 8. Discussion

---

### 8.1 Introduction

In this research project eight new bioceramic formulations were developed using:

i) silicon dioxide, phosphorous pentoxide and boron trioxide as network formers due to their widely demonstrated bioactive potential (Hench, 1998a; Hench, 1998b), distinctive resorbable properties (Knowles, 2003; Abou Neel *et al.*, 2009b), and tailorable degradation rate (Huang *et al.*, 2006; Yao *et al.*, 2007);

ii) a range of different doping agents (*i.e.* MgO, MnO<sub>2</sub>, Al<sub>2</sub>O<sub>3</sub>, CaF<sub>2</sub>, 5Fe<sub>2</sub>O<sub>3</sub>, ZnO, CuO, Cr<sub>2</sub>O<sub>3</sub>) to tailor the properties of the main formulation (Dietrich *et al.*, 2009; Fielding and Bose, 2013; Miola *et al.*, 2014; Stähli *et al.*, 2015; Tarafder *et al.*, 2015; Vyas *et al.*, 2015; Zhao *et al.*, 2015).

The aim of the study was the processing and characterisation of these novel developed glass formulations as potential biomaterials for bone tissue repair and regeneration, according to the following objectives:

**OB1:** development of a series of novel glass compositions containing specific doping agents;

**OB2:** evaluation of the physico-chemical and biological properties of the glass powders;

**OB3:** evaluation of the physico-chemical, mechanical and *in vitro* bioactive properties of dense sintered bioceramic pellets;

**OB4:** optimisation of the methodology for the fabrication of 3D porous glass-derived substitutes;

**OB5:** evaluation of the physico-chemical, mechanical and biological properties of the 3D porous sintered substitutes.

These objectives were all achieved, however limitations in the properties meant that not all the glass formulations were carried through to the later stages.

Table 8.1 provides a summary of the key outcomes, which will be discussed in more detail in the following sections.

**Table 8.1: Summary of the key outcomes deriving from the processing and characterisation of the novel glass formulations.**

CODE	RATIONALE	COMMENTS
NCL1 (SiO <sub>2</sub> -based)	Osteogenic properties, mainly determined by the presence of a high amount of silica.	Cytotoxic.
NCL2 (SiO <sub>2</sub> -based)	Osteogenic properties and tailored degradation rate, mainly for load bearing applications.	Good mechanical properties. Slow dissolution rate.
NCL3 (B <sub>2</sub> O <sub>3</sub> -based)	Improved degradation rate and appropriate level of bioactivity as well as mechanical properties.	Cytotoxic.
NCL4 (B <sub>2</sub> O <sub>3</sub> -based)	Tailored degradation rate and osteogenic effects.	Good mechanical properties as dense material. Quick degradation rate.
NCL5 (P <sub>2</sub> O <sub>5</sub> -based)	Resorbable properties with controlled degradation rate.	Did not form melt at 1500 °C.
NCL6 (P <sub>2</sub> O <sub>5</sub> -based)	Resorbable properties with controlled degradation rate, and improved mechanical strength.	Cytotoxic.
NCL7 (SiO <sub>2</sub> -based)	Antibacterial properties, mainly determined by the presence of silver oxide, and a good level of bioactivity.	Good mechanical properties and bioactive potential. Scaffolds inhibited bacterial growth.
NCL8 (SiO <sub>2</sub> -based)	Osteogenic properties and tailored degradation rate for non-load bearing applications.	Cytotoxic.

## 8.2 Glass melting behaviour

The NCL5 phosphate-based formulation did not form a liquid at 1500°C, therefore the process was terminated and this composition was not pursued. The high melting temperature required was in contrast with other studies, which stated that phosphate-based glasses can be prepared at relatively low temperatures (Abou Neel *et al.*, 2009b). It is considered that the complexity of NCL5 composition (10 oxides in total), in comparison to other phosphate-based formulations developed in the literature (typically 6 oxides) (Navarro *et al.*, 2004; Leonardi *et al.*, 2010; Novajra *et al.*, 2011; Vitale-Brovarone *et al.*, 2011), might have increased the melting point of NCL5 glass.

## 8.3 Sintering temperature selection and sintering behaviour

The selection of the appropriate sintering temperature, usually defined as the temperature where the maximal densification rate is reached (Venturelli, 2011; Bretcanu *et al.*, 2014), is a key step during the manufacturing process to consolidate ceramic-based structures (Dorozhkin, 2010; Palmour *et al.*, 2013).

A summary of the potential sintering temperature ranges, derived from HSM analysis, and the optimal sintering temperatures selected for dense pellets and porous scaffolds is reported in Table 8.2. The silicate-based and phosphate-based glasses showed larger sintering intervals when compared to borate-based glasses. However, no specific correlations were found among the different compositions. This might be due to the complex structure of the novel glasses, containing different network formers in diverse molar percentages.

**Table 8.2: Glass formulations sintering intervals obtained by HSM, and optimal sintering temperatures for dense pellets and porous scaffolds.**

	NCL1	NCL2	NCL3	NCL4	NCL6	NCL7	NCL8	AW
<b>HSM sintering interval (°C)</b>	575-785	600-730	555-625	550-650	580-775	575-785	500-730	800-1225
<b>Optimal sintering temperature (°C) (dense pellets)</b>	625	700	625	625	725	625	625	850
<b>Optimal sintering temperature (°C) (porous scaffolds)</b>	-	700	-	-	-	625	-	1150

From a qualitative point of view, the HSM thermographs (reported in paragraph 6.2.3 and obtained under the same heating conditions) revealed that silicate-based glasses (specifically, NCL1, NCL2, NCL7 and NCL8) displayed a similar thermal profile, characterised by an increase in the samples dimensions after the maximum shrinkage temperature. These results are in good agreement with the findings reported by Baino *et al.*, which found that a silicate-based glass after a first densification step exhibited a significant volumetric expansion (Baino *et al.*, 2013). Similar shrinkage profiles were observed for borate-based glasses (NCL3 and NCL4) and the AW composition, which showed an “elbow” in their curves, as reported in Figure 6.5. These findings support the work published by Arstila *et al.*, who suggested that the elbow indicated the possible sintering interval of the analysed compound (Arstila *et al.*, 2005; Arstila *et al.*, 2008). Regarding the NCL6 phosphate-based glass, although this composition has a network former content similar to another glass reported in the literature (45% P<sub>2</sub>O<sub>5</sub>, 3% SiO<sub>2</sub>, 26% CaO, 7% MgO, 15% Na<sub>2</sub>O and 4% K<sub>2</sub>O) (Bretcanu *et al.*, 2014), its shrinkage profile was more comparable to those of the novel borate-based compositions. This is tentatively attributed to the presence of the network modifiers in the formulation.

Appropriate sintering temperatures can be selected only by a thorough post-processing evaluation, which includes: *i*) the production of sintered structures using different thermal treatments and *ii*) subsequent morphological characterisation using SEM or micro-CT analyses (Baino and Vitale-Brovarone, 2011; Vivanco *et al.*, 2011; Bretcanu *et al.*, 2014).

On the basis of the data obtained from the HSM analysis, different thermal treatments were investigated and optimised to increase the liquid phase of the dense pellets and improve their densification status. It is interesting to note that, although an optimisation process was needed, the outcomes from the heating microscopy were a very useful guide in predicting the optimal sintering temperatures of bioceramic pellets: the temperatures that led to optimal consolidated structures were all in the range of sintering temperatures provided by the HSM.

Moving from compact bioceramic pellets to 3D porous scaffolds, the sintering conditions required a further optimisation process (Baino *et al.*, 2013; Bretcanu *et al.*, 2014). As 3D porous scaffolds have a different internal structures, if compared to dense pellets, it was necessary to burn-out the solid binder, which entails further shrinkage of the structure and thus a major reduction of the final volume. The optimal sintering temperatures for NCL2 and NCL7 scaffolds were consistent with



those applied for the sintering of dense bioceramic pellets. However, as reported in Chapter 7, a gradual adjustment of porous structure sintering conditions needed to be performed. Specifically, following the same heating treatments as implemented on the NCL2 and NCL7 bioceramic pellets, the solid binder was not completely burnt off. Therefore, a 2 steps sintering treatment was developed. However, also in this case the 3D printed parts were poorly consolidated, showing weak structural integrity. A 3 steps heat treatment for both NCL2 and NCL7 scaffolds was necessary in order to obtain mechanically competent 3D porous parts with appropriate densification degree. Particularly, during the first step of the treatment (up to 200°C) the temperature was increased to remove completely the sacrificial porogen. The second step was added in order to allow the gradual consolidation of the bioceramic structure, and finally the last step was required to reach the optimal sintering of the bioceramic structures.

Additionally, observing the sintering behaviour of AW glass-ceramic, the data in Table 8.2 show how moving from dense to porous structures the sintering conditions of the material were affected. Specifically, the optimal sintering temperature of dense AW was 850°C, in agreement with the HSM data presented by Faeghi-Nia (Faeghi-Nia *et al.*, 2009), while the 3D porous AW required an increase of the optimal sintering conditions up to 1150°C, based on the protocol developed by Xiao and subsequently applied by Alharbi (Xiao *et al.*, 2008; Alharbi, 2015). Comparing the heat treatments of NCL2 and NCL7 scaffolds with respect to AW (3 steps vs 2 steps), a further stage during the sintering process was necessary in order to reach a satisfactory densification of the novel bioceramic-based samples. Hence, it can be concluded that the best sintering conditions, assessed by a thorough post-processing analysis, are significantly influenced by the glass composition (Novajra *et al.*, 2015).

#### **8.4 Crystal structure evolution**

XRD analysis indicated that only NCL6 and NCL7 (as raw materials) showed a glass-ceramic behaviour, whereas the other formulations produced XRD patterns characterised by a broad peak detected at  $2\theta$  values between 25° and 30° (Figure 6.3), typical of completely amorphous bioglasses (Boccaccini *et al.*, 2007).

Comparing the XRD patterns of the glass powders with those of the sintered bioceramic pellets, few considerations can be drawn. First of all, the XRD analysis confirmed the amorphous nature of NCL1, NCL2, NCL3, NCL4 and NCL8 compositions even after sintering; the thermal process

did not affect the crystallinity of NCL7 glass-ceramic, which still showed a crystalline phase corresponding to pure silver. The post sintering XRD pattern for NCL2 silicate-based glass revealed the presence of a crystalline phase identified as diopside. Diopside is a Mg-containing compound, which have already been investigated as biomaterials for bone repair in form of powder and dense bulk ceramic (Nonami and Tsutsumi, 1999). Furthermore, diopside-derived scaffolds were found to possess good and stable mechanical properties upon immersion in physiological solution due to their low degradation rate (Wu *et al.*, 2010). Additionally, the sintering process increased the crystallinity of NCL6 glass sample; in fact, as the XRD pattern reported (see Figure 6.37), the initial calcium sodium phosphate phase was complemented by a sodium calcium magnesium phosphate phase after NCL6 thermal treatment. As presented in chapter 2, the use of calcium phosphates is a longstanding area of interest for bone tissue applications due to their high similarity with human bone (Dorozhkin, 2010).

The XRD patterns of AW glass-ceramic revealed the same crystalline phases (hydroxylapatite complemented with  $\beta$ -wollastonite) before and after the sintering process (Xiao *et al.*, 2008). However, the sintered material showed more intense peaks (Figure 6.40(b)) with respect to the raw glass-powder (Figure 6.40(a)), confirming the glass-ceramic nature of this formulation. These results are different from those of Magallanes-Perdomo *et al.*, who worked with raw AW powder which was completely amorphous, and showed that thermal treatment of the powders at 1100°C for 1 hour produced two crystalline phases, apatite and wollastonite respectively. It is thought that differences in the glass production method will have affected the crystallisation behaviour of the compound. Hence, it can be concluded that through a careful optimisation of the post-processing conditions, it is possible to consolidate AW powder which is completely amorphous and AW powder that is partially crystalline, with similar phase composition in the sintered material.

### **8.5 Morphological analysis**

The morphology of the starting glass powders was evaluated through SEM analysis, after the grinding and sieving processes. Glass particles were found to have an average size of 20 $\mu$ m and less than 53 $\mu$ m, and the tendency to agglomerate. From a qualitative perspective, the raw powders showed a microstructure very similar to AW glass-ceramic and also to other glasses produced by the melting route (Baino *et al.*, 2013). Moving from glass powders to dense materials, SEM

observations showed homogenous and microporous structures of compact sintered pellets with no internal cracks.

The microstructures achieved from the processing by indirect 3D printing of NCL2 and NCL7 were porous with different topographies, but with high surface roughness similar to AW-based scaffolds obtained by the same processing route. Additionally, micro-CT investigations offered a more accurate assessment of 3D printed glass-derived scaffolds. 3D reconstructions of NCL2, NCL7 and AW printed bioceramic structures are shown in Figure 7.13, Figure 7.14 and Figure 7.15 respectively. Although the same glass powder/maltodextrin ratio was used, the NCL2 composition exhibited lower micro-porosity with a heterogeneous distribution of the pores. NCL7 micro-CT images revealed an interconnected architecture very similar to 3D printed AW, and characterised by a homogeneous widespread network of micro ( $\sim 20\mu\text{m}$ ) and macro-pores ( $\sim 150\mu\text{m}$ ), which are fundamental for fluid flow, cell migration, bone ingrowth and vascularisation (Liu *et al.*, 2007; Loh and Choong, 2013). Overall, the NCL7 and AW scaffolds showed the most promising structures for clinical application.

## **8.6 Ion release potential and cytotoxicity evaluation**

The ionic release ability of the novel formulations was assessed by immersing the raw glass powders (10 mg/l) in deionised water. A summary of the ion release concentrations for Si, P, B, Ca and Mg, which are the common elements present in almost all the formulations, and derived from the ion release data presented in Chapter 6, is reported in Figure 8.1. It is interesting to observe that, except for NCL2 composition, the amount of silicon released in solution after 28 days of soaking, was proportional to the molar content present in the main formulation. Furthermore, boron was released much quicker than silicon for NCL3, NCL4 and NCL6 composition, in accordance with the findings reported by previous researchers (Huang *et al.*, 2006). The data reported in Figure 8.1 further demonstrate the widely proved reactive nature of  $\text{B}_2\text{O}_3$ -based glasses. Moreover, it was found that phosphorus concentration (Figure 8.1) did not increase with immersion time for all the glasses, except for NCL6 phosphate-based formulation.

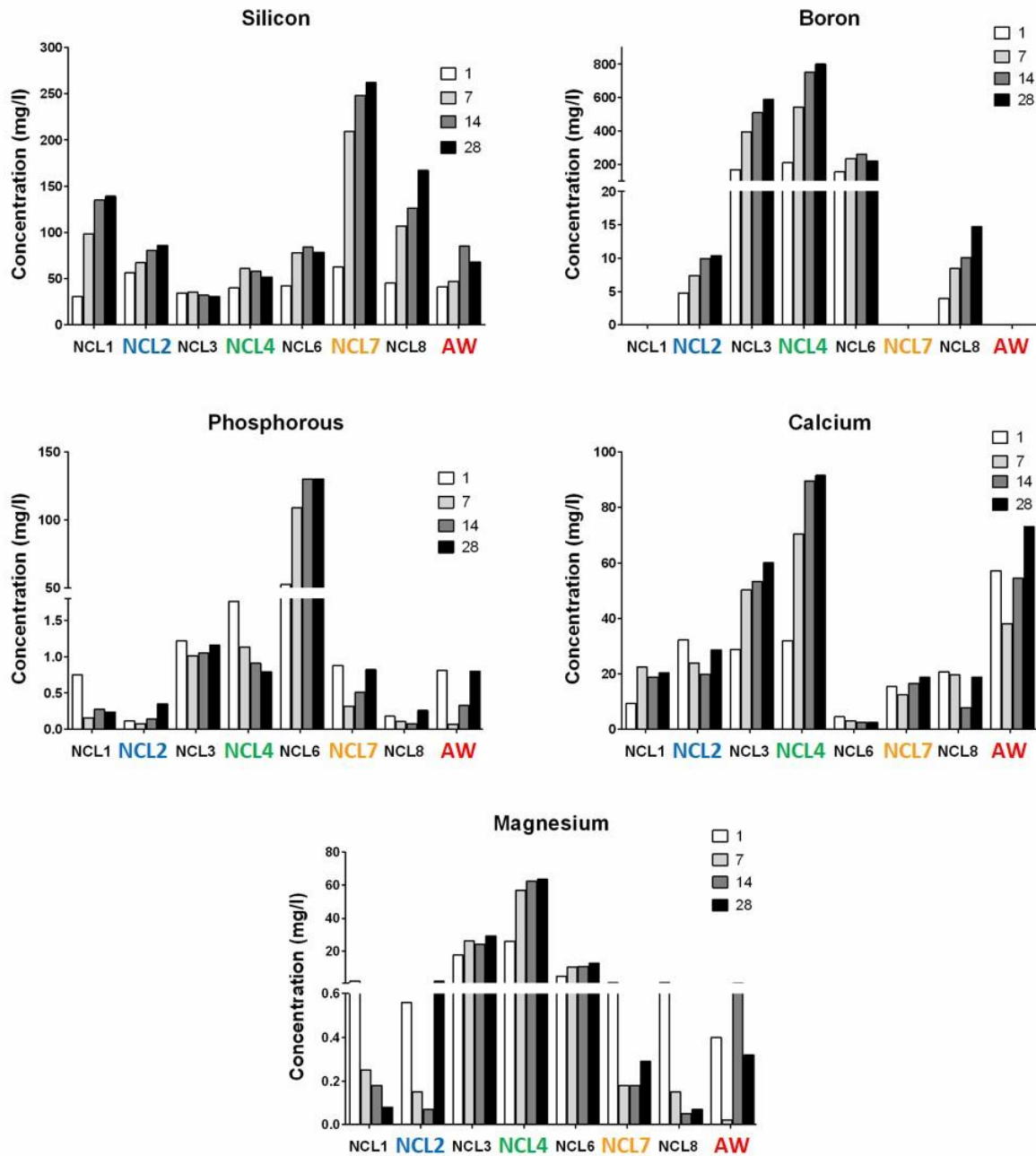


**Figure 8.1: Ionic concentrations of Si, P, B, Ca and Mg released into deionised water from all the formulations, without refreshing the solutions and at different time points (1, 7, 14 and 28 days).**

Additionally, concerning the pH of the solutions, it is well-known that changes in pH values can cause severe damage to OB cells, which prefer a more physiological environment (pH ~ 7.5) (El-Ghannam *et al.*, 1997). The pH values resulting from the immersion of the raw glass powders in deionised water were monitored up to 28 days. All the glasses, even with refreshes of the media,

showed pH levels above 8.5, which can be considered a severe condition for cell viability. However, the values were comparable to those of AW, therefore the pH rise might be due to the high reactivity of glass powders. These results are consistent with the work of other researchers, which found that fine Bioglass® powders (average particle size ~2µm), immersed in different solutions, produced a rapid increase in pH already after 6 hours of soaking; in particular, the pH of deionised water solution reached a value of 10 after the first 30 seconds of immersion (Cerruti *et al.*, 2005)

Following these considerations and looking at the overall data reported in Figure 8.1, no meaningful correlations between the cytotoxic effect of the novel formulations and their ionic release potential of Si, P, B, Ca and Mg can be derived. Cell viability was significantly affected by the presence of the glass powders in the media in particular at high concentrations. These findings are consistent with the results obtained by Santocildes-Romero *et al.*, who found that the addition of Sr-doped bioactive glass powders ( $\geq 6.7\text{mg/ml}$ ) to culture medium, significantly reduced MSCs viability. However, for NCL1, NCL3, NCL6 and NCL8 compositions the cell mitochondrial activity was inhibited even for the indirect method for all three concentrations tested. Considering that no remarkable variation in pH values up to 7 days were detected, it can be stated:

- for NCL1 and NCL3 glass formulations, considering the low concentrations of the majority of the doping agents, it is most likely that the release of vanadium from both these compositions might have had a negative effect on cell mitochondrial activity (Sakai *et al.*, 2002);
- for NCL6 composition, since not many dopants were present in this formulation, and because the release of Co, Cu and Cr after 28 days in immersion was quite low, it is most likely that the high level of phosphorus and boron concentration was the cause of the detrimental effect of this glass;
- considering the doping agents of NCL8 formulation and comparing their effect with those of the other compositions, no clear reasons for the toxicity of this glass were found; hence, the negative effect might be due to the combination of the different oxides present in the main formulation;
- for NCL2 composition the slow release of the doping agents seems to positively influence the cell viability; conversely, the high reactive nature of NCL4 borate-based glass helped the release of strontium at higher level (in comparison to NCL1 glass), which has been

demonstrated to increase proliferation as well as differentiation of osteoblast cells (Gentleman *et al.*, 2010; Hesarakı *et al.*, 2010)

- the positive effect of the NCL7 formulation seems to derive from the combined effect of titanium, iron and copper, which enhance OB proliferation and activity (Mourino *et al.*, 2012).

According to the results of the MTT assay performed on 3D porous structures, no obvious reason for the differences in behaviour can be derived from the formulations alone, but the AW and NCL7 materials showed the best results for apatite formation in SBF, which will be discussed in the next section, and this bioactive response might have influenced cellular behaviour (Dyson *et al.*, 2007; Alharbi, 2015; Lee *et al.*, 2015).

### **8.7 Apatite-forming ability**

No apatite needle-like precipitates were visible on the surface of the three novel compositions, after immersion in SBF. On the contrary, AW glass-ceramic was completely covered after 7 days in immersion, demonstrating its widely proved bioactive behaviour (Zhang *et al.*, 2009; Magallanes-Perdomo *et al.*, 2011; Park and Ozturk, 2013). However, globular shaped aggregates were found on the surface of NCL4 and NCL7 bioceramic pellets after 7 days in immersion, which particularly for the NCL7 composition increased after 28 days. Furthermore, for NCL7 pellets the Ca/P ratio changed from 1.1 at day 7 up to 1.4 at day 28, as demonstrated by EDS and XPS analysis. These precipitates might be considered HCA precursors (octacalcium phosphate) (Dorozhkin, 2010), and therefore suggest the capability of NCL7 composition to induce bioactivity.

Fu *et al.* suggested that the morphology of sample surfaces, after immersion in SBF, changed from needle-like for silicate-based scaffolds to approximately globular shape for borate-based scaffolds (Fu *et al.*, 2010a). On the basis of the SBF testing results conducted in this study, NCL4 and AW compositions can therefore be said to have behaved as expected. Conversely, the cauliflower shape of NCL7 precipitates was not in accordance with the findings reported by previous studies (Huang *et al.*, 2006; Magallanes-Perdomo *et al.*, 2011; Deliormanli, 2013). A possible explanation for this might be the presence of iron in the NCL7 main formulation, which could have affected the morphology of the precipitates (Zhang *et al.*, 2013). If this was the case, it would mean that the differences in precipitate morphology, after immersion in SBF solution, are composition dependent.

The Ca/P ratio of NCL7 precipitates after 28 days in immersion was lower than the one for AW, but the formation of micro-cracks on NCL7 surface was more pronounced than the AW-derived pellets (see Figure 8.2). Crack development is usually a common morphological feature due to the dual reaction of formation of a silica-rich film and growth of the calcium-phosphate HCA layer, which is typical of bioactive materials (Hench, 1991). This suggests that the NCL7 formulation may be considered a bioactive material.

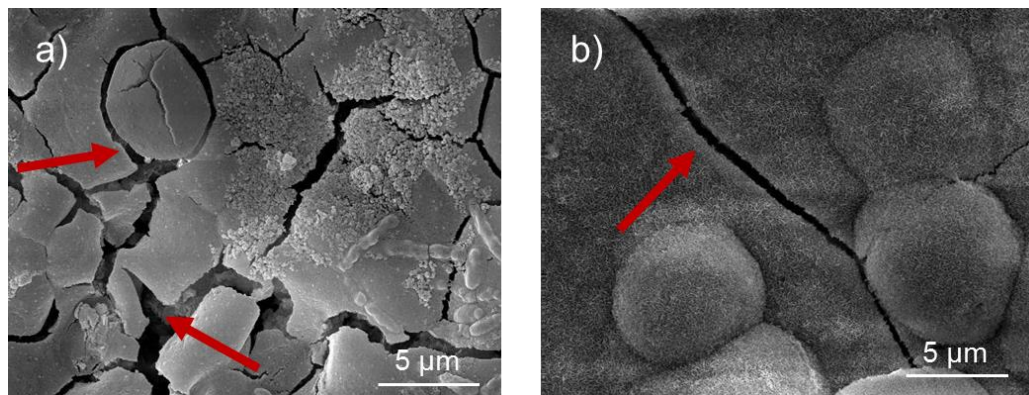


**Figure 8.2:** (a) NCL7 and (b) AW bioceramic pellet after soaking in SBF for 28 days (the red arrows indicate the micro-cracks formation on the pellet surface).

Regarding NCL2 bioceramic pellets, no structural changes were detected, apart from that after 28 days of soaking in SBF the surface appeared homogeneously covered by a thin white layer rich in calcium.

According to the literature, the structure of a glass plays a crucial role in determining its bioactivity (Goel *et al.*, 2012). Specifically, the incorporation of intermediate oxides and the reduction of  $P_2O_5$  content in the glass network can reduce bioactive behaviour (Groh *et al.*, 2014). Hence, the complex formulation of NCL2 glass may explain the absence of even HA precursors. However, it has been also demonstrated that bioactivity tests *in vitro*, using SBF solution, can lead to false positive and false negative results when compared to *in vivo* trials (Bohner and Lemaitre, 2009), and so no strong conclusion can be drawn.

Another aspect that needs to be considered when a biomaterial is immersed in SBF solution is its biodegradation rate. Usually glass-based structures undergo degradation process at a rate defined by the kind of network former (Fu *et al.*, 2010a). In good agreement with the literature, and as anticipated by the ion leaching phenomena, after 28 days of immersion in SBF borate-based samples were characterised by comparatively greater weight loss (Yao *et al.*, 2007; Xin *et al.*,

2010). Silicate-derived structures showed the lowest degradation rate (Huang *et al.*, 2006). Particularly, for NCL2 the negligible weight loss is consistent with the low degradation rate showed by its diopside crystalline phase upon immersion in physiological fluids, as previous studies demonstrated (Wu *et al.*, 2010). These findings indicate that NCL2-based structures, with their high mechanical strength and slower degradation rate (compared to traditional bioactive ceramics) could potentially be used for bone-tissue repair where a controlled slow degradation is desirable.

Additionally, the pH variation of the NCL2, NCL4 and NCL7 compositions during bioactivity tests in SBF solution was monitored up to 28 days. Conversely to the pH trends resulting from the immersion of the raw glass powders in deionised water, it was observed that the pH varied between 7.4 and 7.7. These values are considered optimal for *in vitro* cell culture (El-Ghannam *et al.*, 1997), and are consistent with those of Vitale-Brovarone *et al.*, who evaluated pH variation of dense silicate-based glasses in SBF solution, and reported pH levels around 7.75 (Vitale-Brovarone *et al.*, 2008).

### **8.8 Novel glass formulations printability**

When processed by ZCorp 310 3D printer, the NCL2 and NCL7-based green parts resulted in stable structures similar to AW. On the contrary, NCL4-based green bodies were very weak and powdery, and difficult to handle. A possible explanation for this might be related to the poor flowability of NCL4-based blend, which as stated by Cox *et al.* directly affects the material printability (Cox *et al.*, 2015). The poor printability of NCL4 formulation, in comparison to the other compositions, was qualitatively observed during the spreading phase of the printing process. NCL4 blend particles tended to agglomerate resulting in a non-homogenous powder layer.

### **8.9 Mechanical properties**

Table 8.3 shows that the moduli of the dense bioceramics were close to that of dense AW. However, porosity and interconnectivity are known to be desirable requirements of tissue engineered structures, necessary for correct diffusion of nutrients and for the removal of metabolic waste (Salgado *et al.*, 2004; Polo-Corrales *et al.*, 2014). Total porosity values for 3D printed NCL2, NCL7 and AW scaffolds are reported in Table 8.4 in comparison to human cortical and trabecular bone. All the 3D printed structures had porosity levels higher than cortical bone and lower than trabecular bone (Goldstein, 1987; Keaveny and Hayes, 1993), with no significant differences



between the three materials. However, depending on the clinical need, it might be possible to reach a porosity level closer to cortical or trabecular bone simply redesigning the precursor characteristics (*i.e.* particle size and powder/binder ratio) (Goldstein, 1987; Keaveny and Hayes, 1993; Jones and Hench, 2003b). Furthermore, using a 3D printing approach, it has been shown that combined macro- and micro-porous structures can be created (Dyson *et al.*, 2007; Alharbi, 2015).

**Table 8.3: Compressive modulus (mean $\pm$ SE) of AW and dense bioceramic pellets.**

	<b>Compressive Modulus (GPa)</b>	<b>Porosity (%)</b>
<b>AW</b>	1.29 $\pm$ 0.03	< 2 %
<b>NCL1</b>	1.54 $\pm$ 0.01	< 2 %
<b>NCL2</b>	1.43 $\pm$ 0.03	< 2 %
<b>NCL3</b>	1.53 $\pm$ 0.04	< 2 %
<b>NCL4</b>	1.37 $\pm$ 0.02	< 2 %
<b>NCL6</b>	1.24 $\pm$ 0.01	< 2 %
<b>NCL7</b>	1.32 $\pm$ 0.06	< 2 %
<b>NCL8</b>	1.68 $\pm$ 0.01	< 2 %

**Table 8.4: Total porosity values (vol %) of 3D printed scaffolds (n=5) compared to human bone. The data represent the mean  $\pm$  SE (\* (Goldstein, 1987)).**

<b>NCL2</b>	<b>NCL7</b>	<b>AW</b>	<b>Cortical bone</b>	<b>Trabecular bone</b>
28.7 $\pm$ 1.5	35.3 $\pm$ 2.0	38.4 $\pm$ 3.7	5-10*	50-90*

It has been considered that for powder-based 3D printing systems, grain size and relative distribution of the starting materials are crucial factors for the physical characteristics of the final 3D printed parts. Particularly, these parameters directly influence porosity, which in turn has been seen to impact cell behaviour (attachment, proliferation and differentiation), as well as the resulting mechanical properties of the implant (Spath *et al.*, 2015). However, one of the major critical aspects in developing load-bearing scaffolds for bone tissue is the conflicting balance between porosity and mechanical properties.

Considering the data reported in Table 8.5, the scaffolds fabricated in the current work had flexural strength higher than trabecular bone (10-20MPa) and lower than human cortical bone (135-193MPa) (Fu *et al.*, 2011). Furthermore, the NCL2 and NCL7 3D printed scaffolds showed similar properties to AW scaffolds (Table 8.5). It is of value to highlight that, using a powder-based indirect 3DP technology and novel glass formulations, porous bone-like substitutes with load-bearing capability and tailorable porosity have been manufactured.

#### **8.10 NCL7 antibacterial properties**

The results of the antibacterial tests performed on NCL7 silver-doped composition were presented in the last part of Chapter 7. The porous 3D printed NCL7 scaffolds were able to create a zone where the bacterial growth was slightly inhibited, which was absent for the dense bioceramic pellets. A possible explanation of this effect might be the higher surface area that the porous materials offered with respect to the dense pellets, and presumably the greater release of Ag ions (Sepulveda *et al.*, 2002; Fu *et al.*, 2011; Kolmas *et al.*, 2014). However, the resulting halo, assessed qualitatively *via* the inhibition test, was limited in comparison to the positive control. As Kolmas stated, the method of material synthesis plays a crucial role during the release of doping ions (Kolmas *et al.*, 2014). Specifically, they found that the direct incorporation of Ag ions into the structure of HA lowered their release. Furthermore, dose dependent antibacterial activity was observed for silver-substituted HA, for which higher levels of silver (1.1wt%) led to a more effective bactericidal response (Lim *et al.*, 2013). Hence, it is possible that the antibacterial properties of NCL7 formulation would also be enhanced by increasing the Ag content.

**Table 8.5: Mechanical properties (mean±SE) of 3D printed scaffolds via powder-based indirect 3DP.**

Material	Sintering conditions	Total porosity (vol%)	Flexural strength (MPa)	Reference
NCL2	700°C/1h	28.7±1.5	35.9±2.5	-
NCL7	625°C/1h	35.3±2.0	26.1±2.1	-
AW	1150°C/1h	38.4±3.7	28.6±3.2	-
AW	1150°C/1h	35.3±1.9	35.6±4.7	(Alharbi, 2015)
β-TCP/Bioglass	1000°C	-	14.9±3.6	(Bergmann <i>et al.</i> , 2010)
HA/AW	1200°C/3h	51.5±1.2	21.0±0.1	(Suwanprateeb <i>et al.</i> , 2009)
	1300°C/3h	2.5±0.1	76.8±4.3	
HA	1200°C/2h		21.2±2.2	(Seitz <i>et al.</i> , 2005)
TCP	134°C/2h	28-35%	3.9-5.2	(Klammert <i>et al.</i> , 2010)

### 8.11 Summary

Over the last four decades, considerable progress has been made to develop load-bearing substitutes for diseased, injured or missing bone. Particularly, the science of glass and glass-ceramic together with the last developments in additive manufacturing technology have greatly contributed to address some of the current open problems, mainly poor reproducibility of the grafts, degree of performance needed and strategy for a cost-effective manufacturing process (Ventola, 2014).

However, although numerous research efforts have been made “*the design of advance bioactive biomaterials that can share load with host bone, transmit the load to the cells, and then degrade as the bone repairs*” is a frontier that need to be crossed (Hench and Jones, 2015).

Taken all together, the results of this research work indicated the possibility to design novel bioceramic formulations by adding specific and functional doping agents in order to tailor their properties towards a specific mechanical and biological response. Particularly, ICP analysis proved the high reactive nature of borate-based glass, and the quicker release of boron in comparison to silicon and phosphorous. Furthermore, the data obtained from the HSM represented a useful preliminary guide in the selection of the appropriate sintering temperature for glass-derived structures. Finally, this study demonstrated the excellent capabilities of powder-based 3DP technology to produce 3D bioceramic substitutes, which feature similar properties, such as surface roughness, porosity, interconnectivity, mechanical properties. Moreover *in vitro* biocompatibility of 3D printed bioceramic-derived structures, by using different ceramic-based precursors, has been investigated. Additionally, the use of a binder jetting 3DP technology for the manufacturing of porous structures as potential bone-like substitutes, led to establish that the glass composition significantly impacts the printability of powdered materials, as demonstrated by NCL4 formulation. Hence, a thorough optimisation process is required before the manufacturing phase starts.

## Chapter 9. Conclusion and future work

---

### 9.1 Conclusions

Eight innovative glass compositions, based on silicate, phosphate and borate network formers, were initially proposed for this research work and three of these (NCL2, NCL4 and NCL7 compositions) are considered to have promise in load bearing musculoskeletal applications:

- NCL2 has good mechanical properties and slow degradation rate;
- NCL4 has the highest biodegradation rate of the three, however, NCL4 glass composition significantly influenced the printability of the powder-based precursors;
- NCL7 was more able to form HCA precursors than NCL2 and NCL4-derived pellets, and in the form of a porous scaffold inhibited bacterial growth.

According to the main findings of whole research project, the following conclusions can be drawn:

- the NCL6, NCL7 and AW compositions were glass-ceramic in nature, whilst the NCL1, NCL2, NCL3, NCL4 and NCL8 formulations were completely amorphous;
- the sintering treatment contributed to the development of diopside crystalline phase for NCL2 composition, modifying the nature of the material from glass to glass-ceramic after the sintering;
- hot stage microscopy provides an effective and informative method to support the development of new material sintering conditions;
- the borate-based formulations showed the fastest ion release and degradation rates, with the silicate-based compositions showing the lowest degradation rate;
- all the formulations, processed as dense bioceramic structures, showed mechanical properties comparable to those of dense AW glass-ceramic;
- the NCL7-based bioceramic structures showed a better ability to form HCA precursors than NCL2 and NCL4-based materials;
- binder removal as part of a sintering cycle can be best achieved through the use of a multi-step sintering treatment.
- indirect powder-based 3DP offers an effective route for the production of porous bioceramic scaffolds.

Overall, this research work demonstrated:

- i) the potential of NCL2 and NCL7 glass formulations as smart materials in the field of bone tissue repair and regeneration, with surface roughness, porosity and interconnectivity, mechanical properties and *in vitro* biocompatibility similar to 3D printed AW-derived structures.
- ii) the possibility to process glass powder blends by using a versatile and cost-effective additive manufacturing technology for the production of customised “off-shelf” bone tissue engineered substitutes.

## 9.2 Future work

The findings of the present study complemented those of previous researchers, and contributed to extend the knowledge on the use of ceramic materials with tailorable properties for orthopaedic applications. Nevertheless, future research work that will be valuable to perform is suggested below.

- **Biodegradation rate:**  
the degradation rate of bioglass formulations depends not only on their compositions but also on surface area, geometry of the specimens and pH of the environment (Fu *et al.*, 2010a) (Huang *et al.*, 2006). Therefore, a set of new experimental conditions, based on different geometries (both rectangular and cylindrical shape), level of porosity, and initial pH values of the solution might be useful to be explored in static and dynamic conditions (Pilia *et al.*, 2013). Furthermore, additional studies need to be performed to prove the potential of NCL2 and NCL4 formulations as controlled drug delivery systems.
- **Bioactivity:**  
bioactivity tests in SBF using 3D printed structures should be carried out to establish the potential bone-bonding behaviour of 3D porous materials.
- **Printability:**  
the effects of processing parameters (such as precursor particle distribution, layer thickness and binder saturation level) on mechanical properties of 3D printed structures before and after sintering could be further investigated. Additionally, the printability of the NCL4 formulation, as function of different processing parameters, needs to be further assessed.

- Antibacterial properties:
  - i)* further tests, based on the quantitative evaluation of Ag released during the antibacterial test need to be performed;
  - ii)* in order to deeply investigate the efficiency of the antibacterial activity of the NCL7 composition different types of bacteria need to be carried out;
  - iii)* development and characterisation of new glass compositions with different Ag content could be further evaluated.
- *In vivo* tests:

since *in vitro* tests cannot replicate the complex environment of the human body, animal studies to assess whether or not the novel materials are suitable for bone tissue repair and regeneration applications should be performed.

## REFERENCES

- Abou Neel, E.A., Ahmed, I., Blaker, J.J., Bismarck, A., Boccaccini, A.R., Lewis, M.P., Nazhat, S.N. and Knowles, J.C. (2005) 'Effect of iron on the surface, degradation and ion release properties of phosphate-based glass fibres', *Acta Biomaterialia*, 1(5), pp. 553-63.
- Abou Neel, E.A., Chrzanowski, W., Pickup, D.M., O'Dell, L.A., Mordan, N.J., Newport, R.J., Smith, M.E. and Knowles, J.C. (2009a) 'Structure and properties of strontium-doped phosphate-based glasses', *Journal of the Royal Society Interface*, 6(34), pp. 435-446.
- Abou Neel, E.A., Pickup, D.M., Valappil, S.P., Newport, R.J. and Knowles, J.C. (2009b) 'Bioactive functional materials: a perspective on phosphate-based glasses', *Journal of Materials Chemistry*, 19(6), pp. 690-701.
- Albrektsson, T. and Johansson, C. (2001) 'Osteoinduction, osteoconduction and osseointegration', *European Spine Journal*, 10(2), pp. S96-S101.
- Alharbi, N.A. (2015) *Indirect three dimensional printing of apatite-wollastonite structures for biomedical applications*. Ph.D. thesis. Newcastle University.
- Amini, A.R., Laurencin, C.T. and Nukavarapu, S.P. (2012) 'Bone tissue engineering: Recent advances and challenges', *Critical Reviews in Biomedical Engineering*, 40(5), pp. 363-408.
- Arafat, M.T., Ian, G. and Xu, L. (2014) 'State of the art and future direction of additive manufactured scaffolds-based bone tissue engineering', *Rapid Prototyping Journal*, 20(1), pp. 13-26.
- Arcaute, K., Mann, B. and Wicker, R. (2010) 'Stereolithography of spatially controlled multi-material bioactive poly(ethylene glycol) scaffolds', *Acta Biomaterialia*, 6(3), pp. 1047-1054.
- Arstila, H., Fröberg, L., Hupa, L., Vedel, E., Ylänen, H. and Hupa, M. (2005) 'The sintering range of porous bioactive glasses', *Glass Technology*, 46(2), pp. 138-141.
- Arstila, H., Tukiainen, M., Taipale, S., Kellomäki, M. and Hupa, L. (2008) 'Liquidus temperatures of bioactive glasses', *Advanced Materials Research*, 39-40, pp. 287-292.
- Aubin, J.E. and Triffitt, J.T. (2002) 'Chapter 4 - Mesenchymal Stem Cells and Osteoblast Differentiation', in Rodan, J.P.B.G.R.A. (ed.) *Principles of Bone Biology (Second Edition)*. San Diego: Academic Press, pp. 59-81.



- Baino, F., Ferraris, M., Bretcanu, O., Verné, E. and Vitale-Brovarone, C. (2013) 'Optimization of composition, structure and mechanical strength of bioactive 3-D glass-ceramic scaffolds for bone substitution', *Journal of Biomaterials Applications*, 27(7), pp. 872-890.
- Baino, F., Novajra, G. and Vitale-Brovarone, C. (2015) 'Bioceramics and Scaffolds: A Winning Combination for Tissue Engineering', *Frontiers in Bioengineering and Biotechnology*, 3, p. 202.
- Baino, F. and Vitale-Brovarone, C. (2011) 'Three-dimensional glass-derived scaffolds for bone tissue engineering: Current trends and forecasts for the future', *Journal of Biomedical Materials Research - Part A*, 97 A(4), pp. 514-535.
- Baino, F. and Vitale-Brovarone, C. (2015) 'Ceramics for oculo-orbital surgery', *Ceramics International*, 41(4), pp. 5213-5231.
- Balagna, C., Vitale-Brovarone, C., Miola, M., Verné, E., Canuto, R.A., Saracino, S., Muzio, G., Fucile, G. and Maina, G. (2011) 'Biocompatibility and antibacterial effect of silver doped 3D-glass-ceramic scaffolds for bone grafting', *Journal of Biomaterials Applications*, 25(6), pp. 595-617.
- Balamurugan, A., Balossier, G., Kannan, S., Michel, J., Rebelo, A.H.S. and Ferreira, J.M.F. (2007) 'Development and in vitro characterization of sol-gel derived CaO-P<sub>2</sub>O<sub>5</sub>-SiO<sub>2</sub>-ZnO bioglass', *Acta Biomaterialia*, 3(2), pp. 255-262.
- Barrère, F., van Blitterswijk, C.A. and de Groot, K. (2006) 'Bone regeneration: molecular and cellular interactions with calcium phosphate ceramics', *International Journal of Nanomedicine*, 1(3), pp. 317-332.
- Bartolo, P.J.S., Almeida, H. and Laoui, T. (2009) 'Rapid prototyping and manufacturing for tissue engineering scaffolds', *International Journal of Computer Applications in Technology*, 36(1), pp. 1-9.
- Beard, J.L. (2001) 'Iron biology in immune function, muscle metabolism and neuronal functioning', *The Journal of Nutrition*, 131(2s-2), pp. 568-579;.
- Bellantone, M., Williams, H.D. and Hench, L.L. (2002) 'Broad-spectrum bactericidal activity of Ag<sub>2</sub>O-doped bioactive glass', *Antimicrobial agents and chemotherapy*, 46(6), pp. 1940-1945.

- Bellucci, D., Sola, A. and Cannillo, V. (2011) 'Revised replication method for bioceramic scaffolds', *Bioceramics Development and Applications*, 1(8), p. 2011.
- Bergmann, C., Lindner, M., Zhang, W., Koczur, K., Kirsten, A., Telle, R. and Fischer, H. (2010) '3D printing of bone substitute implants using calcium phosphate and bioactive glasses', *Journal of the European Ceramic Society*, 30(12), pp. 2563-2567.
- Best, S.M., Porter, A.E., Thian, E.S. and Huang, J. (2008) 'Bioceramics: Past, present and for the future', *Journal of the European Ceramic Society*, 28(7), pp. 1319-1327.
- Bielby, R.C., Saravanapavan, P., Polak, J.M. and Hench, L.L. 218-220 (2002) 'Study of osteoblast differentiation and proliferation on the surface of binary bioactive gel-glasses' *Key Engineering Materials*. pp. 269-272.
- Boccaccini, A.R., Chen, Q., Lefebvre, L., Gremillard, L. and Chevalier, J. (2007) 'Sintering, crystallisation and biodegradation behaviour of Bioglass®-derived glass-ceramics', *Faraday Discussions*, 136, pp. 27-44.
- Boccaccini, A.R. and Maquet, V. (2003) 'Bioresorbable and bioactive polymer/Bioglass® composites with tailored pore structure for tissue engineering applications', *Composites Science and Technology*, 63(16), pp. 2417-2429.
- Bohner, M. and Lemaire, J. (2009) 'Can bioactivity be tested in vitro with SBF solution?', *Biomaterials*, 30(12), pp. 2175-2179.
- Bonnelye, E., Chabadel, A., Saltel, F. and Jurdic, P. (2008) 'Dual effect of strontium ranelate: stimulation of osteoblast differentiation and inhibition of osteoclast formation and resorption in vitro', *Bone*, 42(1), pp. 129-38.
- Bosch, C., Melsen, B. and Vargervik, K. (1998) 'Importance of the critical-size bone defect in testing bone-regenerating materials', *Journal of Craniofacial Surgery*, 9(4), pp. 310-316.
- Bose, S., Darsell, J., Hosick, H.L., Yang, L., Sarkar, D.K. and Bandyopadhyay, A. (2002) 'Processing and characterization of porous alumina scaffolds', *Journal of Materials Science: Materials in Medicine*, 13(1), pp. 23-28.
- Bose, S., Roy, M. and Bandyopadhyay, A. (2012) 'Recent advances in bone tissue engineering scaffolds', *Trends in biotechnology*, 30(10), pp. 546-554.

- Bose, S., Vahabzadeh, S. and Bandyopadhyay, A. (2013) 'Bone tissue engineering using 3D printing', *Materials Today*, 16(12), pp. 496-504.
- Boskey, A.L. (2003) 'Biom mineralization: An overview', *Connective Tissue Research*, 44(SUPPL. 1), pp. 5-9.
- Boskey, A.L. (2007) 'Mineralization of bones and teeth', *Elements*, 3(6), pp. 385-391.
- Bracci, B., Torricelli, P., Panzavolta, S., Boanini, E., Giardino, R. and Bigi, A. (2009) 'Effect of  $Mg^{2+}$ ,  $Sr^{2+}$ , and  $Mn^{2+}$  on the chemico-physical and in vitro biological properties of calcium phosphate biomimetic coatings', *Journal of Inorganic Biochemistry*, 103(12), pp. 1666-1674.
- Branda, F., Arcobello-Varlese, F., Costantini, A. and Luciani, G. (2002) 'Effect of the substitution of  $M_2O_3$  ( $M = La, Y, In, Ga, Al$ ) for  $CaO$  on the bioactivity of  $2.5 CaO \cdot 2SiO_2$  glass', *Biomaterials*, 23(3), pp. 711-716.
- Brauer, D.S. (2015) 'Bioactive Glasses—Structure and Properties', *Angewandte Chemie International Edition*, 54(14), pp. 4160-4181.
- Brauer, D.S., Karpukhina, N., O'Donnell, M.D., Law, R.V. and Hill, R.G. (2010) 'Fluoride-containing bioactive glasses: effect of glass design and structure on degradation, pH and apatite formation in simulated body fluid', *Acta Biomaterialia*, 6(8), pp. 3275-82.
- Bredt, J.F. and Anderson, T. (1999) *Method of Three Dimensional Printing*.
- Bredt, J.F., Anderson, T.C. and Russell, D.B. (2003) *Three dimensional printing material system and method*.
- Bretcanu, O., Baine, F., Verné, E. and Vitale-Brovarone, C. (2014) 'Novel resorbable glass-ceramic scaffolds for hard tissue engineering: From the parent phosphate glass to its bone-like macroporous derivatives', *Journal of Biomaterials Applications*, 28(9), pp. 1287-1303.
- Bretcanu, O., Chatzistavrou, X., Paraskevopoulos, K., Conradt, R., Thompson, I. and Boccaccini, A.R. (2009) 'Sintering and crystallisation of 45S5 Bioglass® powder', *Journal of the European Ceramic Society*, 29(16), pp. 3299-3306.
- Bretcanu, O., Samaille, C. and Boccaccini, A. (2008) 'Simple methods to fabricate Bioglass®-derived glass-ceramic scaffolds exhibiting porosity gradient', *Journal of Materials Science*, 43(12), pp. 4127-4134.

- Brink, M. (1997) 'The influence of alkali and alkaline earths on the working range for bioactive glasses', *Journal of Biomedical Materials Research*, 36(1), pp. 109-17.
- Brovarone, C.V., Verné, E. and Appendino, P. (2006) 'Macroporous bioactive glass-ceramic scaffolds for tissue engineering', *Journal of Materials Science: Materials in Medicine*, 17(11), pp. 1069-1078.
- Brown, R.F., Rahaman, M.N., Dwilewicz, A.B., Huang, W., Day, D.E., Li, Y. and Bal, B.S. (2009) 'Effect of borate glass composition on its conversion to hydroxyapatite and on the proliferation of MC3T3-E1 cells', *Journal of Biomedical Materials Research - Part A*, 88(2), pp. 392-400.
- Brydone, A.S., Meek, D. and MacLaine, S. (2010) 'Bone grafting, orthopaedic biomaterials, and the clinical need for bone engineering', *Proceeding Institution of Mechanical Engineering part H*, 224(12), pp. 1329-43.
- Buckwalter, J.A., Glimcher, M.J., Cooper, R.R. and Recker, R. (1996) 'Bone biology. I: Structure, blood supply, cells, matrix, and mineralization', *Instructional course lectures*, 45, pp. 371-386.
- Burg, K.J.L., Porter, S. and Kellam, J.F. (2000) 'Biomaterial developments for bone tissue engineering', *Biomaterials*, 21(23), pp. 2347-2359.
- Butscher, A., Bohner, M., Hofmann, S., Gauckler, L. and Müller, R. (2011) 'Structural and material approaches to bone tissue engineering in powder-based three-dimensional printing', *Acta Biomaterialia*, 7(3), pp. 907-920.
- Butscher, A., Bohner, M., Roth, C., Ernstberger, A., Heuberger, R., Doebelin, N., Rudolf Von Rohr, P. and Müller, R. (2012) 'Printability of calcium phosphate powders for three-dimensional printing of tissue engineering scaffolds', *Acta Biomaterialia*, 8(1), pp. 373-385.
- C773, A. (1988) *Standard Test Method for Compressive (Crushing) Strength of Fired Whiteware Materials*.
- Cancedda, R., Giannoni, P. and Mastrogiacomo, M. (2007) 'A tissue engineering approach to bone repair in large animal models and in clinical practice', *Biomaterials*, 28(29), pp. 4240-4250.
- Cao, H. and Kuboyama, N. (2010) 'A biodegradable porous composite scaffold of PGA/ $\beta$ -TCP for bone tissue engineering', *Bone*, 46(2), pp. 386-395.

- Cao, Y., Croll, T.I., Oconnor, A.J., Stevens, G.W. and Cooper-White, J.J. (2006) 'Systematic selection of solvents for the fabrication of 3D combined macro- and microporous polymeric scaffolds for soft tissue engineering', *Journal of Biomaterials Science, Polymer Edition*, 17(4), pp. 369-402.
- Carlisle, E. 33 (1981) 'Silicon: A requirement in bone formation independent of vitamin D1' *Calcified Tissue International*. 1981/12/01. Springer-Verlag, pp. 27-34 1.
- Carlisle, E.M. (1970) 'Silicon: a possible factor in bone calcification', *Science*, 167(3916), pp. 279-80.
- Carneiro, O.S., Silva, A.F. and Gomes, R. (2015) 'Fused deposition modeling with polypropylene', *Materials & Design*, 83, pp. 768-776.
- Cerruti, M., Greenspan, D. and Powers, K. (2005) 'Effect of pH and ionic strength on the reactivity of Bioglass® 45S5', *Biomaterials*, 26(14), pp. 1665-1674.
- Chachami, G., Simos, G., Hatziefthimiou, A., Bonanou, S., Molyvdas, P.-A. and Paraskeva, E. (2004) 'Cobalt Induces Hypoxia-Inducible Factor-1 $\alpha$  Expression in Airway Smooth Muscle Cells by a Reactive Oxygen Species– and PI3K-Dependent Mechanism', *American Journal of Respiratory Cell and Molecular Biology*, 31(5), pp. 544-551.
- Chellan, P. and Sadler, P.J. (2015) 'The elements of life and medicines', *Philosophical Transactions of the Royal Society of London A: Mathematical, Physical and Engineering Sciences*, 373(2037).
- Chen, Q., Roether, J.A. and Boccaccini, A.R. (2008) 'Tissue engineering scaffolds from bioactive glass and composite materials', *Topics in tissue engineering*, 4.
- Chen, Q., Zhu, C. and Thouas, G. (2012) 'Progress and challenges in biomaterials used for bone tissue engineering: bioactive glasses and elastomeric composites', *Progress in Biomaterials*, 1(1), p. 2.
- Chen, Q.Z. (2011) 'Foaming technology of tissue engineering scaffolds - a review', *Bubble Science, Engineering & Technology*, 3(2), pp. 34-47.
- Chen, Q.Z., Thompson, I.D. and Boccaccini, A.R. (2006) '45S5 Bioglass (R)-derived glass-ceramic scaffolds for bone tissue engineering', *Biomaterials*, 27, pp. 2414 - 2425.

Chu, T.M., Orton, D.G., Hollister, S.J., Feinberg, S.E. and Halloran, J.W. (2002) 'Mechanical and in vivo performance of hydroxyapatite implants with controlled architectures', *Biomaterials*, 23(5), pp. 1283-93.

Ciardelli, G., Chiono, V., Vozzi, G., Pracella, M., Ahluwalia, A., Barbani, N., Cristallini, C. and Giusti, P. (2005) 'Blends of poly-(epsilon-caprolactone) and polysaccharides in tissue engineering applications', *Biomacromolecules*, 6(4), pp. 1961-76.

Cima, L.G. and Cima, M.J. (1996) *Preparation of medical devices by solid free-form fabrication methods*.

Cima, M., Sachs, E., Fan, T., Brecht, J.F., Michaels, S.P., Khanuja, S., Lauder, A., Lee, S.J.J., Brancaccio, D. and Curodeau, A. (1995) *Three-dimensional printing techniques*.

Clarke, B. (2008) 'Normal bone anatomy and physiology', *Clinical journal of the American Society of Nephrology : CJASN*, 3 Suppl 3, pp. S131-139.

Cooke, M.N., Fisher, J.P., Dean, D., Rimnac, C. and Mikos, A.G. (2003) 'Use of stereolithography to manufacture critical-sized 3D biodegradable scaffolds for bone ingrowth', *Journal of Biomedical Materials Research Part B: Applied Biomaterials*, 64B(2), pp. 65-69.

Cordero-Arias, L., Cabanas-Polo, S., Goudouri, O.M., Misra, S.K., Gilabert, J., Valsami-Jones, E., Sanchez, E., Virtanen, S. and Boccaccini, A.R. (2015) 'Electrophoretic deposition of ZnO/alginate and ZnO-bioactive glass/alginate composite coatings for antimicrobial applications', *Materials science & engineering C, Materials for biological applications*, 55, pp. 137-144.

Correia, C.O., Leite, Á.J. and Mano, J.F. (2015) 'Chitosan/bioactive glass nanoparticles scaffolds with shape memory properties', *Carbohydrate Polymers*, 123(0), pp. 39-45.

Cousins, R.J. (1998) 'A role of zinc in the regulation of gene expression', *Proceedings Of The Nutrition Society*, 57, pp. 307 - 311.

Cox, S.C., Thornby, J.A., Gibbons, G.J., Williams, M.A. and Mallick, K.K. (2015) '3D printing of porous hydroxyapatite scaffolds intended for use in bone tissue engineering applications', *Materials Science and Engineering: C*, 47(0), pp. 237-247.

Currey, J.D., Pitchford, J.W. and Baxter, P.D. (2007) 'Variability of the mechanical properties of bone, and its evolutionary consequences', *Journal of the Royal Society Interface*, 4, pp. 127-135.

- Dalton, P.D., Woodfield, T. and Hutmacher, D.W. (2009) 'Snapshot: Polymer scaffolds for tissue engineering', *Biomaterials*, 30(4), pp. 701-2.
- Davis, E.H. and Leach, K.J. (2008) *Hybrid and composite biomaterials in tissue engineering*.
- Dawson, J.I., Kanczler, J., Tare, R., Kassem, M. and Oreffo, R.O. (2014) 'Concise review: bridging the gap: bone regeneration using skeletal stem cell-based strategies - where are we now?', *Stem Cells*, 32(1), pp. 35-44.
- De Long, W.G., Jr., Einhorn, T.A., Koval, K., McKee, M., Smith, W., Sanders, R. and Watson, T. (2007) 'Bone grafts and bone graft substitutes in orthopaedic trauma surgery. A critical analysis', *Journal of bone & Joint Surgery, American Volume*, 89(3), pp. 649-58.
- Delormannli, A.M. (2013) 'Size-dependent degradation and bioactivity of borate bioactive glass', *Ceramics International*, 39(7), pp. 8087-8095.
- Demling, R.H. (2009) 'Nutrition, Anabolism, and the Wound Healing Process: An Overview', *Eplasty*, 9, p. e9.
- Detsch, R., Schaefer, S., Deisinger, U., Ziegler, G., Seitz, H. and Leukers, B. (2011) 'In vitro - Osteoclastic Activity Studies on Surfaces of 3D Printed Calcium Phosphate Scaffolds', *Journal of Biomaterials Applications*, 26(3), pp. 359-380.
- Deville, S. (2008) 'Freeze-Casting of Porous Ceramics: A Review of Current Achievements and Issues', *Advanced Engineering Materials*, 10(3), pp. 155-169.
- Deville, S., Saiz, E., Nalla, R.K. and Tomsia, A.P. (2006a) 'Freezing as a path to build complex composites', *Science*, 311(5760), pp. 515-518.
- Deville, S., Saiz, E. and Tomsia, A.P. (2006b) 'Freeze casting of hydroxyapatite scaffolds for bone tissue engineering', *Biomaterials*, 27(32), pp. 5480-5489.
- Dhandayuthapani, B., Yoshida, Y., Maekawa, T. and Kumar, D.S. (2011) 'Polymeric scaffolds in tissue engineering application: a review', *International Journal of Polymer Science*, 2011.
- Dietrich, E., Oudadesse, H., Lucas-Girot, A. and Mami, M. (2009) 'In vitro bioactivity of melt-derived glass 46S6 doped with magnesium', *Journal of Biomedical Materials Research - Part A*, 88(4), pp. 1087-96.

- Dimitriou, R., Jones, E., McGonagle, D. and Giannoudis, P. (2011) 'Bone regeneration: current concepts and future directions', *BMC Medicine*, 9(1), p. 66.
- Dimitriou, R., Mataliotakis, G., Calori, G. and Giannoudis, P. (2012) 'The role of barrier membranes for guided bone regeneration and restoration of large bone defects: current experimental and clinical evidence', *BMC Medicine*, 10(1), p. 81.
- Dorozhkin, S.V. (2010) 'Calcium Orthophosphates as Bioceramics: State of the Art', *Journal of Functional Biomaterials*, 1(1), pp. 22-107.
- Dorozhkin, S.V. (2011) 'Biocomposites and hybrid biomaterials based on calcium orthophosphates', *Biomatter*, 1(1), pp. 3-56.
- Downey, P.A. and Siegel, M.I. (2006) 'Bone biology and the clinical implications for osteoporosis', *Physical Therapy*, 86(1), pp. 77-91.
- Dressmann, H. (1892) 'Ueber knochenplombierung bei hohlenformigen defekten des knochens', *Beitr Klin Chir*, 9, pp. 804-810.
- Ducheyne, P. and Qiu, Q. (1999) 'Bioactive ceramics: The effect of surface reactivity on bone formation and bone cell function', *Biomaterials*, 20(23-24), pp. 2287-2303.
- Dvir, T., Timko, B.P., Kohane, D.S. and Langer, R. (2011) 'Nanotechnological strategies for engineering complex tissues', *Nature Nanotechnology*, 6(1), pp. 13-22.
- Dyson, J.A., Genever, P.G., Dalgarno, K.W. and Wood, D.J. (2007) 'Development of custom-built bone scaffolds using mesenchymal stem cells and apatite-wollastonite glass-ceramics', *Tissue Engineering*, 13(12), pp. 2891-2901.
- Dzondo-Gadet, M., Mayap-Nzietchueng, R., Hess, K., Nabet, P., Belleville, F. and Dousset, B. (2002) 'Action of boron at the molecular level', *Biological Trace Element Research*, 85(1), pp. 23-33.
- Einhorn, T.A. (1998) 'The cell and molecular biology of fracture healing', *Clinical Orthopaedics and Related Research*, (355 Suppl), pp. S7-21.
- El-Ghannam, A., Ducheyne, P. and Shapiro, I.M. (1997) 'Formation of surface reaction products on bioactive glass and their effects on the expression of the osteoblastic phenotype and the deposition of mineralized extracellular matrix', *Biomaterials*, 18(4), pp. 295-303.



- Emans, P.J., Spaapen, F., Surtel, D.A.M., Reilly, K.M., Cremers, A., van Rhijn, L.W., Bulstra, S.K., Voncken, J.W. and Kuijer, R. (2007) 'A novel in vivo model to study endochondral bone formation; HIF-1 $\alpha$  activation and BMP expression', *Bone*, 40(2), pp. 409-418.
- Erol-Taygun, M., Zheng, K. and Boccaccini, A.R. (2013) 'Nanoscale Bioactive Glasses in Medical Applications', *International Journal of Applied Glass Science*, 4(2), pp. 136-148.
- Erol, M.M., Mouriño, V., Newby, P., Chatzistavrou, X., Roether, J.A., Hupa, L. and Boccaccini, A.R. (2012) 'Copper-releasing, boron-containing bioactive glass-based scaffolds coated with alginate for bone tissue engineering', *Acta Biomaterialia*, 8(2), pp. 792-801.
- Eslami, H., Solati-Hashjin, M. and Tahriri, M. (2010) 'Effect of fluorine ion addition on structural, thermal, mechanical, solubility and biocompatibility characteristics of hydroxyapatite nanopowders', *Advances in Applied Ceramics*, 109(4), pp. 200-212.
- Evans, F.G. (1961) *Biomechanical studies of the musculo-skeletal system*. Literary Licensing, LLC.
- F2792, A. (2012) 'Standard Terminology for Additive Manufacturing Technologies'.
- Fabbri, P., Cannillo, V., Sola, A., Dorigato, A. and Chiellini, F. (2010) 'Highly porous polycaprolactone-45S5 Bioglass® scaffolds for bone tissue engineering', *Composites Science and Technology*, 70(13), pp. 1869-1878.
- Faeghi-Nia, A., Marghussian, V.K., Taheri-Nassaj, E., Pascual, M.J. and Durán, A. (2009) 'Pressureless Sintering of Apatite/Wollastonite-Phlogopite Glass-Ceramics', *Journal of the American Ceramic Society*, 92(7), pp. 1514-1518.
- Farzadi, A., Waran, V., Solati-Hashjin, M., Rahman, Z.A.A., Asadi, M. and Osman, N.A.A. (2015) 'Effect of layer printing delay on mechanical properties and dimensional accuracy of 3D printed porous prototypes in bone tissue engineering', *Ceramics International*, 41(7), pp. 8320-8330.
- Feenstra, F.K. (2005) *Method for making a dental element*.
- Fielding, G. and Bose, S. (2013) 'SiO<sub>2</sub> and ZnO Dopants in 3D Printed TCP Scaffolds Enhances Osteogenesis and Angiogenesis in vivo', *Acta biomaterialia*, 9(11).
- Finney, L., Vogt, S., Fukai, T. and Glesne, D. (2009) 'Copper and angiogenesis: unravelling a relationship key to cancer progression', *Clinical and Experimental Pharmacology and Physiology*, 36(1), pp. 88-94.

Franks, K., Abrahams, I. and Knowles, J.C. (2000) 'Development of soluble glasses for biomedical use Part I: in vitro solubility measurement', *Journal of Materials Science: Materials in Medicine*, 11(10), pp. 609-14.

Franz-Oodendaal, T.A., Hall, B.K. and Witten, P.E. (2006) 'Buried alive: how osteoblasts become osteocytes', *Developmental Dynamics*, 235(1), pp. 176-90.

Fu, H., Rahaman, M.N., Day, D.E. and Huang, W. (2012) 'Long-term conversion of 45S5 bioactive glass-ceramic microspheres in aqueous phosphate solution', *Journal of Materials Science: Materials in Medicine*, 23, pp. 1181 - 1191.

Fu, H.L., Fu, Q., Zhou, N., Huang, W.H., Rahaman, M.N., Wang, D.P. and Liu, X. (2009) 'In vitro evaluation of borate-based bioactive glass scaffolds prepared by a polymer foam replication method', *Materials Science & Engineering C, Materials for biological applications.*, 29, pp. 2275 - 2281.

Fu, Q., Rahaman, M.N., Bal, B.S., Bonewald, L.F., Kuroki, K. and Brown, R.F. (2010a) 'Silicate, borosilicate, and borate bioactive glass scaffolds with controllable degradation rate for bone tissue engineering applications. II. In vitro and in vivo biological evaluation', *Journal of Biomedical Materials Research Part A*, 95(1), pp. 172-179.

Fu, Q., Rahaman, M.N., Bal, B.S., Huang, W. and Day, D.E. (2007) 'Preparation and bioactive characteristics of a porous 13-93 glass, and fabrication into the articulating surface of a proximal tibia', *Journal of Biomedical Materials Research - Part A*, 82(1), pp. 222-229.

Fu, Q., Rahaman, M.N., Bal, B.S., Kuroki, K. and Brown, R.F. (2010b) 'In vivo evaluation of 13-93 bioactive glass scaffolds with trabecular and oriented microstructures in a subcutaneous rat implantation model', *Journal of Biomedical Materials Research - Part A*, 95(1), pp. 235-244.

Fu, Q., Rahaman, M.N., Fu, H. and Liu, X. (2010c) 'Silicate, borosilicate, and borate bioactive glass scaffolds with controllable degradation rate for bone tissue engineering applications. I. Preparation and in vitro degradation', *Journal of Biomedical Materials Research - Part A*, 95(1), pp. 164-71.

Fu, Q., Saiz, E., Rahaman, M.N. and Tomsia, A.P. (2011) 'Bioactive glass scaffolds for bone tissue engineering: State of the art and future perspectives', *Materials Science and Engineering C*, 31(7), pp. 1245-1256.

- Galea, G., Kopman, D. and Graham, B.J. (1998) 'Supply and demand of bone allograft for revision hip surgery in Scotland', *Journal of Bone & Joint Surgery, British Volume*, 80(4), pp. 595-9.
- Gao, C., Deng, Y., Feng, P., Mao, Z., Li, P., Yang, B., Deng, J., Cao, Y., Shuai, C. and Peng, S. (2014) 'Current progress in bioactive ceramic scaffolds for bone repair and regeneration', *International Journal of Molecular Sciences*, 15(3), pp. 4714-4732.
- Gaston, M.S. and Simpson, A.H.R.W. (2007) 'Inhibition of fracture healing', *Journal of Bone & Joint Surgery, British Volume*, 89-B(12), pp. 1553-1560.
- Gbureck, U., Vorndran, E., Muller, F.A. and Barralet, J.E. (2007) 'Low temperature direct 3D printed bioceramics and biocomposites as drug release matrices', *Journal of Control Release*, 122(2), pp. 173-80.
- Gentile, P., Chiono, V., Carmagnola, I. and Hatton, P.V. (2014) 'An Overview of Poly(lactic-co-glycolic) Acid (PLGA)-Based Biomaterials for Bone Tissue Engineering', *International Journal of Molecular Sciences*, 15(3), pp. 3640-3659.
- Gentili, C. and Cancedda, R. (2009) 'Cartilage and bone extracellular matrix', *Current Pharmaceutical Design*, 15(12), pp. 1334-48.
- Gentleman, E., Fredholm, Y.C., Jell, G., Lotfibakhshaiesh, N., O'Donnell, M.D., Hill, R.G. and Stevens, M.M. (2010) 'The effects of strontium-substituted bioactive glasses on osteoblasts and osteoclasts in vitro', *Biomaterials*, 31(14), pp. 3949-3956.
- Gerard, C., Bordeleau, L.J., Barralet, J. and Doillon, C.J. (2010) 'The stimulation of angiogenesis and collagen deposition by copper', *Biomaterials*, 31, pp. 824 - 831.
- Gerhardt, L.C. and Boccaccini, A.R. (2010) 'Bioactive Glass and Glass-Ceramic Scaffolds for Bone Tissue Engineering', *Materials*, 3(7), pp. 3867-3910.
- Giannitelli, S.M., Accoto, D., Trombetta, M. and Rainer, A. (2014) 'Current trends in the design of scaffolds for computer-aided tissue engineering', *Acta Biomaterialia*, 10(2), pp. 580-594.
- Giannoudis, P.V., Dinopoulos, H. and Tsiridis, E. (2005) 'Bone substitutes: an update', *Injury*, 36 Suppl 3, pp. S20-7.
- Gibson, I., Rosen, D. and Stucker, B. (2014) *Additive Manufacturing Technologies: 3D Printing, Rapid Prototyping, and Direct Digital Manufacturing*. Springer New York.

- Gloria, A., De Santis, R. and Ambrosio, L. (2010) 'Polymer-based composite scaffolds for tissue engineering', *Journal of Applied Biomaterials and Biomechanics*, 8(2), pp. 57-67.
- Goel, A., Kapoor, S., Rajagopal, R.R., Pascual, M.J., Kim, H.W. and Ferreira, J.M. (2012) 'Alkali-free bioactive glasses for bone tissue engineering: a preliminary investigation', *Acta Biomaterialia*, 8(1), pp. 361-72.
- Goldstein, S.A. (1987) 'The mechanical properties of trabecular bone: Dependence on anatomic location and function', *Journal of Biomechanics*, 20(11-12), pp. 1055-1061.
- Goodridge, R.D., Wood, D.J., Ohtsuki, C. and Dalgarno, K.W. (2007) 'Biological evaluation of an apatite-mullite glass-ceramic produced via selective laser sintering', *Acta Biomaterialia*, 3(2), pp. 221-31.
- Goodship, A.E. (1987) 'The Law of Bone Remodelling', *Journal of Anatomy*, 155, pp. 217-217.
- Greil, P. (2000) 'Polymer derived engineering ceramics', *Advanced Engineering Materials*, 2(6), pp. 339-348.
- Griffith, L.G. (2000) 'Polymeric biomaterials', *Acta Materialia*, 48(1), pp. 263-277.
- Groh, D., Döhler, F. and Brauer, D.S. (2014) 'Bioactive glasses with improved processing. Part 1. Thermal properties, ion release and apatite formation', *Acta Biomaterialia*, 10(10), pp. 4465-4473.
- Gruber, R., Koch, H., Doll, B.A., Tegtmeier, F., Einhorn, T.A. and Hollinger, J.O. (2006) 'Fracture healing in the elderly patient', *Experimental Gerontology*, 41(11), pp. 1080-1093.
- Habibovic, P., Gbureck, U., Doillon, C.J., Bassett, D.C., van Blitterswijk, C.A. and Barralet, J.E. (2008) 'Osteoconduction and osteoinduction of low-temperature 3D printed bioceramic implants', *Biomaterials*, 29(7), pp. 944-953.
- Hadjidakis, D.J. and Androulakis, II (2006) 'Bone remodeling', *Annals of the New York Academy of Sciences*, 1092, pp. 385-96.
- Hall, B.K. (1992) *Bone: A Treatise*. Taylor & Francis.
- Heaney, R.P. (2008) 'Chapter 79 - Calcium', in Martin, J.P.B.G.R.J. (ed.) *Principles of Bone Biology (Third Edition)*. San Diego: Academic Press, pp. 1697-1710.

- Heino, T.J. and Hentunen, T.A. (2008) 'Differentiation of osteoblasts and osteocytes from mesenchymal stem cells', *Current Stem Cell Research and Therapy*, 3(2), pp. 131-145.
- Hench, L.L. (1991) 'Bioceramics: From Concept to Clinic', *Journal of the American Ceramic Society*, 74(7), pp. 1487-1510.
- Hench, L.L. (1998a) 'Bioactive materials: the potential for tissue regeneration', *Journal of Biomedical Materials Research*, 41(4), pp. 511-8.
- Hench, L.L. (1998b) 'Bioceramics', *Journal of the American Ceramic Society*, 81, pp. 1705 - 1728.
- Hench, L.L. (1998c) 'Biomaterials: a forecast for the future', *Biomaterials*, 19(16), pp. 1419-23.
- Hench, L.L. (1999) 'Bioactive glasses and glasses-ceramics', *Bioceramics -applications of ceramic and glass materials in medicine*, pp. 37 - 64.
- Hench, L.L. and Jones, J.R. (2015) 'Bioactive glasses: Frontiers and challenges', *Frontiers in Bioengineering and Biotechnology*, 3.
- Hench, L.L., Splinter, R.J., Allen, W.C. and Greenlee, T.K. (1971) 'Bonding mechanisms at the interface of ceramic prosthetic materials', *Journal of Biomedical Materials Research*, 2, pp. 117 - 141.
- Hench, L.L. and West, J.K. (1990) 'The sol-gel process', *Chemical Reviews*, 90(1), pp. 33-72.
- Hench, L.L. and Wilson, J. (1993) *An Introduction to Bioceramics*. World Scientific, Singapore.
- Henkel, J., Woodruff, M.A., Epari, D.R., Steck, R., Glatt, V., Dickinson, I.C., Choong, P.F.M., Schuetz, M.A. and Hutmacher, D.W. (2013) 'Bone Regeneration Based on Tissue Engineering Conceptions — A 21st Century Perspective', *Bone Research*, 1, p. 216.
- Hernandez, C.J., Beaupre, G.S., Keller, T.S. and Carter, D.R. (2001) 'The influence of bone volume fraction and ash fraction on bone strength and modulus', *Bone*, 29(1), pp. 74-8.
- Hesaraki, S., Alizadeh, M., Nazarian, H. and Sharifi, D. (2010) 'Physico-chemical and in vitro biological evaluation of strontium/calcium silicophosphate glass', *Journal of Materials Science: Materials in Medicine*, 21(2), pp. 695-705.
- Hing, K.A. (2004) 'Bone repair in the twenty-first century: biology, chemistry or engineering?', *Philos Trans A Math Phys Eng Sci*, 362(1825), pp. 2821-50.

- Ho, S.T., Hutmacher, D.W., Ekaputra, A.K., Hitendra, D. and Hui, J.H. (2010) 'The evaluation of a biphasic osteochondral implant coupled with an electrospun membrane in a large animal model', *Tissue Engineering Part A*, 16(4), pp. 1123-41.
- Hogekamp, S. and Pohl, M. (2004) 'Methods for characterizing wetting and dispersing of powder', *Chemie-Ingenieur-Technik*, 76(4), pp. 385-390.
- Hollinger, J.O. (2011) *An Introduction to Biomaterials, Second Edition*. CRC Press.
- Hollinger, J.O., Einhorn, T.A., Doll, B. and Sfeir, C. (2004) *Bone tissue engineering*. CRC Press.
- Hollister, S.J., Maddox, R.D. and Taboas, J.M. (2002) 'Optimal design and fabrication of scaffolds to mimic tissue properties and satisfy biological constraints', *Biomaterials*, 23(20), pp. 4095-4103.
- Hoppe, A., Brandl, A., Bleiziffer, O., Arkudas, A., Horch, R.E., Jokic, B., Janackovic, D. and Boccaccini, A.R. (2015) 'In vitro cell response to Co-containing 1393 bioactive glass', *Materials Science and Engineering: C*, 57, pp. 157-163.
- Hoppe, A., Guldal, N.S. and Boccaccini, A.R. (2011) 'A review of the biological response to ionic dissolution products from bioactive glasses and glass-ceramics', *Biomaterials*, 32, pp. 2757 - 2774.
- Hoppe, A., Jokic, B., Janackovic, D., Fey, T., Greil, P., Romeis, S., Schmidt, J., Peukert, W., Lao, J., Jallot, E. and Boccaccini, A.R. (2014) 'Cobalt-releasing 1393 bioactive glass-derived scaffolds for bone tissue engineering applications', *ACS Applied Materials & Interfaces*, 6(4), pp. 2865-77.
- Hoppe, A., Meszaros, R., Stahli, C., Romeis, S., Schmidt, J., Peukert, W., Marelli, B., Nazhat, S.N., Wondraczek, L., Lao, J., Jallot, E. and Boccaccini, A.R. (2013) 'In vitro reactivity of Cu doped 45S5 Bioglass[registered sign] derived scaffolds for bone tissue engineering', *Journal of Materials Chemistry B*, 1(41), pp. 5659-5674.
- Hoppe, U. (1996) 'A structural model for phosphate glasses', *Journal of Non-Crystalline Solids*, 195(1-2), pp. 138-147.
- Hordyjewska, A., Popiolek, L. and Kocot, J. (2014) 'The many “faces” of copper in medicine and treatment', *Biometals*, 27(4), pp. 611-621.
- Horner, E.A., Kirkham, J., Wood, D., Curran, S., Smith, M., Thomson, B. and Yang, X.B. (2010) 'Long bone defect models for tissue engineering applications: criteria for choice', *Tissue engineering. Part B*, 16(2), pp. 263-271.

- Hsin, I.C. and Yiwei, W. (2011) *Cell Responses to Surface and Architecture of Tissue Engineering Scaffolds*.
- Hu, G.F. (1998) 'Copper stimulates proliferation of human endothelial cells under culture', *Journal of Cellular Biochemistry*, 69, pp. 326 - 335.
- Huang, W., Rahaman, M.N., Day, D.E. and Li, Y. (2006) 'Mechanisms for converting bioactive silicate, borate, and borosilicate glasses to hydroxyapatite in dilute phosphate solution', *Physics and Chemistry of Glasses: European Journal of Glass Science and Technology Part B*, 47(6), pp. 647-658.
- Hull, C.W. (1986) *Apparatus for production of three-dimensional objects by stereolithography*.
- Hum, J. and Boccaccini, A.R. (2012) 'Bioactive glasses as carriers for bioactive molecules and therapeutic drugs: a review', *Journal of Materials Science: Materials in Medicine*, 23(10), pp. 2317-2333.
- Hutmacher, D.W. (2000) 'Scaffolds in tissue engineering bone and cartilage', *Biomaterials*, 21(24), pp. 2529-2543.
- Hutmacher, D.W. (2001) 'Scaffold design and fabrication technologies for engineering tissues - State of the art and future perspectives', *Journal of Biomaterials Science, Polymer Edition*, 12(1), pp. 107-124.
- Hutmacher, D.W., Sittinger, M. and Risbud, M.V. (2004) 'Scaffold-based tissue engineering: Rationale for computer-aided design and solid free-form fabrication systems', *Trends in Biotechnology*, 22(7), pp. 354-362.
- Inzana, J.A., Olvera, D., Fuller, S.M., Kelly, J.P., Graeve, O.A., Schwarz, E.M., Kates, S.L. and Awad, H.A. (2014) '3D printing of composite calcium phosphate and collagen scaffolds for bone regeneration', *Biomaterials*, 35(13), pp. 4026-34.
- Irsen, S.H., Leukers, B., Höckling, C., Tille, C. and Seitz, H. (2006a) 'Bioceramic granulates for use in 3D printing: Process engineering aspects', *Materials Science & Engineering Technology*, 37(6), pp. 533-537.

Irsen, S.H., Leukers, B., Höckling, C., Tille, C. and Seitz, H. (2006b) 'Bioceramic granulates for use in 3D printing: Process engineering aspects', *Materialwissenschaft und Werkstofftechnik*, 37(6), pp. 533-537.

Jarcho, M. (1981) 'Calcium phosphate ceramics as hard tissue prosthetics', *Clinical Orthopaedics and Related Research*, (157), pp. 259-78.

Jayabalan, M., Shalumon, K.T., Mitha, M.K., Ganesan, K. and Epple, M. (2010) 'Effect of hydroxyapatite on the biodegradation and biomechanical stability of polyester nanocomposites for orthopaedic applications', *Acta Biomaterialia*, 6(3), pp. 763-775.

Jeans, L.A., Gilchrist, T. and Healy, D. (2007) 'Peripheral nerve repair by means of a flexible biodegradable glass fibre wrap: a comparison with microsurgical epineurial repair', *Journal of Plastic, Reconstructive & Aesthetic Surgery*, 60(12), pp. 1302-1308.

Jegoux, F., Aguado, E., Cognet, R., Malard, O., Moreau, F., Daculsi, G. and Goyenvalle, E. 361-363 II (2008) 'Repairing segmental defect with a composite associating collagen membrane and MBCP® combined with total bone marrow graft in irradiated bone defect: An experimental study in rabbit' *Key Engineering Materials*. pp. 1245-1248.

*Joint Reconstruction and Replacement: Materials, Technologies, and Global Markets* (2014). Available at: <http://www.bccresearch.com/>.

Jones, J., Ahir, S. and Hench, L. (2004) 'Large-Scale Production of 3D Bioactive Glass Macroporous Scaffolds for Tissue Engineering', *Journal of Sol-Gel Science and Technology*, 29(3), pp. 179-188.

Jones, J. and Clare, A. (2012) *Bio-Glasses : An Introduction*. Wiley.

Jones, J.R. (2013) 'Review of bioactive glass: from Hench to hybrids', *Acta Biomaterialia*, 9(1), pp. 4457-86.

Jones, J.R., Ehrenfried, L.M. and Hench, L.L. (2006) 'Optimising bioactive glass scaffolds for bone tissue engineering', *Biomaterials*, 27(7), pp. 964-973.

Jones, J.R. and Hench, L.L. (2003a) 'Effect of surfactant concentration and composition on the structure and properties of sol-gel-derived bioactive glass foam scaffolds for tissue engineering', *Journal of Materials Science*, 38(18), pp. 3783-3790.



- Jones, J.R. and Hench, L.L. (2003b) 'Regeneration of trabecular bone using porous ceramics', *Current Opinion in Solid State & Materials Science* 7, pp. 301 - 307.
- Josko, O. (2011) 'Copper and zinc, biological role and significance of copper/zinc imbalance', *Journal of Clinical Toxicology*, S3:001.
- Jung, S.B., Day, D.E., Brown, R.F. and Bonewald, L.F. (2013) 'Potential toxicity of bioactive borate glasses in-vitro and in-vivo', *Ceramic Engineering and Science Proceedings*, 33(6), pp. 65-74.
- Kalita, S.J., Bose, S., Hosick, H.L. and Bandyopadhyay, A. (2003) 'Development of controlled porosity polymer-ceramic composite scaffolds via fused deposition modeling', *Materials Science and Engineering: C*, 23(5), pp. 611-620.
- Kanczler, J.M. and Oreffo, R.O. (2008) 'Osteogenesis and angiogenesis: the potential for engineering bone', *European Cells and Materials*, 15, pp. 100-14.
- Karageorgiou, V. and Kaplan, D. (2005) 'Porosity of 3D biomaterial scaffolds and osteogenesis', *Biomaterials*, 26(27), pp. 5474-5491.
- Karaplis, A.C. (2002) 'Chapter 3 - Embryonic Development of Bone and the Molecular Regulation of Intramembranous and Endochondral Bone Formation', in Rodan, J.P.B.G.R.A. (ed.) *Principles of Bone Biology (Second Edition)*. San Diego: Academic Press, pp. 33-IV.
- Kaur, G., Pandey, O.P., Singh, K., Homa, D., Scott, B. and Pickrell, G. (2013) 'A review of bioactive glasses: Their structure, properties, fabrication, and apatite formation', *Journal of Biomedical Materials Research - Part A*, 102(1), pp. 254-274.
- Keaveny, T.M. and Hayes, W.C. (1993) 'Mechanical properties of cortical and trabecular bone', *Bone. A treatise, volume 7: bone growth*, pp. 285 - 344.
- Khalyfa, A., Vogt, S., Weisser, J., Grimm, G., Rechtenbach, A., Meyer, W. and Schnabelrauch, M. (2007) 'Development of a new calcium phosphate powder-binder system for the 3D printing of patient specific implants', *Journal of Materials Science: Materials in Medicine*, 18(5), pp. 909-916.
- Khan, Y., Yaszemski, M.J., Mikos, A.G. and Laurencin, C.T. (2008) 'Tissue engineering of bone: material and matrix considerations', *Journal of Bone & Joint Surgery, American Volume*, 90 Suppl 1, pp. 36-42.

- Kim, S.S., Utsunomiya, H., Koski, J.A., Wu, B.M., Cima, M.J., Sohn, J., Mukai, K., Griffith, L.G. and Vacanti, J.P. (1998) 'Survival and function of hepatocytes on a novel three-dimensional synthetic biodegradable polymer scaffold with an intrinsic network of channels', *Annals of Surgery*, 228(1), pp. 8-13.
- Kimmel, D.B. (1993) 'A paradigm for skeletal strength homeostasis', *Journal of Bone and Mineral Research*, 8 Suppl 2, pp. S515-22.
- Kini, U. and Nandeesh, B.N. (2012) 'Physiology of Bone Formation, Remodeling, and Metabolism', in Fogelman, I., Gnanasegaran, G. and van der Wall, H. (eds.) *Radionuclide and Hybrid Bone Imaging*. Springer Berlin Heidelberg, pp. 29-57.
- Klammert, U., Gbureck, U., Vorndran, E., Rödiger, J., Meyer-Marcotty, P. and Kübler, A.C. (2010) '3D powder printed calcium phosphate implants for reconstruction of cranial and maxillofacial defects', *Journal of Cranio-Maxillofacial Surgery*, 38(8), pp. 565-570.
- Knowles, J.C. (2003) 'Phosphate based glasses for biomedical applications', *Journal of Materials Chemistry*, 13(10), pp. 2395-2401.
- Kobayashi, S., Takahashi, H.E., Ito, A., Saito, N., Nawata, M., Horiuchi, H., Ohta, H., Ito, A., Iorio, R., Yamamoto, N. and Takaoka, K. (2003) 'Trabecular minimodeling in human iliac bone', *Bone*, 32(2), pp. 163-9.
- Kokubo, T. (1990) 'Surface chemistry of bioactive glass-ceramics', *Journal of Non-Crystalline Solids*, 120(1-3), pp. 138-151.
- Kokubo, T. (1999) 'A/W glass-ceramic: processing and properties', *An introduction to bioceramics*, pp. 75 - 88.
- Kokubo, T. (2008) *Bioceramics and their Clinical Applications*. Woodhead Publishing Ltd.
- Kokubo, T., Kim, H.M. and Kawashita, M. (2003) 'Novel bioactive materials with different mechanical properties', *Biomaterials*, 24(13), pp. 2161-2175.
- Kokubo, T., Kushitani, H., Sakka, S., Kitsugi, T. and Yamamuro, T. (1990) 'Solutions able to reproduce in vivo surface-structure changes in bioactive glass-ceramic A-W', *Journal of Biomedical Materials Research*, 24(6), pp. 721-34.

- Kokubo, T., Shigematsu, M., Nagashima, Y., Tashiro, M., Nakamura, T., Yamamuro, T. and Higashi, S. (1982) 'KURENAI: Kyoto University Research Information Repository', *Bull. Inst. Chem. Res., Kyoto Univ*, 60(3-4).
- Kokubo, T. and Takadama, H. (2006) 'How useful is SBF in predicting in vivo bone bioactivity?', *Biomaterials*, 27(15), pp. 2907-2915.
- Kolmas, J., Groszyk, E., Kwiatkowska, R., xf, x17c and ycka, D. (2014) 'Substituted Hydroxyapatites with Antibacterial Properties', *BioMed Research International*, 2014, p. 15.
- Krishnan, V. and Lakshmi, T. (2013) 'Bioglass: A novel biocompatible innovation', *Journal of Advanced Pharmaceutical Technology & Research*, 4(2), pp. 78-83.
- Lai, Y.L. and Yamaguchi, M. (2005) 'Effects of copper on bone component in the femoral tissues of rats: anabolic effect of zinc is weakened by copper', *Biological and Pharmaceutical Bulletin*, 28, pp. 2296 - 2301.
- Lakhkar, N.J., Lee, I.H., Kim, H.W., Salih, V., Wall, I.B. and Knowles, J.C. (2013) 'Bone formation controlled by biologically relevant inorganic ions: role and controlled delivery from phosphate-based glasses', *Advanced Drug Delivery Reviews*, 65(4), pp. 405-20.
- Landis, W.J., Song, M.J., Leith, A., McEwen, L. and McEwen, B.F. (1993) 'Mineral and organic matrix interaction in normally calcifying tendon visualized in three dimensions by high-voltage electron microscopic tomography and graphic image reconstruction', *Journal of Structural Biology*, 110(1), pp. 39-54.
- Lang, C., Murgia, C., Leong, M., Tan, L.W., Perozzi, G., Knight, D., Ruffin, R. and Zalewski, P. (2007) 'Anti-inflammatory effects of zinc and alterations in zinc transporter mRNA in mouse models of allergic inflammation', *American journal of physiology. Lung cellular and molecular physiology*, 292, pp. L577 - L584.
- Langer, R. and Vacanti, J.P. (1993) 'Tissue engineering', *Science*, 260(5110), pp. 920-926.
- Lee, I.H., Shin, S.H., Foroutan, F., Lakhkar, N.J., Gong, M.S. and Knowles, J.C. (2013) 'Effects of magnesium content on the physical, chemical and degradation properties in a MgO-CaO-Na<sub>2</sub>O-P<sub>2</sub>O<sub>5</sub> glass system', *Journal of Non-Crystalline Solids*, 363(1), pp. 57-63.

- Lee, J.A., Knight, C.A., Kun, X., Yang, X.B., Wood, D.J., Dalgarno, K.W. and Genever, P.G. (2015) 'In vivo biocompatibility of custom-fabricated apatite-wollastonite-mesenchymal stromal cell constructs', *Journal of Biomedical Materials Research - Part A*, 103(10), pp. 3188-3200.
- Lee, M., Dunn, J.C.Y. and Wu, B.M. (2005) 'Scaffold fabrication by indirect three-dimensional printing', *Biomaterials*, 26(20), pp. 4281-4289.
- Lee, Y.J. (2010) 'Spectroscopic investigation of arsenate and selenate incorporation into hydroxylapatite', *Current Applied Physics*, 10(1), pp. 158-163.
- Leonardi, E., Ciapetti, G., Baldini, N., Novajra, G., Verné, E., Baino, F. and Vitale-Brovarone, C. (2010) 'Response of human bone marrow stromal cells to a resorbable  $\text{P2O5-SiO2-CaO-MgO-Na2O-K2O}$  phosphate glass ceramic for tissue engineering applications', *Acta Biomaterialia*, 6(2), pp. 598-606.
- Leong, K.F., Cheah, C.M. and Chua, C.K. (2003) 'Solid freeform fabrication of three-dimensional scaffolds for engineering replacement tissues and organs', *Biomaterials*, 24(13), pp. 2363-2378.
- Leukers, B., Güllkan, H., Irsen, S.H., Milz, S., Tille, C., Schieker, M. and Seitz, H. (2005) 'Hydroxyapatite scaffolds for bone tissue engineering made by 3D printing', *Journal of Materials Science: Materials in Medicine*, 16(12), pp. 1121-1124.
- Li, P., Yang, Q., Zhang, F. and Kokubo, T. (1992) 'The effect of residual glassy phase in a bioactive glass-ceramic on the formation of its surface apatite layer in vitro', *Journal of Materials Science: Materials in Medicine*, 3, pp. 452 - 456.
- Liang, W., Rahaman, M.N., Day, D.E., Marion, N.W., Riley, G.C. and Mao, J.J. (2008) 'Bioactive borate glass scaffold for bone tissue engineering', *Journal of Non-Crystalline Solids*, 354(15-16), pp. 1690-1696.
- Lichte, P., Pape, H.C., Pufe, T., Kobbe, P. and Fischer, H. (2011) 'Scaffolds for bone healing: concepts, materials and evidence', *Injury*, 42(6), pp. 569-73.
- Lickorish, D., Guan, L. and Davies, J.E. (2007) 'A three-phase, fully resorbable, polyester/calcium phosphate scaffold for bone tissue engineering: Evolution of scaffold design', *Biomaterials*, 28(8), pp. 1495-1502.

- Lim, P.N., Teo, E.Y., Ho, B., Tay, B.Y. and Thian, E.S. (2013) 'Effect of silver content on the antibacterial and bioactive properties of silver-substituted hydroxyapatite', *Journal of Biomedical Materials Research - Part A*, 101(9), pp. 2456-64.
- Liu, C., Xia, Z. and Czernuszka, J.T. (2007) 'Design and development of three-dimensional scaffolds for tissue engineering', *Chemical Engineering Research and Design*, 85(7 A), pp. 1051-1064.
- Liu, X., Huang, W., Fu, H., Yao, A., Wang, D., Pan, H., Lu, W., Jiang, X. and Zhang, X. (2009) 'Bioactive borosilicate glass scaffolds: in vitro degradation and bioactivity behaviors', *Journal of Materials Science: Materials in Medicine*, 20(6), pp. 1237-1243.
- Liu, X., Xie, Z., Zhang, C., Pan, H., Rahaman, M.N., Zhang, X., Fu, Q. and Huang, W. (2010) 'Bioactive borate glass scaffolds: in vitro and in vivo evaluation for use as a drug delivery system in the treatment of bone infection', *Journal of Materials Science: Materials in Medicine*, 21(2), pp. 575-82.
- Liu, Y., Lim, J. and Teoh, S.H. (2013) 'Review: Development of clinically relevant scaffolds for vascularised bone tissue engineering', *Biotechnology Advances*, 31(5), pp. 688-705.
- Logeart-Avramoglou, D., Anagnostou, F., Bizios, R. and Petite, H. (2005) 'Engineering bone: challenges and obstacles', *Journal of Cellular and Molecular Medicine*, 9(1), pp. 72-84.
- Loh, Q.L. and Choong, C. (2013) 'Three-dimensional scaffolds for tissue engineering applications: Role of porosity and pore size', *Tissue Engineering - Part B: Reviews*, 19(6), pp. 485-502.
- Lovell, N.C. (1990) 'Structure function, and adaptation of compact bone.', *American Journal of Physical Anthropology*, 82(1), pp. 116-117.
- Low, S.W., Ng, Y.J., Yeo, T.T. and Chou, N. (2009) 'Use of Osteoplug polycaprolactone implants as novel burr-hole covers', *Singapore Medical Journal*, 50(8), pp. 777-80.
- Lu, T., Li, Y. and Chen, T. (2013) 'Techniques for fabrication and construction of three-dimensional scaffolds for tissue engineering', *International Journal of Nanomedicine*, 8, pp. 337-350.

- Lu, Y., Mapili, G., Suhali, G., Chen, S. and Roy, K. (2006) 'A digital micro-mirror device-based system for the microfabrication of complex, spatially patterned tissue engineering scaffolds', *Journal of Biomedical Materials Research Part A*, 77A(2), pp. 396-405.
- Luo, S.H., Xiao, W., Wei, X.J., Jia, W.T., Zhang, C.Q., Huang, W.H., Jin, D.X., Rahaman, M.N. and Day, D.E. (2010) 'In vitro evaluation of cytotoxicity of silver-containing borate bioactive glass', *Journal of Biomedical Materials Research Part B: Applied Biomaterials*, 95(2), pp. 441-8.
- Macon, A.L., Kim, T.B., Valliant, E.M., Goetschius, K., Brow, R.K., Day, D.E., Hoppe, A., Boccaccini, A.R., Kim, I.Y., Ohtsuki, C., Kokubo, T., Osaka, A., Vallet-Regi, M., Arcos, D., Fraile, L., Salinas, A.J., Teixeira, A.V., Vueva, Y., Almeida, R.M., Miola, M., Vitale-Brovarone, C., Verne, E., Holand, W. and Jones, J.R. (2015) 'A unified in vitro evaluation for apatite-forming ability of bioactive glasses and their variants', *Journal of Materials Science: Materials in Medicine*, 26(2), p. 115.
- Maeno, S., Niki, Y., Matsumoto, H., Morioka, H., Yatabe, T., Funayama, A., Toyama, Y., Taguchi, T. and Tanaka, J. (2005) 'The effect of calcium ion concentration on osteoblast viability, proliferation and differentiation in monolayer and 3D culture', *Biomaterials*, 26(23), pp. 4847-4855.
- Magallanes-Perdomo, M., Luklinska, Z.B., De Aza, A.H., Carrodegua, R.G., De Aza, S. and Pena, P. (2011) 'Bone-like forming ability of apatite-wollastonite glass ceramic', *Journal of the European Ceramic Society*, 31(9), pp. 1549-1561.
- Mankin, H.J., Hornicek, F.J. and Raskin, K.A. (2005) 'Infection in massive bone allografts', *Clinical Orthopaedics and Related Research*, (432), pp. 210-6.
- Mano, J.F., Sousa, R.A., Boesel, L.F., Neves, N.M. and Reis, R.L. (2004) 'Bioinert, biodegradable and injectable polymeric matrix composites for hard tissue replacement: state of the art and recent developments', *Composites Science and Technology*, 64(6), pp. 789-817.
- Marie, P.J. (2010) 'The calcium-sensing receptor in bone cells: A potential therapeutic target in osteoporosis', *Bone*, 46, pp. 571 - 576.
- Marie, P.J., Ammann, P., Boivin, G. and Rey, C. (2001) 'Mechanisms of action and therapeutic potential of strontium in bone', *Calcified tissue international*, 69, pp. 121 - 129.

- Marion, N.W., Liang, W., Reilly, G.C., Day, D.E., Rahaman, M.N. and Mao, J.J. (2005) 'Borate glass supports the in vitro osteogenic differentiation of human mesenchymal stem cells', *Mechanics of Advanced Materials and Structures*, 12, pp. 239 - 246.
- Marion, N.W. and Mao, J.J. (2006) 'Mesenchymal Stem Cells and Tissue Engineering', *Methods in enzymology*, 420, pp. 339-361.
- Marks Jr, S.C. and Odgren, P.R. (2002) 'Chapter 1 - Structure and Development of the Skeleton', in Rodan, J.P.B.G.R.A. (ed.) *Principles of Bone Biology (Second Edition)*. San Diego: Academic Press, pp. 3-15.
- Marks Jr, S.C. and Popoff, S.N. (1988) 'Bone cell biology: The regulation of development, structure, and function in the skeleton', *American Journal of Anatomy*, 183(1), pp. 1-44.
- Martin, R.B., Burr, D. B., Sharkey, N. A. *Skeletal Tissue Mechanics* Elsevier.
- Matsumine, A., Myoui, A., Kusuzaki, K., Araki, N., Seto, M., Yoshikawa, H. and Uchida, A. (2004) 'Calcium hydroxyapatite ceramic implants in bone tumour surgery. A long-term follow-up study', *Journal of Bone & Joint Surgery, British Volume*, 86(5), pp. 719-25.
- Melchels, F.P., Feijen, J. and Grijpma, D.W. (2009) 'A poly(D,L-lactide) resin for the preparation of tissue engineering scaffolds by stereolithography', *Biomaterials*, 30(23-24), pp. 3801-9.
- Melchels, F.P.W., Domingos, M.A.N., Klein, T.J., Malda, J., Bartolo, P.J. and Hutmacher, D.W. (2012) 'Additive manufacturing of tissues and organs', *Progress in Polymer Science*, 37(8), pp. 1079-1104.
- Melchels, F.P.W., Feijen, J. and Grijpma, D.W. (2010) 'A review on stereolithography and its applications in biomedical engineering', *Biomaterials*, 31(24), pp. 6121-6130.
- Meunier, P.J., Slosman, D.O., Delmas, P.D., Sebert, J.L., Brandi, M.L., Albanese, C., Lorenc, R., Pors-Nielsen, S., de Vernejoul, M.C., Roces, A. and Reginster, J.Y. (2002) 'Strontium ranelate: dose-dependent effects in established postmenopausal vertebral osteoporosis - a 2-year randomized placebo controlled trial', *The Journal of Clinical Endocrinology & Metabolism*, 87, pp. 2060 - 2066.
- Miguez-Pacheco, V., Hench, L.L. and Boccaccini, A.R. (2015) 'Bioactive glasses beyond bone and teeth: Emerging applications in contact with soft tissues', *Acta Biomaterialia*, 13, pp. 1-15.

- Miola, M., Brovarone, C.V., Maina, G., Rossi, F., Bergandi, L., Ghigo, D., Saracino, S., Maggiora, M., Canuto, R.A., Muzio, G. and Verne, E. (2014) 'In vitro study of manganese-doped bioactive glasses for bone regeneration', *Materials Science and Engineering C*, 38, pp. 107-18.
- Mitra, J., Tripathi, G., Sharma, A. and Basu, B. (2013) 'Scaffolds for bone tissue engineering: role of surface patterning on osteoblast response', *RSC Advances*, 3(28), pp. 11073-11094.
- Molladavoodi, S., Gorbet, M., Medley, J. and Ju Kwon, H. (2013) 'Investigation of microstructure, mechanical properties and cellular viability of poly(L-lactic acid) tissue engineering scaffolds prepared by different thermally induced phase separation protocols', *Journal of the Mechanical Behavior of Biomedical Materials*, 17, pp. 186-197.
- Morsi, Y.S., Wong, C.S. and Patel, S.S. (2008) 'Virtual Prototyping of Biomanufacturing in Medical Applications', in Bidanda, B. and Bártolo, P. (eds.) *Virtual Prototyping & Bio Manufacturing in Medical Applications*. Springer US, pp. 129-148.
- Mota, C., Puppi, D., Chiellini, F. and Chiellini, E. (2015) 'Additive manufacturing techniques for the production of tissue engineering constructs', *Journal of Tissue Engineering and Regenerative Medicine*, 9(3), pp. 174-90.
- Mourino, V., Cattalini, J.P. and Boccaccini, A.R. (2012) 'Metallic ions as therapeutic agents in tissue engineering scaffolds: an overview of their biological applications and strategies for new developments', *Journal of the Royal Society Interface*, 9(68), pp. 401-19.
- Mozafari, M. and Moztarzadeh, F. (2014) 'Synthesis, characterization and biocompatibility evaluation of sol-gel derived bioactive glass scaffolds prepared by freeze casting method', *Ceramics International*, 40(4), pp. 5349-5355.
- Muralithran, G. and Ramesh, S. (2000) 'The effects of sintering temperature on the properties of hydroxyapatite', *Ceramics International*, 26(2), pp. 221-230.
- Murphy, S., Boyd, D., Moane, S. and Bennett, M. (2009) 'The effect of composition on ion release from Ca-Sr-Na-Zn-Si glass bone grafts', *Journal of Materials Science: Materials in Medicine*, 20(11), pp. 2207-2214.
- Murphy, S., Wren, A.W., Towler, M.R. and Boyd, D. (2010) 'The effect of ionic dissolution products of Ca-Sr-Na-Zn-Si bioactive glass on in vitro cytocompatibility', *Journal of Materials Science: Materials in Medicine*, 21(10), pp. 2827-34.



- Nalla, R.K., Kruzic, J.J., Kinney, J.H., Balooch, M., Ager, J.W. and Ritchie, R.O. (2006) 'Role of microstructure in the aging-related deterioration of the toughness of human cortical bone', *Materials Science and Engineering: C*, 26(8), pp. 1251-1260.
- Narayan, R. (2009) *Biomedical Materials*. Springer US.
- Navarro, M., Del Valle, S., Martínez, S., Zeppetelli, S., Ambrosio, L., Planell, J.A. and Ginebra, M.P. (2004) 'New macroporous calcium phosphate glass ceramic for guided bone regeneration', *Biomaterials*, 25(18), pp. 4233-4241.
- Navarro, M., Michiardi, A., Castaño, O. and Planell, J.A. (2008) 'Biomaterials in orthopaedics', *Journal of the Royal Society Interface*, 5(27), pp. 1137-1158.
- Neel, E.A.A., Ahmed, I., Pratten, J., Nazhat, S.N. and Knowles, J.C. (2005) 'Characterisation of antibacterial copper releasing degradable phosphate glass fibres', *Biomaterials*, 26(15), pp. 2247-2254.
- Nerem, R.M. (2006) 'Tissue engineering: The hope, the hype, and the future', *Tissue Engineering*, 12(5), pp. 1143-1150.
- Neve, A., Corrado, A. and Cantatore, F.P. (2011) 'Osteoblast physiology in normal and pathological conditions', *Cell and Tissue Research*, 343(2), pp. 289-302.
- Nielsen, F.H. 'Boron in human and animal nutrition', *Plant and Soil*, 193(1), pp. 199-208.
- Nielsen, F.H. (1990) 'New essential trace elements for the life sciences', *Biological Trace Element Research*, 26-27, pp. 599-611.
- Nielsen, F.H. and Poellot, R. (2004) 'Dietary silicon affects bone turnover differently in ovariectomized and sham-operated growing rats', *The Journal of Trace Elements in Experimental Medicine*, 17(3), pp. 137-149.
- Ning, J., Yao, A., Wang, D., Huang, W., Fu, H., Liu, X., Jiang, X. and Zhang, X. (2007) 'Synthesis and in vitro bioactivity of a borate-based bioglass', *Materials Letters*, 61(30), pp. 5223-5226.
- Nonami, T. and Tsutsumi, S. (1999) 'Study of diopside ceramics for biomaterials', *Journal of Materials Science: Materials in Medicine*, 10(8), pp. 475-479.
- Novajra, G., Perdika, P., Pisano, R., Miola, M., Bari, A., Jones, J.R., Detsch, R., Boccaccini, A.R. and Vitale-Brovarone, C. (2015) 'Structure optimisation and biological evaluation of bone scaffolds

prepared by co-sintering of silicate and phosphate glasses', *Advances in Applied Ceramics*, 114, pp. S48-S55.

Novajra, G., Vitale-Brovarone, C., Knowles, J.C., Maina, G., Aina, V., Ghigo, D. and Bergandi, L. (2011) 'Effects of TiO<sub>2</sub>-containing phosphate glasses on solubility and in vitro biocompatibility', *Journal of Biomedical Materials Research - Part A*, 99 A(2), pp. 295-306.

O'Donnell, M.D. (2012) 'Melt-Derived Bioactive Glass', in *Bio-Glasses*. John Wiley & Sons, Ltd, pp. 13-27.

Ohsawa, K., Neo, M., Okamoto, T., Tamura, J. and Nakamura, T. (2004) 'In vivo absorption of porous apatite-and wollastonite-containing glass-ceramic', *Journal of Materials Science: Materials in Medicine*, 15(8), pp. 859-864.

Oryan, A., Alidadi, S., Moshiri, A. and Maffulli, N. (2014) 'Bone regenerative medicine: Classic options, novel strategies, and future directions', *Journal of Orthopaedic Surgery and Research*, 9(1).

Oryan, A., Monazzah, S. and Bigham-Sadegh, A. (2015) 'Bone Injury and Fracture Healing Biology', *Biomedical and Environmental Sciences*, 28(1), pp. 57-71.

Ossification, I. (2004) 'Developmental Biology of the Skeletal System', *Bone Tissue Engineering*, p. 1.

Oudadesse, H., Dietrich, E., Gal, Y.L., Pellen, P., Bureau, B., Mostafa, A.A. and Cathelineau, G. (2011) 'Apatite forming ability and cytocompatibility of pure and Zn-doped bioactive glasses', *Journal of Biomedical Materials Research*, 6(3), p. 035006.

Owen, M. (1988) 'Marrow stromal stem cells', *Journal of Cell Science*, 10, pp. 63-76.

Pal, S. (2014) 'Mechanical Properties of Biological Materials', in *Design of Artificial Human Joints & Organs*. Springer US, pp. 23-40.

Palmer, L.C., Newcomb, C.J., Kaltz, S.R., Spoerke, E.D. and Stupp, S.I. (2008) 'Biomimetic systems for hydroxyapatite mineralization inspired by bone and enamel', *Chemical Reviews*, 108(11), pp. 4754-4783.

Palmour, H., Spriggs, R.M. and Uskokovic, D.P. (2013) *Science of Sintering: New Directions for Materials Processing and Microstructural Control*. Springer US.

- Pan, H.B., Zhao, X.L., Zhang, X., Zhang, K.B., Li, L.C., Li, Z.Y., Lam, W.M., Lu, W.W., Wang, D.P., Huang, W.H., Lin, K.L. and Chang, J. (2010) 'Strontium borate glass: Potential biomaterial for bone regeneration', *Journal of the Royal Society Interface*, 7(48), pp. 1025-1031.
- Park, J. and Ozturk, A. (2013) 'Bioactivity of apatite-wollastonite glass-ceramics produced by melting casting', *Surface Review and Letters*, 20(1).
- Park, J.K., Shim, J.-H., Kang, K.S., Yeom, J., Jung, H.S., Kim, J.Y., Lee, K.H., Kim, T.-H., Kim, S.-Y., Cho, D.-W. and Hahn, S.K. (2011) 'Solid Free-Form Fabrication of Tissue-Engineering Scaffolds with a Poly(lactic-co-glycolic acid) Grafted Hyaluronic Acid Conjugate Encapsulating an Intact Bone Morphogenetic Protein-2/Poly(ethylene glycol) Complex', *Advanced Functional Materials*, 21(15), pp. 2906-2912.
- 'Performance Standards for Antimicrobial Disk Susceptibility Tests; Approved Standard—Eleventh Edition ', (2012).
- Petite, H., Viateau, V., Bensaid, W., Meunier, A., de Pollak, C., Bourguignon, M., Oudina, K., Sedel, L. and Guillemin, G. (2000) 'Tissue-engineered bone regeneration', *Nature Biotechnology*, 18(9), pp. 959-63.
- Pilia, M., Guda, T. and Appleford, M. (2013) 'Development of composite scaffolds for load-bearing segmental bone defects', *BioMed Research International*, 2013.
- Pittenger, M.F., Mackay, A.M., Beck, S.C., Jaiswal, R.K., Douglas, R., Mosca, J.D., Moorman, M.A., Simonetti, D.W., Craig, S. and Marshak, D.R. (1999) 'Multilineage potential of adult human mesenchymal stem cells', *Science*, 284(5411), pp. 143-7.
- Planell, J.A., Best, S.M., Lacroix, D. and Merolli, A. (2009) *Bone repair biomaterials*. Woodhead Publishing Ltd.
- Polo-Corrales, L., Latorre-Esteves, M. and Ramirez-Vick, J.E. (2014) 'Scaffold design for bone regeneration', *Journal of Nanoscience and Nanotechnology*, 14(1), pp. 15-56.
- Prakasam, M., Locs, J., Salma-Ancane, K., Loca, D., Largeteau, A. and Berzina-Cimdina, L. (2015) 'Fabrication, Properties and Applications of Dense Hydroxyapatite: A Review', *Journal of Functional Biomaterials*, 6(4), pp. 1099-1140.

- Rahaman, M.N., Bal, B.S. and Huang, W. (2014) 'Review: Emerging developments in the use of bioactive glasses for treating infected prosthetic joints', *Materials Science and Engineering: C*, 41(0), pp. 224-231.
- Rahaman, M.N., Day, D.E., Bal, B.S., Fu, Q., Jung, S.B., Bonewald, L.F. and Tomsia, A.P. (2011) 'Bioactive glass in tissue engineering', *Acta Biomaterialia*, 7(6), pp. 2355-73.
- Rahaman, M.N., Liang, W.E.N., Day, D.E., Marion, N.W., Reilly, G.C. and Mao, J.J. (2005) *Ceramic engineering and science proceedings*. American Ceramic Society.
- Rai, B., Lin, J.L., Lim, Z.X.H., Guldberg, R.E., Hutmacher, D.W. and Cool, S.M. (2010) 'Differences between in vitro viability and differentiation and in vivo bone-forming efficacy of human mesenchymal stem cells cultured on PCL-TCP scaffolds', *Biomaterials*, 31(31), pp. 7960-7970.
- Rainer, A., Giannitelli, S.M., Abbruzzese, F., Traversa, E., Licoccia, S. and Trombetta, M. (2008) 'Fabrication of bioactive glass–ceramic foams mimicking human bone portions for regenerative medicine', *Acta Biomaterialia*, 4(2), pp. 362-369.
- Raucci, M.G., Guarino, V. and Ambrosio, L. (2010) 'Hybrid composite scaffolds prepared by sol–gel method for bone regeneration', *Composites Science and Technology*, 70(13), pp. 1861-1868.
- Raucci, M.G., Guarino, V. and Ambrosio, L. (2012) 'Biomimetic strategies for bone repair and regeneration', *Journal of functional biomaterials*, 3(3), pp. 688-705.
- Reffitt, D.M., Ogston, N., Jugdaohsingh, R., Cheung, H.F., Evans, B.A., Thompson, R.P., Powell, J.J. and Hampson, G.N. (2003) 'Orthosilicic acid stimulates collagen type 1 synthesis and osteoblastic differentiation in human osteoblast-like cells in vitro', *Bone*, 32(2), pp. 127-35.
- Reilly, D.T., Burstein, A.H. and Frankel, V.H. (1974) 'The elastic modulus for bone', *Journal of Biomechanics*, 7(3), pp. 271-5.
- Reis, R.L. and Román, J.S. (2004) *Biodegradable Systems in Tissue Engineering and Regenerative Medicine*. CRC Press.
- Renghini, C., Komlev, V., Fiori, F., Verné, E., Baino, F. and Vitale-Brovarone, C. (2009) 'Micro-CT studies on 3-D bioactive glass-ceramic scaffolds for bone regeneration', *Acta Biomaterialia*, 5(4), pp. 1328-1337.

- Rezwan, K., Chen, Q.Z., Blaker, J.J. and Boccaccini, A.R. (2006) 'Biodegradable and bioactive porous polymer/inorganic composite scaffolds for bone tissue engineering', *Biomaterials*, 27(18), pp. 3413-3431.
- Rho, J.-Y., Kuhn-Spearing, L. and Zioupos, P. (1998) 'Mechanical properties and the hierarchical structure of bone', *Medical Engineering & Physics*, 20(2), pp. 92-102.
- Rho, J.Y., Hobatho, M.C. and Ashman, R.B. (1995) 'Relations of mechanical properties to density and CT numbers in human bone', *Medical Engineering & Physics*, 17(5), pp. 347-55.
- Roberts, W.E., Huja, S. and Roberts, J.A. (2004) 'Bone modeling: biomechanics, molecular mechanisms, and clinical perspectives', *Seminars in Orthodontics*, 10(2), pp. 123-161.
- Rodriguez, J.P., Rios, S. and Gonzalez, M. (2002) 'Modulation of the proliferation and differentiation of human mesenchymal stem cells by copper', *Journal of Cellular Biochemistry*, 85, pp. 92 - 100.
- Rose, F.R. and Oreffo, R.O. (2002) 'Bone tissue engineering: hope vs hype', *Biochemical and Biophysical Research Communications*, 292(1), pp. 1-7.
- Rucci, N. (2008) 'Molecular biology of bone remodelling', *Clinical Cases in Mineral and Bone Metabolism*, 5(1), pp. 49-56.
- Rude, R.K., Gruber, H.E., Wei, L.Y., Frausto, A. and Mills, B.G. (2003) 'Magnesium deficiency: effect on bone and mineral metabolism in the mouse', *Calcified tissue international*, 72(1), pp. 32-41.
- Sachlos, E., Czernuszka, J.T., Gogolewski, S. and Dalby, M. (2003) 'Making tissue engineering scaffolds work. Review on the application of solid freeform fabrication technology to the production of tissue engineering scaffolds', *European Cells and Materials*, 5, pp. 29-40.
- Sachs, E., Cima, M., Williams, P., Brancazio, D. and Cornie, J. (1992) 'Three dimensional printing. Rapid Tooling and prototypes directly from a CAD model', *Journal of engineering for industry*, 114(4), pp. 481-488.
- Sachs, E.M. (2000) *Powder Dispensing Apparatus Using Vibration*.

- Saikia, K.C., Bhattacharya, T.D., Bhuyan, S.K., Talukdar, D.J., Saikia, S.P. and Jitesh, P. (2008) 'Calcium phosphate ceramics as bone graft substitutes in filling bone tumor defects', *Indian Journal of Orthopaedics*, 42(2), pp. 169-172.
- Sakai, T., Takeda, S. and Nakamura, M. (2002) 'The effects of particulate metals on cell viability of osteoblast-like cells in vitro', *Dental Materials*, 21(2), pp. 133-46.
- Salgado, A.J., Coutinho, O.P. and Reis, R.L. (2004) 'Bone tissue engineering: State of the art and future trends', *Macromolecular Bioscience*, 4(8), pp. 743-765.
- Salinas, A.J. and Vallet-Regi, M. (2013) 'Bioactive ceramics: from bone grafts to tissue engineering', *RSC Advances*, 3(28), pp. 11116-11131.
- Saltman, P.D. and Strause, L.G. (1993) 'The role of trace minerals in osteoporosis', *Journal of the American College of Nutrition*, 12(4), pp. 384-389.
- Samavedi, S., Whittington, A.R. and Goldstein, A.S. (2013) 'Calcium phosphate ceramics in bone tissue engineering: A review of properties and their influence on cell behavior', *Acta Biomaterialia*, 9(9), pp. 8037-8045.
- Sansone, V., Pagani, D. and Melato, M. (2013) 'The effects on bone cells of metal ions released from orthopaedic implants. A review', *Clinical Cases in Mineral and Bone Metabolism*, 10(1), pp. 34-40.
- Santos, C.F.L., Silva, A.P., Lopes, L., Pires, I. and Correia, I.J. (2012) 'Design and production of sintered  $\beta$ -tricalcium phosphate 3D scaffolds for bone tissue regeneration', *Materials Science and Engineering: C*, 32(5), pp. 1293-1298.
- Saranti, A., Koutselas, I. and Karakassides, M.A. (2006) 'Bioactive glasses in the system CaO–B<sub>2</sub>O<sub>3</sub>–P<sub>2</sub>O<sub>5</sub>: Preparation, structural study and in vitro evaluation', *Journal of Non-Crystalline Solids*, 352(5), pp. 390-398.
- Scholze, H. (2012) *Glass: nature, structure, and properties*. Springer Science & Business Media.
- Schroeder, J.E. and Mosheiff, R. (2011) 'Tissue engineering approaches for bone repair: Concepts and evidence', *Injury*, 42(6), pp. 609-613.
- Schulze, D. (1995) 'Flowability of Bulk Solids-Definition and Measuring Principles', *Chemie Ingenieur Technik*, 67(1), pp. 60-68.

- Seal, B.L., Otero, T.C. and Panitch, A. (2001) 'Polymeric biomaterials for tissue and organ regeneration', *Materials Science and Engineering: R: Reports*, 34(4-5).
- Seeman, E. (2009) 'Bone modeling and remodeling', *Critical Reviews™ in Eukaryotic Gene Expression*, 19(3), pp. 219-33.
- Seitz, H., Rieder, W., Irsen, S., Leukers, B. and Tille, C. (2005) 'Three-dimensional printing of porous ceramic scaffolds for bone tissue engineering', *Journal of Biomedical Materials Research Part B: Applied Biomaterials*, 74(2), pp. 782-788.
- Sepulveda, P., Jones, J.R. and Hench, L.L. (2002) 'Bioactive sol-gel foams for tissue repair', *Journal of Biomedical Materials Research*, 59(2), pp. 340-348.
- Services., U.S.D.o.H.a.H. (2004) *Bone Health and Osteoporosis: A Report of the Surgeon General*.
- Shanjani, Y., De Croos, J.N., Pilliar, R.M., Kandel, R.A. and Toyserkani, E. (2010) 'Solid freeform fabrication and characterization of porous calcium polyphosphate structures for tissue engineering purposes', *Journal of Biomedical Materials Research Part B: Applied Biomaterials*, 93(2), pp. 510-9.
- Sharma, K., Deo, M.N. and Kothiyal, G.P. (2012) 'Effect of iron oxide addition on structural properties of calcium silico phosphate glass/glass-ceramics', *Journal of Non-Crystalline Solids*, 358(16), pp. 1886-1891.
- Sheng, M.H., Lau, K.H. and Baylink, D.J. (2014) 'Role of Osteocyte-derived Insulin-Like Growth Factor I in Developmental Growth, Modeling, Remodeling, and Regeneration of the Bone', *Journal of Bone Metabolism*, 21(1), pp. 41-54.
- Silver, I.A., Deas, J. and Erecińska, M. (2001) 'Interactions of bioactive glasses with osteoblasts in vitro: effects of 45S5 Bioglass®, and 58S and 77S bioactive glasses on metabolism, intracellular ion concentrations and cell viability', *Biomaterials*, 22(2), pp. 175-185.
- Singh, K. and Bahadur, D. (1999) 'Characterization of SiO<sub>2</sub>-Na<sub>2</sub>O-Fe<sub>2</sub>O<sub>3</sub>-CaO-P<sub>2</sub>O<sub>5</sub>-B<sub>2</sub>O<sub>3</sub> glass ceramics', *Journal of Materials Science: Materials in Medicine*, 10(8), pp. 481-4.
- Singh, K., Bala, I. and Kumar, V. (2009) 'Structural, optical and bioactive properties of calcium borosilicate glasses', *Ceramics International*, 35(8), pp. 3401-3406.

- Singh, R.K. and Srinivasan, A. (2010) 'Bioactivity of SiO<sub>2</sub>–CaO–P<sub>2</sub>O<sub>5</sub>–Na<sub>2</sub>O glasses containing zinc–iron oxide', *Applied Surface Science*, 256(6), pp. 1725-1730.
- Soetan, K.O., Olaiya, C.O. and Oyewole, O.E. (2010) 'The importance of mineral elements for humans, domestic animals and plants: A review', *African Journal of Food Science*, 4(5), pp. 200-222.
- Sofie, S.W. and Dogan, F. (2001) 'Freeze Casting of Aqueous Alumina Slurries with Glycerol', *Journal of the American Ceramic Society*, 84(7), pp. 1459-1464.
- Sommerfeldt, D. and Rubin, C. (2001) 'Biology of bone and how it orchestrates the form and function of the skeleton', *European Spine Journal*, 10(SUPPL. 2), pp. S86-S95.
- Song, J.H., Koh, Y.H., Kim, H.E., Li, L.H. and Bahn, H.J. (2006) 'Fabrication of a porous bioactive glass-ceramic using room-temperature freeze casting', *Journal of the American Ceramic Society*, 89(8), pp. 2649-2653.
- Sosinsky, G.E. and Nicholson, B.J. (2005) 'Structural organization of gap junction channels', *Biochimica et Biophysica Acta*, 1711(2), pp. 99-125.
- Spath, S., Drescher, P. and Seitz, H. (2015) 'Impact of Particle Size of Ceramic Granule Blends on Mechanical Strength and Porosity of 3D Printed Scaffolds', *Materials*, 8(8), pp. 4720-4732.
- Spori, D.M., Drobek, T., Zürcher, S., Ochsner, M., Sprecher, C., Mühlebach, A. and Spencer, N.D. (2008) 'Beyond the lotus effect: Roughness influences on wetting over a wide surface-energy range', *Langmuir*, 24(10), pp. 5411-5417.
- Stähli, C., James-Bhasin, M., Hoppe, A., Boccaccini, A.R. and Nazhat, S.N. (2015) 'Effect of ion release from Cu-doped 45S5 Bioglass® on 3D endothelial cell morphogenesis', *Acta Biomaterialia*, 19, pp. 15-22.
- Stahli, C., Muja, N. and Nazhat, S.N. (2013) 'Controlled copper ion release from phosphate-based glasses improves human umbilical vein endothelial cell survival in a reduced nutrient environment', *Tissue Engineering - Part A*, 19(3-4), pp. 548-57.
- Standard (2009) 'ISO 10993-5:2009 - Biological evaluation of medical devices. Tests for in vitro cytotoxicity'.



Office for National Statistics, (2012) *Population Ageing in the United Kingdom, its Constituent Countries and the European Union*. [Online]. Available at: [http://www.ons.gov.uk/ons/dcp171776\\_258607.pdf](http://www.ons.gov.uk/ons/dcp171776_258607.pdf).

Stevens, M.M. (2008) 'Biomaterials for bone tissue engineering', *Materials Today*, 11(5), pp. 18-25.

Sun, H. and Yang, H.L. (2015) 'Calcium phosphate scaffolds combined with bone morphogenetic proteins or mesenchymal stem cells in bone tissue engineering', *Chinese Medical Journal*, 128(8), pp. 1121-1127.

Sun, W., Darling, A., Starly, B. and Nam, J. (2004) 'Computer-aided tissue engineering: overview, scope and challenges', *Biotechnology and Applied Biochemistry*, 39(1), pp. 29-47.

Sun, Z.P., Ercan, B., Evis, Z. and Webster, T.J. (2010) 'Microstructural, mechanical, and osteocompatibility properties of Mg<sup>2+</sup>/F(-)-doped nanophase hydroxyapatite', *Journal of Biomedical Materials Research - Part A*, 94(3), pp. 806-15.

Sung-Hoon, A., Michael, M., Dan, O., Shad, R. and Paul, K.W. (2002) 'Anisotropic material properties of fused deposition modeling ABS', *Rapid Prototyping Journal*, 8(4), pp. 248-257.

Suwanprateeb, J. and Chumnanklang, R. (2006) 'Three-dimensional printing of porous polyethylene structure using water-based binders', *Journal of Biomedical Materials Research Part B: Applied Biomaterials*, 78(1), pp. 138-45.

Suwanprateeb, J., Sanngam, R., Suvannapruk, W. and Panyathanmaporn, T. (2009) 'Mechanical and in vitro performance of apatite-wollastonite glass ceramic reinforced hydroxyapatite composite fabricated by 3D-printing', *Journal of Materials Science: Materials in Medicine*, 20(6), pp. 1281-9.

Swift, K.G. and Booker, J.D. (2013) 'Chapter 8 - Rapid Prototyping Processes', in Booker, K.G.S.D. (ed.) *Manufacturing Process Selection Handbook*. Oxford: Butterworth-Heinemann, pp. 227-241.

Tarafder, S., Balla, V.K., Davies, N.M., Bandyopadhyay, A. and Bose, S. (2013) 'Microwave Sintered 3D Printed Tricalcium Phosphate Scaffolds for Bone Tissue Engineering', *Journal of tissue engineering and regenerative medicine*, 7(8), pp. 631-641.

- Tarafder, S., Dernell, W.S., Bandyopadhyay, A. and Bose, S. (2015) 'SrO- and MgO-doped microwave sintered 3D printed tricalcium phosphate scaffolds: Mechanical properties and in vivo osteogenesis in a rabbit model', *Journal of Biomedical Materials Research - Part B Applied Biomaterials*, 103(3), pp. 679-690.
- Thavornnyutikarn, B., Chantarapanich, N., Sitthiseripratip, K., Thouas, G. and Chen, Q. (2014) 'Bone tissue engineering scaffolding: computer-aided scaffolding techniques', *Progress in Biomaterials*, 3(2-4), pp. 61-102.
- Thompson, I.D. and Hcnch, L.L. (1998) 'Mechanical properties of bioactive glasses, glass-ceramics and composites', *Proceedings of the Institution of Mechanical Engineers, Part H: Journal of Engineering in Medicine*, 212(2), pp. 127-136.
- Tilley, R.J.D. (2013) *Understanding Solids: The Science of Materials*. Wiley.
- Tranquilli Leali, P., Doria, C., Zachos, A., Ruggiu, A., Milia, F. and Barca, F. (2009) 'Bone fragility: current reviews and clinical features', *Clinical Cases in Mineral and Bone Metabolism*, 6(2), pp. 109-113.
- Tsuboi, S., Nakagaki, H., Ishiguro, K., Kondo, K., Mukai, M., Robinson, C. and Weatherell, J.A. (1994) 'Magnesium distribution in human bone', *Calcified tissue international*, 54(1), pp. 34-37.
- Turner, C.H. (1998) 'Three rules for bone adaptation to mechanical stimuli', *Bone*, 23(5), pp. 399-407.
- Utela, B., Anderson, R.L. and Kuhn, H. (2006a) *17th Solid Freeform Fabrication Symposium, SFF 2006*.
- Utela, B., Anderson, R.L. and Kuhn, H. (2006b) *Solid Freeform Fabrication Symposium Proceeding*.
- Utela, B., Storti, D., Anderson, R. and Ganter, M. (2008) 'A review of process development steps for new material systems in three dimensional printing (3DP)', *Journal of Manufacturing Processes*, 10(2), pp. 96-104.
- Utela, B.R., Storti, D., Anderson, R.L. and Ganter, M. (2010) 'Development process for custom three-dimensional printing (3DP) material systems', *Journal of Manufacturing Science and Engineering, Transactions of the ASME*, 132(1), pp. 0110081-0110089.

- Uysal, T., Ustidal, A., Sonmez, M.F. and Ozturk, F. (2009) 'Stimulation of bone formation by dietary boron in an orthopedically expanded suture in rabbits', *The Angle Orthodontist*, 79(5), pp. 984 - 990.
- Vacanti, J.P., Cima, L.G. and Cima, M.J. (2001) *Vascularized tissue regeneration matrices formed by solid free form fabrication techniques*.
- Vacanti, J.P. and Vacanti, C.A. (2013) 'The History and Scope of Tissue Engineering', in *Principles of Tissue Engineering: Fourth Edition*. Elsevier Inc., pp. 3-8.
- Valappil, S.P., Pickup, D.M., Carroll, D.L., Hope, C.K., Pratten, J., Newport, R.J., Smith, M.E., Wilson, M. and Knowles, J.C. (2007) 'Effect of silver content on the structure and antibacterial activity of silver-doped phosphate-based glasses', *Antimicrobial agents and chemotherapy*, 51(12), pp. 4453-4461.
- Vallet, R., xed, Mar and xed (2012) 'Mesoporous Silica Nanoparticles: Their Projection in Nanomedicine', *ISRN Materials Science*, 2012, p. 20.
- Van Lieshout, E.M.M., Van Kralingen, G.H., El-Massoudi, Y., Weinans, H. and Patka, P. (2011) 'Microstructure and biomechanical characteristics of bone substitutes for trauma and orthopaedic surgery', *BMC Musculoskeletal Disorders*, 12, pp. 34-34.
- Velleman, S.G. (2000) 'The role of the extracellular matrix in skeletal development', *Poultry Science*, 79(7), pp. 985-9.
- Ventola, C.L. (2014) 'Medical Applications for 3D Printing: Current and Projected Uses', *Pharmacy and Therapeutics*, 39(10), pp. 704-711.
- Venturelli, C. (2011) 'Heating Microscopy and its Applications', *Microscopy Today*, 19(01), pp. 20-25.
- Vickers, W.O.M. (2013) *The Effect of Strontium Substitution on Apatite-wollastonite Glass-ceramics*. PhD thesis. University of Leeds (School of Mechanical Engineering) [Online]. Available at: <https://books.google.co.uk/books?id=r4bIoAEACAAJ>.
- Vitale-Brovarone, C., Bairo, F., Bretcanu, O. and Verné, E. (2009) 'Foam-like scaffolds for bone tissue engineering based on a novel couple of silicate-phosphate specular glasses: Synthesis and properties', *Journal of Materials Science: Materials in Medicine*, 20(11), pp. 2197-2205.

- Vitale-Brovarone, C., Baino, F. and Verne, E. (2010) 'Feasibility and tailoring of bioactive glass-ceramic scaffolds with gradient of porosity for bone grafting', *Journal of Biomaterials Applications*, 24(8), pp. 693-712.
- Vitale-Brovarone, C., Ciapetti, G., Leonardi, E., Baldini, N., Bretcanu, O., Verné, E. and Baino, F. (2011) 'Resorbable glass-ceramic phosphate-based scaffolds for bone tissue engineering: Synthesis, properties, and in vitro effects on human marrow stromal cells', *Journal of Biomaterials Applications*, 26(4), pp. 465-489.
- Vitale-Brovarone, C., Verné, E., Robiglio, L., Martinasso, G., Canuto, R.A. and Muzio, G. (2008) 'Biocompatible glass-ceramic materials for bone substitution', *Journal of Materials Science: Materials in Medicine*, 19(1), pp. 471-478.
- Vivanco, J., Slane, J., Nay, R., Simpson, A. and Ploeg, H.L. (2011) 'The effect of sintering temperature on the microstructure and mechanical properties of a bioceramic bone scaffold', *Journal of the Mechanical Behavior of Biomedical Materials*, 4(8), pp. 2150-60.
- Vogel, W. (2013) *Structure and Crystallization of Glasses*. Elsevier Science.
- Vorndran, E., Klarner, M., Klammert, U., Grover, L.M., Patel, S., Barralet, J.E. and Gbureck, U. (2008) '3D Powder Printing of  $\beta$ -Tricalcium Phosphate Ceramics Using Different Strategies', *Advanced Engineering Materials*, 10(12), pp. B67-B71.
- Vrouwenvelde, W.C.A., Groot, C.G. and De Groot, K. (1994) 'Better histology and biochemistry for osteoblasts cultured on titanium-doped bioactive glass: bioglass 45S5 compared with iron-, titanium-, fluorine- and boron-containing bioactive glasses', *Biomaterials*, 15(2), pp. 97-106.
- Vyas, V., Kumar, A., Prasad, S., Singh, S.P. and Pyare, R.A.M. (2015) 'Bioactivity and mechanical behaviour of cobalt oxide-doped bioactive glass', *Bulletin of Materials Science*, 38(4), pp. 957-964.
- Wagoner Johnson, A.J. and Herschler, B.A. (2011) 'A review of the mechanical behavior of CaP and CaP/polymer composites for applications in bone replacement and repair', *Acta Biomaterialia*, 7(1), pp. 16-30.
- Wan, C., Gilbert, S.R., Wang, Y., Cao, X., Shen, X., Ramaswamy, G., Jacobsen, K.A., Alaq, Z.S., Eberhardt, A.W., Gerstenfeld, L.C., Einhorn, T.A., Deng, L. and Clemens, T.L. (2008) 'Activation of the hypoxia-inducible factor-1 $\alpha$  pathway accelerates bone regeneration', *Proceedings of the National Academy of Sciences*, 105(2), pp. 686-691.

- Wang, H., Zhao, S., Zhou, J., Shen, Y., Huang, W., Zhang, C., Rahaman, M.N. and Wang, D. (2014) 'Evaluation of borate bioactive glass scaffolds as a controlled delivery system for copper ions in stimulating osteogenesis and angiogenesis in bone healing', *Journal of Materials Chemistry B*, 2(48), pp. 8547-8557.
- Wang, M. (2003) 'Developing bioactive composite materials for tissue replacement', *Biomaterials*, 24(13), pp. 2133-2151.
- Wang, P., Zhao, L., Liu, J., Weir, M.D., Zhou, X. and Xu, H.H.K. (2015) 'Bone tissue engineering via nanostructured calcium phosphate biomaterials and stem cells', *Bone Research*, 2.
- Warnke, P.H., Seitz, H., Warnke, F., Becker, S.T., Sivananthan, S., Sherry, E., Liu, Q., Wiltfang, J. and Douglas, T. (2010) 'Ceramic scaffolds produced by computer-assisted 3D printing and sintering: characterization and biocompatibility investigations', *Journal of Biomedical Materials Research Part B: Applied Biomaterials*, 93(1), pp. 212-7.
- Whitney, E.N. and Rolfes, S.R. (2013) *Understanding nutrition*. Australia; Belmont, CA: Wadsworth, Cengage Learning.
- Will, J., Gerhardt, L.C. and Boccaccini, A.R. (2012) 'Bioactive glass-based scaffolds for bone tissue engineering', *Advances in biochemical engineering/biotechnology*, 126, pp. 195-226.
- Will, J., Melcher, R., Treul, C., Travitzky, N., Kneser, U., Polykandriotis, E., Horch, R. and Greil, P. (2008) 'Porous ceramic bone scaffolds for vascularized bone tissue regeneration', *Journal of Materials Science: Materials in Medicine*, 19(8), pp. 2781-90.
- Williams, D.F. (2009) 'On the nature of biomaterials', *Biomaterials*, 30(30), pp. 5897-5909.
- Wu, C., Fan, W., Gelinsky, M., Xiao, Y., Simon, P., Schulze, R., Doert, T., Luo, Y. and Cuniberti, G. (2011) 'Bioactive SrO-SiO<sub>2</sub> glass with well-ordered mesopores: characterization, physiochemistry and biological properties', *Acta Biomaterialia*, 7(4), pp. 1797-806.
- Wu, C., Ramaswamy, Y. and Zreiqat, H. (2010) 'Porous diopside (CaMgSi<sub>2</sub>O<sub>6</sub>) scaffold: A promising bioactive material for bone tissue engineering', *Acta Biomaterialia*, 6(6), pp. 2237-2245.
- Wu, C. and Xiao, Y. (2009) 'Evaluation of the in vitro bioactivity of bioceramics', *Bone and Tissue Regeneration Insights*, 2, pp. 25-29.

- Wu, C., Zhou, Y., Xu, M., Han, P., Chen, L., Chang, J. and Xiao, Y. (2013) 'Copper-containing mesoporous bioactive glass scaffolds with multifunctional properties of angiogenesis capacity, osteostimulation and antibacterial activity', *Biomaterials*, 34(2), pp. 422-433.
- Xiao, K., Dalgarno, K.W., Wood, D.J., Goodridge, R.D. and Ohtsuki, C. (2008) 'Indirect selective laser sintering of apatite-wollastonite glass-ceramic', *Proceeding Institution of Mechanical Engineering part H*, 222(7), pp. 1107-14.
- Xiao, W., Gu, Y.F., Wang, D.P., Huang, W.H., Pan, H.B. and Lu, W.J. (2009) 'Application of borate glass in the field of biomaterials', *Journal of Clinical Rehabilitative Tissue Engineering Research*, 13(34), pp. 6741-6744.
- Xin, L., Haobo, P., Hailuo, F., Qiang, F., Mohamed, N.R. and Wenhai, H. (2010) 'Conversion of borate-based glass scaffold to hydroxyapatite in a dilute phosphate solution', *Biomedical Materials*, 5(1), p. 015005.
- Xu, C., Su, P., Chen, X., Meng, Y., Yu, W., Xiang, A.P. and Wang, Y. (2011) 'Biocompatibility and osteogenesis of biomimetic Bioglass-Collagen-Phosphatidylserine composite scaffolds for bone tissue engineering', *Biomaterials*, 32(4), pp. 1051-1058.
- Xynos, I.D., Edgar, A.J., Buttery, L.D.K., Hench, L.L. and Polak, J.M. (2000a) 'Ionic products of bioactive glass dissolution increase proliferation of human osteoblasts and induce insulin-like growth factor II mRNA expression and protein synthesis', *Biochemical and Biophysical Research Communications*, 276, pp. 461 - 465.
- Xynos, I.D., Edgar, A.J., Buttery, L.D.K., Hench, L.L. and Polak, J.M. (2001) 'Gene-expression profiling of human osteoblasts following treatment with the ionic products of Bioglass(R) 45S5 dissolution', *Journal of Biomedical Materials Research*, 55, pp. 151 - 157.
- Xynos, I.D., Hukkanen, M.V.J., Batten, J.J., Buttery, L.D., Hench, L.L. and Polak, J.M. (2000b) 'Bioglass (R)45S5 stimulates osteoblast turnover and enhances bone formation in vitro: implications and applications for bone tissue engineering', *Calcified Tissue International*, 67, pp. 321 - 329.
- Yamaguchi, M. (1998) 'Role of zinc in bone formation and bone resorption', *The Journal of Trace Elements in Experimental Medicine*, 11(2-3), pp. 119-135.

- Yamasaki, K. and Hagiwara, H. (2009) 'Excess iron inhibits osteoblast metabolism', *Toxicology Letters*, 191(2-3), pp. 211-5.
- Yang, S., Leong, K.F., Du, Z. and Chua, C.K. (2001) 'The design of scaffolds for use in tissue engineering. Part I. Traditional factors', *Tissue Engineering*, 7(6), pp. 679-689.
- Yao, A., Wang, D., Huang, W., Fu, Q., Rahaman, M.N. and Day, D.E. (2007) 'In vitro bioactive characteristics of borate-based glasses with controllable degradation behavior', *Journal of the American Ceramic Society*, 90(1), pp. 303-306.
- Yao, J., Radin, S.S., Leboy, P. and Ducheyne, P. (2005) 'The effect of bioactive glass content on synthesis and bioactivity of composite poly (lactic-co-glycolic acid)/bioactive glass substrate for tissue engineering', *Biomaterials*, 26, pp. 1935 - 1943.
- Yin, Y., Ye, F., Cui, J., Zhang, F., Li, X. and Yao, K. (2003) 'Preparation and characterization of macroporous chitosan-gelatin/beta-tricalcium phosphate composite scaffolds for bone tissue engineering', *Journal of Biomedical Materials Research Part A*, 67(3), pp. 844-55.
- Yoo, D.-J. (2014) 'Recent trends and challenges in computer-aided design of additive manufacturing-based biomimetic scaffolds and bioartificial organs', *International Journal of Precision Engineering and Manufacturing*, 15(10), pp. 2205-2217.
- Yoshikawa, H. and Myoui, A. (2005) 'Bone tissue engineering with porous hydroxyapatite ceramics', *Journal of Artificial Organs*, 8(3), pp. 131-6.
- Younger, E.M. and Chapman, M.W. (1989) 'Morbidity at bone graft donor sites', *Journal of Orthopaedic Trauma*, 3(3), pp. 192-5.
- Zein, I., Hutmacher, D.W., Tan, K.C. and Teoh, S.H. (2002) 'Fused deposition modeling of novel scaffold architectures for tissue engineering applications', *Biomaterials*, 23(4), pp. 1169-1185.
- Zhang, H., Hussain, I., Brust, M., Butler, M.F., Rannard, S.P. and Cooper, A.I. (2005) 'Aligned two- and three-dimensional structures by directional freezing of polymers and nanoparticles', *Nature Materials*, 4(10), pp. 787-793.
- Zhang, H., Ye, X.-J. and Li, J.-S. (2009) 'Preparation and biocompatibility evaluation of apatite/wollastonite-derived porous bioactive glass ceramic scaffolds', *Biomedical Materials*, 4(4), p. 045007.

- Zhang, Y., Liu, Y., Li, M., Lu, S. and Wang, J. (2013) 'The effect of iron incorporation on the in vitro bioactivity and drug release of mesoporous bioactive glasses', *Ceramics International*, 39(6), pp. 6591-6598.
- Zhao, S., Wang, H., Zhang, Y., Huang, W., Rahaman, M.N., Liu, Z., Wang, D. and Zhang, C. (2015) 'Copper-doped borosilicate bioactive glass scaffolds with improved angiogenic and osteogenic capacity for repairing osseous defects', *Acta biomaterialia*, 14, pp. 185-196.
- Zhao, Y.S., Zhang, X., Xiang, W.D., Wang, D.P., Huang, W.H., Pan, H.B. and Lv, W.J. (2010) 'Research of borosilicate glass with strontium on bioactivity and biodegradability in vitro', *Gongneng Cailiao/Journal of Functional Materials*, 41(3), pp. 439-442.
- Zheng, K., Yang, S.B., Wang, J.J., Russel, C., Liu, C.S. and Liang, W. (2012) 'Characteristics and biocompatibility of  $\text{Na}_2\text{O-K}_2\text{O-CaO-MgO-SrO-B}_2\text{O}_3\text{-P}_2\text{O}_5$  borophosphate glass fibers', *Journal of Non-Crystalline Solids*, 358, pp. 387 - 391.
- Zhu, N. and Chen, X. (2013) *Biofabrication of Tissue Scaffolds*. INTECH Open Access Publisher.
- Zipkin, I. (1970) 'Chapter 3. The Inorganic Composition of Bones and Teeth', in Schraer, H. (ed.) *Biological Calcification: Cellular and Molecular Aspects*. Springer US, pp. 69-103.
- Zreiqat, H., Howlett, C.R., Zannettino, A., Evans, P., Schulze-Tanzil, G., Knabe, C. and Shakibaei, M. (2002) 'Mechanisms of magnesium-stimulated adhesion of osteoblastic cells to commonly used orthopaedic implants', *Journal of Biomedical Materials Research - Part A*, 62(2), pp. 175-84.